UNIVERSIDADE DE SÃO PAULO
ESCOLA DE ENGENHARIA DE SÃO CARLOS

Lucas Sales Neves

Fast Methods for Voltage Stability Analysis and Control Selection Considering Parameter Uncertainties

São Carlos

2022

Lucas Sales Neves

Fast Methods for Voltage Stability Analysis and Control Selection Considering Parameter Uncertainties

Tese apresentada à Escola de Engenharia de São Carlos da Universidade de São Paulo, para obtenção do título de Doutor em Ciências - Programa de Pós-Graduação em Engenharia Elétrica.

Área de concentração: Sistemas Elétricos de Potência

Orientador: Prof. Luís Fernando Costa Alberto

São Carlos

2022

Trata-se da versão corrigida da tese. A versão original se encontra disponível na EESC/USP que aloja o Programa de Pós-Graduação de Engenharia Elétrica.

Ficha catalográfica elaborada pela Biblioteca Prof. Dr. Sérgio Rodrigues Fontes da EESC/USP com os dados inseridos pelo(a) autor(a).

Sales Neves, Lucas
S511f Fast methods for voltage stability analysis and control selection considering parameter uncertainties / Lucas Sales Neves; orientador Luís Fernando Costa Alberto. São Carlos, 2022.

Tese (Doutorado) - Programa de Pós-Graduação em Engenharia Elétrica e Área de Concentração em Sistemas Elétricos de Potência -- Escola de Engenharia de São Carlos da Universidade de São Paulo, 2022.

1. Voltage Stability. 2. Bifurcation Surface. 3. Parameter Uncertainties. 4. Voltage Stability Margin. 5. Preventive Control Selection. I. Título.

Eduardo Graziosi Silva - CRB - 8/8907

FOLHA DE JULGAMENTO

Candidato: Engenheiro **LUCAS SALES NEVES.**

Título da tese: "Métodos rápidos de análise de estabilidade de tensão e seleção de controles considerando incertezas de parâmetros".

Data da defesa: 11/03/2022.

Comissão Julgadora	**Resultado**
Prof. Titular **Luís Fernando Costa Alberto (Orientador)** (Escola de Engenharia de São Carlos/EESC-USP)	__Aprovado___
Prof. Dr. **João Alberto Passos Filho** (Universidade Federal de Juíz de Fora/UFJF)	__Aprovado___
Prof. Dr. **Antonio Carlos Zambroni de Souza** (Universidade Federal de Itajubá/UNIFEI)	__Aprovado___
Prof. Dr. **Glauco Nery Taranto** (Universidade Federal do Rio de Janeiro/UFRJ)	__Aprovado___
Prof. Dr. **Marcos Julio Rider Flores** (Universidade Estadual de Campinas/UNICAMP)	__Aprovado___

Coordenador do Programa de Pós-Graduação em Engenharia Elétrica:
Prof. Dr. **João Bosco Augusto London Junior**

Presidente da Comissão de Pós-Graduação:
Prof. Titular **Murilo Araujo Romero**

ACKNOWLEDGEMENTS

I acknowledge my family, friends, professors and colleagues, who directly or indirectly influenced this work. I acknowledge USP and FAPESP (grants 2018/24815-7, 2014/50851-0 and 2018/20104-9) for the financial and institutional support.

ABSTRACT

Neves, L. S. **Fast Methods for Voltage Stability Analysis and Control Selection Considering Parameter Uncertainties**. 2022. 199p. Tese (Doutorado) - Escola de Engenharia de São Carlos, Universidade de São Paulo, São Carlos, 2022.

With the ongoing load increase in current power systems, voltage stability analysis has become an essential tool to ensure that a power system can withstand different loading variations. In this scenario, this work deals with parameter uncertainties and control selection in voltage stability analysis of power systems.

The main contributions of this thesis are related to:

- Modelling:
  - A new static power system model is proposed. The new model enables an unified analysis of different voltage instability mechanisms. Specifically, all static bifurcations are transformed into saddle-node bifurcations.
  - A new model to take parameter uncertainties into account is proposed, where parametric variations are represented by a Brownian motion and the uncertainty region is described by a cone.
- Voltage stability margin computation:
  - A new method for contingency ranking is proposed. The proposed method is both fast and accurate in computing the contingency ranking, and is able to compute different bifurcation types.
  - A new method is proposed to compute the voltage stability margin. The method is robust to different parameter variation scenarios and is able to compute different bifurcation types. The method is also fast, with a execution time equivalent to a few continuation power flow computations.
- Voltage stability margin control: A new method is proposed to select control actions which aim for increasing the voltage stability margin. The method takes uncertainties into account, and results show that proposed method is fast on selecting a small number of control actions that are sufficient to increase the voltage stability margin to a predefined value.

All propositions were tested by means of several simulations on different test-systems. Implementation results corroborate that the proposed methods are fast and robust, with potential for online voltage stability assessment of large-scale power systems.

Keywords: Voltage Stability. Bifurcation Surface. Parameter Uncertainties. Voltage Stability Margin. Preventive Control Selection.

RESUMO

Neves, L. S. **Métodos Rápidos de Análise de Estabilidade de Tensão e Seleção de Controles Considerando Incertezas de Parâmetros**. 2022. 199p. Tese (Doutorado) - Escola de Engenharia de São Carlos, Universidade de São Paulo, São Carlos, 2022.

Com o aumento de carga nos sistemas de potência atuais, estabilidade de tensão se tornou uma ferramenta essencial para garantir que um sistema de potênca pode suportar diferentes variações de carregamento. Neste contexto, este trabalho aborda incertezas de parâmetros e seleção de controles na análise de estabilidade de tensão de sistemas de potência.

Esta tese apresenta contribuições relacionadas a:

- Modelagem:
  - A proposição de um novo modelo estático para sistemas de potência. O novo modelo permite uma análise unificada de diferentes mecanismos que podem levar à instabilidade de tensão. Especificamente, todas as bifurcações estáticas são transformadas em bifurcações sela-nó.
  - Um modelo para tratamento de incertezas é proposto. As variações paramétricas são representadas por um movimento Browniano e a região de incertezas é representada por um cone.
- Cálculo da margem de estabilidade de tensão:
  - Um novo método para análise de contingências foi desenvolvido. O método proposto é preciso no cálculo do ranqueamento das contingências, e é capaz de detectar diferentes tipos de bifurcação.
  - Um novo método de cálculo da margem de estabilidade de tensão foi proposto. O método é robusto a diferentes cenários de variação paramétrica e é capaz de detectar diferentes tipos de bifurcação. O método também é rápido, com um tempo de execução equivalente a alguns cálculos de fluxo de potência continuado.
- Controle da margem de estabilidade de tensão: Um novo método foi proposto para a seleção de ações de controle com o objetivo de aumentar a margem de estabilidade de tensão. O método leva incertezas em consideração, e resultados mostram que o método proposto pode rapidamente selecionar um pequeno conjunto de ações de controle capaz de aumentar a margem para um valor pré-definido.

Todas as proposições foram testadas por meio de diversas simulações em diferentes sistemas-teste. Resultados de implementação corroboram que os métodos propostos são rápidos e robustos, com potencial para avaliação em tempo real de estabilidade de tensão em sistemas de grande porte.

Palavras-chave: Estabilidade de Tensão. Superfície de Bifurcações. Incertezas Paramétricas. Margem de Estabilidade de Tensão. Seleção de Controles Preventivos.

LIST OF FIGURES

LIST OF TABLES

CONTENTS

1 INTRODUCTION

Power system stability analysis is concerned about quantifying operating margins and maintaining power system security. This stability refers to the ability of the power system to reach an appropriate equilibrium state (where operating constraints are satisfied) after a disturbance. The goal of power system stability assessment is to ensure that the system can withstand different disturbances without major failures. In other words, stability assessment aims for maintaining the power system in the *normal state*, where frequency and voltage are properly controlled between their acceptable limits and the system can resist to any credible contingency.

Power system stability is generally divided into three fields of study[1], regarding the nature of the instability issue: *angle stability*, *frequency stability* or *voltage stability*. In *angle stability*, the concern is to maintain synchronous generators "in step" after a (small or large) disturbance. Following a fault and a subsequent tripping of a transmission line, for example, a nearby generator may lose synchronism with the system. In this situation, the rotor speed varies, followed by large power flow oscillations due to the uncontrolled variation of the rotor angle.

Even when generator rotors remain synchronized, their speed may still increase or decrease, leading to frequency deviations in relation to the nominal value. This characterizes the field of *frequency stability*. Power flow oscillations are not necessarily an issue in frequency instability, but frequency deviations may suddenly trigger protection devices to avoid damages to equipment.

In contrast, *voltage instability* refers to the inability of the power system to maintain the voltage levels at load buses. For example, as with angle instability, voltage instability issues may also arise from the loss of a transmission line. In this case, nearby transmission lines may get overloaded and the load-end voltage might start decreasing. The load dynamics usually try to restore the power by increasing its current, which will increase the current flow in the overloaded transmission system, leading to a further voltage drop. The unstable situation is clear and blackouts may occur if countermeasures (like load shedding) are not taken.

It is usually difficult to separate these instability mechanisms in practical situations. These effects can occur concomitantly when a contingency occurs, for example. Nevertheless, a natural distinction between angle/frequency instability and voltage instability is the source of the problem: angle/frequency instability occurs due to an uncontrolled variation

[1] Recent studies (HATZIARGYRIOU et al., 2021) extend this division to include *resonance stability* and *converter-driven stability*.

of the rotor speed of generators, while voltage instability occurs when the dynamics of a load/voltage restoration mechanism becomes unstable. As a result, it is common to associate angle/frequency instability with the generation-side dynamics, while voltage instability is associated with the load-side dynamics. Nevertheless, load dynamics are not the only source of voltage instability problems, which can also be driven by renewable, uncontrollable generation resources.

This work deals with voltage stability. Specifically, this work approaches *long-term voltage stability in relation to parameter variations*. Let this subject of study be described by a simple example.

1.1 Voltage Stability Example

Consider a DC load R_L connected to an ideal DC voltage source E by means of resistance R, as shown in Figure 1.

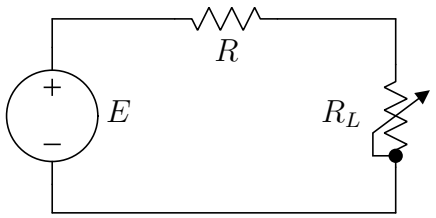

Figure 1 – Voltage Stability Example

Let the load dynamics be a first-order power restoration dynamics:

$$R'_L(t) = P_L(t) - P_{\text{ref}} = R_L(t)\frac{E^2}{(R + R_L(t))^2} - P_{\text{ref}}\,, \tag{1.1}$$

where P_{ref} is the power reference. Note that the steady-state model of this load is a constant power model. The equilibrium $R'_L(t) = 0$ is a quadratic equation with respect to R_L. The two solutions of this equation are:

$$R_{L,\text{eq}} = \frac{E^2 - 2P_{\text{ref}}R \pm E\sqrt{E^2 - 4P_{\text{ref}}R}}{2P_{\text{ref}}}\,, \tag{1.2}$$

which are represented in Figure 2 for $E = 1$ and $R = 0.25$. This figure shows that the maximum power that can be delivered to the load is $P_L = 1$.

The phase portrait of equation (1.1) is shown in Figure 3. This figure shows that the upper equilibrium of R_L is stable, while the lower solution is unstable. With the increase of P_{ref}, these two solutions approach each other and coalesce at $P_{\text{ref}} = 1$.

If the variation of P_{ref} is sufficiently slow, the power system operating point simply follows the trajectory of stable equilibrium points up to $P_{\text{ref}} = 1$. For example, assume that P_{ref} slowly increases starting from 0.8. The trajectory of R_L with the quasi-static increase of P_{ref} is shown in Figure 4, where a collapse occurs at $P_{\text{ref}} = 1$.

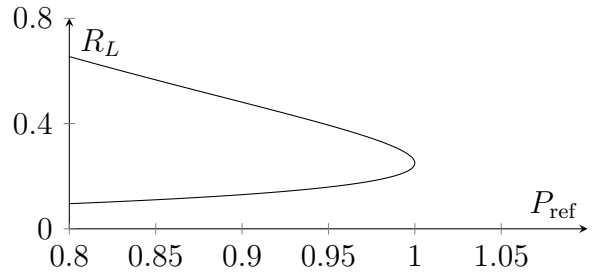

Figure 2 – Equilibrium branch of equation (1.1).

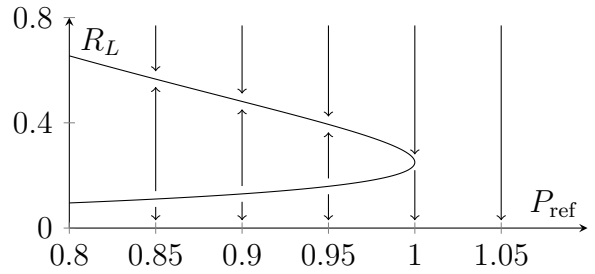

Figure 3 – Phase portrait of equation (1.1).

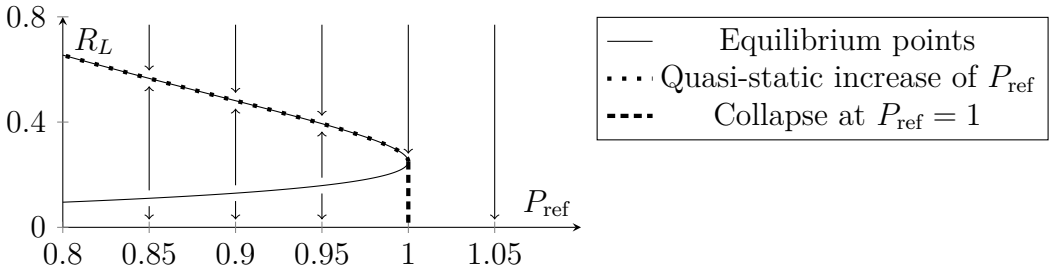

Figure 4 – Quasi-static variation of P_{ref} followed by a collapse.

Figures 2, 3 and 4 can also be projected in the $P_{\text{ref}}V_L$-plane instead of the $P_{\text{ref}}R_L$-plane, where V_L is the load voltage. Since $V_L = \sqrt{P_L\, R_L}$ and $P_L = P_{\text{ref}}$ on the equlibrium branch, one can see that these figures in the $P_{\text{ref}}V_L$-plane present the same behavior shown in Figures 2, 3 and 4. When P_{ref} reaches 1, V_L will inevitably decrease to zero, resulting in a voltage collapse.

To illustrate the temporal variation of V_L during a voltage collapse, assume that P_{ref} increases from 0.9999 to 1.0001 at $t = 0$. Equation (1.2) indicates that the stable equilibrium at $P_{\text{ref}} = 0.9999$ is $R_{L,\text{eq}} \approx 0.255$. Equation (1.1) is numerically integrated for $P_{\text{ref}} = 1.0001$ starting from $R_L(0) \approx 0.255$, and $R_L(t)$ is obtained. The value of $V_L(t) = \sqrt{1.0001 R_L(t)}$ is shown in Figure 5.

Note that, even though the fast decrease in V_L only occurs after $t = 100$ s, the unstable situation was present from the very beginning. The difference from a slow and fast dynamics in this unstable trajectory is due to the fact that the initial point is near the saddle-node point $(P_{\text{ref}}, R_L) = (1, 0.25)$. The saddle-node point is the "nose point" in Figure 3, where two equilibrium points (one stable and one unstable) collide with the

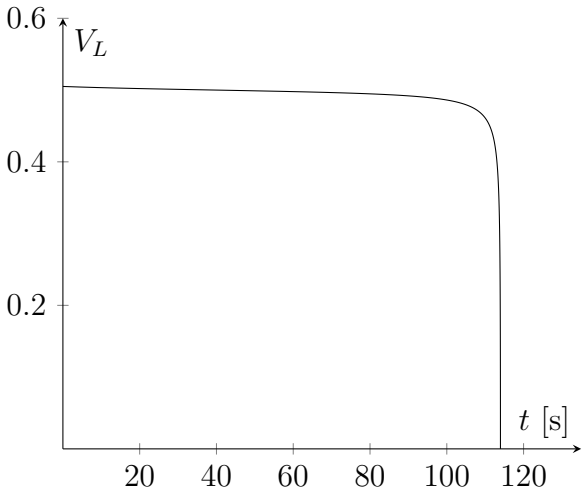

Figure 5 – Voltage collapse.

increase of P_{ref}. The unstable trajectory starting from $R_L(0) \approx 0.255$ with $P_{\text{ref}} = 1.0001$ is near the unstable part of the center manifold of this saddle-node point (which was depicted by the heavy dashed line in Figure 4).

Albeit simple, the example detailed above highlights important characteristics of voltage instability:

- Voltage instability is intrinsically linked to the inability of the transmission system to deliver the power demanded by the load;
- The mechanism that leads to the collapse is the voltage/power restoration dynamics;
- Voltage instability issues are not exclusively related to reactive power;
- Long-term voltage instability due to slow parametric variations occur due to loss of equilibrium points (typically the collision of a stable equilibrium and an unstable equilibrium).

These observations generalize to larger and more complex systems, where there are several dynamics involved. Moreover, this example is representative of the current situation of electric power systems: current power systems are highly loaded, i.e., they often operate near their loadability limits. As a consequence, Voltage Stability Assessment (VSA) became even more important nowadays.

1.2 Voltage Stability of Large Power Systems

Despite the several mechanisms that lead a power system to voltage instability, this thesis deals specifically with voltage instability issues triggered by small, slow parameter variations. In this scenario, the example of Section 1.1 captures the essence of voltage instability in current power systems: the composition of the generation system and the transmission system can suddenly become unable to meet the power demands of the distribution centers. This can be thought as a weakness of either the generation system

or the transmission system, where either the generated power cannot be increased or an increase in the generated power does not reflect in an increase in load power.

Real power systems are not radial as the example of Section 1.1: the transmission system can be thought as a graph, where the vertices represent power system buses and edges represent power system branches (generally transmission lines or transformers). This graph is usually meshed, in a way that is usually difficult to predict, without computational simulation, the direction of the power flowing on a given edge. Without knowing the direction of the power flow in the transmission system, it is difficult to predict a voltage collapse. In this situation, computational tools are needed to analyze the system from the point of view of voltage stability.

In traditional power systems, it is generally well defined which buses are generation buses and which ones are load buses. Several devices are connected to these load buses, where each device has a particular dynamical characteristic. In general, however, the dynamics of load devices try to maintain the demanded power at a specified value, independent of the terminal voltage. Examples of such equipment are induction motors and thermostatic loads (CUTSEM; VOURNAS, 1998). In other words, there are several loads in the system that roughly behave like the one in the example of Section 1.1. All these dynamics generate a set of differential equations of the power system, which can then be used to compute the current equilibrium point.

The power demanded by load devices vary with time (e.g., the mechanical load of a induction machine may increase). As a result, the state of the system changes to a new equilibrium point as load varies. Clearly, the system loading cannot increase indefinitely. For example, the increase of the system loading (i.e., the increase of the power demanded by load devices) can cause the loss of the equilibrium point, exactly as exemplified in Section 1.1. In this situation, the loss of an equilibrium point due to loading variations simply means the specified power demanded by the set of all load buses cannot be meet, because:

- generators cannot increase (or decrease) the generated power due to operational limits;
- transmission lines are not able to deliver the specified power, i.e., much of the power absorbed in the generation-end of the line become transmission losses, which do not propagate to the load-end of the line.

The collapse usually occurs with the variation of several parameters in the power system. With the aid of numerical methods (sensitivity analysis, for example), we can identify which devices most influence the occurring collapse. However, it must be emphasized that there is not an unique device triggering the voltage collapse: the collapse is a combination of the effects of the dynamic characteristics of several equipment.

1.3 Power System Control

In the context of stability, power system control refers to the set of controls available to maintain and restore the normal state. Preventive actions are taken to keep the system away from an unstable condition (which can lead to outages, for example), while corrective actions are taken in extreme cases to avoid an incoming collapse.

Different control actions are taken in different circumstances. For example, frequency deviations are intrinsically linked to active power unbalance of generation units (via the swing equation). Hence, frequency control is directly employed in the generator prime mover. This control occurs at different levels. In a primary (faster) level, speed governors ensure the synchronization between a generation unit and the power system. In a secondary (slower) level, the power output of multiple generators is adjusted to correct frequency mismatches.

On the other hand, voltage-related issues usually arise at the load-end of overloaded transmission systems. Due to the intrinsically inductive characteristic of transmission systems, voltage deviations from the nominal value generally occur due to differences between the required and available reactive power reserves. Voltage control is a result of a concatenation of controls spread from generation to load. These controls are divided among several devices, such as automatic voltage regulators, load tap changers, static var compensators, synchronous compensators, etc. All these controls must be combined and properly coordinated to ensure that voltage limits at the load-end are satisfied.

In face of an incoming voltage instability, the system operator must know which control action is most effective in avoiding the collapse. For example, in a situation where the collapse occurs due to the limit of a generator, control actions which increase the power generated in the system may be promising in ensuring voltage stability. When generation limits are not an issue, series compensation may help alleviate transmission losses. Nevertheless, in large, highly connected systems, it is difficult to define the best control actions to avoid the collapse. In this case, computational tools are often employed to define the most promising controls to ensure voltage stability.

When the voltage at the receiving end is low, voltage instability problems may also occur due to a device that is itself trying to restore the voltage levels. A typical example is the dynamic of a load tap changer: a tap increase, which usually increases the load voltage in stable operation, might end up decreasing this voltage even more. This occurs when the voltage increase due to the tap increase is less than the voltage drop due to the increased current flowing in the transmission system.

All aforementioned control actions are usually performed by controllers, which do not need human intervention. However, there are control devices which need manual operation, in contrast to being operated by controllers. A typical example in voltage

stability is a mechanically switched capacitor, which can be connected or disconnected from the system according to an external (human) action.

Even though controllers automatically regulate the power system voltage, their parameters can still be tuned in order to avoid a voltage collapse. For example, the voltage setpoint of a static var compensator may be externally adjusted to increase the power system robustness.

In this work, control selection refers to the procedure of determining a set of (manual) control actions needed to improve power system stability. These control actions may either directly influence the power system performance (which is the case of a manual load shedding, for example) or tune parameters of controllers, which in turn influence the power system behavior.

Next, a simple example will be presented to demonstrate the effects of a control variable in voltage stability.

1.3.1 Example

Consider the two-bus AC system shown in Figure 6, comprising an infinite bus (with unlimited capacity of generation and voltage regulation) and a load bus whose steady-state characteristic is given by a constant power model (similarly to the steady state characteristic of the load in Section 1.1).

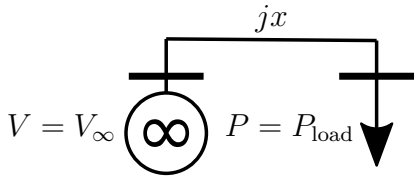

Figure 6 – Voltage Stability Control

The complex power demanded by the load is given by:

$$S = P + jQ = E\overline{I} = E\overline{\frac{E_\infty - E}{jx}}\,, \tag{1.3}$$

where E and I are the complex voltage at the load bus and the complex current flowing through the transmission line, respectively. For a given complex value S, (1.3) is used to compute the complex load voltage E. In this small example, this solution is analytical.

Equation (1.3) is rewritten as follows:

$$V^2 - jxS = V^2 - jxP + xQ = E\overline{E_\infty}\,, \tag{1.4}$$

where $V = |E|$. Taking the squared modulus on both sides leads to:

$$(V^2 + xQ)^2 + (xP)^2 = V^2 V_\infty^2\,, \tag{1.5}$$

where $V_\infty = |E_\infty|$.

Equation (1.5) is a quadratic equation on V^2, whose solution (if it exists) is given by:

$$V^2 = \frac{V_\infty^2 - 2xQ \pm \sqrt{(V_\infty^2 - 2xQ)^2 - 4x^2|S|^2}}{2}, \tag{1.6}$$

where $|S|^2 = P^2 + Q^2$. Since $V \geq 0$:

$$V = \sqrt{\frac{V_\infty^2 - 2xQ \pm \sqrt{(V_\infty^2 - 2xQ)^2 - 4x^2|S|^2}}{2}}, \tag{1.7}$$

which shows that, usually, there are two solutions for equation (1.3) for a given $S = P + jQ$. Let us assume that the load consumes no reactive power, so $Q = 0$ and (1.7) reduces to:

$$V = \sqrt{\frac{V_\infty^2 \pm \sqrt{V_\infty^4 - 4x^2P^2}}{2}}, \tag{1.8}$$

which has two solutions for $P = 0$ and these solutions coalesce when $|P| = \frac{V_\infty^2}{2x}$. The PV-curve representing equation (1.8) is shown in Figure 7. Note the resemblance between Figure 7 and Figure 2.

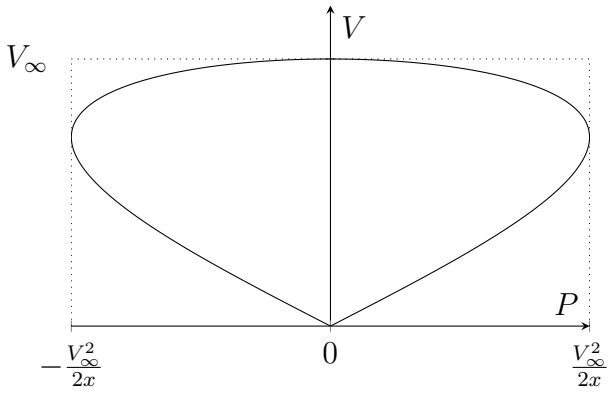

Figure 7 – PV-curve of equation (1.8).

For each value of P, there are two solution points for V. These are equilibria of the underlying dynamical system that model the dynamics of the load. Which equilibrium is stable and which is unstable will be defined by these dynamics. For example, if the upper equilibrium branch is stable (which is usually the case), then the phase portrait for this system will look like the one in Figure 3.

Assume that the load is demanding a level of active power close to $P_{\max} = \frac{V_\infty^2}{2x}$, such that small variations of this load can surpass this limit, causing a voltage collapse (similarly to the one in Figure 4). Hence, it is desirable to increase the limit and avoid instability. Consider that there is a capacitor with susceptance b_c available at the load bus.

When the capacitor is connected to the system, equation (1.3) changes to

$$S - jQ_c = P + j(Q - Q_c) = E\overline{I} = E\overline{\frac{E_\infty - E}{jx}}, \tag{1.9}$$

where $Q_c = b_c V^2$ is the reactive power supplied by the capacitor. Following the same steps presented above, the solution V for (1.9) is:

$$V = \sqrt{\frac{V_\infty^2 - 2(1 - xb_c)xQ \pm \sqrt{(V_\infty^2 - 2(1 - xb_c)xQ)^2 - 4(1 - xb_c)^2 x^2 |S|^2}}{2(1 - xb_c)^2}}, \tag{1.10}$$

which reduces to

$$V = \sqrt{\frac{V_\infty^2 \pm \sqrt{V_\infty^4 - 4(1 - xb_c)^2 x^2 P^2}}{2(1 - xb_c)^2}}, \tag{1.11}$$

when $Q = 0$. Again, two solution points exist for $P = 0$, but now they coalesce for $|P| = \frac{V_\infty^2}{2x(1-xb_c)}$. Observe that the maximum value of P grew by a factor of $\frac{1}{1-xb_c}$. Along with the curve in Figure 7, the PV-curve from equation (1.11) is shown in Figure 8. Note that the maximum value of V also grows by a factor of $\frac{1}{1-xb_c}$, so the size of the capacitor must be carefully chosen to avoid violating the voltage upper bound for the load bus.

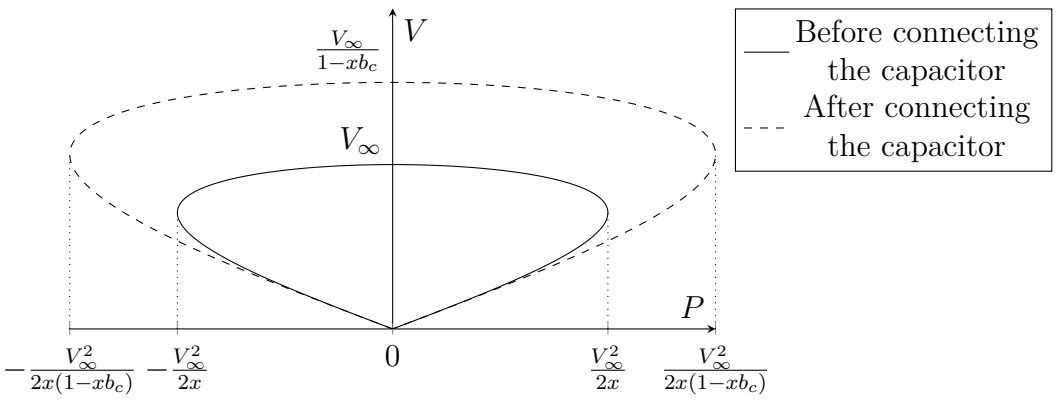

Figure 8 – PV-curve of equation (1.8).

In this case, connecting the capacitor is a control action in the system that results in a increase in the power transfer capability, thus providing a way of ensuring voltage stability when the system is highly loaded.

This example illustrated how external control actions can influence voltage stability. In this example, the effect of connecting a capacitor to the system was calculated analytically. In real systems, with several control actions available, computational tools must be employed to accurately define which control action is more appropriate to each situation.

1.4 Motivation

The description of the voltage instability phenomena given in Section 1.1 and in Section 1.2 shows that voltage instability issues generally occur in highly-loaded systems. Indeed, this is the case of current power systems, due to the ongoing load increase, where a loading variation can suddenly lead to a voltage collapse. Furthermore, the increasingly

use of renewable, uncontrollable generation sources make the power system operating point harder to predict, which further raises concerns related to voltage instability. Therefore, computational tools must be employed to constantly monitor the power system operating point (by means of state estimation) and to ensure that the system is not prone to instability.

To judge if the system is susceptible to voltage instability, we usually define voltage stability indicators, such as the voltage stability margin, to quantify "how far" the current operating point is from a collapse. By "how far", we compute a distance from the current operating point to the limit point where the system becomes unstable. In Figure 4, for example, we may define the voltage stability margin as 0.2, which is the difference between the load parameter in the collapse ($P_{\text{ref}} = 1$) and the same parameter in the current operating point ($P_{\text{ref}} = 0.8$).

In contrast to the example of Section 1.1, practical power systems have several parameters (usually thousands of parameters) that vary simultaneously with respect to time. Computational tools are then used to compute how the stable equilibrium point changes with these parameter variations. It is hard to accurately predict how these parameters will change. In this condition, the traditional VSA literature generally can be divided into two approaches:

- A literature which assumes that parameter variations can be predicted with accuracy. By knowing in advance how the system parameters will change, this literature is composed of several methods to assess voltage stability given a particular *parameter variation scenario*. A common method in this literature is the continuation power flow (IBA et al., 1991; AJJARAPU; CHRISTY, 1992; CANIZARES; ALVARADO, 1993; ZENG et al., 1993; CHIANG et al., 1995).
- A literature which disregards any predictability information about how parameters will change. Methods in this literature aim for computing worst case *scenarios*. Control actions are selected based on this worst case *scenario*. A common method in this literature is the closest bifurcation method (DOBSON; LU, 1993; ALVARADO; DOBSON; HU, 1994; DOBSON, 2004).

The influence of intermittent generation (such as solar generation and wind generation) makes it difficult to predict how parameters will vary. In this case, not only loading parameters are uncontrollable, but also the power generated by non-dispatchable renewable energy sources. In addition, the increase of distributed generation blurs the distinction between load buses and generation buses. As a consequence, the uncertainty in predicting the system future behavior is intensified nowadays, which harms the accuracy of continuation methods in predicting a voltage collapse.

On the other hand, results provided by worst case methods are restricted to critical situations which are unlikely to occur in practice. For example, the closest bifurcation

method may warn the operator that the system is near a collapse in a situation where the load at a critical, remote bus is increased. However, we know that such a pattern of parameter variation is unlikely to happen, and thus the system is not that close to a collapse.

Clearly, none of these approaches is realistic. While the first approach ignores any uncertainty related to how parameters *will* vary, the second approach ignores how parameters *are expected* to vary. The first approach usually gives optimistic results in voltage stability analysis, while the second approach provides pessimistic results.

This work takes place between the two aforementioned approaches. We assume that it is possible to predict how parameters will change. However, uncertainties about this predictability are not overlooked. In this way, all information available about parameter variations are taken into account when assessing voltage stability, leading to more realistic results that better reflect the power system future behavior.

Besides computing the distance to a voltage collapse, computational tools must also provide a set of preventive actions to ensure the normal operation of the power system. If the power system operating point approach an unstable condition, a set of control actions must be available to avoid instability. This control selection should be particularly fast in critical situations, where the system is near a collapse.

Both the computation and control of the distance to collapse should be constantly executed during power system operation. It is impossible to predict exactly how the power system will behave in the near future, thus measures of the voltage stability margin must be constantly updated to help operators maintain the system normal state. Hence, computational tools employed to perform online voltage stability analyses should be both fast and robust.

Lastly, an implementation concern (from the mathematical point of view) regarding the characterization of the point of collapse is related to the different mechanisms that can lead the system to instability. These different mechanisms are associated with different *bifurcations* that a power system is subject to (these concepts will be introduced in Chapter 3). Methods on voltage stability analysis must take into account that a system can undergo different bifurcations, whose mathematical treatment is not necessarily the same.

Considering multiple bifurcation types in voltage stability is even more relevant when parameter uncertainties are taken into account, specially considering the lack of studies in the literature approaching uncertainties for bifurcations other than the saddle-node bifurcation. To take multiple bifurcation types into account when proposing methods for voltage stability, there are two possible approaches:

- Develop a method that is itself able to compute and detect arbitrary bifurcation

types;

- Develop a new model that transforms every generic static bifurcation into a specific type of bifurcation, and then propose methods for dealing with this specific bifurcation.

This thesis will address the second approach, motivated by the following reasons:

- Methods that deal with any bifurcation type usually are more complex than methods that deal with one type of bifurcation, because, in the former, the implementation must internally select different branches to compute and detect different bifurcations;
- While transforming every bifurcation into a specific bifurcation, not only the proposed method can take advantage of this model, but also any method that works with this specific type of bifurcation can be used.

Since the majority of the static voltage stability literature explores the characteristic of saddle-node bifurcations, a new model that converts generic bifurcations into saddle-node bifurcations is useful, allowing the study of generic bifurcations by most of the methods proposed in the literature that deals with saddle-node bifurcations.

1.5 PhD Contributions

The contribution of this thesis is the development of the foundations, of algorithms and computational tools to assess voltage stability in an efficient way.

A new, enhanced power flow model is proposed to unify and simplify the search for bifurcations. The proposed (smooth) model is supported by a solid theoretical background.

On top of this new model, several algorithms were developed for voltage stability assessment. The formulation of these algorithms is also supported by a strong mathematical foundation, and they do not make approximations or assumptions about the power system model. These algorithms can be gathered into a new, comprehensive framework, that is able to (i) estimate if the current operating point is near a voltage collapse and (ii) select preventive and corrective control actions to ensure that the system is far from a voltage collapse. Specifically, the proposed framework meets the following requisites:

- parameter uncertainties are addressed;
- different mechanisms leading to a voltage collapse are addressed;
- it is fast, with potential for online VSA of practical power systems;
- it is robust, in the sense that it works for different power systems under different operating conditions;
- control actions are selected to maintain the *normal state* of the system.

It should be emphasized that all models and methods presented in this thesis make distinct contributions in relation to the current literature on voltage stability. Some of these unique contributions are highlighted below, whose details are given throughout this

thesis:

- The new power flow model proposed here can support not only the methods proposed in this thesis, but also any method on the VSA literature that deals with saddle-node bifurcations. Any method that computes saddle-node bifurcations can be take advantage of the proposed model to produce more complete analyses in voltage stability.
- In relation to the literature, the method proposed for contingency ranking gives special attention to quality of the results. While methods in the current literature prioritize speed rather than accuracy, the proposed method is not only fast but also accurate on ranking contingencies with respect to voltage stability.
- The new treatment for parameter uncertainties proposed in this document is founded on a statistically solid background. This model clearly shows why the uncertainty region can be represented by a cone, and it further develops the foundations of uncertainty models in the VSA literature.
- The new method for voltage stability margin computation considering parameter uncertainties is more robust than the alternatives in the literature. This robustness comes from distinct steps for computing bifurcation points and for taking uncertainties into account. Moreover, the method is fast, with good potential for real time analysis of large systems.
- The method proposed for control selection is fast on selecting a minimum number of control actions that improve voltage stability. To our knowledge, this is the first method to deal with control selection to improve a robust measure of voltage stability margin, where uncertainties are taken into account. The promising results also show that the method scales well to large systems, which shows potential to real time voltage stability assessment.

1.6 Document structure

The remainder of this document is structured in the following chapters:

- **Chapter 2** describes the traditional power flow model by means of the several devices that constitute a power system.
- **Chapter 3** presents an overview of the current state of the model-based VSA literature, with special focus on methods that directly influenced the methodology proposed in this document.
- **Chapter 4** proposes a new modelling to mathematically represent power systems. The formulation proposed in Chapter 4 is the starting point of all methods proposed in the chapters following it.
- **Chapter 5** proposes a new method for contingency analysis in voltage stability assessment. The proposed method applies a homotopy to compute the post-contingency

voltage stability margin starting from the pre-contingency voltage stability margin.

- **Chapter 6** proposes a new foundation to the treatment of parameter uncertainties in voltage stability analysis. Based on this treatment of uncertainties, a new voltage stability index is proposed and a fast way to compute this index is developed.
- **Chapter 7** proposes proposes a new method for control selection on VSA. The proposed method is developed on top of the method of Chapter 6 and aims for selecting a small number fo control actions that are able to increase the voltage stability margin to a predefined value.
- **Chapter 8** presents the conclusions of this research and summarizes the contributions of this work.

2 TRADITIONAL POWER SYSTEM MODELLING

In order to computationally simulate the power system, a mathematical representation of the system is necessary. This chapter provides a brief review of the current and traditional literature on static power system modelling. With this modelling, the power system is represented by a set of nonlinear algebraic equations (usually referred to as power flow equations). A solution of this set of equations represent an equilibrium of the underlying dynamical power system. This work deals with electric power transmission systems, where three-phase loads are assumed to be balanced and single-phase equivalent models are used to represent the system. Note, however, that all methods proposed in this document are generic and can be used in poly-phase power system models as well.

At the end of this chapter, the power system steady-state behavior will be represented by a set of nonlinear equations (which correspond to the power system equilibrium equations). In addition, all system operational limits will be represented by a set of inequality constraints. In the next chapters, the complete mathematical model described here will then be used in computational tools to analyze the power system with respect to voltage stability.

2.1 Introduction

Most equations in the power flow model come from a nodal analysis of the system buses. The Kirchhoff's current law establishes that, for a given bus k, the following equation is satisfied:

$$\sum_{b \in B_k} I_b = 0\,, \tag{2.1}$$

where B_k is the set of all equipment connected to bus k and I_b is the current injected by a device b at bus k. The complex current I_b is a function of the complex voltage of all buses in which device b is connected to. Therefore, the variables in equation (2.1) are the voltages of all buses connected to all devices in B_k.

Power flow equations generally are modelled in terms of power, where equation (2.1) is conjugated and multiplied by the complex voltage E_k:

$$E_k \overline{\sum_{b \in B_k} I_b} = \sum_{b \in B_k} E_k \overline{I_b} = \sum_{b \in B_k} S_b = 0\,, \tag{2.2}$$

where S_b is the power that device b injects at bus k.

Different sections of this chapter describe different components in set B_k. These sections explain how to compute the power S_b for each device b.

Note that, in (2.2), all power variables are either injected or demanded from bus k. Thus, even though each section below explains the computation of S_b using a specific notation, care must be taken on picking the sign of S_b when adding this variable in (2.2).

2.2 Load

In voltage stability studies, loads are often represented by a constant power model, disregarding its terminal voltage.

The main reason for this is the fact that, in voltage stability studies, the constant power model leads to conservative results regarding loadability limits: voltage instability is intrinsically related to an inability of the transmission system to supply the system load, hence constant power models are conservative in the sense that they indicate that the system is closer to instability than it actually is.

If voltage-dependent load models were employed (e.g., constant impedance or constant current load models), the voltage drop caused by the increase in the system loading would be balanced by a decrease in how much power is demanded by such loading, diminishing the stress of the system.

The aforementioned comments and the constant power steady state characteristic of many dynamic loads justify the use of loads represented mainly by constant power terms. However, sometimes it is desirable to include the effect of voltage-dependent loads in the power system model. Consider the following ZIP load model (IEEE Task Force on Load Representation for Dynamic Performance, 1993) connected to bus k:

$$S_k = P + I \times V_k + Z \times V_k^2 \,, \tag{2.3}$$

where S_k is the power demanded from bus k. The coefficients Z, I and P are generically complex and are chosen to satisfy a specific distribution (e.g., when the voltage is given by $V_k = V_{\text{ref}}$, the load power is composed of 10% of constant impedance-like loads, 20% of constant current-like loads and 70% of constant power-like loads). In this work, loads will be modelled as constant power (i.e., the coefficients I and Z will be set to zero), unless stated otherwise.

2.2.1 Voltage Limits

Loads generally have pre-specified lower and upper voltage limits. These limits must be satisfied to guarantee the proper operation of the load.

When a certain load connected to bus k, the following inequality constraint should be satisfied:

$$V_{\min} \leq V_k \leq V_{\max} \,, \tag{2.4}$$

where V_k is the magnitude of the voltage at bus k. Once these limits are violated, one of the following countermeasures must be taken:

- The load voltage must be controlled inside its interval of safe operation. Several devices can be used in this control, such as switched capacitors or load tap changers. This control can be either automatic or manual.
- The load can be shed to avoid damages. Again, this action can be either automatic (via protection systems) or manual.

2.3 Generation

In contrast to load buses, generation buses are generally modelled as "PV" buses, meaning that generators are able to regulate their terminal voltages by means of a variable reactive power output. The active power, on the other hand, is directly determined by its prime mover. When generator losses are neglected, its (electric) output power is equal to its (mechanical) input power:

$$P = P_g \,. \tag{2.5}$$

On static analyses of power systems, one usually defines a *slack bus*, which is responsible for counterbalancing the active power mismatch in the system, zeroing out the difference between the generated power and the power demanded by the loads and the losses. This is somewhat similar to saying that one of the generators (the slack generator) has a *speed-droop* much closer to zero than the other generators, which indicates that frequency variations are compensated basically by the slack generator.

Generators also regulate the terminal voltage by means of its field current using an automatic voltage regulator (AVR). With the aid of power system stabilizers (PSSs), AVRs usually provide a negligible steady-state error. Thus, it is generally acceptable to assume that the voltage can be perfect controlled at the specified value:

$$V = V_{\text{ref}} \,, \tag{2.6}$$

where V_{ref} is the voltage reference defined in the AVR.

Even though the controlled voltage usually is the generator terminal voltage, it can generically be any voltage in the power system. The same way as for loads, the terminal voltage of a generator must also obey lower and upper bounds.

2.3.1 Active Power Limits

To maintain a proper behavior of the machine, the active power on generators must obey pre-defined lower and upper bounds:

$$P_{\text{min}} \leq P_G \leq P_{\text{max}} \,. \tag{2.7}$$

When computing the solution of the power flow equations, these inequality constraints must be monitored for all generation units whose active power is variable. When

slack generators are defined, only the active power of these generators are variable and must be monitored.

On the other hand, voltage stability studies typically vary the system loading, which often include varying the active power of generators. In these cases, special attention should be paid to clamp these active power values between its respective lower and upper bounds.

For example, suppose the active load at a given bus i is increased. To meet this load increase, the active power of a generator j is also increased (where this generator is not a *slack* generator). By assuming that the increase in $P_{G,j}$ is linear in relation to the increase in $P_{L,i}$, Figure 9 is drawn.

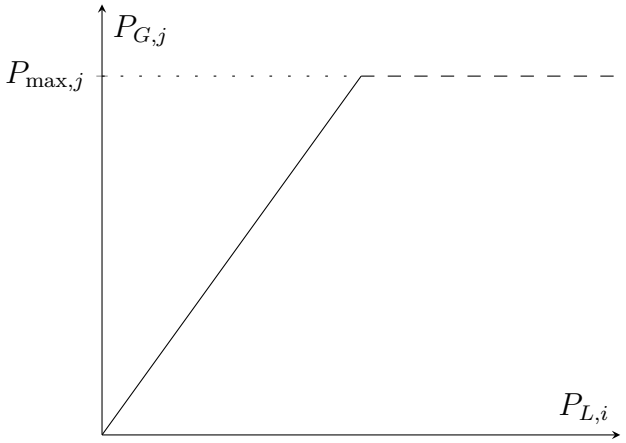

Figure 9 – Active power limits in the parameter space.

Initially, the power system operates at the origin of Figure 9. The increase in $P_{L.i}$ is compensated by the increase in $P_{G,j}$, as indicated by the solid line. When $P_{G,j}$ reaches $P_{\max,j}$, the active power of generator j is clamped at this maximum value, in order to avoid damages. In the parameter space, this clamping corresponds to the change from the solid line to the dashed line.

2.3.2 Reactive Power Limits

Generators control the terminal voltage at one of the system buses by means of actuation on the field current using an AVR. The field current must also be limited between lower and upper bounds. These limits directly determine the AVR behavior by means of underexcitation and overexcitation limiters. In the PQ plane, these limits are presented as capability curves[1]. From capability curves, one can define functions $Q_{\min}(P,V)$ and $Q_{\max}(P,V)$ to represent lower and upper bounds for the reactive power:

$$Q_{\min}(P,V) \leq Q \leq Q_{\max}(P,V)\,. \tag{2.8}$$

[1] Capability curves are defined not only by field current limits but also by other limits such as armature current limits, underexcitation limits and end region heating limits (KUNDUR, 1994).

When underexcitation or overexcitation limiters are not active, the reactive power output of the machine is adjusted to control the voltage magnitude at a given bus (typically the generator terminal). On the other hand, when either $Q_{\min}$ or $Q_{\max}$ is reached, the machine loses the ability to control the voltage, which in turn starts to increase or decrease, depending on which limit was reached:

$$\begin{cases} Q = Q_{\min}(P, V) & \text{if } V_c > V_{\text{ref}}\,, \\ Q_{\min}(P, V) \leq Q \leq Q_{\max}(P, V) & \text{if } V_c = V_{\text{ref}}\,, \\ Q = Q_{\max}(P, V) & \text{if } V_c < V_{\text{ref}}\,, \end{cases} \tag{2.9}$$

where V_c is the voltage magnitude at the controlled bus, V is the voltage magnitude at the machine terminal, and $P + jQ$ is the complex power generated in the machine. Note that the controlled bus is often the machine terminal, in which case $V = V_c$.

2.4 Transmission Line

The steady-state, single-phase model of transmission lines is generally derived from the single-phase differential model shown in Figure 10, where:

- l is the length of the line
- x is a spatial coordinate and varies from 0 to l;
- $z = r + jx$ is the series impedance per unit length;
- $y = g + jc$ is the shunt admittance per unit length;
- $E(x)$ is the complex voltage as a function of x;
- $I(x)$ is the complex current as a function of x.

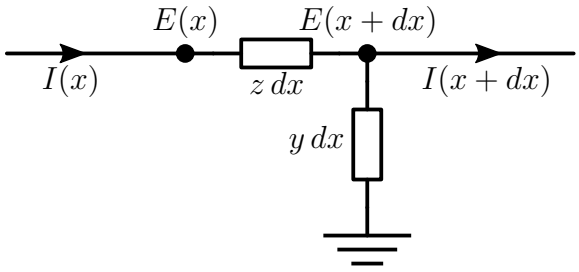

Figure 10 – Single-phase differential model of a transmission line (KUNDUR, 1994).

The differential equations associated with Figure 10 result in a wave equation, whose solution is given by:

$$I(0) = \frac{\coth(\gamma l)}{Z_c} E(0) - \frac{\operatorname{csch}(\gamma l)}{Z_c} E(l)\,, \tag{2.10a}$$

$$I(l) = \frac{\operatorname{csch}(\gamma l)}{Z_c} E(0) - \frac{\coth(\gamma l)}{Z_c} E(l)\,, \tag{2.10b}$$

where $\gamma \equiv \sqrt{yz}$ and $Z_c \equiv \gamma / y$. $E(0)$, $E(l)$, $I(0)$ and $I(l)$ are the voltages and currents at the line terminals, using the same notation as Figure 10.

By rearranging the coefficients in (2.10), it is possible to show that these equations actually represent a π-circuit. The coefficients of this circuit will be clarified in Section 2.5.

2.4.1 Thermal Limit of Transmission Lines

The increase of the current flowing through the line increases the losses by Joule effect, which increases the line temperature. As a consequence, the line expands and the clearance to ground decreases. The clearance to ground must be higher than a pre-defined value, thus there is a maximum current allowed to a given transmission line, which defines the ampacity of the line.

The thermal constant of a transmission line is generally high (on the order of 10 to 20 minutes (KUNDUR, 1994)). Hence, it is common to define a thermal limit for transmission lines in continuous operation and a short-term thermal limit (in emergency situations, for example).

Besides representing the line thermal limit as a current limit, it is common to define the thermal limit by means of other measures, e.g., apparent power:

$$S \leq S_{\max} \,. \tag{2.11}$$

2.5 Transformer

Transformers are generally modelled as shown in Figure 11. From this figure, the following equations are derived:

$$I_1 = |t|^2 (y_{\text{se}} + y_{\text{sh}}) E_1 - \bar{t} y_{\text{se}} E_2 \tag{2.12a}$$

$$I_2 = -t y_{\text{se}} E_1 + (y_{\text{se}} + y_{\text{sh}}) E_2 \tag{2.12b}$$

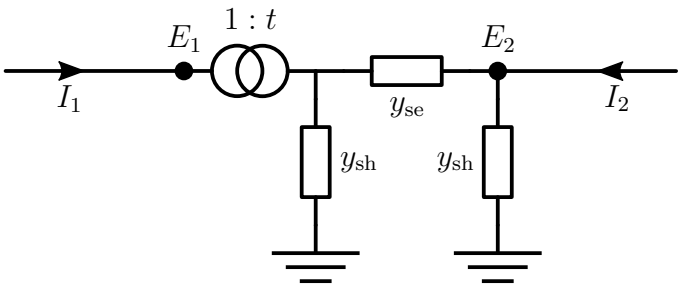

Figure 11 – Single-phase representation of a fixed-tap transformer.

Note that the transmission line model of equation (2.10) actually is one instance of this model, in which $t = 1$, $y_{\text{se}} = \frac{\operatorname{csch}(\gamma l)}{Z_c}$ and $y_{\text{sh}} = \frac{1}{Z_c} \tanh\left(\frac{\gamma l}{2}\right)$.

The same way as for transmission lines, transformers also have thermal limits that must be satisfied. These limits are often in the form of MVA ratings.

2.5.1 Load Tap Changer

Load Tap Changers (LTCs) are transformers whose tap ratio can be adjusted without de-energization. The tap-changing can be either automatic or manual. Automatic LTCs are discrete devices that aim for controlling the voltage of a remote bus (typically one the transformer terminals) within a pre-specified deadband. The instant at which the controlled voltage leaves this admissible range starts a timer which defines when the tap-changing will be performed, in case the voltage remains out of limits. Time delays for the consecutive tap changes are generically given by a composition of an inverse time characteristic and a constant term (CUTSEM; VOURNAS, 1998).

In static analyses, the sequence of tap changes cannot be captured, thus the aforementioned discrete behavior is not well defined. One alternative is to approximate the discontinuous tap variations by a continuous characteristic. If the deadband is neglected and a controller with zero steady-state error is assumed:

$$\begin{cases} \tau = \tau_1, & \text{if } V < V_{\text{spec}}, \\ \min\{\tau_1, \tau_2\} \leq \tau \leq \max\{\tau_1, \tau_2\}, & \text{if } V = V_{\text{spec}}, \\ \tau = \tau_2, & \text{if } V > V_{\text{spec}}, \end{cases} \tag{2.13}$$

where τ is the tap position, given by $\tau = |t|$ in Figure 11. If an increase in τ attempts to increase the voltage V, then $\tau_1 = \tau_{\max}$ and $\tau_2 = \tau_{\min}$.

2.5.2 Phase Shifting Transformer

In Phase Shifting Transformers (PSTs), the transformer phase angle is adjusted to control the power flow through the transformer. Similarly to LTCs, PSTs also are discrete devices whose changes in phase shift are discontinuous. PSTs can also be approximated by a continuous characteristic in static analyses:

$$\begin{cases} \phi = \phi_{\max}, & \text{if } P < P_{\text{spec}}, \\ \phi_{\min} \leq \phi \leq \phi_{\max}, & \text{if } P = P_{\text{spec}}, \\ \phi = \phi_{\min}, & \text{if } P > P_{\text{spec}}, \end{cases} \tag{2.14}$$

where P is the active power flow from left to right in Figure 11, and $\phi = \sphericalangle(t)$ is the phase angle of the transformer. In (2.14), the PST deadband was neglected.

The value of P is calculated from the active power injected at one of the terminals (say P_{from}) and the active power demanded at the other terminal (say P_{to}). One way to define P is the mean of P_{from} and P_{to}:

$$P = \frac{P_{\text{from}} + P_{\text{to}}}{2}\,. \tag{2.15}$$

2.6 HVDC Links

An HVDC Link basically consists of two converters and one DC line. One of the converters act as a rectifier and the other act as an inverter. The AC power system is connected to the converters through transformers, which usually are LTCs. Figure 12 shows the representation of a HVDC link. Smoothing reactors are low-pass current filters that maintain the DC current almost constant. This work assumes that these filters are ideal, thus the ripple current in I_{DC} is negligible.

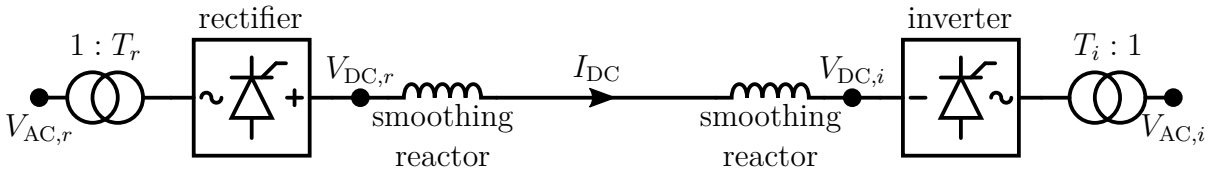

Figure 12 – Representation of a HVDC Link.

Equations for the rectifier side of the Line-Commutated Converter HVDC are:

$$V_r = \frac{3}{\pi} \times \sqrt{2} T_r V_{\mathrm{AC},r} \,, \tag{2.16a}$$

$$V_{\mathrm{DC},r} = V_r \cos\alpha - R_r I_{\mathrm{DC}} \,, \tag{2.16b}$$

$$P_r = V_{\mathrm{DC},r} I_{\mathrm{DC}} \,, \tag{2.16c}$$

$$S_r = V_r I_{\mathrm{DC}} \,, \tag{2.16d}$$

where α is the firing angle of the rectifier. P_r and S_r are the active and apparent power injected by the AC side to the DC Line. Note that losses both in the transformer and in the converter are neglected.

Resistance R_r is a "commutating resistance", which is a fictitious resistance that accounts for the nonzero commutation time of AC side due to the leakage reactance of the transformer (TAYLOR, 1994). This resistance does not consume power.

The factor $\sqrt{2}$ is due to the conversion of the line-to-line RMS voltage $V_{\mathrm{AC},r}$ to peak, while the first factor is due to the three-phase six-pulse converter (KUNDUR, 1994):

$$\frac{3}{\pi} = \frac{6}{2\pi} \int_{-\pi/6}^{\pi/6} \cos t \, dt \,. \tag{2.17}$$

Equations for the inverter side are similar:

$$V_i = \frac{3}{\pi} \times \sqrt{2} T_i V_{\mathrm{AC},i} \,, \tag{2.18a}$$

$$V_{\mathrm{DC},i} = V_i \cos\gamma - R_i I_{\mathrm{DC}} \,, \tag{2.18b}$$

$$P_i = V_{\mathrm{DC},i} I_{\mathrm{DC}} \,, \tag{2.18c}$$

$$S_i = V_i I_{\mathrm{DC}} \,, \tag{2.18d}$$

where γ is the extinction angle. The computation of I_{DC} is given by:

$$I_{\mathrm{DC}} = \max\left\{0, \frac{V_{\mathrm{DC},r} - V_{\mathrm{DC},i}}{R_L}\right\}, \tag{2.19}$$

where R_L is the DC line resistance. I_{DC} is always non-negative, which ensures that the current always flows from the rectifier side to the inverter side.

Even though I_{DC} is positive, it is possible to transfer active power from the inverter side to the rectifier side by making $\cos\alpha$ and $\cos\gamma$ negative. In this case, $V_{\mathrm{DC},r}$ and $V_{\mathrm{DC},i}$ are negative and the power flow is reversed. It is important to note that reactive power is consumed at both ends of the HVDC link, even though one of the HVDC link terminals deliver active power to the AC system. Therefore, the reactive power computed by

$$Q_r = \sqrt{S_r^2 - P_r^2} \tag{2.20}$$

and

$$Q_i = \sqrt{S_i^2 - P_i^2} \tag{2.21}$$

always flow to the HVDC link. Capacitor banks and synchronous condensers are often employed to supply this demand of reactive power.

2.6.1 Control of a HVDC Link

There are four actuation variables for the HVDC link, namely T_r, α, T_i and γ. Bounds are imposed to all these variables, and generally the control strategy changes when some of these variables reach their limits. In most control strategies, one regulates either voltage terminals, DC current or DC power.

In steady-state studies, converter angles α and γ are usually fixed. In this work, assume that T_r and T_i are both used to control I_{DC}. However, to avoid undesirable oscillations due to the interaction between the rectifier and inverter controls, the setpoint value for both controls are different.

An increase of T_r increases V_r, which in turn increases I_{DC}. Therefore, the rectifier control characteristic is written as:

$$\begin{cases} T_r = T_{r,\max}, & \text{if } I_{\mathrm{DC}} < I_{\mathrm{spec},r}, \\ T_{r,\min} \leq T_r \leq T_{r,\max}, & \text{if } I_{\mathrm{DC}} = I_{\mathrm{spec},r}, \\ T_r = T_{r,\min}, & \text{if } I_{\mathrm{DC}} > I_{\mathrm{spec},r}. \end{cases} \tag{2.22}$$

An increase of T_i increases V_i, which in turn decreases I_{DC}. Therefore, the inverter control characteristic is written as:

$$\begin{cases} T_i = T_{i,\min}, & \text{if } I_{\mathrm{DC}} < I_{\mathrm{spec},i}, \\ T_{i,\min} \leq T_i \leq T_{i,\max}, & \text{if } I_{\mathrm{DC}} = I_{\mathrm{spec},i}, \\ T_i = T_{i,\max}, & \text{if } I_{\mathrm{DC}} > I_{\mathrm{spec},i}. \end{cases} \tag{2.23}$$

Equations (2.22) and (2.23) assume a control with no steady-state error. In practical situations, the integral controller may be replaced with a proportional controller with a high gain.

From equation (2.16b), $V_{\mathrm{DC},r}$ can be computed from the rectifier variables as follows:

$$V_{\mathrm{DC},r} = V_r \cos\alpha - R_r I_{\mathrm{DC}} \,. \tag{2.24}$$

From equations (2.18) and (2.19), $V_{\mathrm{DC},r}$ can be computed from the inverter variables as follows:

$$V_{\mathrm{DC},r} = V_i \cos\gamma + (R_L - R_i)\, I_{\mathrm{DC}} \,. \tag{2.25}$$

Assuming that $I_{\mathrm{spec},r} > I_{\mathrm{spec},i}$, equations (2.24) and (2.25) (where V_r and V_i are calculated using (2.22) and (2.23), respectively) can be sketched in the $V_{\mathrm{DC},r}I_{\mathrm{DC}}$-plane as shown in Figure 13. The intersection between the shown curves determine the operating point. Note that, in the situation shown in Figure 13, T_r controls the current on the DC line, while T_i is held at $T_{i,\max}$. In this situation, $V_{\mathrm{DC},r}$ is positive and the power flows from the rectifier to the inverter.

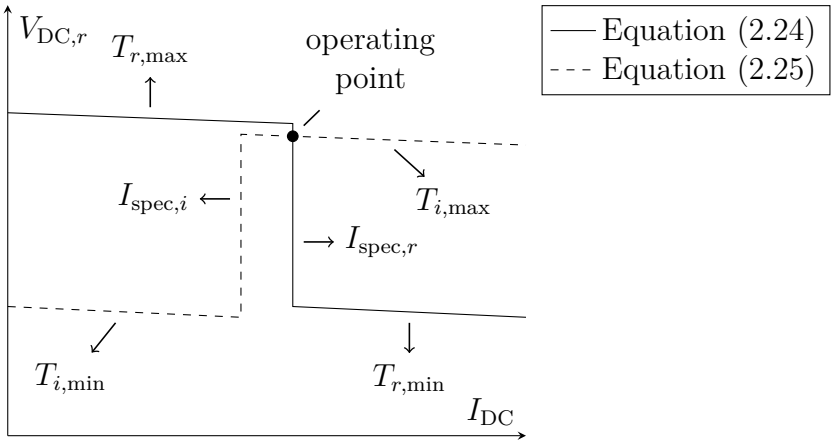

Figure 13 – Control characteristic of a HVDC link.

In order to reverse the power flow direction, voltages V_r and V_i should be reversed. In Figure 14, α and γ are increased such that $\cos\alpha < 0$ and $\cos\gamma < 0$. The operating point in this figure shows that $P_r = V_{\mathrm{DC},r} I_{DC} < 0$, indicating that the power flow has been reversed.

2.7 Reactive Power Compensation

Voltage stability can often be improved by reactive power compensation devices. These devices provide a reactive power reserve to a portion of the power system, which usually alleviates the stress of the transmission lines and increase the power transfer capability. Furthermore, these devices can be used to control the voltage of remote buses of the system.

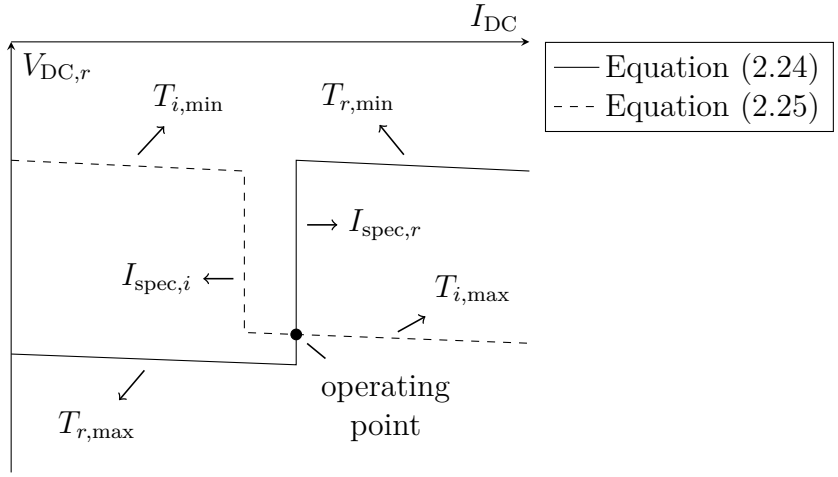

Figure 14 – Control characteristic of a HVDC link — power flow reversed.

The simplest form of reactive power compensation (either series compensation or shunt compensation) are in the form of switched capacitors and reactors. For example, series capacitors reduce the impedance of transmission lines, "reducing the distance" between generation and load centers, which increases the power transfer capability of a particular transmission line. On the other hand, shunt reactors can reduce the voltage of a bus, when this voltage is undesirably high.

Besides switched capacitors and reactors, fine voltage control can be attained with Flexible Alternating Current Transmission System (FACTS) devices. In the remainder of this section, static Var compensators and static synchronous compensators will be briefly described.

2.7.1 Static Var Compensator

Static Var Compensators (SVCs) are devices which provide voltage control for a remote bus by means of thyristor controlled reactors and capacitors. With the aim of controlling the voltage V_i at bus i, the following susceptance is connected at bus j (CUTSEM; VOURNAS, 1998):

$$b = \min\{\max\{b_{\min}, K(V_{\mathrm{ref}} - V_i)\}, b_{\max}\}\,, \tag{2.26}$$

where V_{ref} is the voltage setpoint and K is the proportional gain. The minimum and maximum values of susceptance are given by $b_{\min}$ and $b_{\max}$, respectively.

If an integral controller is used as opposed to a proportional controller, a zero steady state error is assumed and equation (2.26) is replaced by the following:

$$\begin{cases} b = b_{\max}, & \text{if } V_i < V_{\mathrm{ref}}, \\ b_{\min} \leq b \leq b_{\max}, & \text{if } V_i = V_{\mathrm{ref}}, \\ b = b_{\min}, & \text{if } V_i > V_{\mathrm{ref}}. \end{cases} \tag{2.27}$$

The reactive power injected at bus j (note that i and j may be equal) is given by:

$$Q_j = b \times V_j^2 \,. \tag{2.28}$$

When the SVC is limited, it behaves merely as a fixed capacitor or reactor. Thus, equation (2.28) shows that the reactive power capability of a SVC decays quadratically with the voltage at bus j. This is unfavorable considering that buses i and j are usually near each other, such that V_i and V_j are close. At the same time that V_i decreases and more reactive power is desirable, the decrease in V_j reduces the reactive power reserve.

To circumvent this problem, better reactive power support is provided by static synchronous compensators, explained next.

2.7.2 Static Synchronous Compensator

Static Synchronous Compensator (STATCOM) devices inject reactive power into the power system using a capacitor connected to the system by means of a voltage-source converter. The amount of reactive power delivered to the system is a function of the capacitor voltage, which in turn is controlled by the firing angle of the converter.

In contrast with SVCs, STATCOMs behave as a constant reactive current at their limits. Hence, its reactive current can be modelled as follows:

$$I = \min\{\max\{I_{\min}, K(V_{\text{ref}} - V_i)\}, I_{\max}\} \,, \tag{2.29}$$

where I is the current injected at bus j and i is the controlled bus.

If an integral controller is used as opposed to a proportional controller, the steady state error is zero, and the STATCOM can be modelled as:

$$\begin{cases} I = I_{\max}, & \text{if } V_i < V_{\text{ref}}, \\ I_{\min} \leq I \leq I_{\max}, & \text{if } V_i = V_{\text{ref}}, \\ I = I_{\min}, & \text{if } V_i > V_{\text{ref}}. \end{cases} \tag{2.30}$$

The reactive power injected at bus j is given by:

$$Q_j = I \times V_j \,. \tag{2.31}$$

2.8 Active Power Interchange Control

Interconnected power systems can be divided into different areas with different generation and load patterns. The power flow between different areas is often controlled.

Suppose that the active power exported by area k should be controlled at a pre-specified value. In a static analysis, this control action represents one extra equality

constraint to the power flow model. To match the number of equations and variables, a previously fixed variable in the power flow model must be released. Since the exported active power ought to be controlled, it is reasonable to free the active power of one of the generators in area k. In this way, the active power of this generator will be adjusted so that the scheduled area interchange is meet.

Another possibility is to assign participation factors to all generators in area k. In this way, the active power of all generators would be varied to meet the desired power exportation. In this case, a new variable λ is added to the power flow model, and the active power supplied by each (non-slack) generator i in area k is given by:

$$P_i = P_{0,i} + F_i\lambda\,, \tag{2.32}$$

where $P_{0,i}$ is the original active power provided by generation i and F_i is its respective participation factor.

2.9 Ensuring Voltage Limits are Satisfied

Some equipment can be designed to only operate when voltage limits are reached. For example, when the voltage reaches a minimum admissible value, a SVC may be connected to the system. Other examples include mechanical devices, such as switchable capacitor banks, which might start to operate only when voltage limits are violated. If the reactive power injection Q_j at bus j is used to control the voltage V_i at bus i, then:

$$\begin{cases} V_i = V_{\min} & \text{if } Q_j > Q_{\text{ref}}\,, \\ V_{\min} \leq V_i \leq V_{\max} & \text{if } Q_j = Q_{\text{ref}}\,, \\ V_i = V_{\max} & \text{if } Q_j < Q_{\text{ref}}\,, \end{cases} \tag{2.33}$$

where i and j are generally equal.

Even though reactive power support devices that operate like (2.33) are atypical, the inclusion of such equations into computational frameworks can be advantageous not only to voltage stability studies but also to other power system planning and security analyses. By ensuring that voltage limits are satisfied, it is possible to detect regions of the power system with shortage or excess of reactive power.

In the literature, there is not a specific name for a device whose behavior is given by equation (2.33). A bus whose characteristic is (2.33) is usually referred to as a "PQ" bus with voltage limits (PIERCE JR et al., 1973). Throughout this document, each device that generates reactive power according to equation (2.33) will be denoted by *Voltage Limit Imposition Device* (VLID).

2.10 Complete Power System Model

This chapter presented the modelling of different devices that compose a static power system model. Let the power system be composed of:

- n_{bus} buses;
- n_{area} areas with controlled exportation;
- n_{slack} slack generators;
- n_{gen} non-slack generators;
- n_{branch} transmission lines and fixed tap transformers;
- n_{LTC} LTCs;
- n_{PST} PSTs;
- n_{DC} HVDC links;
- n_{SVC} SVCs;
- n_{STATCOM} STATCOMs;
- n_{VLID} VLIDs (defined in Section 2.9).

The variables for the power flow model are:

- $n_{\text{bus}} - 1$ variables of voltage angle (assuming that there is only one reference bus);
- n_{bus} variables of voltage magnitude;
- n_{slack} variables of active power in slack generators;
- n_{slack} variables of reactive power in slack generators;
- n_{gen} variables of reactive power in non-slack generators;
- n_{LTC} variables of tap position in LTCs;
- n_{PST} variables of phase shift in PSTs;
- n_{PST} variables of active power in PSTs;
- n_{DC} variables of DC current in HVDC links;
- n_{DC} variables of firing angle in HVDC links;
- n_{DC} variables of extinction angle in HVDC links;
- n_{SVC} variables of susceptance in SVCs;
- n_{STATCOM} variables of reactive current in STATCOMs;
- n_{VLID} variables of reactive power injected by VLIDs.

The equations for the power flow model are:

- $2n_{\text{bus}}$ real equations from nodal analysis (real and imaginary parts of (2.2));
- n_{area} equations of power interchange control;
- n_{slack} instances of equation (2.9) for slack generators;
- n_{gen} instances of equation (2.9) for non-slack generators;
- n_{LTC} instances of equation (2.13);
- n_{PST} instances of equation (2.14);
- n_{PST} instances of equation (2.15);

- n_{DC} instances of equation (2.19);
- n_{DC} instances of equation (2.22);
- n_{DC} instances of equation (2.23);
- n_{SVC} instances of either equation (2.26) or (2.27);
- n_{STATCOM} instances of either equation (2.29) or (2.30);
- n_{VLID} instances of equation (2.33).

Hereinafter, the set of all variables in the power system model will be denoted by $\mathbf{x}$, while the set of equations of the power flow model will be grouped into a function $\mathbf{f}$. Therefore, the aforementioned power system equations are written simply as:

$$\mathbf{f}(\mathbf{x}) = \mathbf{0}\,. \tag{2.34}$$

This power flow model also includes inequality constraints, e.g., inequations (2.4), (2.7) and (2.11). All these inequality constraints will be grouped into a function $\mathbf{g}$:

$$\mathbf{g}(\mathbf{x}) \geq \mathbf{0}\,. \tag{2.35}$$

In order to have the number of variables equal to the number of equations, it is necessary that $n_{\mathrm{slack}} = n_{\mathrm{area}} + 1$. Note that one slack generator is responsible for compensating the active power mismatch due to losses in the transmission system, as explained in Section 2.3. The other n_{area} slack generators belong to each one of the n_{area} areas with interchange control, as explained in Section 2.8.

Many equations in the power flow model represent the control characteristic of a device. Invariably, this control characteristic can be divided into the following conditions:

- The control variable is not saturated: in this situation, the control variable can be adjusted so that the controllable variable is maintained at the desired value.
- The control variable is saturated: in this situation, the control variable has reached its limit and should be fixed to avoid damages to the equipment. As a consequence, the controllable variable no longer can be maintained at the desired value.

The most common example of such control in power flow analysis is voltage control by the actuation of the reactive power of a generator. The control characteristic is given by equation (2.9), the control variable is Q and the controllable variable is V. When the control variable is not saturated, then $Q_{\min} < Q < Q_{\max}$ and equation (2.9) indicates that the voltage can be controlled at the setpoint value. On the other hand, when the control variable is saturated, the voltage is allowed to increase or decrease, depending on whether $Q_{\min}$ or $Q_{\max}$ has been reached.

Suppose a solution of the power flow equations has been computed. For this solution, each control variable in the system can be classified as either saturated or non-saturated. While the parameters of the system change (for example, new loads are connected to

the system), the solution point also changes. Eventually, one of the control variables will change from saturated mode to non-saturated mode or vice versa. When this happens, we say that the **structure** of the system changes, since the mode of operation of one device in the system changes.

In order to compute a solution point of (2.34), the literature traditionally approaches the resolution of the power flow equations in the following way:

Step 1 Make an estimate of the current *structure* of the power system based on the current estimate of the solution point;

Step 2 Using an iterative method (e.g., the Newton's method or Fast-Decoupled method), update vector $\mathbf{x}$ with a new estimate of the power flow solution for the system under the current estimated *structure*.

Step 3 For the computed solution point, check if the estimated *structure* is correct. If not, update the system *structure* and return to the previous step.

There are several variations of this procedure in the literature. In Step 2, for example, it is common to execute only one iteration of the Newton (or Fast-Decoupled) method, in order to not expend much time solving the power flow equations for a possibly incorrect *structure*. On the other hand, it is also possible to execute the entire power flow computation, solving one system of nonlinear equations in each execution of Step 2. In relation to Step 3, one could update one misclassified device at a time, or several devices could be updated simultaneously as an attempt to reduce the number of iterations of Steps 2 and 3.

In Chapter 4, a new power flow model is proposed. With the new model, it is not necessary to iteratively update the power system *structure*. In this way, one does not need to resort to the iterative procedure described above, and the proposed power system model can be seamlessly solved by any numerical solver.

Lastly, equations (2.34) and (2.35) can be joined to compose the complete static power system model:

$$\mathbf{f}(\mathbf{x}, \mathbf{p}, \mathbf{u}) = \mathbf{0}\,, \tag{2.36a}$$

$$\mathbf{g}(\mathbf{x}, \mathbf{p}, \mathbf{u}) \geq \mathbf{0}\,. \tag{2.36b}$$

In comparison to equations (2.34) and (2.35), functions $\mathbf{f}$ and $\mathbf{g}$ in (2.36) explicitly take vectors $\mathbf{p}$ and $\mathbf{u}$ as arguments. These vectors include any variables in the power flow model other than the variables in vector $\mathbf{x}$. Vector $\mathbf{p}$ represents uncontrollable parameters, such as the coefficients Z, I and P in the load model (equation (2.3)). On the other hand, vector $\mathbf{u}$ represents controllable parameters, such as the voltage setpoint and active power output of a generator.

The following chapters will be developed based on the power system model (2.36).

Vector **p** will be used to compute voltage stability indicators (e.g., the voltage stability margin), while vector **u** represents the set of control actions available to improve voltage stability.

3 LITERATURE REVIEW ON MODEL-BASED STATIC VSA

The previous chapter provided a mathematical model to represent the steady-state behavior of a power system. With this model, the power system equilibrium equations are written by equation (2.36a), while power system operational limits are represented by equation (2.36b). By using this mathematical model, we are able to simulate and analyze power systems in steady-state condition. This chapter presents the foundations of voltage stability, as well as it describes some traditional methods for voltage stability analyses. These analyses are usually performed on equation (2.36) to judge if the power system is prone to a voltage collapse.

This chapter presents a review of some existing well accepted approaches of the literature on static voltage stability analysis. These studies are the foundations of the methodology proposed in this document. The focus of the studies described here is model-based VSA, as opposed to measurement-based VSA. The latter does not make assumptions about the power system layout, and only measurements are generally used to infer about voltage stability. The former, on the other hand, makes use of the system model to provide results about the system. These results often are much more accurate than the results computed by measurement-based methodologies, provided that the employed system model is correct.

Section 3.1 briefly presents the foundations of voltage stability analysis and the goal of voltage stability assessment. Section 3.2 describes the bifurcation surface and how this surface is composed of different bifurcation types. Section 3.3 explains how continuation methods can be used to compute the voltage stability margin. Section 3.5 presents a simple method to calculate the minimum voltage stability margin in the parameter space. Section 3.6 describes how the current literature deals with parameter uncertainties in voltage stability. Section 3.7 presents some studies on selection of preventive and corrective controls in voltage stability. Finally, Section 3.8 presents an overview of other studies in the VSA literature, covering VSA indices other than voltage stability margin, contingency analyses, sensitivity analyses, and modal analyses.

3.1 Voltage Stability and Bifurcations

Static voltage stability analysis is mainly concerned with the study of the power system behavior when its parameters change. Recall that the power flow model is represented by equation (2.36) and assume that vector $\mathbf{u}$ is constant in the analysis (i.e., all controllable variables are left unchanged in the period of study). In this situation, equation (2.36a) is written as:

$$\mathbf{f}(\mathbf{x}, \mathbf{p}) = \mathbf{0}\,. \tag{3.1}$$

Assume that the power system is operating at the current point given by $(\mathbf{x}_1, \mathbf{p}_1)$ (where $\mathbf{f}(\mathbf{x}_1, \mathbf{p}_1) = \mathbf{0}$). In normal operation, the solution $\mathbf{x}_1$ represents a stable equilibrium point of the power system for the current value of $\mathbf{p} = \mathbf{p}_1$.

As time changes, vector $\mathbf{p}$ also changes (the variables in this vector are uncontrollable and hence cannot be intentionally held constant), say from $\mathbf{p}_1$ to $\mathbf{p}_2$. For this new value of $\mathbf{p}$, the previous solution point $\mathbf{x}_1$ does not satisfy (3.1) anymore (i.e., $\mathbf{f}(\mathbf{x}_1, \mathbf{p}_2) \neq \mathbf{0}$). In this situation, the power system behavior invariably follows one of two possibilities:

- Variable $\mathbf{x}$ dynamically changes in the direction of a new solution $\mathbf{x}_2$ (where $\mathbf{f}(\mathbf{x}_2, \mathbf{p}_2) = \mathbf{0}$);
- Variable $\mathbf{x}$ is not able to reach a solution of (3.1) starting from $\mathbf{x}_1$.

By using only the static power flow model given by (3.1), it is not possible to infer which of these possibilities will occur. In fact, to predict either the system will be able to reach the equilibrium point $\mathbf{x}_2$ or not, it is necessary to analyze the underlying dynamical system in which equation (3.1) is based. In this case, the system is mathematically represented by a set of differential-algebraic equations, and the stability analysis of these equations can judge whether the system will converge to the new equilibrium $\mathbf{x}_2$ or not. Generically, the system will converge to $\mathbf{x}_2$ if and only if:

- the equilibrium $\mathbf{x}_2$ is stable, and
- the initial point $\mathbf{x}_1$ is inside the stability region of equilibrium $\mathbf{x}_2$.

The computational cost of checking whether an equilibrium point is stable or not is basically the cost of computing eigenvalues[1]. On the other hand, computing the stability region of $\mathbf{x}_2$ is very costly, and it is often unfeasible even for small power systems.

In general, dynamic tools to assess voltage stability are too costly to be applied to real time voltage stability studies during the operation of power systems. These tools are usually applied to small portions of the system in offline analyses, while the use of static tools on online voltage stability assessment of large-scale power systems is still widespread nowadays.

In static voltage stability assessment (static VSA), only the static power flow model (2.36) is used to infer the system behavior (VENIKOV et al., 1975; ABE et al., 1978; TAMURA; MORI; IWAMOTO, 1983; KWATNY; PASRIJA; BAHAR, 1986; SAUER; PAI, 1990; FLATABO; OGNEDAL; CARLSEN, 1990; SCHLUETER et al., 1991; CUTSEM, 1991; MORISON; GAO; KUNDUR, 1993; CANIZARES, 1995). Since this model cannot provide all the information necessary to judge if the system will reach the equilibrium point $\mathbf{x}_2$ (the static model can only predict the existence or not of $\mathbf{x}_2$), some assumptions are needed:

[1] considering that the hypotheses of the Hartman-Grobman theorem (HALE; KOCAK, 1991) are satisfied

[I] parameter variations are assumed to be sufficiently slow (in comparison to the power system dynamics), implying that $\mathbf{p}_2$ is sufficiently close to $\mathbf{p}_1$ if the interval of time for $\mathbf{p}$ to change from $\mathbf{p}_1$ to $\mathbf{p}_2$ is small;

[II] if there is a solution $\mathbf{x}_2$ (such that $\mathbf{f}(\mathbf{x}_2, \mathbf{p}_2) = \mathbf{0}$) close to the original point $\mathbf{x}_1$, then this solution is assumed stable. Moreover, it is assumed that $\mathbf{x}$ will converge to $\mathbf{x}_2$.

These assumptions are reasonable in most situations. It is unusual for the system parameters to change abruptly in normal operation[2]. Moreover, the existence of a new equilibrium $\mathbf{x}_2$ sufficiently close to the previous equilibrium $\mathbf{x}_1$ generally means the existence of an equilibrium branch from $\mathbf{x}_1$ to $\mathbf{x}_2$ when vector $\mathbf{p}$ changes from $\mathbf{p}_1$ to $\mathbf{p}_2$. Unless the stability properties of the equilibrium branch change in the halfway between $\mathbf{x}_1$ and $\mathbf{x}_2$, $\mathbf{x}_2$ will also be stable.

If the system dynamics are much faster than the variation of $\mathbf{p}$, the state variable $\mathbf{x}$ basically moves along the equilibrium branch (as shown in Figure 4 of Section 1.1), as long as this equilibrium branch remains stable. Therefore, since the system is assumed to be operating at the (stable) equilibrium point, there is no need to verify if the current operating point is inside the stability region.

In face of assumptions [I] and [II], the goal of static voltage stability assessment is:

- to check whether the solution $\mathbf{x}$ of (2.36) will disappear with the variation $\mathbf{p}$;
- to compute the values of $\mathbf{p}$ at which this solution point vanishes;
- to determine corrective and preventive actions to avoid the loss of this solution point.

The usual consequence of the loss of a solution point usually is an abrupt variation of the state vector $\mathbf{x}$, as a consequence of the system dynamics. In power systems context, this abrupt variation is noticeable in load buses, whose voltage suddenly and quickly decreases, possibly leading to blackouts. This phenomenon is referred to as voltage collapse and was sketched in Figure 5.

If a solution $\mathbf{x}_2$ that satisfies both (2.36a) and (2.36b) does not exist, this means that the power system lost its solution point for $\mathbf{p}$ between $\mathbf{p}_1$ and $\mathbf{p}_2$. The exact value of $\mathbf{p}$ at which the solution $\mathbf{x}$ disappears is named **bifurcation point** (BP). Basically, a bifurcation point is a limit point at which the system undergoes a qualitative change. When using the static model (2.36), this qualitative change essentially means either birth or death of solution points.

It should be mentioned that there might be cases where assumptions [I] and [II] are invalid. For example, a load shedding cannot be represented as a slow parameter variation, violating assumption [I]. On the other hand, assumption [II] is violated when a Hopf

[2] Contingency analysis is often employed to study large disturbances in static voltage stability.

bifurcation[3], for example, occurs on the equilibrium branch. Note that these examples are intrinsic limitations of the static model, and these situations cannot be approached without the (computationally more expensive) dynamical model.

3.2 Voltage Stability Margin and Bifurcation Surface

Assume that a bifurcation occurs while $\mathbf{p}$ changes from $\mathbf{p} = \mathbf{p}_1$ to $\mathbf{p} = \mathbf{p}_2$. In other words, there is $\mathbf{x}_1$ that satisfies (2.36) for $\mathbf{p} = \mathbf{p}_1$, while there is not $\mathbf{x}_2$ that satisfies (2.36) for $\mathbf{p} = \mathbf{p}_2$, or vice versa. Assume that this bifurcation occurs precisely at $\mathbf{p} = \widehat{\mathbf{p}}$. This situation is sketched in Figure 15. In this figure, the solid line indicates the existence of $\mathbf{x}$ satisfying (2.36), while there is no solution $\mathbf{x}$ for the dashed line.

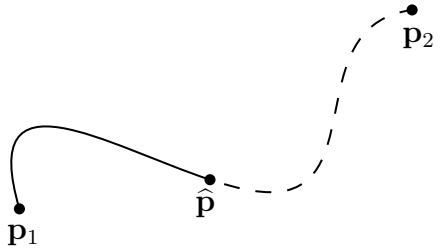

Figure 15 – Bifurcation in the parameter space.

Hereinafter, each path that describes the variation of $\mathbf{p}$ over time (as the one shown in Figure 15) will be named **parameter variation scenario** or simply **scenario**. Hence, a *scenario* essentially is a trajectory described by $\mathbf{p}$ as time changes.

Ideally, the power system should operate at a point $\mathbf{p}_1$ that is far from a bifurcation. In other words, the distance between the operating point $\mathbf{p}_1$ and the bifurcation point $\widehat{\mathbf{p}}$ should be larger than a threshold. This distance is defined as the **Voltage Stability Margin** (VSM), which is written mathematically as:

$$\text{VSM} = d(\mathbf{p}_1, \widehat{\mathbf{p}}) \,, \tag{3.2}$$

where d computes the distance between two vectors $\mathbf{p}_1$ and $\widehat{\mathbf{p}}$. Different definitions of function d will be given throughout this document.

The existence or non-existence of a solution $\mathbf{x}$ for a given $\mathbf{p}$ is an attribute of vector $\mathbf{p}$ itself, and not of the path described by this vector. As a consequence, there will always be a bifurcation between $\mathbf{p}_1$ and $\mathbf{p}_2$ in Figure 15, independently of the path that connects these two endpoints. Figure 16 shows two more *scenarios* connecting $\mathbf{p}_1$ and $\mathbf{p}_2$, and their corresponding bifurcation points. Note that there is a specific VSM (computed according to (3.2)) associated with each BP. Therefore, each particular *scenario* is associated with a particular VSM.

[3] In contrast to stationary bifurcations (SEYDEL, 2010), a Hopf bifurcation is a qualitative change where the stability of an equilibrium point changes, as opposed to a change in the number of equilibria.

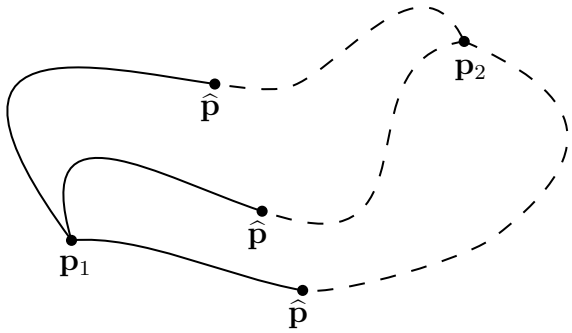

Figure 16 – Bifurcations associated with different paths.

As can be seen, there is a "barrier" of bifurcation points delimiting the region in which $\mathbf{p}$ is allowed to move without losing the solution $\mathbf{x}$. If $\mathbf{p}$ is a m-dimensional vector, then this barrier is a $(m-1)$-dimensional hypersurface, called **bifurcation surface**, which is the set of all bifurcation points in the m-dimensional parameter space. Figure 17 shows the bifurcation surface associated with Figure 16 as a dotted line.

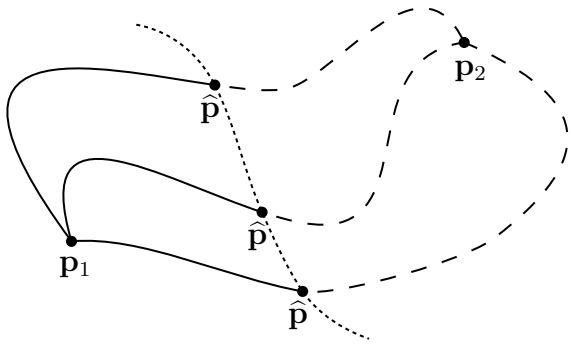

Figure 17 – Sketch of a bifurcation surface.

The set of bifurcation points corresponds to a surface that splits the parameter space into two disjoint sets. For all $\mathbf{p}$ in one of these sets, there is $\mathbf{x}$ satisfying (2.36), while this solution does not exist in the other set. Let these sets be denoted by

$$\mathbb{A} = \{\mathbf{p} \in \mathbb{R}^m | \text{there is } \mathbf{x} \text{ satisfying (2.36)}\} \tag{3.3}$$

and

$$\mathbb{B} = \mathbb{R}^m \backslash \mathbb{A}\,. \tag{3.4}$$

Any bifurcation point $\widehat{\mathbf{p}}$ is adherent to both $\mathbb{A}$ and $\mathbb{B}$, i.e., any bifurcation point is arbitrarily close to both $\mathbb{A}$ and $\mathbb{B}$. The converse is also true: by definition, any vector $\mathbf{p}$ adherent to both $\mathbb{A}$ and $\mathbb{B}$ is a bifurcation point.

3.2.1 Bifurcation Types

The loss of a solution of (2.36) in a bifurcation point $(\widehat{\mathbf{x}}, \widehat{\mathbf{p}})$ (the control vector $\mathbf{u}$ is omitted for simplicity) can be caused by two factors:

- *Equation* (2.36a)*:* The system reaches the limit of function $\mathbf{f}$ itself. Even though inequation (2.36b) allows a variation of vector $\widehat{\mathbf{p}}$ (i.e., all elements of $\mathbf{g}(\widehat{\mathbf{x}}, \widehat{\mathbf{p}})$ are strictly positive[4]), there is a vector $\widetilde{\mathbf{p}}$ arbitrarily close to $\widehat{\mathbf{p}}$ such that equation $\mathbf{f}(\mathbf{x}, \widetilde{\mathbf{p}}) = \mathbf{0}$ does not admit a solution $\widetilde{\mathbf{x}}$ close to $\widehat{\mathbf{x}}$.
- *Inequation* (2.36b)*:* In this case, equation (2.36a) admits solutions $\mathbf{x}$ for any $\mathbf{p}$ in an arbitrarily small neighborhood of $\widehat{\mathbf{p}}$. However, some of these solutions violate one of the inequality constraints in (2.36b). Since $\mathbf{g}$ is continuous, this means that at least one of the elements of $\mathbf{g}(\widehat{\mathbf{x}}, \widehat{\mathbf{p}})$ is zero.

Hence, a bifurcation can be categorized according to the mechanism that originated it. In this work, we denote by Constraint Violation Induced Bifurcation[5] (CVIB) a bifurcation induced by inequation (2.36b), since the disappearance of the solution point occurs specifically due to a constraint violation.

In relation to bifurcations due to equation (2.36a), they can be further divided according to the Implicit Function Theorem (SEYDEL, 2010):

Theorem 1 (Implicit Function Theorem)**.** *Suppose a solution* $(\widetilde{\mathbf{x}}, \widetilde{\mathbf{p}})$ *of*

$$\mathbf{f}(\mathbf{x}, \mathbf{p}) = \mathbf{0} \tag{3.5}$$

is known, and assume that the following conditions are satisfied:

- *Function* $\mathbf{f}$ *is continuously differentiable at* $(\widetilde{\mathbf{x}}, \widetilde{\mathbf{p}})$*;*
- *The Jacobian matrix* $\partial_{\mathbf{x}}\mathbf{f}$ *is nonsingular at* $(\widetilde{\mathbf{x}}, \widetilde{\mathbf{p}})$*.*

Then, there is an unique implicit function $\mathbf{x}(\mathbf{p})$*, also continuously differentiable, defined in a neighborhood* $\mathbb{U}$ *of* $\widetilde{\mathbf{p}}$*, such that:*

- $\mathbf{x}(\widetilde{\mathbf{p}}) = \widetilde{\mathbf{x}}$*;*
- $\mathbf{f}(\mathbf{x}(\mathbf{p}), \mathbf{p}) = \mathbf{0}\ \forall\ \mathbf{p} \in \mathbb{U}$*.*

If the assumptions of the Implicit Function Theorem are satisfied for a solution $(\widetilde{\mathbf{x}}, \widetilde{\mathbf{p}})$ of (2.36a), then there is a solution $\mathbf{x}$ of (2.36a) for all $\mathbf{p}$ in a neighborhood $\mathbb{U}$ of $\widetilde{\mathbf{p}}$. The existence of this neighborhood implies that $\widetilde{\mathbf{p}}$ is not adherent to the set $\mathbb{B}$ (note that $\mathbb{U} \subset \mathbb{A}$). This indicates that $\widetilde{\mathbf{p}}$ is not a bifurcation point caused by (2.36a). Therefore, for every bifurcation point $(\widehat{\mathbf{x}}, \widehat{\mathbf{p}})$ due to (2.36a), one of the following conditions is satisfied:

- $\mathbf{f}$ is not continuously differentiable at $(\widehat{\mathbf{x}}, \widehat{\mathbf{p}})$;
- if $\mathbf{f}$ is C^1 at $(\widehat{\mathbf{x}}, \widehat{\mathbf{p}})$, then the Jacobian matrix $\partial_{\mathbf{x}}\mathbf{f}$ is singular at $(\widehat{\mathbf{x}}, \widehat{\mathbf{p}})$.

These two conditions allow the definition of two bifurcation types due to (2.36a):

[4] Note that function $\mathbf{g}$ is continuous.

[5] Note that there is no standard nomenclature for this type of bifurcation (there is not even a consensus if this constraint violation should be named "bifurcation"). However, this phenomenon will be called bifurcation here, since it agrees with our definition of bifurcation (see page 55).

- When $\mathbf{f}$ is C^1 but $\partial_{\mathbf{x}}\mathbf{f}$ is singular at the bifurcation point, the bifurcation is generically named Saddle-Node Bifurcation (SNB)[6]. This nomenclature agrees with the respective bifurcation of the underlying dynamical system in which system (2.36) is based.
- When $\mathbf{f}$ is not C^1 at the bifurcation point, then the bifurcation is named Limit-Induced Bifurcation (LIB), since the bifurcation occurs when the *structure*[7] of the system changes due to a limit.

With these definitions, the bifurcation surface is composed of three types of bifurcations, namely SNBs, LIBs and CVIBs. For example, it might be the case that each of the three bifurcation points shown in Figure 17 is associated with a different bifurcation type.

In this section, three bifurcation types were defined based on the mechanisms that can lead to the loss of a solution point. A mathematical definition of each of these three bifurcations will be given in Chapter 4.

3.3 Continuation Method

In the course of time, $\mathbf{p}$ will slowly vary, which causes a variation on the solution $\mathbf{x}$. Eventually, for a specific value of $\mathbf{p}$, the system may undergo a bifurcation. This bifurcation point is not known beforehand, thus numerical methods must be employed to compute it.

Assume that the value of $\mathbf{p}$ with respect to time can be tracked by a time-varying function $\mathbf{p}(t)$, where $\mathbf{p}(0)$ represents the current value of $\mathbf{p}$. In the nomenclature of this document, $\mathbf{p}(t)$ represents a *parameter variation scenario*. Assume that the current operating point $(\mathbf{x}_0, \mathbf{p}(0))$ is known. The goal is to compute the corresponding function $\mathbf{x}(t)$, defined in an interval $\mathcal{I} = [0, t_{\max}]$, such that

- $\mathbf{x}(0) = \mathbf{x}_0$, and
- $\mathbf{f}(\mathbf{x}(t), \mathbf{p}(t)) = \mathbf{0} \; \forall \; t \in \mathcal{I}$;

In order to such a function exist, a bifurcation point must not occur in the interior of $\mathcal{I}$. Moreover, in order to the value $t_{\max}$ be maximum, there must not be any solution $\mathbf{x}$ for $t > t_{\max}$, which implies that $\mathbf{p}(t_{\max})$ must be a bifurcation point.

The objective is then to compute the path of solutions from the current operating point $(\mathbf{x}(0), \mathbf{p}(0))$ to the bifurcation point $(\mathbf{x}(t_{\max}), \mathbf{p}(t_{\max}))$. This is sketched in Figure 18, where $t_{\max}$ is the first value of t at which $\mathbf{p}(t)$ touches the bifurcation surface.

The computation of new points $(\mathbf{x}, t)$ starting from a previously known solution

[6] In reality, *simple bifurcations* (SEYDEL, 2010) also occur when the Jacobian matrix is singular. However, simple bifurcations are not generic, so they are unlikely to occur in practical situations.

[7] Recall the definition of the system *structure* given in Section 2.10.

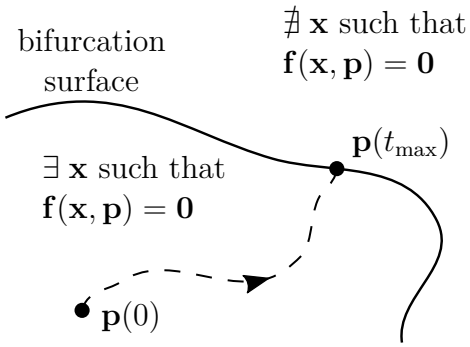

Figure 18 – *Scenario* described by function $\mathbf{p}(t)$.

$(\mathbf{x}_0, 0)$ is the exact use case of continuation methods. These methods aim at computing solution branches of systems of n equations and $n+1$ variables.

Continuation methods compute a sequence of points $\{(\mathbf{x}_0, t_0), (\mathbf{x}_1, t_1) \dots\}$ basically by iterating the following four steps:

Step 1) Parameterization: In order to compute a new solution $(\mathbf{x}_1, t_1)$ starting from $(\mathbf{x}_0, t_0)$, it is necessary to define a new equation $h(\mathbf{x}, t) = 0$. Thereby, the system of $n+1$ equations

$$\mathbf{f}(\mathbf{x}, \mathbf{p}(t)) = \mathbf{0}\,, \tag{3.6a}$$

$$h(\mathbf{x}, t) = 0\,, \tag{3.6b}$$

and $n+1$ variables $(\mathbf{x}, t)$ can be solved by a numeric solver. Each choice of h defines a new parameterization of the continuation procedure. If the goal is to increase t, the most obvious choice of h is

$$h(x, t) = t - (t_0 + \Delta t)\,, \tag{3.7}$$

where t_0 is the previous solution and Δt is the step length (which is adjusted iteratively by Step 4). With this choice of parameterization, the Jacobian of equation (3.6) is

$$\begin{bmatrix} \partial_{\mathbf{x}}\mathbf{f} & \partial_{\mathbf{p}}\mathbf{f}\,\partial_t\mathbf{p} \\ \mathbf{0} & 1 \end{bmatrix}, \tag{3.8}$$

which clearly becomes ill-conditioned near a saddle-node bifurcation (where $\partial_{\mathbf{x}}\mathbf{f}$ is singular). The ill-conditioning of this system of equations near a SNB makes it difficult for the corrector of Step 3 to converge near the bifurcation point. There are several parameterization alternatives in the literature. One of those is the arc-length parameterization (CHIANG et al., 1995):

$$h(\mathbf{x}, t) = \sum_i (x_i - x_{0,i})^2 + (t - t_0)^2 - \Delta s^2 \tag{3.9}$$

where x_i and $x_{0,i}$ are the ith elements of vectors $\mathbf{x}$ and $\mathbf{x}_0$, respectively. In this parameterization, the step length is quantified by Δs.

Step 2) Prediction: After choosing a parameterization, the system of equations (3.6) should be solved by an iterative numerical solver. These solvers require an initial estimate $(\widetilde{\mathbf{x}}, \widetilde{t})$ of the solution of (3.6).

A trivial estimate of the solution is the previous solution point, given by

$$(\widetilde{\mathbf{x}}, \widetilde{t}) = (\mathbf{x}_0, t_0)\,. \tag{3.10}$$

If the parameterization is given by (3.7), then this estimate can be slightly improved by

$$(\widetilde{\mathbf{x}}, \widetilde{t}) = (\mathbf{x}_0, t_0 + \Delta t)\,. \tag{3.11}$$

When two previous solutions $(\mathbf{x}_0, t_0)$ and $(\mathbf{x}_{-1}, t_{-1})$ are known, the estimate can be computed by linear extrapolation:

$$(\widetilde{\mathbf{x}}, \widetilde{t}) = (\mathbf{x}_0, t_0) + \lambda((\mathbf{x}_0, t_0) - (\mathbf{x}_{-1}, t_{-1}))\,, \tag{3.12}$$

where λ must be chosen appropriately, according to the parameterization and the step size.

In the tangent predictor, vector $\mathbf{v}$, tangent to the solution branch at $(\mathbf{x}_0, t_0)$, is used in the estimate. Vector $\mathbf{v}$ satisfies the following:

$$\begin{bmatrix}\partial_{\mathbf{x}}\mathbf{f} & \partial_{\mathbf{p}}\mathbf{f}\ \partial_t\mathbf{p}\end{bmatrix}\ \mathbf{v} = \mathbf{0}\,, \tag{3.13}$$

where the Jacobian is evaluated at $(\mathbf{x}, \mathbf{p}) = (\mathbf{x}_0, \mathbf{p}(t_0))$. The estimate is then computed similarly to equation (3.12):

$$(\widetilde{\mathbf{x}}, \widetilde{t}) = (\mathbf{x}_0, t_0) + \lambda\mathbf{v}\,. \tag{3.14}$$

Step 3) Correction: This step refers to the numerical solver used to solve equation (3.6). Common choices are the Newton's method and its variations, such as the Fast-Decoupled method used in power flow computations.

Step 4) Step Length Control: When the main goal is to fast compute the bifurcation point, it is desirable to compute as few intermediary steps as possible. To this end, step length control is used to adaptatively adjust the distance between consecutive points in the solution branch and to guarantee a good progress towards increasing t. The step length control basically determines the value of Δt or Δs in equations (3.7) and (3.9), respectively.

A common choice for step length control is to monitor the number of iterations that the corrector of Step 3 needs to compute the solution. If it needs many iterations, then the corrector is struggling to compute the solution, so the step size should be decreased. If, on the other hand, the corrector quickly converges towards the solution, then the step size could be increased to reduce the number of continuation steps.

Another choice is to monitor the distance between the prediction $(\widetilde{\mathbf{x}}, \widetilde{t})$ and the correction $(\mathbf{x}_1, t_1)$. If the distance between these points is small, then the step size can be increased.

It can be noted that the function of step length control is basically to balance the work of the corrector and the number of continuation steps. If the step size is too small, the computational time will be high because too many continuation steps will be computed. If the step size is too large, the corrector will hardly converge to the desired solution point.

These four steps are not completely independent/orthogonal. For example, the parameterization may influence the prediction step: if the arc-length parameterization (3.9) is being applied, then the predictor (3.10) cannot be used.

By following these four steps, it is possible to compute new solutions $(\mathbf{x}, t)$ in the solution branch for increasing values of t. As the bifurcation point is approached, the continuation method will either (I) stop converging (as a consequence of ill-conditioning and the loss of the solution point) or (II) start to decrease t (t decreases after the BP). Parameterization plays a crucial role on which possibility will occur: possibility (I) occurs when using parameterization (3.7), while possibility (II) typically occurs when using parameterization (3.9).

An example of a continuation procedure is shown in Figure 19. In this example, arc-length parameterization (3.9) is used together with the prediction of equation (3.12). In this figure, two previous solutions $(\mathbf{x}_{-1}, t_{-1})$ and $(\mathbf{x}_0, t_0)$ of $\mathbf{f}(\mathbf{x}, \mathbf{p}) = \mathbf{0}$ are known, and the initial estimate of the new solution $(\mathbf{x}_1, t_1)$ (provided by the predictor step) is given by $(\widetilde{\mathbf{x}}, \widetilde{t})$. This estimate is then corrected by the correction step.

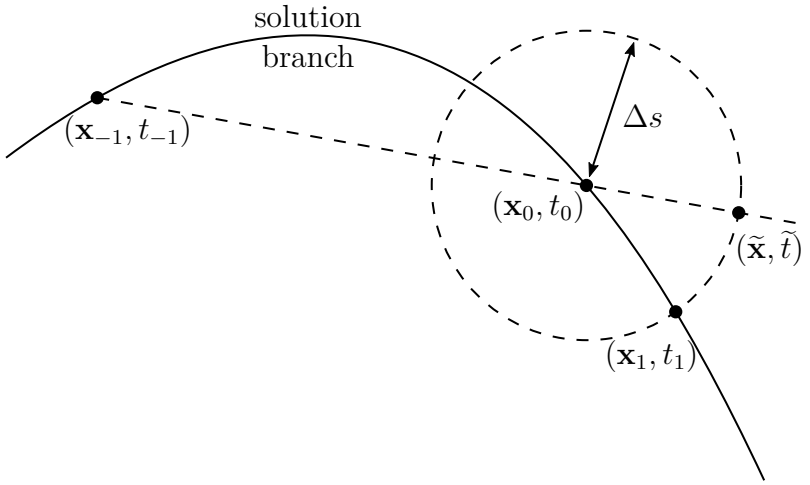

Figure 19 – Example of a continuation procedure.

Continuation methods have been extensively applied in the voltage stability literature (IBA et al., 1991; AJJARAPU; CHRISTY, 1992; CANIZARES; ALVARADO, 1993;

ZENG et al., 1993; CHIANG et al., 1995; HISKENS; CHAKRABARTI, 1996; FENG; AJJARAPU; LONG, 2000; ZHU; TAYLOR; IRVING, 2008; AVALOS et al., 2009), in which they are commonly referred to as continuation power flow. Continuation methods are one of the most used tools for model-based static voltage stability assessment.

It should be mentioned that, even though the continuation method was presented based in equation (2.36a), this method could be easily adapted to handle the inequality constraints in (2.36b).

3.4 Point of Collapse Method

In Subsection 3.2.1, a saddle-node bifurcation point is described as a point where matrix $\partial_{\mathbf{x}}\mathbf{f}$ exists and is singular. Hence, a direct method of computing a SNB point consists of searching specifically for the singularity of the Jacobian.

Matrix $\partial_{\mathbf{x}}\mathbf{f}$ is singular when it has at least one null eigenvalue. Associated with this eigenvalue, there is a right eigenvector $\mathbf{v}$ satisfying

$$\partial_{\mathbf{x}}\mathbf{f}\,\mathbf{v} = \lambda\,\mathbf{v} = \mathbf{0} \tag{3.15}$$

and a left eigenvector $\mathbf{w}$ satisfying

$$\mathbf{w}^T\,\partial_{\mathbf{x}}\mathbf{f} = \lambda\,\mathbf{w}^T = \mathbf{0}\,, \tag{3.16}$$

where both $\mathbf{v}$ and $\mathbf{w}$ are nontrivial ($\mathbf{v} \neq \mathbf{0}$ and $\mathbf{w} \neq \mathbf{0}$).

For a particular *scenario* $\mathbf{p}(t)$, the direct method to compute saddle-node bifurcations is naturally given by the resolution of either equation

$$\mathbf{f}(\mathbf{x}, \mathbf{p}(t)) = \mathbf{0}\,, \tag{3.17a}$$
$$\partial_{\mathbf{x}}\mathbf{f}(\mathbf{x}, \mathbf{p}(t))\,\mathbf{v} = \mathbf{0}\,, \tag{3.17b}$$
$$\|\mathbf{v}\| = 1\,, \tag{3.17c}$$

or equation

$$\mathbf{f}(\mathbf{x}, \mathbf{p}(t)) = \mathbf{0}\,, \tag{3.18a}$$
$$\partial_{\mathbf{x}}\mathbf{f}(\mathbf{x}, \mathbf{p}(t))^T\,\mathbf{w} = \mathbf{0}\,, \tag{3.18b}$$
$$\|\mathbf{w}\| = 1\,, \tag{3.18c}$$

depending on which eigenvector should be computed for a particular analysis.

Both (3.17) and (3.18) are composed of $2n + 1$ equations and $2n + 1$ variables, which can be solved, e.g., using the Newton's method. However, choosing initial estimates for the eigenvector is usually difficult, so better approaches are often needed to solve these equations. The computation of the bifurcation point by solving these equations

directly is known in the literature as Point of Collapse method (CANIZARES et al., 1992; CANIZARES; ALVARADO, 1993).

It should be emphasized that this method works specifically for SNB points.

3.5 Closest Bifurcation Point

The use of continuation methods is based on the assumption that the path $\mathbf{p}(t)$, on which $\mathbf{p}$ will vary with the increase of time, can be predicted. In general, however, this path cannot be accurately estimated, and alternative approaches must be taken. One of these approaches is to compute the closest bifurcation to the current operating point.

The aim of the closest bifurcation method is to solve the following optimization problem:

$$\begin{aligned} \min_{\mathbf{p}} \quad & d(\mathbf{p}, \mathbf{p}_0) \\ \text{subject to} \quad & \mathbf{p} \in \text{bifurcation surface} \end{aligned} \tag{3.19}$$

where $\mathbf{p}_0$ is the current operating point and d corresponds to VSM, as defined in equation (3.2). For this section, let the distance d be the usual Euclidean distance:

$$\mathrm{d}(\mathbf{a}, \mathbf{b}) = \|\mathbf{a} - \mathbf{b}\|_2 = \sqrt{\sum_i (a_i - b_i)^2} \tag{3.20}$$

where $\mathbf{a}$ and $\mathbf{b}$ are arbitrary m-dimensional vectors.

Solving problem (3.19) is not easy, mainly because it is difficult to obtain a convenient representation of the bifurcation surface. In this section, assume that the bifurcation surface is composed only of SNB points.

Assume that a SNB point $(\widehat{\mathbf{x}}, \widehat{\mathbf{p}})$ on the bifurcation surface has been computed. By differentiating (3.1) at $(\widehat{\mathbf{x}}, \widehat{\mathbf{p}})$:

$$\partial_{\mathbf{x}} \mathbf{f}(\widehat{\mathbf{x}}, \widehat{\mathbf{p}})\, d\mathbf{x} + \partial_{\mathbf{p}} \mathbf{f}(\widehat{\mathbf{x}}, \widehat{\mathbf{p}})\, d\mathbf{p} = \mathbf{0}\,. \tag{3.21}$$

Since a SNB occurs at $(\widehat{\mathbf{x}}, \widehat{\mathbf{p}})$, then $\partial_{\mathbf{x}} \mathbf{f}(\widehat{\mathbf{x}}, \widehat{\mathbf{p}})$ is singular. Let $\mathbf{w}$ be the eigenvector associated with the null eigenvalue of this matrix. Then, by pre-multiplying (3.21) by $\mathbf{w}^T$:

$$\cancel{\mathbf{w}^T \partial_{\mathbf{x}} \mathbf{f}(\widehat{\mathbf{x}}, \widehat{\mathbf{p}})\, d\mathbf{x}} + \mathbf{w}^T\, \partial_{\mathbf{p}} \mathbf{f}(\widehat{\mathbf{x}}, \widehat{\mathbf{p}})\, d\mathbf{p} = \mathbf{w}^T\, \partial_{\mathbf{p}} \mathbf{f}(\widehat{\mathbf{x}}, \widehat{\mathbf{p}})\, d\mathbf{p} = 0\,. \tag{3.22}$$

Equation (3.22) shows a cheap way of computing a vector $\mathbf{n}$ that is normal to the bifurcation surface at $(\widehat{\mathbf{x}}, \widehat{\mathbf{p}})$:

$$\mathbf{n}^T\, (\mathbf{p} - \widehat{\mathbf{p}}) = 0\,, \tag{3.23}$$

where $\mathbf{n} = \partial_{\mathbf{p}} \mathbf{f}(\widehat{\mathbf{x}}, \widehat{\mathbf{p}})^T\, \mathbf{w}$. This method of computing the normal vector was introduced in (DOBSON, 1992).

Since it is cheap to compute the normal vector, an efficient way of computing the closest bifurcation is to iterate the following steps (DOBSON; LU, 1993; ALVARADO; DOBSON; HU, 1994):

Step 1) For a given *scenario* $\mathbf{p}(t) = \mathbf{p}_0 + t\mathbf{d}$ of variation of $\mathbf{p}$, compute the BP;

Step 2) Ensure that the BP is a SNB point and compute the normal vector as in (3.23);

Step 3) Update vector $\mathbf{d} \leftarrow \mathbf{n}$ and return to Step 1.

The update $\mathbf{d} \leftarrow \mathbf{n}$ in Step 3 simply comes from the fact that $\mathbf{n}$ is the direction of the solution of problem (3.19), when the bifurcation surface is replaced by the linearized plane (3.23). To see this, problem (3.19) is conveniently reformulated as follows:

$$\begin{aligned} \min_{\mathbf{p}} \quad & \tfrac{1}{2}\|\mathbf{p} - \mathbf{p}_0\|_2^2 \\ \text{subject to} \quad & \mathbf{n}^T(\mathbf{p} - \widehat{\mathbf{p}}) = 0 \end{aligned} \tag{3.24}$$

The first-order optimality conditions of problem (3.24) (NOCEDAL; WRIGHT, 1999; LUENBERGER; YE, 2008) result in the following linear system:

$$\mathbf{p} + \lambda\,\mathbf{n} = \mathbf{p}_0\,, \tag{3.25a}$$

$$\mathbf{n}^T(\mathbf{p} - \widehat{\mathbf{p}}) = 0\,, \tag{3.25b}$$

where λ is the Lagrange multiplier associated with constraint $\mathbf{n}^T(\mathbf{p} - \widehat{\mathbf{p}}) = 0$. The first equation is simply $\mathbf{p} = \mathbf{p}_0 - \lambda\,\mathbf{n}$, showing that $\mathbf{n}$ is the direction of the solution of (3.24).

Step 1 aims for computing the bifurcation point for a given *scenario* $\mathbf{p}(t)$. This BP can be computed using continuation methods, as discussed in Section 3.3. Since it is assumed that the BP is a SNB point, another possibility is to compute the SNB point directly using equation (3.18), assuming that an estimate of the eigenvector $\mathbf{w}$ is available.

This procedure of computing the closest bifurcation will be referred to as *Closest Bifurcation Method*. A graphical visualization of this method is given in Figure 20.

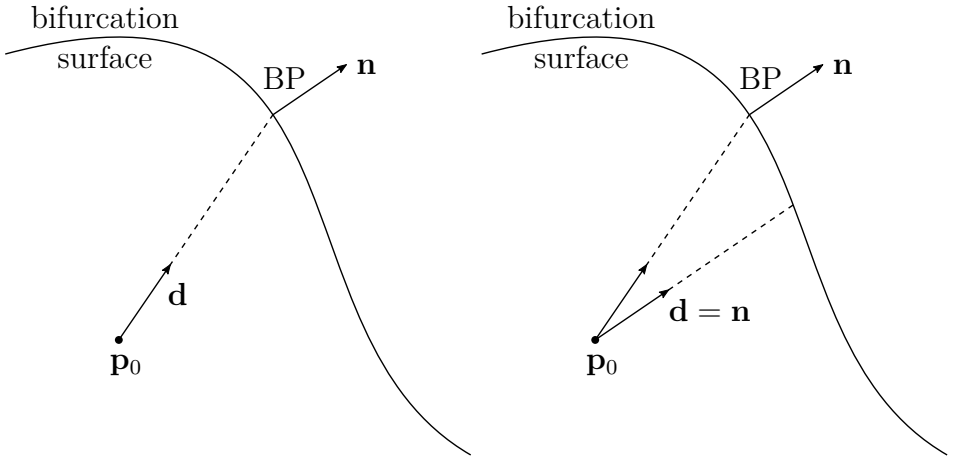

(a) Computing the BP and $\mathbf{n}$. (b) The new direction $\mathbf{d}$.

Figure 20 – Computation of the closest bifurcation.

Lastly, it should be emphasized the clear limitation of this method on assuming that the BP is a SNB point. In other words, it is assumed that:

- function $\mathbf{f}$ is C^1 at the bifurcation point, which discards the possibility of LIBs;
- any solution of equation (2.36a) satisfies inequation (2.36b), which discards the possibility of CVIBs.

In Chapter 4, a new power flow model is proposed to circumvent the aforementioned issues, removing these limitations of the closest bifurcation method.

3.6 Regarding Parameter Uncertainties

Section 3.3 presented a traditional method of computing the bifurcation point using a continuation strategy. This method is well-suited for situations where the *parameter variation scenario* $\mathbf{p}(t)$ can be precisely predicted.

On the other hand, when no information is provided about the variation of $\mathbf{p}$, Section 3.5 presents a method capable of computing the closest BP in the entire parameter space (provided that all BPs are SNB points).

Both approaches are non-realistic in real power systems:

- The first approach, while assuming that the system future behavior can be accurately estimated, ignores parameter uncertainties. In this sense, the continuation method can provide nonconservative measures of VSM, as there might exist other credible *scenarios* associated with lower values of VSM.
- The second approach assumes no knowledge about how $\mathbf{p}$ will change over time. As a consequence, this approach computes the worst case *scenario*, which is very unlikely to occur in practical situations. Therefore, this approach often provides too conservative results.

Some studies (KATAOKA, 2003; NEVES; ALBERTO, 2020) are placed between the two aforementioned approaches. They assume that a most likely *scenario* can be predicted (this would be the scenario considered in a continuation method). However, they do not overlook uncertainties related to this *scenario*.

Specifically, the uncertainty in these studies is modelled by a hypercone, as shown in Figure 21. The axis of this hypercone represents the most likely scenario, and all scenarios inside the hypercone are considered credible (according to some threshold) and must be taken into account while computing a robust value of VSM.

The portion of the bifurcation surface in the interior of the cone (shown in Figure 21 as a heavy solid line) is the set of bifurcation points that can be reached from credible scenarios. Each of these bifurcation points is associated with a specific value of VSM, as defined in (3.2).

Since VSM is a security index, it should not be overestimated. Ideally, the value of VSM should be as realistic as possible, but in the presence of uncertainty the returned

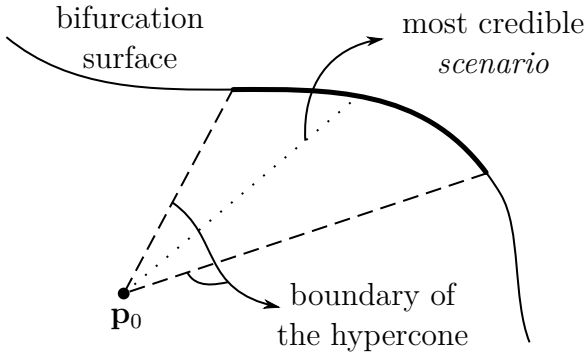

Figure 21 – Representing uncertainties using a hypercone model. Any *scenario* inside the hypercone is considered credible.

VSM should rather be conservative than optimistic. Therefore, the minimum VSM among all credible *scenarios* should be computed (NEVES; ALBERTO, 2020):

$$\begin{aligned} \min_{\mathbf{p}} \quad & d(\mathbf{p}, \mathbf{p}_0) \\ \text{subject to} \quad & \mathbf{p} \in \text{bifurcation surface} \\ & \mathbf{p} \in \text{hypercone} \end{aligned} \tag{3.26}$$

The feasible region of this optimization problem is the heavy solid line of Figure 21. If distance d is the usual Euclidean distance, then the solution of (3.26) is sketched in Figure 22. The solution of (3.26) basically establishes that the power system will not undergo a bifurcation for any vector $\mathbf{p}$ inside the shaded area shown in Figure 22 (for any $\mathbf{p}$ inside this shaded area, there is a vector $\mathbf{x}$ satisfying $\mathbf{f}(\mathbf{x}, \mathbf{p}) = \mathbf{0}$).

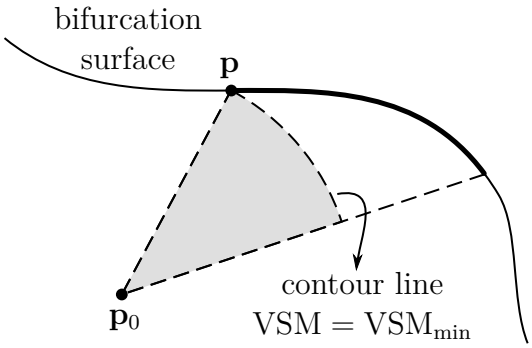

Figure 22 – Representing uncertainties using a hypercone model. For any $\mathbf{p}$ inside the shaded area, there is a solution $\mathbf{x}$ of $\mathbf{f}(\mathbf{x}, \mathbf{p}) = \mathbf{0}$.

The method proposed in (NEVES; ALBERTO, 2020) to solve problem (3.26) can be summarized as follows:

- *Stage I:* Compute the bifurcation point associated with the most credible *scenario*.
- *Stage II:* Minimize VSM by moving along the bifurcation surface, constrained to the hypercone model.

In *Stage I*, the following equations are solved for the most credible scenario $\mathbf{p}(t)$:

$$\mathbf{f}(\mathbf{x}, \mathbf{p}(t)) = \mathbf{0}\,, \tag{3.27a}$$

$$\partial_{\mathbf{x}}\mathbf{f}(\mathbf{x}, \mathbf{p}(t))\,\mathbf{v} = \mathbf{0}\,, \tag{3.27b}$$

$$\|\mathbf{v}\| = 1\,. \tag{3.27c}$$

These equations guarantee the singularity of $\partial_{\mathbf{x}}\mathbf{f}$, as explained in Section 3.4.

In *Stage II*, the bifurcation surface of problem (3.26) is replaced by equation (3.27), and the resulting optimization problem is solved efficiently. The initial point for this optimization method is the BP computed in *Stage I*.

The same way as for the closest bifurcation method (presented in Section 3.5), the resolution of (3.26) proposed in (NEVES; ALBERTO, 2020) assumes that all BPs are SNB points. However, a smooth formulation was presented in (NEVES; ALBERTO, 2020) to represent generator reactive power limits (equation (2.9), specifically), which allows LIBs caused by generator Q-limits to be transformed into SNBs. Hence, these LIBs can be computed using equation (3.27). The smooth formulation proposed in (NEVES; ALBERTO, 2020) will be generalized in Chapter 4 to the entire power system model.

It should be noted that several studies in the literature (ZHANG; DOBSON; ALVARADO, 2004; HAESEN et al., 2009; ZHANG et al., 2010; WANG; CHIANG; WANG, 2013; JIANFEN et al., 2016) deal with a probabilistic approach of computing VSM as a function of the random variables of the system. Some of these studies propose to roughly estimate the probability density function of VSM at the expense of several continuation power flow executions. Therefore, most of these methods are not suitable to analyze large-scale power systems.

3.7 Control Selection in Voltage Stability

In previous sections, the problem of voltage instability was stated and the voltage stability margin, which quantifies the distance from the current operating point to the bifurcation point, was defined. Some methods for computing VSM were also presented. This section presents how the current literature approaches the selection of preventive and corrective controls to improve voltage stability.

After computing VSM, two situations are possible:

- If VSM is *high enough*, the system is not operating near the bifurcation surface and thus it is considered stable from the point of view of static voltage stability. Hence, control actions are not necessary to guarantee stability.
- Otherwise, small variations of $\mathbf{p}$ can suddenly lead the system to a voltage collapse. Countermeasures should be taken to guarantee stability, which are quantified by a change in vector $\mathbf{u}$ in equation (2.36).

The meaning of *high enough* is subjective. Usually, there is a threshold defined in regulations to determine the minimum admissible value for VSM. This threshold should take into account which distance function is used in the definition of VSM, given by (3.2).

In Section 3.5, a cheap method was presented for computing the normal vector of the bifurcation surface at a specific BP. It is intuitive that the normal vector gives the (locally) optimal direction in which $\mathbf{p}$ must be varied to increase VSM. To maximize the increase in VSM for a given change $\Delta\mathbf{p}$ in $\mathbf{p}$, $\Delta\mathbf{p}$ should be parallel to $\mathbf{n}$. Mathematically, this can be proven with the following optimization problem (illustrated in Figure 23):

$$\begin{aligned} \max_{t,\Delta\mathbf{p}} \quad & \|t\mathbf{d}\| \\ \text{subject to} \quad & \mathbf{n}^T\left(\mathbf{p}_0 + \Delta\mathbf{p} + t\mathbf{d} - \widehat{\mathbf{p}}\right) = 0 \\ & \|\Delta\mathbf{p}\|_2^2 = 1 \end{aligned} \tag{3.28}$$

where:

- $\mathbf{p}(t) = \mathbf{p}_0 + t\mathbf{d}$ is the current *parameter variation scenario*, for which a bifurcation occurs at $\widehat{\mathbf{p}}$;
- $\mathbf{n}$ is the normal vector to the bifurcation surface at point $\widehat{\mathbf{p}}$;
- after perturbing the current operating point from $\mathbf{p}_0$ to $\mathbf{p}_0 + \Delta\mathbf{p}$, the new *scenario* is given by $\mathbf{p}(t) = \mathbf{p}_0 + \Delta\mathbf{p} + t\mathbf{d}$;
- distance d in the definition of VSM (equation (3.2)) is induced by the vector norm $\|\cdot\|$, therefore the objective function is given by $\|(\mathbf{p}_0 + \Delta\mathbf{p} + t\mathbf{d}) - (\mathbf{p}_0 + \Delta\mathbf{p})\| = \|t\mathbf{d}\|$.

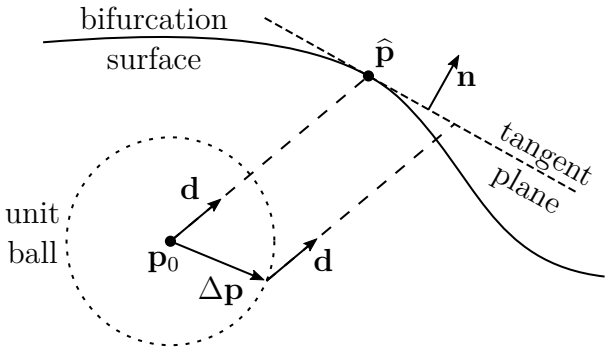

Figure 23 – Graphical representation of problem (3.28).

The first constraint basically establishes that the approximation of the new bifurcation point should lie in the hyperplane tangent to the bifurcation surface at $\mathbf{p} = \widehat{\mathbf{p}}$. The second constraint restricts the size of the perturbation $\Delta\mathbf{p}$.

The Lagrangian (LUENBERGER; YE, 2008) of this optimization problem is:

$$\mathcal{L}(t, \Delta\mathbf{p}, \lambda_1, \lambda_2) = \|t\mathbf{d}\| + \lambda_1\mathbf{n}^T\left(\mathbf{p}_0 + \Delta\mathbf{p} + t\mathbf{d} - \widehat{\mathbf{p}}\right) + \lambda_2(\|\Delta\mathbf{p}\|_2^2 - 1)\,, \tag{3.29}$$

and the KKT condition (LUENBERGER; YE, 2008) $\partial_{\Delta\mathbf{p}}\mathcal{L} = \mathbf{0}$ is:

$$\lambda_1\mathbf{n} + 2\lambda_2\Delta\mathbf{p} = \mathbf{0}\,, \tag{3.30}$$

which clearly shows that the optimal vector $\Delta\mathbf{p}$ is parallel to $\mathbf{n}$.

In the case where vector $\mathbf{p}$ is composed by loading parameters, the normal vector indicates which loads should be shed to increase the distance to the bifurcation. Several studies in the literature suggest this approach to increase VSM and restore solvability (DOBSON, 1992; DOBSON; LU, 1992a; ALVARADO; DOBSON; HU, 1994; OVERBYE, 1994; FENG; AJJARAPU; MARATUKULAM, 1998; WANG; LASSETER, 2000; WU et al., 2001; CAPITANESCU; CUTSEM, 2002).

The approach described above shows directly how to move $\mathbf{p}$ to avoid the bifurcation, but it does not provide information on how to change vector $\mathbf{u}$ in (2.36) to increase VSM. Assume that a particular *scenario* $\mathbf{p}(t)$ is known. For this scenario, the bifurcation point $(\mathbf{x}_{\text{bif}}(\mathbf{u}), t_{\max}(\mathbf{u}))$ is uniquely defined for a particular vector $\mathbf{u}$ (equation (3.27) has one solution for a given $\mathbf{u}$). The derivatives of $\mathbf{x}$ and t with respect to $\mathbf{u}$ could be obtained directly by differentiating equation

$$\mathbf{f}(\mathbf{x}, \mathbf{p}(t), \mathbf{u}) = \mathbf{0}\,, \tag{3.31a}$$

$$\partial_{\mathbf{x}}\mathbf{f}(\mathbf{x}, \mathbf{p}(t), \mathbf{u})\,\mathbf{v} = \mathbf{0}\,, \tag{3.31b}$$

$$\|\mathbf{v}\| = 1\,. \tag{3.31c}$$

with respect to $\mathbf{u}$, but once again the left eigenvector $\mathbf{w}$ of the null eigenvalue of $\partial_{\mathbf{x}}\mathbf{f}$ provides a cheap way of computing $\partial_{\mathbf{u}}t$:

$$\mathbf{w}^T\,(\partial_{\mathbf{x}}\mathbf{f}\,\partial_{\mathbf{u}}\mathbf{x} + \partial_{\mathbf{p}}\mathbf{f}\,\partial_t\mathbf{p}\,\partial_{\mathbf{u}}t + \partial_{\mathbf{u}}\mathbf{f}) = 0\,, \tag{3.32}$$

where the expression inside the parentheses is the Jacobian of $\mathbf{f}(\mathbf{x}, \mathbf{p}(t), \mathbf{u})$ with respect to $\mathbf{u}$. Since $\mathbf{w}^T\partial_{\mathbf{x}}\mathbf{f} = \mathbf{0}$:

$$\mathbf{w}^T\,\partial_{\mathbf{p}}\mathbf{f}\,\partial_t\mathbf{p}\,\partial_{\mathbf{u}}t + \mathbf{w}^T\,\partial_{\mathbf{u}}\mathbf{f} = 0 \Rightarrow \partial_{\mathbf{u}}t = -\frac{\mathbf{w}^T\,\partial_{\mathbf{u}}\mathbf{f}}{\mathbf{w}^T\,\partial_{\mathbf{p}}\mathbf{f}\,\partial_t\mathbf{p}}\,. \tag{3.33}$$

The use of equation (3.33) in the selection of most promising controls to improve VSM were reported in (GREENE; DOBSON; ALVARADO, 1997; CANIZARES, 1998; FENG; AJJARAPU; MARATUKULAM, 2000; ZHAO et al., 2006).

Since the singularity of $\partial_{\mathbf{x}}\mathbf{f}$ is used to compute the derivative in (3.33), this is another method that can only be applied to SNB points, ignoring the possibility of LIB and CVIB points.

3.8 Overview of the VSA literature

Up to this point, all sections in this chapter described methodologies that directly guide how VSA is approached in this document. However, many other works have indirectly influenced the foundations of voltage stability and they should be acknowledged. This

section presents an overview of other approaches in the literature that deal with voltage instability and voltage collapse in electric power systems.

Since the Jacobian matrix $\partial_{\mathbf{x}}\mathbf{f}$ becomes singular at a SNB point, some studies propose to use the singular values of this matrix as an index of voltage stability (TIRANUCHIT et al., 1988; LOF et al., 1992; LEE; LEE, 1991). The use of singular values to improve static voltage stability was proposed in (TIRANUCHIT; THOMAS, 1988), in which the minimum singular value of $\partial_{\mathbf{x}}\mathbf{f}$ (say $\sigma_{\min}$) is maximized using a continuation technique to determine the change in vector $\mathbf{u}$. A drawback of these methods is that the relation between $\sigma_{\min}$ and VSM is nonlinear and unpredictable, hence the choice of $\sigma_{\min}$ as a measure of the distance to bifurcation can be misleading (e.g., there might be operating points for which $\sigma_{\min}$ is high, even though VSM is low).

The right eigenvector $\mathbf{v}$ associated with the null eigenvalue of $\partial_{\mathbf{x}}\mathbf{f}$ plays an important role in the behavior of the system undergoing a SNB (DOBSON; CHIANG, 1989; CHIANG et al., 1990). This vector is tangent to the (unique) unstable part of the center manifold associated with the saddle-node equilibrium point. Hence, vector $\mathbf{v}$ basically defines which elements of the state vector $\mathbf{x}$ would initiate the collapse. The equipment/buses associated with these elements of $\mathbf{x}$ can be thought as the "source" of the instability, and they show where preventive controls are promising in improving voltage stability. The use of eigenvectors associated with the eigenvalues with smallest magnitude has been addressed in the literature of voltage stability (GAO; MORISON; KUNDUR, 1992; CANIZARES; ALVARADO, 1993; GAO; MORISON; KUNDUR, 1996; AFFONSO et al., 2004).

Instead of computing eigenvectors, some studies assess voltage stability using sensitivities (OBADINA; BERG, 1990; FLATABO et al., 1993; CUTSEM, 1995; SOUZA, 1998; CAPITANESCU; CUTSEM, 2005). Large sensitivities may indicate that the operating point is near a bifurcation point, and the sign of the sensitivities may predict a voltage collapse. The use of sensitivities to assess stability is intrinsically linked to the foundations of measurement-based voltage stability assessment. In model-based VSA, sensitivity analysis is generally associated with the tangent vector. On the other hand, in measurement-based VSA, sensitivity analysis is usually associated with the difference between consecutive measures of the state vector.

In general, it is desirable to guarantee static voltage stability not only for the base-case power system, but also to maintain stability in face of a contingency. Typical examples are the loss of a transmission line due to faults or the loss of generation units. In these cases, a perturbed version of system (2.36) is studied. Many methods in the literature have been proposed to fast compute VSM for a set of credible contingencies (EJEBE et al., 1996; CHIANG; WANG; FLUECK, 1997; GREENE; DOBSON; ALVARADO, 1999; VAAHEDI et al., 1999; FLUECK; DONDETI, 2000; JIA; JEYASURYA, 2000; FLUECK; GONELLA; DONDETI, 2002; CAPITANESCU et al., 2007; NEVES; ALBERTO; CHIANG, 2020).

On the other hand, some studies address the selection of corrective/preventive controls to restore solvability/increase VSM (WANG et al., 1997; CAPITANESCU; CUTSEM, 2002; SONG et al., 2003; ZHAO; CHIANG; LI, 2005; MANSOUR et al., 2013; MANSOUR; ALBERTO; RAMOS, 2016; WANG; CHIANG, 2020).

4 PROPOSED POWER SYSTEM MODELLING

In the previous chapter, several methods were presented for voltage stability analysis of a power system whose mathematical model is given by equation (2.36). Those methods basically search for bifurcation points of equation (2.36), i.e., they search for points at which the power system loses its equilibrium point. Following the loss of the solution of equation (2.36), the underlying power system usually undergoes a voltage collapse.

Most methods mentioned in Chapter 3 for voltage stability assessment were developed on the assumption that bifurcation points are generically saddle-node bifurcation points. However, as described in Subsection 3.2.1, the saddle-node bifurcation is not the only mechanism in which a solution of system (2.36) disappears. Specifically, limit-induced bifurcations and constraint violation induced bifurcations could also lead to the loss of a solution point.

In this chapter, a new power system modelling is proposed to ensure that all BPs in the bifurcation surface are generically saddle-node bifurcations. The main goal of this chapter is to represent a generic power system (which includes all types of devices listed in Chapter 2) by only one equation of the form

$$\mathbf{h}(\mathbf{z}, \mathbf{p}, \mathbf{u}) = \mathbf{0}\,, \tag{4.1}$$

where $\mathbf{h}$ is a continuously differentiable function in the entire domain. $\mathbf{z}$ is the state vector of equation (4.1), and it is equivalent to vector $\mathbf{x}$ for system (2.36). Compared to the power system model given by equation (2.36), equation (4.1) presents the following differences:

- Function $\mathbf{h}$ is C^1 (continuously differentiable) in the entire domain, which is not the case of function $\mathbf{f}$ in (2.36a). When using (4.1) instead of (2.36), it is not necessary to check which is the correct *structure* of the power system for a particular operating point.
- All inequality constraints in inequation (2.36b) are directly incorporated in function $\mathbf{h}$, thus there is no need to check if these inequality constraints are satisfied for a particular solution of equation (4.1).

Under the assumption that the power system can be represented by equation (4.1), the Implicit Function Theorem ensures that all static bifurcations points, without exception, are points where $\partial_{\mathbf{z}}\mathbf{h}$ exists and is singular. Note that this is the only characteristic of a saddle-node bifurcation explored by many of the methods described in Chapter 3, thus all those methods can be applied to the new power system model, proposed in this chapter, without checking the bifurcation type.

Even though this chapter describes how to transform the power system model described in Chapter 2 into the form of equation (4.1), the ideas presented in this chapter

are generic and can be extended to incorporate new devices besides those presented in Chapter 2.

Initially, a precise definition of SNBs, LIBs and CVIBs will be provided in Section 4.1. These definitions are needed to formally demonstrate that all SNBs, LIBs and CVIBs in the original power system (2.36) generically correspond to SNBs in the proposed power system (4.1).

After Section 4.1, several sections and theorems are provided to demonstrate how the original power system model can be described by (4.1).

4.1 Mathematical definition of bifurcation types

Before proceeding with the description of how the power system can be represented by equation (4.1), some clarification is needed about the precise definitions of SNBs, LIBs and CVIBs which will be used throughout this chapter. Each of these bifurcations will be described in one of the following subsections.

4.1.1 Saddle-Node Bifurcation

In Subsection 3.2.1, the saddle-node bifurcation point was defined as a BP where $\partial_{\mathbf{x}}\mathbf{f}$ exists and is singular. The precise definition of a saddle-node bifurcation is given in Definition 1:

Definition 1 (Saddle-Node Bifurcation)**.** *The system of n equations and $n+1$ variables given by*

$$\mathbf{f}(\mathbf{x}, t) = \mathbf{0}\,, \tag{4.2}$$

where:

- $\mathbf{x} \in \mathbb{R}^n$*;*
- $t \in \mathbb{R}$*;*
- $\mathbf{f} : \mathbb{R}^n \times \mathbb{R} \to \mathbb{R}^n$*;*

undergoes a saddle-node bifurcation at point $(\widehat{\mathbf{x}}, \widehat{t})$ if the following conditions hold:

[I] $\mathbf{f}(\widehat{\mathbf{x}}, \widehat{t}) = \mathbf{0}$*;*

[II] $\mathbf{f}$ *is continuously differentiable at* $(\widehat{\mathbf{x}}, \widehat{t})$*;*

[III] $\partial_{\mathbf{x}}\mathbf{f}(\widehat{\mathbf{x}}, \widehat{t})$ *is singular;*

[IV] *There is an unique solution branch passing through $(\widehat{\mathbf{x}}, \widehat{t})$, which can be parameterized by $s \in \mathbb{R}$ and denoted by $(\mathbf{x}(s), t(s))$ such that $(\mathbf{x}(s), t(s)) = (\widehat{\mathbf{x}}, \widehat{t})$ when $s = \widehat{s}$. In addition, $s = \widehat{s}$ is a* critical point[1] *of function $t(s)$.*

[1] The definition of *critical point* used in this situation is the following: $\widehat{\mathbf{x}}$ is a critical point of function $f(\mathbf{x})$ if there is a neighborhood $\mathbb{U}$ of $\widehat{\mathbf{x}}$ such that:

- $f(\mathbf{x}) \geq f(\widehat{\mathbf{x}})\ \forall\ \mathbf{x} \in \overline{\mathbb{U}}$ and $f(\mathbf{x}) > f(\widehat{\mathbf{x}})\ \forall\ \mathbf{x} \in \partial\mathbb{U}$; or

A sketch of a SNB is given in Figure 24, where the solution $\mathbf{x}$ disappear with the increase of t. From this figure, it can be seen that a SNB point is simply the maximum value of t along a unique solution branch. For this reason, the SNB point is also called turning point in the literature (SEYDEL, 2010).

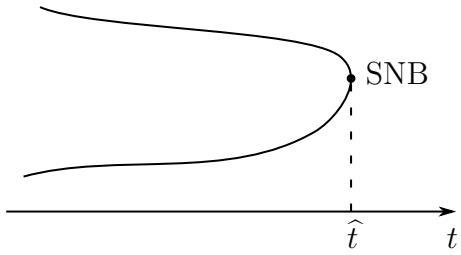

Figure 24 – Sketch of a SNB point.

The definition of SNB given in the literature (SEYDEL, 2010; HALE; KOCAK, 1991) differs from the definition used in this document mainly in relation to condition [IV], usually referred to as the transversality condition of SNB (CUTSEM; VOURNAS, 1998). In the literature, this condition is usually replaced by two separate conditions:

- $\operatorname{rank}\left(\begin{bmatrix}\partial_{\mathbf{x}}\mathbf{f} & \partial_t\mathbf{f}\end{bmatrix}\right) = n$ at the BP. This condition guarantees (according to the Implicit Function Theorem) that there is an unique solution branch that passes through $(\widehat{\mathbf{x}}, \widehat{t})$, and that this point is neither the start nor the end of the solution branch.
- A condition which imposes that $(\widehat{\mathbf{x}}, \widehat{t})$ is a turning point. This condition is usually written as $t''(s) \neq 0$, where s parameterizes the solution branch that passes through $(\widehat{\mathbf{x}}, \widehat{t})$. Equivalent expressions using second-order derivatives of $\mathbf{f}$ also appear in the literature.

Note that every point that satisfies these conditions also satisfy condition [IV]. Therefore, all SNBs according to the literature are also SNBs according to our definition. The converse, however, is not true: our definition does not assume a nonzero curvature of the solution branch at the BP. In fact, our definition does not even assume that second order derivatives exist. This definition was used in this document exactly to require less information about the power system model, by allowing any C^1 function to encounter SNB points.

Even though this definition of SNB is less restrictive, it still requires the existence of an unique solution branch, which filters out degenerate bifurcations, e.g. isolated solutions or bifurcations where several solution branches meet.

- $f(\mathbf{x}) \leq f(\widehat{\mathbf{x}})\ \forall\ \mathbf{x} \in \overline{\mathbb{U}}$ and $f(\mathbf{x}) < f(\widehat{\mathbf{x}})\ \forall\ \mathbf{x} \in \partial\mathbb{U}$.

This definition does not assume that a *critical point* is isolated. In fact, there might be a region of critical points in which $f(\mathbf{x})$ is constant.

4.1.2 Limit-Induced Bifurcation

In Subsection 3.2.1, the limit-induced bifurcation point was defined as a BP where f is not C^1. The precise definition of a limit-induced bifurcation is given in Definition 2:

Definition 2 (Limit-Induced Bifurcation)**.** *The system of n equations and $n+1$ variables given by*

$$\mathbf{f}(\mathbf{x}, t) = \mathbf{0}\,, \tag{4.3a}$$

$$\begin{cases} a(\mathbf{x}, t) = 0, & \text{if } b(\mathbf{x}, t) > 0\,, \\ a(\mathbf{x}, t) \geq 0, & \text{if } b(\mathbf{x}, t) = 0\,, \end{cases} \tag{4.3b}$$

where:

- $\mathbf{x} \in \mathbb{R}^n$;
- $t \in \mathbb{R}$;
- $\mathbf{f} : \mathbb{R}^n \times \mathbb{R} \to \mathbb{R}^{n-1}$;
- $a : \mathbb{R}^n \times \mathbb{R} \to \mathbb{R}$;
- $b : \mathbb{R}^n \times \mathbb{R} \to \mathbb{R}$;

undergoes a limit-induced bifurcation at point $(\widehat{\mathbf{x}}, \widehat{t})$ if the following conditions hold:

[I] $\mathbf{f}(\widehat{\mathbf{x}}, \widehat{t}) = \mathbf{0}$, $a(\widehat{\mathbf{x}}, \widehat{t}) = 0$ *and* $b(\widehat{\mathbf{x}}, \widehat{t}) = 0$;

[II] $\mathbf{f}$, a *and* b *are continuously differentiable at* $(\widehat{\mathbf{x}}, \widehat{t})$;

[III] *both* $\begin{bmatrix} \partial_{\mathbf{x}} \mathbf{f} \\ \partial_{\mathbf{x}} a \end{bmatrix}$ *and* $\begin{bmatrix} \partial_{\mathbf{x}} \mathbf{f} \\ \partial_{\mathbf{x}} b \end{bmatrix}$ *are nonsingular at* $(\widehat{\mathbf{x}}, \widehat{t})$;

[IV] $(\partial_{\mathbf{x}} b\, \boldsymbol{\alpha} + \partial_t b)\,(\partial_{\mathbf{x}} a\, \boldsymbol{\beta} + \partial_t a) > 0$ *at* $(\widehat{\mathbf{x}}, \widehat{t})$, *where* $\boldsymbol{\alpha}$ *is the unique solution of* $\begin{bmatrix} \partial_{\mathbf{x}} \mathbf{f} \\ \partial_{\mathbf{x}} a \end{bmatrix} \boldsymbol{\alpha} + \begin{bmatrix} \partial_t \mathbf{f} \\ \partial_t a \end{bmatrix} = \mathbf{0}$ *and* $\boldsymbol{\beta}$ *is the unique solution of* $\begin{bmatrix} \partial_{\mathbf{x}} \mathbf{f} \\ \partial_{\mathbf{x}} b \end{bmatrix} \boldsymbol{\beta} + \begin{bmatrix} \partial_t \mathbf{f} \\ \partial_t b \end{bmatrix} = \mathbf{0}$.

This definition restricts LIB points to points where the system *structure* changes from being governed by equations

$$\mathbf{f}(\mathbf{x}, t) = \mathbf{0}\,, \tag{4.4a}$$

$$a(\mathbf{x}, t) = 0\,, \tag{4.4b}$$

to being governed by equations

$$\mathbf{f}(\mathbf{x}, t) = \mathbf{0}\,, \tag{4.5a}$$

$$b(\mathbf{x}, t) = 0\,, \tag{4.5b}$$

or vice versa. Note that this usage of the word *structure* is equivalent to the usage of Section 2.10, and that every point where function $\mathbf{f}$ of equation (2.36a) is non-differentiable is a point where the system *structure* changes.

Conditions [II] and [III] of a LIB guarantee, by the Implicit Function Theorem, that there are two implicit functions, namely $\mathbf{x}_a(t)$ and $\mathbf{x}_b(t)$, defined in a vicinity $\mathcal{I}$ of $t = \widehat{t}$, such that:

$$x_a(\widehat{t}) = \widehat{\mathbf{x}}\,, \tag{4.6a}$$

$$\mathbf{f}(\mathbf{x}_a(t), t) = \mathbf{0}\ \forall\ t \in \mathcal{I}\,, \tag{4.6b}$$

$$a(\mathbf{x}_a(t), t) = 0\ \forall\ t \in \mathcal{I}\,, \tag{4.6c}$$

and

$$x_b(\widehat{t}) = \widehat{\mathbf{x}}\,, \tag{4.7a}$$

$$\mathbf{f}(\mathbf{x}_b(t), t) = \mathbf{0}\ \forall\ t \in \mathcal{I}\,, \tag{4.7b}$$

$$b(\mathbf{x}_b(t), t) = 0\ \forall\ t \in \mathcal{I}\,. \tag{4.7c}$$

Condition [IV] of a LIB guarantees the existence of an arbitrarily small neighborhood $\mathcal{I}$ of $t = \widehat{t}$ such that exactly one of the following possibilities is true:

- $a(\mathbf{x}_b(t), t) > 0$ and $b(\mathbf{x}_a(t), t) > 0$ for $t \in \mathcal{I}$ such that $t < \widehat{t}$, while $a(\mathbf{x}_b(t), t) < 0$ and $b(\mathbf{x}_a(t), t) < 0$ for $t \in \mathcal{I}$ such that $t > \widehat{t}$;
- $a(\mathbf{x}_b(t), t) < 0$ and $b(\mathbf{x}_a(t), t) < 0$ for $t \in \mathcal{I}$ such that $t < \widehat{t}$, while $a(\mathbf{x}_b(t), t) > 0$ and $b(\mathbf{x}_a(t), t) > 0$ for $t \in \mathcal{I}$ such that $t > \widehat{t}$.

In the first possibility, two distinct solution branches $(\mathbf{x}_a(t), t)$ and $(\mathbf{x}_b(t), t)$ exist for $t < \widehat{t}$, they coallesce at $t = \widehat{t}$ and disappear for $t > \widehat{t}$. In the second possibility, the two solution branches coalesce and disappear when t is decreased.

Figure 25 shows how two solution branches for the system under two different *structures* coalesce and disappear on a LIB point. The dashed lines in this figure emphasize that the individual solution branches $(\mathbf{x}_a(t), t)$ (of equation (4.4)) and $(\mathbf{x}_b(t), t)$ (of equation (4.5)) still exist for $t > \widehat{t}$, but they both violate either constraint $a(\mathbf{x}, t) \geq 0$ or constraint $b(\mathbf{x}, t) \geq 0$.

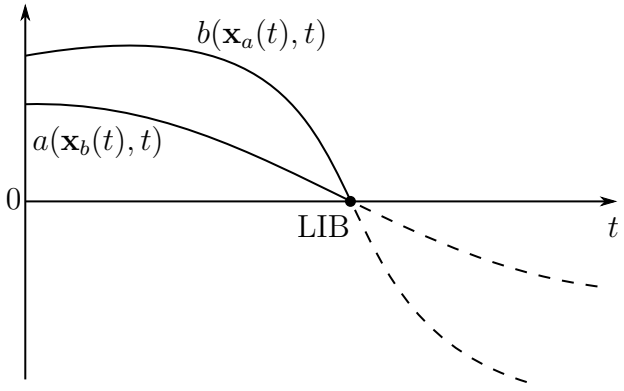

Figure 25 – Sketch of a LIB point.

In the same nomenclature used for the definition of SNB, condition [IV] of a LIB is a transversality condition, which is sufficient to guarantee that there is a solution point in one side of $t = \widehat{t}$, and that this solution vanishes on the other side.

For completeness, it should be emphasized that not all points where the system *structure* changes are bifurcation points. It might be the case that the system is governed by equation (4.4) for $t < \widehat{t}$, the structure changes at $t = \widehat{t}$ and the system can continue to operate for $t > \widehat{t}$ under equation (4.5). A generic point where the system structure changes is called **Transition Point** (TP). The case where the TP is not a BP is sketched in Figure 26. Again, the dashed lines in this figure indicate points that violate either constraint $a(\mathbf{x}, t) \geq 0$ or constraint $b(\mathbf{x}, t) \geq 0$.

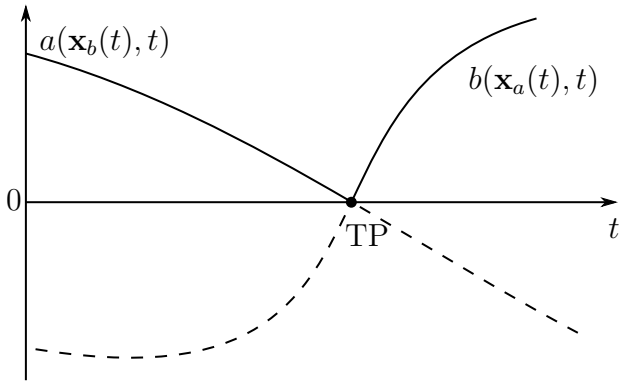

Figure 26 – Sketch of a TP.

The only difference between the case shown in Figure 25 and the case shown in Figure 26 is that Figure 26 does not satisfy condition [IV] of a LIB. Specifically, it can be shown that $(\partial_{\mathbf{x}} b\, \boldsymbol{\alpha} + \partial_t b)\,(\partial_{\mathbf{x}} a\, \boldsymbol{\beta} + \partial_t a) < 0$ for Figure 26, since the derivatives of $a(\mathbf{x}_b(t), t)$ and $b(\mathbf{x}_a(t), t)$ with respect to t have opposite signs at $t = \widehat{t}$.

Example

The usual example of transition points and limit-induced bifurcations in voltage stability is due to Q-limits of synchronous generators (equation (2.9)). Assume that, with the increase of t, the generator changes from being modelled by equation $V = V_{\text{spec}}$ to equation $Q = Q_{\max}$. In the notation used in this subsection, functions a and b are given by:

- $a(\mathbf{x}, t) \equiv Q_{\max} - Q$;
- $b(\mathbf{x}, t) \equiv V_{\text{spec}} - V$.

Note that both V and Q are variables that belong to vector $\mathbf{x}$.

If the change from equation $b(\mathbf{x}, t) = 0$ (i.e., the generator is modelled as constant V) to equation $a(\mathbf{x}, t) = 0$ (i.e., the generator is modelled as constant Q) does not induce

a bifurcation, then this change represents a transition point as the one shown in Figure 26. For this particular example, Figure 26 is redrawn in Figure 27. In this figure, the generator initially is modelled with $V = V_{\text{spec}}$, while the reactive power increases with the increase of t. After the TP, the generator no longer can be modelled with $V = V_{\text{spec}}$ because it would violate constraint $Q \leq Q_{\max}$. As a result, the generator model changes from $V = V_{\text{spec}}$ to $Q = Q_{\max}$.

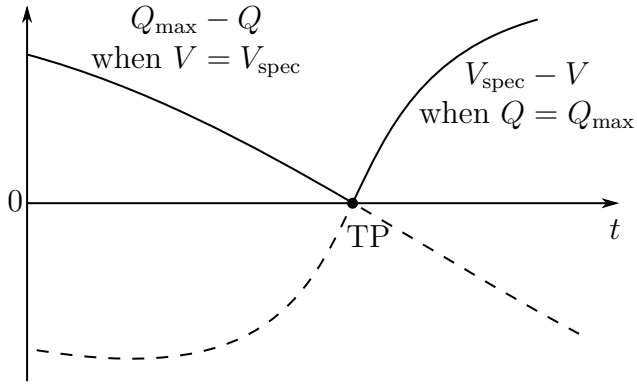

Figure 27 – Sketch of a TP due to the Q-limit of a generator.

From Figure 27, the generator can be modelled as $Q = Q_{\max}$ after the TP because $V \leq V_{\text{spec}}$. Thus, the TP is not a BP. The other possibility was sketched in Figure 25, where the generator cannot be modelled neither with $V = V_{\text{spec}}$ nor with $Q = Q_{\max}$ after the TP, because either constraint $Q \leq Q_{\max}$ or $V \leq V_{\text{spec}}$ (respectively) is violated. Hence, the TP is a LIB point in this case.

4.1.3 Constraint Violation Induced Bifurcation

In Subsection 3.2.1, the constraint violation induced bifurcation point was defined as a BP where inequation (2.36b) is violated. The precise definition of a constraint violation induced bifurcation is given in Definition 3:

Definition 3 (Constraint Violation Induced Bifurcation)**.** *The system of n equations,* 1 *inequation and $n+1$ variables given by*

$$\mathbf{f}(\mathbf{x}, t) = \mathbf{0}\,, \tag{4.8a}$$

$$g(\mathbf{x}, t) \geq 0\,, \tag{4.8b}$$

where:

- $\mathbf{x} \in \mathbb{R}^n$*;*
- $t \in \mathbb{R}$*;*
- $\mathbf{f} : \mathbb{R}^n \times \mathbb{R} \to \mathbb{R}^n$*;*
- $g : \mathbb{R}^n \times \mathbb{R} \to \mathbb{R}$*;*

undergoes a constraint violation induced bifurcation at point $(\widehat{\mathbf{x}}, \widehat{t})$ if the following conditions hold:

[I] $\mathbf{f}(\widehat{\mathbf{x}}, \widehat{t}) = \mathbf{0}$ *and* $g(\widehat{\mathbf{x}}, \widehat{t}) = 0$*;*
[II] $\mathbf{f}$ *and* g *are continuously differentiable at* $(\widehat{\mathbf{x}}, \widehat{t})$*;*
[III] $\partial_{\mathbf{x}}\mathbf{f}(\widehat{\mathbf{x}}, \widehat{t})$ *is nonsingular;*
[IV] $\partial_{\mathbf{x}} g\,\mathbf{v} + \partial_t g \neq 0$ *at* $(\widehat{\mathbf{x}}, \widehat{t})$*, where* $\mathbf{v}$ *is the unique solution of* $\partial_{\mathbf{x}}\mathbf{f}\,\mathbf{v} + \partial_t \mathbf{f} = \mathbf{0}$*.*

Conditions [II] and [III] guarantee that there is an unique solution branch $\mathbf{x}(t)$, defined in $\mathcal{I}$, such that:

$$\mathbf{x}(\widehat{t}) = \widehat{\mathbf{x}}\,, \tag{4.9a}$$

$$\mathbf{f}(\mathbf{x}(t), t) = \mathbf{0}\ \forall\ t \in \mathcal{I}\,, \tag{4.9b}$$

Therefore, $(\widehat{\mathbf{x}}, \widehat{t})$ is not a bifurcation point of equation $\mathbf{f}(\mathbf{x}, t) = \mathbf{0}$. However, condition [IV] guarantees that $g(\mathbf{x}(t), t) < 0$ either for $t < \widehat{t}$ or for $t > \widehat{t}$.

A sketch of a CVIB is shown in Figure 28. In this figure, the dashed line indicates solutions of $\mathbf{f}(\mathbf{x}, t) = \mathbf{0}$ that do not satisfy $g(\mathbf{x}(t), t) \geq 0$.

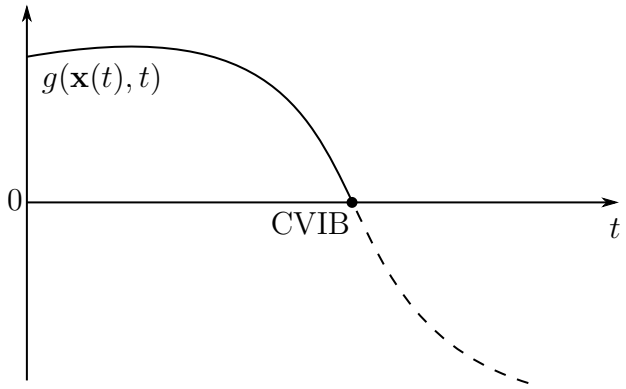

Figure 28 – Sketch of a CVIB point.

The same way as for SNB and LIB, condition [IV] of a CVIB is the transversality condition that guarantees that point $(\widehat{\mathbf{x}}, \widehat{t})$ is in fact a bifurcation point, where the solution disappears for either $t < \widehat{t}$ or $t > \widehat{t}$.

4.1.3.1 Voltage instability caused by a CVIB

When a power system encounters a SNB or a LIB, the equilibrium point is lost and the system actually becomes unstable due to the dynamics. Figures 24 and 25 show that the bifurcation is the collision of two equilibrium points. Typically, one of these points is a type zero equilibrium point and the other one is a type one equilibrium point (DOBSON; CHIANG, 1989; DOBSON; LU, 1992b).

On the other hand, Figure 28 shows that a CVIB is the disappearance of an unique solution branch due to an inequality constraint. In reality, this inequality constraint represents a soft limit (e.g., an undervoltage limit) that does not directly lead the system

to an unstable situation. A violation of a soft limit leads the system to an emergency condition, which in turn might eventually lead to an unstable situation due to the tripping of protection schemes.

For example, assume that one of the inequality constraints of (2.36) is given by $S \leq S_{\max}$, which represents the MVA rating of a transmission line. For a reasonably short time, the system may still operate when this constraint is violated, but eventually the transmission line will be tripped by the protection system. The tripping of an overloaded transmission line may lead to a voltage collapse due to a reduction in the power transfer capability of the transmission system.

Compare this characteristic to the behavior of a power system undergoing a SNB (DOBSON; CHIANG, 1989): in the SNB case, the system moves along the (one-dimensional) center manifold of the SNB point, which consists of a slow dynamics followed by a subsequent fast dynamics that leads to a voltage collapse. This is somewhat similar to the expected behavior of a CVIB, where the transition from a "slow" dynamics to a "fast" dynamics occurs when a protection device is triggered.

Lastly, we reiterate that there is no consensus whether the violation of an inequality constraint should be named a bifurcation. In this document, we adopt this convention following the definition of bifurcation given in Chapter 3, where a bifurcation of equation (2.36) simply is a point where the number of solutions $\mathbf{x}$ of (2.36) changes.

4.2 Handling the clamping effect in controllers

In the modelling shown in Chapter 2, there is a similarity in the mathematical representation of every control characteristic in which a controllable variable y is maintained at a pre-specified setpoint value y_{spec} by means of a control variable u, which must be clamped between its lower bound $u_{\min}$ and upper bound $u_{\max}$. Using a block diagram, this control system is represented by the closed-loop schematic shown in Figure 29.

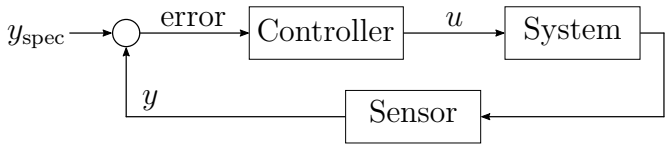

Figure 29 – Closed-loop control system.

If the controller has an integral term and assuming that the control action is stable, the steady-state error is zero, which implies that, in steady-state:

$$y = y_{\text{spec}} \,. \tag{4.10}$$

However, the controller output is limited by the minimum and maximum values of the control variable u. When these bounds are reached, the controller loses the ability

to maintain y at the specified value, and the steady-state representation of the system changes from equation (4.10) to one of the following:

$$u = u_{\min}\,, \tag{4.11a}$$

$$u = u_{\max}\,. \tag{4.11b}$$

Hence, the steady-state characteristic of this control is given by:

$$\begin{cases} u = u_1 & \text{if } y < y_{\text{spec}}\,, \\ \min\{u_1, u_2\} \leq u \leq \max\{u_1, u_2\} & \text{if } y = y_{\text{spec}}\,, \\ u = u_2 & \text{if } y > y_{\text{spec}}\,, \end{cases} \tag{4.12}$$

where $u_1 = u_{\max}$ and $u_2 = u_{\min}$ if, in normal operation, an increase in u leads to an increase in y. On the other hand, if an increase in u leads to a decrease in y, then $u_1 = u_{\min}$ and $u_2 = u_{\max}$.

It should be noted the set of equations

$$\mathbf{f}(\mathbf{x}, t) = \mathbf{0}\,, \tag{4.13a}$$

$$\begin{cases} u = u_1 & \text{if } y < y_{\text{spec}}\,, \\ \min\{u_1, u_2\} \leq u \leq \max\{u_1, u_2\} & \text{if } y = y_{\text{spec}}\,, \\ u = u_2 & \text{if } y > y_{\text{spec}}\,, \end{cases} \tag{4.13b}$$

is locally an instance of equation (4.3). For example, if u is away from u_2, then (4.35) locally becomes:

$$\mathbf{f}(\mathbf{x}, t) = \mathbf{0}\,, \tag{4.14a}$$

$$\begin{cases} u = u_1 & \text{if } y < y_{\text{spec}}\,, \\ \min\{u_1, u_2\} \leq u \leq \max\{u_1, u_2\} & \text{if } y = y_{\text{spec}}\,, \end{cases} \tag{4.14b}$$

and if we assume that $u_1 < u_2$, then:

$$\mathbf{f}(\mathbf{x}, t) = \mathbf{0}\,, \tag{4.15a}$$

$$\begin{cases} u = u_1 & \text{if } y < y_{\text{spec}}\,, \\ u_1 \leq u \leq u_2 & \text{if } y = y_{\text{spec}}\,, \end{cases} \tag{4.15b}$$

but since u is away from u_2, we can (locally) ignore the upper bound, thus:

$$\mathbf{f}(\mathbf{x}, t) = \mathbf{0}\,, \tag{4.16a}$$

$$\begin{cases} u = u_1 & \text{if } y < y_{\text{spec}}\,, \\ u_1 \leq u & \text{if } y = y_{\text{spec}}\,, \end{cases} \tag{4.16b}$$

which is the same as:

$$\mathbf{f}(\mathbf{x}, t) = \mathbf{0}\,, \tag{4.17a}$$

$$\begin{cases} u - u_1 = 0 & \text{if } y_{\text{spec}} - y > 0\,, \\ u - u_1 \geq 0 & \text{if } y_{\text{spec}} - y = 0\,, \end{cases} \tag{4.17b}$$

showing that (4.35) is (4.3) with $a(\mathbf{x}, t) = u - u_1$ and $b(\mathbf{x}, t) = y_{\text{spec}} - y$. In this case, variables u and y are elements of vector $\mathbf{x}$. Since (4.35) locally is a particular case of (4.3), the system (4.35) is subject to TPs and LIBs the same way as (4.3).

For conciseness, equation (4.12) will sporadically be represented as:

$$f_{\text{control}}(y, u) = 0\,, \tag{4.18}$$

where parameters y_{spec}, u_1 and u_2 are omitted for convenience.

The set of solutions of (4.18) can be represented in the yu-plane as shown in Figure 30, where it is assumed that $u_1 < u_2$. For any solution of the power system model, point (y, u) should belong to this solution set. In this figure, the points where the system *structure* changes between saturated and unsaturated modes are highlighted as transition points. These are exactly the same transition points defined in Subsection 4.1.2.

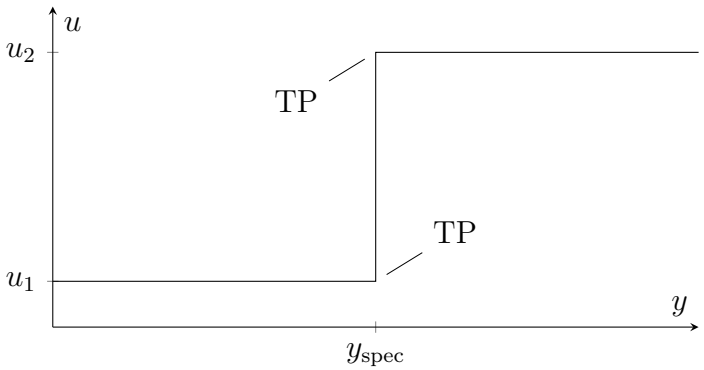

Figure 30 – Solution set of equation (4.18).

The generic control characteristic with no steady-state error shown in equation (4.18) was encountered in several devices in Chapter 2, namely:

- Generator equation (2.9), where $y = V$ and $u = Q$;
- LTC equation (2.13), where $y = V$ and $u = \tau$;
- PST equation (2.14), where $y = P$ and $u = \phi$;
- HVDC link rectifier equation (2.22), where $y = I_{\text{DC}}$ and $u = \alpha$;
- HVDC link inverter equation (2.23), where $y = I_{\text{DC}}$ and $u = \gamma$;
- SVC equation (2.27), where $y = V$ and $u = b$;
- STATCOM equation (2.30), where $y = V$ and $u = I$;
- VLID equation (2.33), where $y = Q$ and $u = V$.

Therefore, the discontinuities in all these equations are instances of the discontinuities in Figure 30. If we demonstrate that it is possible to transform LIBs associated with the TPs of equation (4.18) into corresponding SNBs, then it is demonstrated that LIBs corresponding to all devices listed above can be transformed into SNBs. In fact, a new model to represent equation (4.18) is proposed in the next subsection.

4.2.1 Proposed representation of equation (4.18)

Let a *smooth step function* be defined as follows:

Definition 4 (Smooth step function)**.** *A* smooth step function *is a family of* C^1 *functions* $g_\gamma : \mathbb{R}^4 \to \mathbb{R}$*, parameterized by a scalar variable* $\gamma > 0$ *and satisfying the following properties:*

[I] $\lim_{\gamma\to 0^+} g_\gamma(y, y_{spec}, u_1, u_2) = u_1 \; \forall \; y < y_{spec}$*;*
[II] $\lim_{\gamma\to 0^+} g_\gamma(y, y_{spec}, u_1, u_2) = u_2 \; \forall \; y > y_{spec}$*;*
[III] *there is* $\alpha \in (0, |u_1 - u_2|)$ *such that* $\min\{u_1, u_2\} + \alpha \leq g_\gamma(y_{spec}, y_{spec}, u_1, u_2) \leq \max\{u_1, u_2\} - \alpha$ *for all* γ*;*
[IV] *there is* $\zeta > 0$ *such that* $\min\{u_1, u_2\} \leq g_\gamma(y, y_{spec}, u_1, u_2) \leq \max\{u_1, u_2\} \; \forall \; y \in [y_{spec} - \zeta, y_{spec} + \zeta]$ *for all* γ*;*
[V] *for all* γ*,* g_γ *changes concavity in relation to* y *only at* $y = y_{spec}$*.*

Hereinafter, smooth step functions *will be written in the simplified form given by* $g_\gamma(y)$*.*

An example of a *smooth step function* that will be used throughout this document is:

$$g_\gamma(y) = \begin{cases} u_1, & \text{if } y \leq y_{\text{spec}} - \gamma/2\,, \\ u_2, & \text{if } y \geq y_{\text{spec}} + \gamma/2\,, \\ p(y), & \text{otherwise}\;, \end{cases} \tag{4.19}$$

where p is a cubic polynomial in variable y whose four coefficients satisfy the following equations:

$$p\left(y_{\text{spec}} - \frac{\gamma}{2}\right) = u_1\,, \qquad p\left(y_{\text{spec}} + \frac{\gamma}{2}\right) = u_2\,, \tag{4.20a}$$

$$p'\left(y_{\text{spec}} - \frac{\gamma}{2}\right) = 0\,, \qquad p'\left(y_{\text{spec}} + \frac{\gamma}{2}\right) = 0\,. \tag{4.20b}$$

By solving the respective linear system, polynomial p is given by:

$$p(y) = \frac{u_1 + u_2}{2} + \frac{u_2 - u_1}{2}\left(3\left(\frac{y - y_{\text{spec}}}{\gamma}\right) - 4\left(\frac{y - y_{\text{spec}}}{\gamma}\right)^3\right) \tag{4.21}$$

It can be easily shown that function g_γ defined in (4.19) is C^1 in the entire domain of $(y, y_{\text{spec}}, u_1, u_2)$. Also, properties [I] and [II] of a *smooth step function* are easily verified.

From equations (4.19) and (4.21), $g_\gamma(y_{\text{spec}}) = p(y_{\text{spec}}) = \frac{u_1+u_2}{2}$. Hence, property [III] is satisfied whenever $u_1 \neq u_2$.

By definition, the two critical points of the cubic polynomial p are $y = y_{\text{spec}} - \gamma/2$ (where $p(y) = u_1$) and $y = y_{\text{spec}} + \gamma/2$ (where $p(y) = u_2$). Hence, $u_1 \leq p(y) \leq u_2 \; \forall \; y \in [y_{\text{spec}} - \gamma/2, y_{\text{spec}} + \gamma/2]$, which demonstrates property [IV].

Function g_γ of equation (4.19) changes concavity only when p changes concavity. A cubic polynomial only changes concavity in the mean of its critical points, so g_γ changes concavity at $\frac{(y_{\text{spec}}-\gamma/2)+(y_{\text{spec}}+\gamma/2)}{2} = y_{\text{spec}}$, which demonstrates property [V].

Function (4.19) is graphically shown in Figure 31. The curve in this figure is identical to the one in Figure 30, except in the interval $\left(y_{\text{spec}} - \frac{\gamma}{2}, y_{\text{spec}} + \frac{\gamma}{2}\right)$ which has length γ. As γ approaches zero, the behavior of the following equation:

$$u = g_\gamma(y)\,, \tag{4.22}$$

approaches the behavior of equation (4.18). This is not a particularity of equation (4.19), but rather it is a characteristic of every instance of a *smooth step function*.

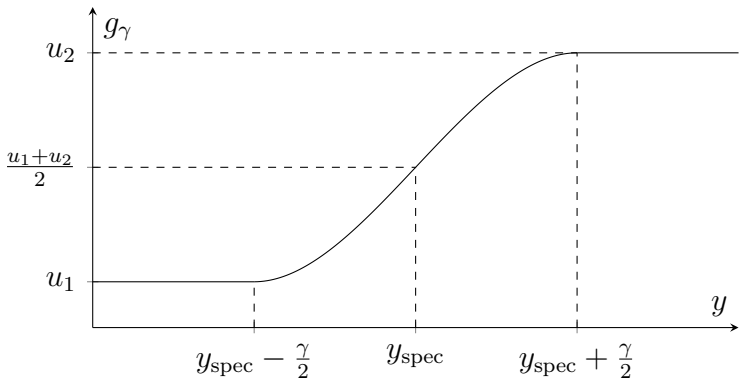

Figure 31 – Graphical representation of function (4.19).

In the remainder of this section, let the power system (2.36) be written as:

$$\mathbf{f}_a(y, u, \mathbf{z}, t) = \mathbf{0}\,, \tag{4.23a}$$

$$f_b(y, u) = 0\,, \tag{4.23b}$$

where:

- $\mathbf{z} \in \mathbb{R}^{n-2}$;
- $y, u \in \mathbb{R}$;
- $\mathbf{x}^T = \begin{bmatrix}\mathbf{z}^T & y & u\end{bmatrix}$ (recall that $\mathbf{x} \in \mathbb{R}^n$);
- $\mathbf{f}_a : \mathbb{R} \times \mathbb{R} \times \mathbb{R}^{n-2} \times \mathbb{R} \to \mathbb{R}^{n-1}$;
- $f_b : \mathbb{R} \times \mathbb{R} \to \mathbb{R}$;
- $\mathbf{f}(\mathbf{x}, t) \equiv \begin{bmatrix}\mathbf{f}_a(y, u, \mathbf{z}, t) \\ f_b(y, u)\end{bmatrix}$ (recall that $\mathbf{f} : \mathbb{R}^n \times \mathbb{R} \to \mathbb{R}^n$).

Vector $\mathbf{x}$ is the state vector of system (2.36), while function f_b is an instance of f_{control}. To simplify notation, vectors $\mathbf{p}$ and $\mathbf{u}$ of system (2.36) are omitted in (4.23). Furthermore, inequation (2.36b) is assumed to be satisfied in this section for simplicity (these inequality constraints will be handled in Section 4.4).

In this work, we propose to replace equation (4.23b) in (4.23) by one instance of equation (4.22), where g_γ is a *smooth step function*. Hence, system (4.23) is transformed into:

$$\mathbf{f}_a(y, u, \mathbf{z}, t) = \mathbf{0}\,, \tag{4.24a}$$

$$u = g_\gamma(y)\,. \tag{4.24b}$$

Hereinafter, system (4.23) will be denoted by the "original system", while system (4.24) will be referred to as the "smoothed system".

In the following subsections, several theorems are presented to demonstrate that the behavior of the original system can be properly approximated by the behavior of the smoothed system.

4.2.2 The validity of the smoothed system

We say that system (4.23) can be correctly approximated by system (4.24) if any solution of (4.23) is arbitrarily near to a solution of (4.24), and vice versa. In this subsection, four theorems are provided to demonstrate that the smoothed system is a valid approximation of the original system, and the accuracy of the smoothed system can be controlled by parameter γ in equation (4.24b).

In order to prove that the smoothed system (4.24) is a valid approximation of the original system (4.23), we initially prove that equation (4.24b) (which is one instance of (4.22)) is a valid approximation of (4.23b) (which is one instance of (4.18)). This is demonstrated by Theorems 2 and 3.

The following theorem proves that any solution of (4.18) is arbitrarily close to a solution of (4.22).

Theorem 2. *For a sufficiently small $\gamma > 0$, equation* (4.22) *admits a solution arbitrarily close to any solution $(\widehat{y}, \widehat{u})$ of equation* (4.18).

Proof. The proof is given in Section A.1. □

The next theorem establishes that the converse of Theorem 2 is also true: any solution of (4.22) is arbitrarily close to a solution of (4.18).

Theorem 3. *For a sufficiently small $\gamma > 0$, equation* (4.18) *admits a solution arbitrarily close to any solution $(\widehat{y}, g_\gamma(\widehat{y}))$ of equation* (4.22).

Proof. The proof is given in Section A.2. □

Supported by Theorem 2, the following theorem establishes that any solution of (4.23) is arbitrarily close to a solution of (4.24):

Theorem 4. *Assume that* $\mathbf{f}_a$ *is* C^1 *in a neighborhood of a solution* $(\widehat{y}, \widehat{u}, \widehat{\mathbf{z}}, \widehat{t})$ *of* (4.23).

Then, for a sufficiently small $\gamma > 0$*, the smoothed system* (4.24) *generically admits a solution* $(\widetilde{y}(\gamma), \widetilde{u}(\gamma), \widetilde{\mathbf{z}}(\gamma), \widetilde{t}(\gamma))$ *(implicitly parameterized by* γ*) arbitrarily close to the solution* $(\widehat{y}, \widehat{u}, \widehat{\mathbf{z}}, \widehat{t})$ *of the original system* (4.23).

Proof. The proof is given in Section A.3. □

Supported by Theorem 3, the following theorem establishes that any solution of (4.24) is arbitrarily close to a solution of (4.23):

Theorem 5. *Assume that* $\mathbf{f}_a$ *is* C^1 *in a neighborhood of a solution* $(\widetilde{y}(\gamma), \widetilde{u}(\gamma), \widetilde{\mathbf{z}}(\gamma), \widetilde{t}(\gamma))$ *(implicitly parameterized by* γ*) of* (4.24).

Then, for a sufficiently small $\gamma > 0$*, the original system* (4.23) *generically admits a solution* $(\widehat{y}, \widehat{u}, \widehat{\mathbf{z}}, \widehat{t})$ *arbitrarily close to the solution* $(\widetilde{y}(\gamma), \widetilde{u}(\gamma), \widetilde{\mathbf{z}}(\gamma), \widetilde{t}(\gamma))$ *of the smoothed system* (4.24).

Proof. The proof is given in Section A.4. □

Theorem 4 demonstrates that all solutions of the original system are near solutions of the smoothed system. Similarly, Theorem 5 establishes that all solutions of the smoothed system are near solutions of the original system. Together, these theorems prove that the smoothed system (4.24) is indeed a valid approximation of system (4.23).

4.2.2.1 Example

The following example illustrates the results of Theorems 4 and 5, showing that solution points of the smoothed system (4.24) are arbitrarily close to solution points of the original system (4.23), and vice versa.

We apply the *smooth step function* formulation to model the Q-limits of a synchronous generator of the three-bus system shown in Figure 32, composed of one infinite bus (bus 1), one generation bus (bus 2), and one load bus (bus 3). The generator connected at bus 2 operates as a synchronous condenser, thus its active power is zero. Parameters y_{se} and y_{sh} are the series and shunt admittance of the transmission line, according to equation (2.12). These parameters are the same for both transmission lines. The power

flow equations for this system are:

$$jQ_2 - S_2(E_2, E_3) = 0\,, \tag{4.25a}$$

$$-S_3(t) - S_3(E_2, E_3) = 0\,, \tag{4.25b}$$

$$f_{\text{control}}(V_2, Q_2) = 0\,, \tag{4.25c}$$

where E_2 and E_3 are the complex voltages at buses 2 and 3 and Q_2 is the reactive power output of the generator at bus 2. $S_2(E_2, E_3)$ and $S_3(E_2, E_3)$ are the complex powers demanded at buses 2 and 3 computed by means of the transmission system (equation (2.12)), while $S_3(t) = (0.8 + j0.6)t$ is the specified load at bus 3. This system of 5 real variables and 5 real equations can be solved for a given t. When $t \approx 0.5054$, the generator operates at the TP $(V_2, Q_2) = (V_{\text{spec}}, Q_{\text{min}})$ (this will later be verified in the solution curve of Figure 39). The solution for $t \approx 0.5054$ is given in the last row of Table 1.

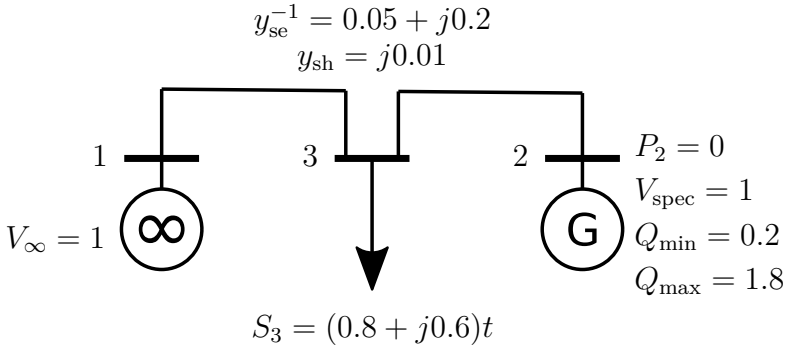

Figure 32 – The three-bus system.

In the smooth model, we replace (4.25c) by $Q_2 = g_\gamma(V_2)$. Using (4.19) as the *smooth step function*, solution points for this system are shown in Table 1. Note that, with the decrease of γ, the smooth solution point approaches the original one.

Table 1 – Three-bus system: solution points for $t \approx 0.5054$.

Model	E_2	E_3	Q_2
$\gamma = 0.5$	$1.108\angle{-0.1151}$	$1.014\angle{-0.09179}$	0.512
$\gamma = 0.2$	$1.06\angle{-0.1045}$	$0.9892\angle{-0.08656}$	0.3655
$\gamma = 0.02$	$1.009\angle{-0.09339}$	$0.9625\angle{-0.08141}$	0.2225
$\gamma = 0.002$	$1.001\angle{-0.09175}$	$0.9586\angle{-0.08068}$	0.2025
Original	$1\angle{-0.09155}$	$0.9581\angle{-0.08059}$	0.2

4.2.3 Transforming generic bifurcations into SNBs

The original system (4.23) can generically undergo two bifurcation types: SNB and LIB. Assuming that $\mathbf{f}_a$ is C^1, an LIB may only occur if the BP is the TP of equation (4.23b). These TPs were graphically sketched in Figure 30. On the other hand, system (4.23) undergoes a SNB if the BP is not a TP of equation (4.23b).

Bifurcation diagrams are typically represented as in Figures 24 and 25. However, it is also possible to represent the variation of a solution point with the change in t in the state space, as shown in Figures 33 and 34. These figures show several possibilities of how two distinct solution points, projected in the yu-plane, can coalesce in a bifurcation point. In all these figures, the dots indicate solution points and the arrows indicate how a particular solution point moves with the increase of t. All bifurcation points shown in Figures 33 and 34 are bifurcations where two solutions disappear with the increase of t. If the arrows were reversed, the bifurcation points would represent points where two solutions are born with the increase of t.

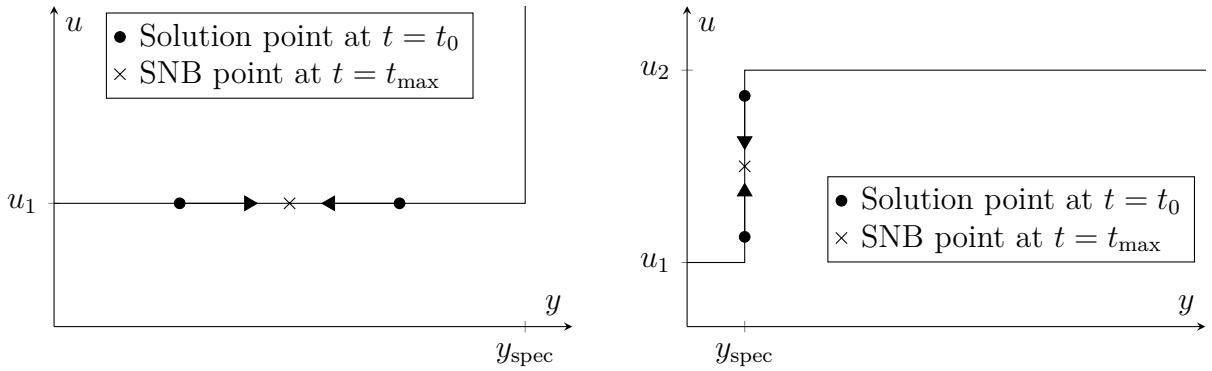

(a) BP for $u = u_1$. (b) BP for $y = y_{\text{spec}}$.

Figure 33 – The SNB occurrence in the yu-plane, assuming that $u_1 < u_2$ and two solutions disappear with the increase of t. The arrows indicate the direction of variation of the solution point when t is increased.

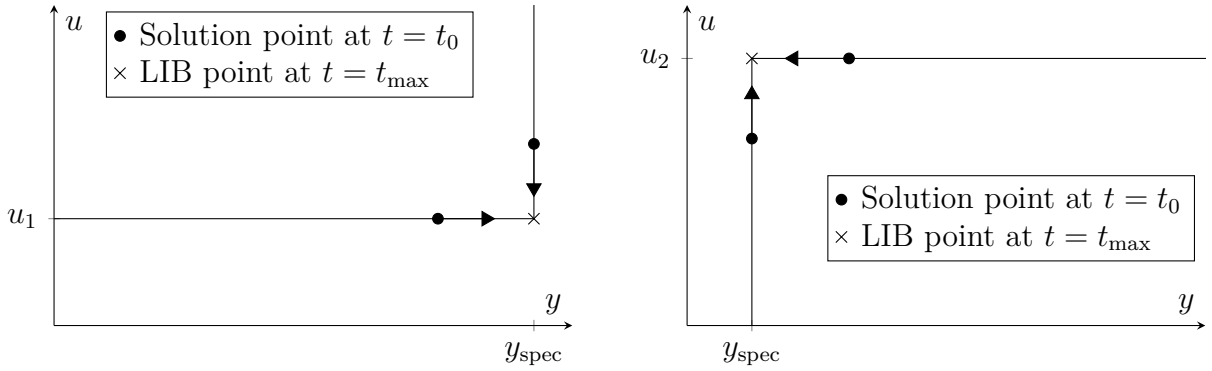

(a) BP at (y_{spec}, u_1). (b) BP at (y_{spec}, u_2).

Figure 34 – The LIB occurrence due to (4.18) in the yu-plane, assuming that $u_1 < u_2$ and two solutions disappear with the increase of t. The arrows indicate the direction of variation of the solution point when t is increased.

Note that Figures 33 and 34 represent exactly the same behavior as Figures 24 and 25, respectively. The only difference between these figures is the bi-dimensional plane in which the multidimensional solution branches are projected.

Figures 33 and 34 show that bifurcations are intrinsically related to how t varies when the current point (y, u) is shifted along the set of solutions of Figure 30. Thus,

conditions for the existence of bifurcations in both the original system and the smoothed system can be easily written in terms of intermediary theorems. These intermediary theorems, namely Theorem 6 and Theorem 7, will then be used to demonstrate that generic bifurcations of the original system are transformed into SNBs in the smoothed system.

The next two theorems (Theorems 6 and 7) are written in terms of a generic function $h(y,u)$. This function will become an implicit function $t(y,u)$ in Theorems 8, 9 and 10, which prove the equivalency between bifurcation points of systems (4.23) and (4.24). Function $t(y,u)$ simply represents how t in the solution of systems (4.23) and (4.24) varies when a solution point moves in the yu-plane.

Theorem 6. *Let $h(y,u):\mathbb{R}\times\mathbb{R}\to\mathbb{R}$ be any C^1 function defined in a neighborhood of a solution $(\widehat{y},\widehat{u})$ of (4.18) such that $\widehat{y}\neq y_{spec}$. Assume that $\partial_y h(\widehat{y},\widehat{u})\neq 0$.*

Define $\mu(y)\equiv h(y,g_\gamma(y))$, where g_γ is a smooth step function.

Then, for a sufficiently small $\gamma>0$, $\mu'(\widetilde{y})\,\partial_y h(\widehat{y},\widehat{u})>0$, where $(\widetilde{y},g_\gamma(\widetilde{y}))$ is arbitrarily close to $(\widehat{y},\widehat{u})$.

Proof. The proof is given in Section A.5. □

Albeit abstract, the result of Theorem 6 is directly explored in Corollary 1.

Corollary 1. *Let $h(y,u):\mathbb{R}\times\mathbb{R}\to\mathbb{R}$ be any C^1 function defined in a neighborhood of $(\widehat{y},\widehat{u})$, where $(\widehat{y},\widehat{u})$ is a solution of (4.18) such that $\widehat{y}\neq y_{spec}$.*

For a sufficiently small $\gamma>0$, Theorem 2 guarantees the existence of a solution $(\widetilde{y},\widetilde{u})$ of (4.22) arbitrarily close to $(\widehat{y},\widehat{u})$.

Assume that both solutions $(\widehat{y},\widehat{u})$ and $(\widetilde{y},\widetilde{u})$ can move along the solution sets of (4.18) and (4.22), respectively.

Then, in order to increase h, both solutions $(\widehat{y},\widehat{u})$ and $(\widetilde{y},\widetilde{u})$ should move in the same direction of y, i.e., they both should either increase y or decrease y.

Proof. The proof is given in Section A.6. □

Figure 35 illustrates the result of Corollary 1. This corollary establishes that $(\widehat{y},\widehat{u})$ and $(\widetilde{y},\widetilde{u})$ are arbitrarily close to each other (i.e., the dotted circle in Figure 35 can be arbitrarily small), and that h will increase when these points move in the same direction of y. In this figure, the arrows indicate that h increases when both points move to the right.

Theorem 7. *Let $h(y,u):\mathbb{R}\times\mathbb{R}\to\mathbb{R}$ be any C^1 function defined in a neighborhood of $(y_{spec},\widehat{u})$, where $\min\{u_1,u_2\}<\widehat{u}<\max\{u_1,u_2\}$. Assume that $\partial_u h(y_{spec},\widehat{u})\neq 0$*

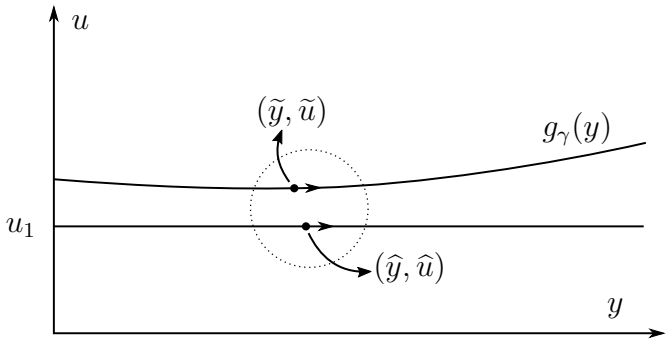

Figure 35 – Graphical visualization of Corollary 1.

Define $\mu(y) \equiv h(y, g_\gamma(y))$*, where* g_γ *is a* smooth step function.

Then, for a sufficiently small $\gamma > 0$*,* $(u_2 - u_1)\,\mu'(\widetilde{y})\,\partial_u h(y_{spec}, \widehat{u}) > 0$*, where* $(\widetilde{y}, g_\gamma(\widetilde{y}))$ *is arbitrarily close to* $(y_{spec}, \widehat{u})$*.*

Proof. The proof is given in Section A.7. □

Corollary 2. *Let* $h(y, u) : \mathbb{R} \times \mathbb{R} \to \mathbb{R}$ *be any* C^1 *function defined in a neighborhood of* $(y_{spec}, \widehat{u})$*, where* $(y_{spec}, \widehat{u})$ *is any solution of* (4.18) *such that* $\min\{u_1, u_2\} < \widehat{u} < \max\{u_1, u_2\}$*.*

For a sufficiently small $\gamma > 0$*, Theorem 2 guarantees the existence of a solution* $(\widetilde{y}, \widetilde{u})$ *of* (4.22) *arbitrarily close to* $(\widehat{y}, \widehat{u})$*.*

Assume that both solutions $(\widehat{y}, \widehat{u})$ *and* $(\widetilde{y}, \widetilde{u})$ *can move along the solution sets of* (4.18) *and* (4.22)*, respectively.*

Then, in order to increase h*, both solutions* $(\widehat{y}, \widehat{u})$ *and* $(\widetilde{y}, \widetilde{u})$ *should move in the same direction of* u*, i.e., they both should either increase* u *or decrease* u*.*

Proof. The proof is given in Section A.8. □

While Corollary 1 establishes how h varies with y, Corollary 2 establishes how h varies with u. Figure 36 illustrates the result of Corollary 2, in a similar way to how Figure 35 illustrates Corollary 1.

Together, Corollaries 1 and 2 can be used to prove that every generic bifurcation of the original system (4.23) corresponds to a saddle-node bifurcation of the smoothed system (4.24). The converse is also true: every saddle-node bifurcation of the smoothed system (4.24) corresponds to a generic bifurcation of the original system (4.23). These results are established by Theorems 8, 9 and 10.

Theorem 8. *Consider that* $\mathbf{f}_a$ *is* C^1 *in a neighborhood of a SNB point* $(\widehat{y}, \widehat{u}, \widehat{\mathbf{z}}, \widehat{t})$ *of the original system.*

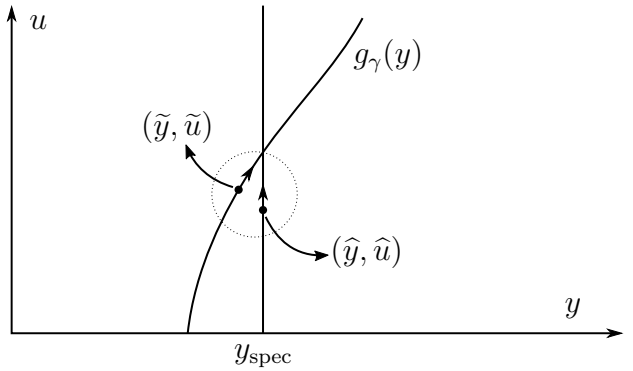

Figure 36 – Graphical visualization of Corollary 2.

Then, for a sufficiently small $\gamma > 0$, the smoothed system (4.24) *generically admits a SNB point $(\widetilde{y}(\gamma), \widetilde{u}(\gamma), \widetilde{\mathbf{z}}(\gamma), \widetilde{t}(\gamma))$ (implicitly parameterized by γ) arbitrarily close to the SNB point of the original system* (4.23).

Proof. The proof is given in Section A.9. □

With the results of Corollaries 1 and 2, Theorem 8 establishes the existence of a SNB by proving the birth or death of two solution points. Figure 37 illustrates how Theorem 8 proves the existence of the SNB of the smoothed system. The arrows indicate the direction of variation of the solution point with the increase of t, thus two solutions are originated at both bifurcation points with the increase of t. Since the enclosing ellipse can be arbitrarily small, both BPs are arbitrarily close to each other.

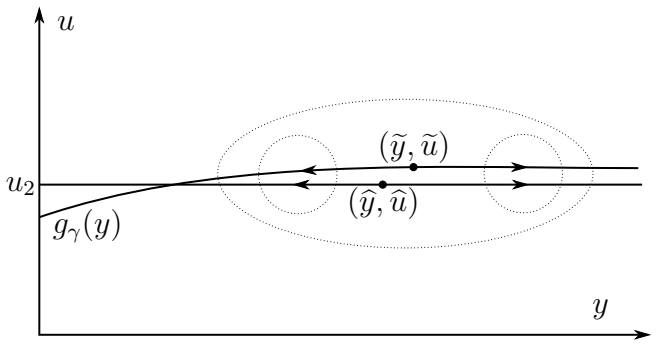

Figure 37 – Graphical visualization of Theorem 8.

Theorem 9. *For a sufficiently small $\gamma > 0$, the smoothed system* (4.24) *admits a SNB point $(\widetilde{y}(\gamma), \widetilde{u}(\gamma), \widetilde{\mathbf{z}}(\gamma), \widetilde{t}(\gamma))$ (implicitly parameterized by γ) arbitrarily close to the LIB point $(\widehat{y}, \widehat{u}, \widehat{\mathbf{z}}, \widehat{t})$ of the original system* (4.23) *due to* (4.24b).

Moreover, if the solution point disappears with the increase of t, then $\widetilde{t} < \widehat{t}$. If the solution point disappears with the decrease of t, then $\widetilde{t} > \widehat{t}$.

Proof. The proof is given in Section A.10. □

Figure 38 illustrates how Theorem 9 proves the existence of a SNB of the smoothed system corresponding to the LIB of the original system. The arrows indicate the direction of variation of the solution point with the increase of t, thus two solutions coalesce and disappear at both bifurcation points with the increase of t. Since the enclosing ellipse can be arbitrarily small, both BPs are arbitrarily close to each other. Figure 38 also emphasizes the intervals α and ζ (given from the definition of a *smooth step function*) which guarantee that $\widetilde{t} < \widehat{t}$. This property is important, as it establishes that the smooth formulation is conservative: if, for a given t, there is a solution of (4.24) close to a LIB point of (4.23), then there is also a solution of (4.23) for the same t.

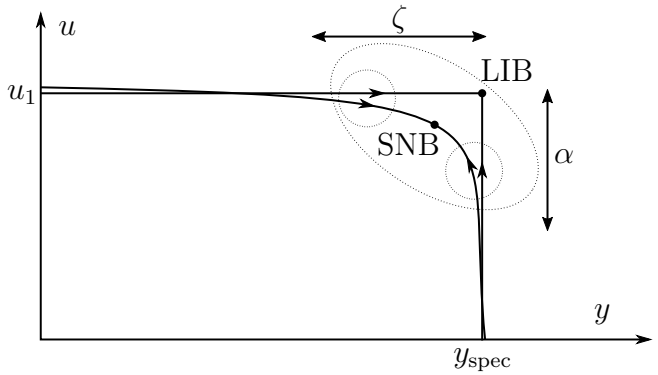

Figure 38 – Graphical visualization of Theorem 9.

Theorem 10. *Consider that* $\mathbf{f}_a$ *is* C^1 *in a neighborhood of a SNB point* $(\widetilde{y}(\gamma), \widetilde{u}(\gamma), \widetilde{\mathbf{z}}(\gamma), \widetilde{t}(\gamma))$ *(implicitly parameterized by* γ*) of the smoothed system,.*

Then, for a sufficiently small $\gamma > 0$*, the original system* (4.23) *generically undergoes either a SNB or a LIB at a point* $(\widehat{y}, \widehat{u}, \widehat{\mathbf{z}}, \widehat{t})$ *arbitrarily close to the SNB point* $(\widetilde{y}(\gamma), \widetilde{u}(\gamma), \widetilde{\mathbf{z}}(\gamma), \widetilde{t}(\gamma))$ *of the smoothed system* (4.24)*.*

Proof. The proof is given in Section A.11. □

4.2.3.1 Example

This subsection illustrates that saddle-node bifurcation points of the smoothed system (4.24) are arbitrarily close to generic bifurcation points of the original system (4.23) (namely saddle-node bifurcations and limit-induced bifurcations), and vice-versa. These are the statements of Theorems 8, 9 and 10.

To illustrate the results of these theorems, the three-bus system of Figure 32 is analyzed again. Solution branches are shown in Figure 39 for this system. Corroborating the results of Theorems 4 and 5, Figure 39 shows that the solution branch of the smoothed system approaches the solution branch of the original system when γ is decreased. Corroborating the results of Theorems 9 and 10, the BPs of the original and smoothed systems approach each other when γ is decreased.

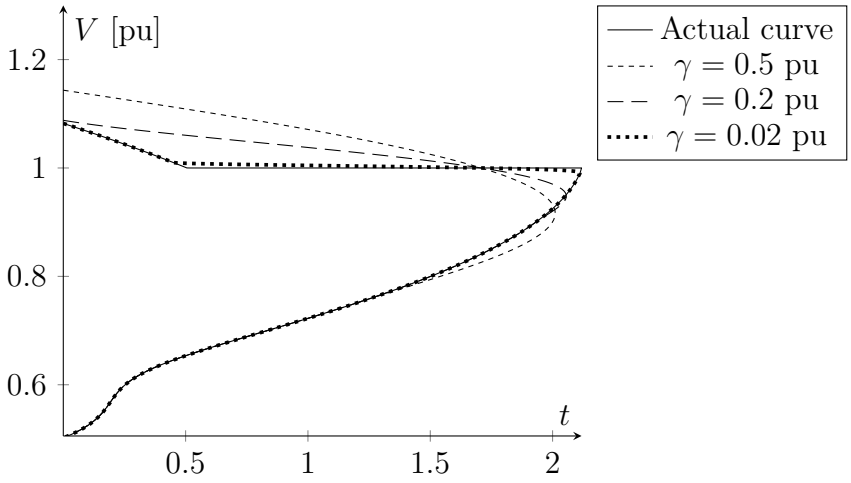

Figure 39 – Three-bus system: Solution branches for bus 2.

It is possible to infer that the BP of the original system is an LIB by noticing that the BP is the collision of two solution branches under two different *structures*[2]. Specifically, equation (4.23b) is equation $V = V_{\text{spec}}$ for one solution branch and $Q = Q_{\max}$ for the other one.

Another important result of Theorem 9 is that the maximum value of t for at the SNB point of the smoothed system is less than the maximum value of t for the LIB point of the original system. This result is shown in Figure 39, and indicates that the VSM for the smoothed system is conservative in relation to the original value of VSM. This emphasizes that the smooth formulation provides conservative results.

Assume now that S_3 in equation (4.25) is not constrained by the straight line $S_3(t) = (0.8 + j0.6)t$, but rather it can be any value $P_3 + jQ_3$ such that $Q_3 > 0$. This three-bus system now can undergo different bifurcations depending on which direction $|S_3|$ increases. Moreover, different bifurcation points may lead to different bifurcation types. Figure 40 shows different bifurcations of the original system (4.25) in the complex plane of S_3. From this figure, the original power system can undergo SNBs when $f_{\text{control}}(V_2, Q_2)$ in equation (4.25) is either $V_2 - V_{\text{spec}}$ or $Q_2 - Q_{\max}$. Between these SNB points, the system encounters LIBs where $(V_2, Q_2) = (V_{\text{spec}}, Q_{\max})$. Note that the Jacobian of (4.25) is *not* singular at these LIB points (in fact, this Jacobian is not even defined).

In addition to the bifurcation surface of Figure 40, Figure 41 shows the bifurcation surface when (4.25c) is replaced by $Q_2 = g_\gamma(V_2)$. Two bifurcation surfaces are shown, one for $\gamma = 1$ pu and one for $\gamma = 0.1$ pu. It can be seen that, as γ approaches zero, the bifurcation surface of the smoothed system approaches the original bifurcation surface (corroborating the result of Theorems 8, 9 and 10). The main difference between bifurcations of the original system and the smoothed system, however, is the fact that all bifurcation points of the smoothed system are generically SNBs. Indeed, the Implicit Function Theorem

[2] see Subsection 4.1.2

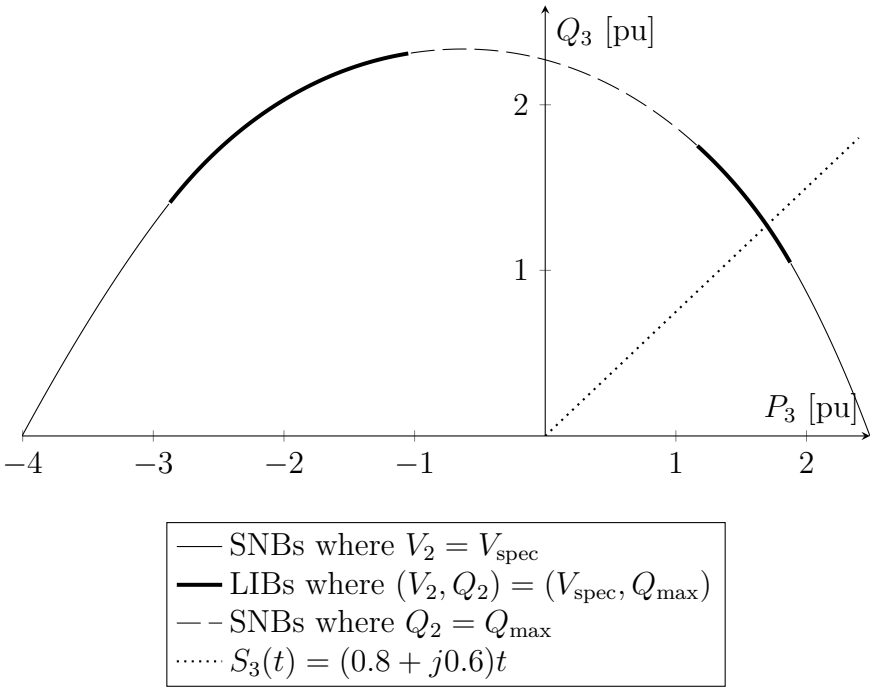

Figure 40 – Bifurcation surface in the complex plane.

guarantees that every bifurcation point of the smoothed system (say $\mathbf{h}(\mathbf{z}) = \mathbf{0}$) is a point where the Jacobian $\partial_{\mathbf{z}}\mathbf{h}(\mathbf{x})$ is singular. Hence, all bifurcation points can be computed in a unified way, because all bifurcation points, without exception, satisfy the following equations:

$$\mathbf{h}(\mathbf{z}) = \mathbf{0}\,, \tag{4.26a}$$

$$\partial_{\mathbf{z}}\mathbf{h}(\mathbf{z})\,\mathbf{v} = \mathbf{0}\,, \tag{4.26b}$$

$$\|\mathbf{v}\| = 1\,. \tag{4.26c}$$

Lastly, the dotted straight line in Figures 40 and 41 represents the load increase given by $S_3(t) = (0.8 + j0.6)t$, used to produce the solution branches in Figure 39. Figure 40 reiterates that the bifurcation point of the smoothed system occurs *before* the bifurcation of the original system, which agrees with the statement of Theorem 9. In this way, the smoothed system is guaranteed to provide conservative measures of voltage stability margin.

4.2.4 Alternative approach to handle equation (4.18)

Throughout this section, several theorems were presented to show that the original power flow model can be accurately approximated by a smooth power flow model, where one instance of equation (4.18) is replaced by one instance of equation (4.22). The validity of this approximation is verified both in the sense that solutions of the original model and the smooth model are arbitrarily close to each other, and in the sense that generic

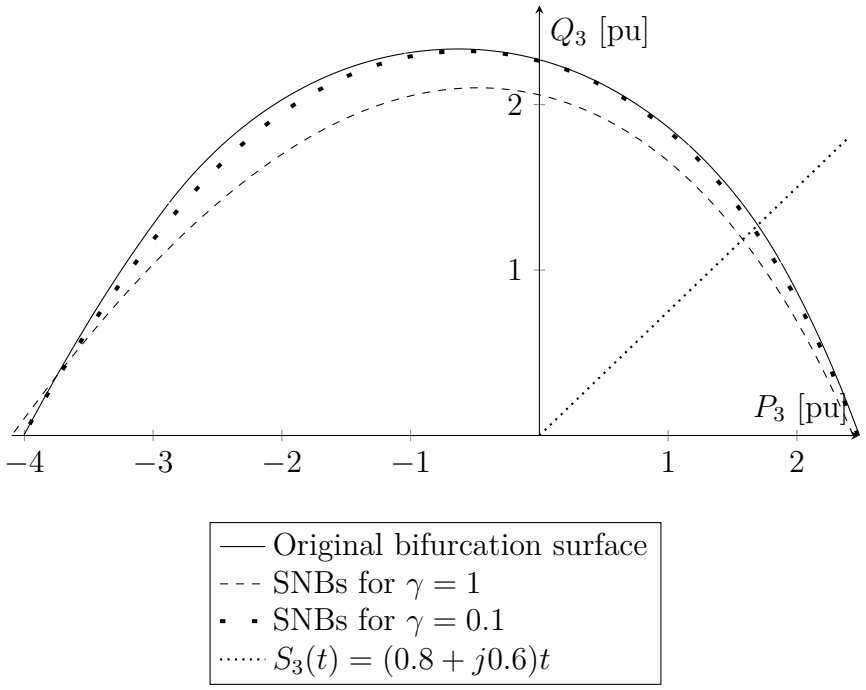

Figure 41 – Bifurcation surface of the smoothed system.

bifurcations of the original model and SNBs of the smooth model are arbitrarily close to each other.

One might argue, however, that the smoothed system (4.24) worse conditioning properties than the original system (4.23). In fact this is true: by observing that the set of solutions in Figure 30 is being approximated by one equation $u = g_\gamma(y)$, the following limit is satisfied:

$$\lim_{\gamma \to 0^+} |g'_\gamma(y_{\text{spec}})| = \infty \,. \tag{4.27}$$

This basically means that some particular elements of the Jacobian of the smoothed system will explode when γ approaches zero. In practical situations where numerical solvers are employed to solve equation (4.24), this means that γ cannot be reduced indefinitely, otherwise the numerical solver will not be able to converge.

This problem is not restricted to *smooth step functions*, but rather to any equation of the form $u = f(y)$ trying to approximate the behavior of Figure 30. Then, the only alternative is to avoid using one equation of the form $u = f(y)$ to approximate this behavior. This alternative is briefly explained in this subsection.

When equation (4.18) was presented as an alternative representation of equation (4.12), we did not explicitly write down how function f_{control} can be implemented. This section provides one possible implementation of f_{control}.

From Figure 30, any function f_{control} clearly is not C^1. However, this function can be continuous. In this case, $f_{\text{control}}(y, u) > 0$ for all (y, u) on one side of the solution branch shown in Figure 30, while $f_{\text{control}}(y, u) < 0$ for the other side. Obviously $f_{\text{control}}(y, u) = 0$

at the solution branch.

Function f_{control} must be written in terms of conditional statements to distinguish between the three straight lines shown in Figure 30. Thus, f_{control} has the following form:

$$f_{\text{control}}(y,u) = \begin{cases} f_1(y,u), & \text{if } (y,u) \in \mathbb{S}_1\,, \\ f_2(y,u), & \text{if } (y,u) \in \mathbb{S}_2\,, \\ f_3(y,u), & \text{if } (y,u) \in \mathbb{S}_3\,, \end{cases} \tag{4.28}$$

where $\mathbb{S}_1$, $\mathbb{S}_2$ and $\mathbb{S}_3$ are disjoint sets such that $\mathbb{S}_1 \cup \mathbb{S}_2 \cup \mathbb{S}_3 = \mathbb{R}^2$. In Figure 42, for example, the dashed lines represent the boundaries of sets $\mathbb{S}_1$, $\mathbb{S}_2$ and $\mathbb{S}_3$. $\mathbb{S}_1$ is the lower left set, $\mathbb{S}_2$ is the upper right set and $\mathbb{S}_3$ is the middle set. The sign of functions f_1, f_2 and f_3 are given in the figure. Note that $f_{\text{control}}(y,u) < 0$ for all (y,u) below the solution curve, while $f_{\text{control}}(y,u) > 0$ for all (y,u) above the solution curve.

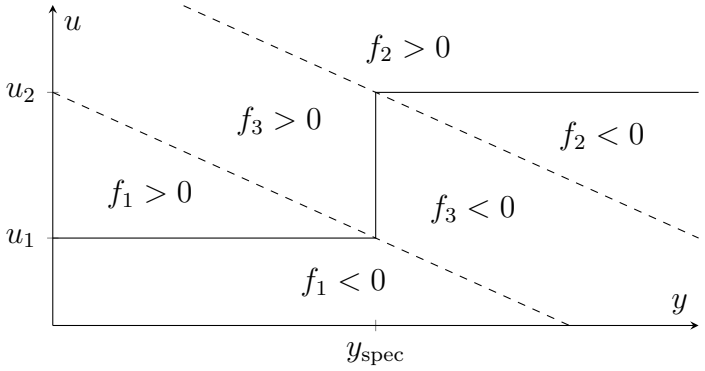

Figure 42 – Defining an instance of function f_{control}.

Motivated by Figure 42, f_{control} can be defined in the following way:

$$f_{\text{control}}(y,u) = \begin{cases} u - u_1, & \text{if } y + u \leq y_{\text{spec}} + u_1\,, \\ u - u_2, & \text{if } y + u \geq y_{\text{spec}} + u_2\,, \\ y_{\text{spec}} - y, & \text{otherwise}\,. \end{cases} \tag{4.29}$$

This definition only works when $u_1 \leq u_2$. If $u_1 > u_2$, one instance of f_{control} is:

$$f_{\text{control}}(y,u) = \begin{cases} u - u_1, & \text{if } y - u \leq y_{\text{spec}} - u_1\,, \\ u - u_2, & \text{if } y - u \geq y_{\text{spec}} - u_2\,, \\ y - y_{\text{spec}}, & \text{otherwise}\,. \end{cases} \tag{4.30}$$

This definition of f_{control} allows one to write any equation of the form (4.12) by means of a well defined, single-valued function. Just by using this definition of f_{control}, it is not necessary to manually keep track of the system *structure* while $\mathbf{p}$ varies in equation (2.36a), because f_{control} itself decides how the system should be modelled.

Even though f_{control} is well defined by equations (4.29) and (4.30), note that this function is not C^1, so system (2.36a) may still undergo a bifurcation at a point where f_{control} is not differentiable. However, it is possible to approximate f_{control} by a C^1 function and follow a similar procedure to the one shown in Subsections 4.2.1, 4.2.2 and 4.2.3. This smooth formulation would have better conditioning properties than the formulation proposed in Subsection 4.2.1.

The reason why we follow the approach proposed in Subsection 4.2.1 is simple: when equation (4.18) is replaced by equation (4.22), the value of u is automatically defined by the value of y, which means that it is not necessary to keep u explicitly as a variable in the state vector $\mathbf{x}$. Thus, for each equation (4.18) that we replace by (4.22), we can remove u from the state vector $\mathbf{x}$ and remove (4.22) from the set of equations in (2.36a).

To clarify this reasoning, compare equations (4.23) and (4.24) again. These equations are given by

$$\mathbf{f}_a(y, u, \mathbf{z}, t) = \mathbf{0}\,, \tag{4.31a}$$

$$f_{\text{control}}(y, u) = 0\,, \tag{4.31b}$$

and

$$\mathbf{f}_a(y, u, \mathbf{z}, t) = \mathbf{0}\,, \tag{4.32a}$$

$$u = g_\gamma(y)\,, \tag{4.32b}$$

respectively. When we replace $f_{\text{control}}(y, u) = 0$ by $u = g_\gamma(y)$, we not only transform LIBs into SNBs, but we also can reduce the system by one equation and one variable:

$$\mathbf{f}_a(y, g_\gamma(y), \mathbf{z}, t) = \mathbf{0}\,. \tag{4.33}$$

Thus, the dimensionality of the system can be greatly reduced if many instances of $f_{\text{control}}(y, u) = 0$ are replaced by instances of $u = g_\gamma(y)$.

There is a trade-off between the conditioning of the power flow model and the number of power flow equations. The choice between whether to replace equation $f_{\text{control}}(y, u) = 0$ by equation $u = g_\gamma(y)$ or by an arbitrary smooth equation $h(y, u) = 0$ (where h is a C^1 function) is basically a choice of how small γ must be in order to approximate the original system satisfactorily.

If there is a value of $\gamma > 0$ small enough to represent the power flow model accurately but large enough to not harm numerical solvers, then it is better to use equation $u = g_\gamma(y)$, because the reduction in the number of equations can reduce the computational cost of the analysis. In the results reported in this work, γ was chosen to provide accurate results, while maintaining the numerical stability of the proposed analysis.

4.3 Handling the saturation functions

Besides equation (4.18), the modelling shown in Chapter 2 also presents non-differentiability associated with saturation functions (also called clamp functions or clip functions):

$$u = \text{sat}(y, y_{\min}, y_{\max}) \equiv \min\{\max\{y_{\min}, y\}, y_{\max}\} \equiv \begin{cases} y_{\min}, & \text{if } y < y_{\min}\,, \\ y, & \text{if } y_{\min} \leq y \leq y_{\max}\,, \\ y_{\max}, & \text{if } y_{\max} < y\,. \end{cases} \tag{4.34}$$

This function is represented in the yu-plane as shown in Figure 43. In this figure, the points where the system *structure* changes between saturated and unsaturated modes are highlighted as transition points. These are exactly the same transition points defined in Subsection 4.1.2. In fact, it can be shown that equation

$$\mathbf{f}(\mathbf{x}, t) = \mathbf{0}\,, \tag{4.35a}$$

$$\begin{cases} y_{\min}, & \text{if } y < y_{\min}\,, \\ y, & \text{if } y_{\min} \leq y \leq y_{\max}\,, \\ y_{\max}, & \text{if } y_{\max} < y\,. \end{cases} \tag{4.35b}$$

is locally an instance of equation (4.3). The proof is completely analogous to the one relating (4.35) to (4.3).

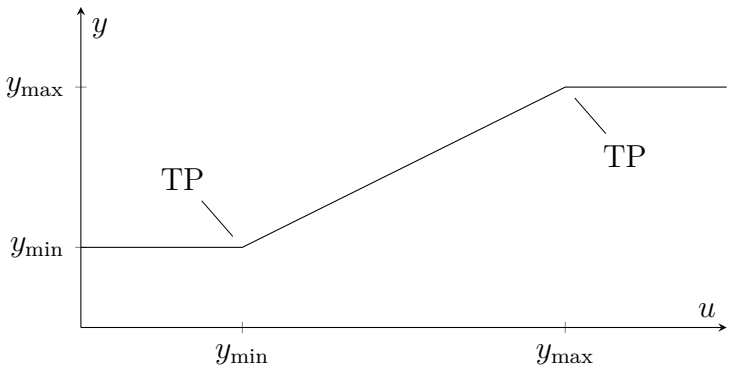

Figure 43 – Solution set of equation (4.34).

The saturation function was explicitly used in equations (2.26) and (2.29) in Chapter 2. However, this function can be used in any control system that have a nonzero steady-state error.

Saturation functions are suitable for other situations as well. For example, equation (2.7) establishes active power limits for the output of a generator. The active power P of this generator does not belong to vector $\mathbf{x}$ in equation (2.36), but it *can* belong either to vector $\mathbf{p}$ or to vector $\mathbf{u}$. This was shown, for example, in Figure 9. It is convenient to leave

to function **f** itself to determine whether the generator is at its active power limit or not. In this case, instead of using P directly in the power flow equations, one could just use $\text{sat}(P, P_{\min}, P_{\max})$, where P is one element of either **p** or **u**.

The same way as LIBs can occur at the TPs of Figure 30, LIBs can also occur at the TPs of Figure 43. As in Section 4.2, the remainder of this section is dedicated to propose a new function to approximate a saturation function, and to demonstrate that LIBs of the original saturation function are SNBs in the proposed smooth function.

4.3.1 Proposed representation of equation (4.34)

Let a *smooth saturation function* be defined as follows:

Definition 5 (Smooth saturation function)**.** *A* smooth saturation function *is a family of* C^1 *functions* $g_\gamma : \mathbb{R}^3 \to \mathbb{R}$*, parameterized by a scalar* $\gamma > 0$ *and satisfying the following properties:*

[I] $\lim_{\gamma \to 0^+} g_\gamma(y, y_{min}, y_{max}) = \text{sat}(y, y_{min}, y_{max}) \; \forall \; y, y_{min}, y_{max}$*;*

[II] *there is a* $\zeta > 0$ *such that, for all* γ*:*

- $g_\gamma(y, y_{min}, y_{max}) \geq \text{sat}(y, y_{min}, y_{max}) \; \forall \; [y_{min} - \zeta, y_{min} + \zeta]$*;*
- $g_\gamma(y, y_{min}, y_{max}) \leq \text{sat}(y, y_{min}, y_{max}) \; \forall \; [y_{max} - \zeta, y_{max} + \zeta]$*;*

[III] *there is* $y_{crit} \in (y_{min} + \zeta, y_{max} - \zeta)$ *such that, for all* γ*,* g_γ *changes concavity in relation to* y *only at* y_{crit}*.*

Hereinafter, smooth saturation functions *will be written in the simplified form given by* $g_\gamma(y)$*.*

The example of a *smooth saturation function* that will be used throughout this document is:

$$g_\gamma(y) = \begin{cases} y_{\min}, & \text{if } y \leq y_{\min} - \gamma/4\,, \\ p_1(y), & \text{if } y_{\min} - \gamma/4 < y < y_{\min} + \gamma/4\,, \\ y, & \text{if } y_{\min} + \gamma/4 \leq y \leq y_{\max} - \gamma/4\,, \\ p_2(y), & \text{if } y_{\max} - \gamma/4 < y < y_{\max} + \gamma/4\,, \\ y_{\max}, & \text{if } y \geq y_{\max} - \gamma/4\,, \end{cases} \tag{4.36}$$

where p_1 and p_2 are quadratic polynomials in y chosen to make g_γ continuously differentiable, while γ is implicitly constrained to the interval $[0, 2(y_{\max} - y_{\min})]$. By solving the respective

linear systems, one obtains:

$$p_1(y) = y_{\min} + \frac{\left(y - y_{\min} + \frac{\gamma}{4}\right)^2}{\gamma}\,, \tag{4.37a}$$

$$p_2(y) = y_{\max} - \frac{\left(y - y_{\max} - \frac{\gamma}{4}\right)^2}{\gamma}\,. \tag{4.37b}$$

It can be easily shown that function g_γ defined in (4.36) is C^1 in the entire domain of $(y, y_{\min}, y_{\max})$. Also, property [I] of a *smooth saturation function* is easily verified.

The minimum value of $p_1(y)$ is obviously $y_{\min}$, while the maximum value of $p_2(y)$ is $y_{\max}$. Thus, property [II] of a *smooth saturation function* holds for (4.36).

The quadratic coefficient of p_1 is positive, which shows that this function is convex. The quadratic coefficient of p_2 is negative, and this function is concave. This proves property [III] of a *smooth saturation function*.

Function (4.36) is graphically shown in Figure 44. The curve in this figure is identical to the one in Figure 43, except in the intervals $\left(y_{\min} - \frac{\gamma}{4}, y_{\min} + \frac{\gamma}{4}\right)$ and $\left(y_{\max} - \frac{\gamma}{4}, y_{\max} + \frac{\gamma}{4}\right)$. As γ approaches zero, function g_γ approaches a saturation function. This is not only a particularity of equation (4.36), but rather it is a characteristic of every instance of a *smooth saturation function*.

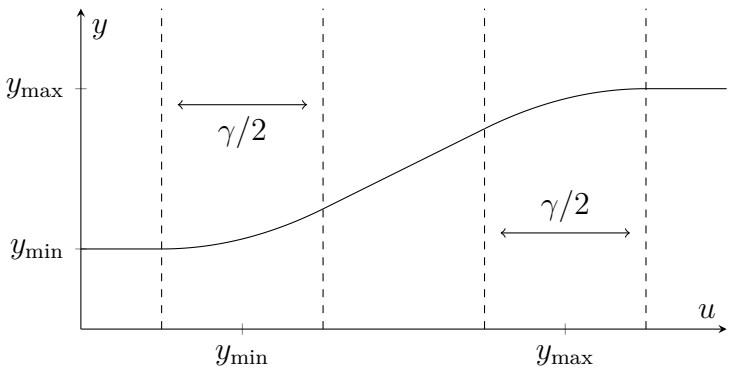

Figure 44 – Graphical representation of function (4.36).

In the remainder of this section, let the power system (2.36) be splitted into the two following equations:

$$\mathbf{f}_a(y, u, \mathbf{z}, t) = \mathbf{0}\,, \tag{4.38a}$$

$$u = \mathrm{sat}(y)\,, \tag{4.38b}$$

where:

- $\mathbf{z} \in \mathbb{R}^{n-2}$;
- $y, u \in \mathbb{R}$;
- $\mathbf{x}^T = \begin{bmatrix}\mathbf{z}^T & y & u\end{bmatrix}$ (recall that $\mathbf{x} \in \mathbb{R}^n$);

- $\mathbf{f}_a : \mathbb{R} \times \mathbb{R} \times \mathbb{R}^{n-2} \times \mathbb{R} \to \mathbb{R}^{n-1}$;
- $\mathbf{f}(\mathbf{x}, t) \equiv \begin{bmatrix} \mathbf{f}_a(y, u, \mathbf{z}, t) \\ u - \text{sat}(y) \end{bmatrix}$ (recall that $\mathbf{f} : \mathbb{R}^n \times \mathbb{R} \to \mathbb{R}^n$).

$\mathbf{x}$ is the state vector of system (2.36), while sat is an instance of the saturation function (4.34). To simplify notation, vectors $\mathbf{p}$ and $\mathbf{u}$ of system (2.36) are omitted in (4.38). Furthermore, inequation (2.36b) is assumed to be satisfied in this section for simplicity (these inequality constraints will be handled in Section 4.4).

In this work, we propose to replace function sat in (4.38) by one instance of a *smooth saturation function*. Hence, (4.38) is transformed into:

$$\mathbf{f}_a(y, u, \mathbf{z}, t) = \mathbf{0}\,, \tag{4.39a}$$

$$u = g_\gamma(y)\,. \tag{4.39b}$$

Hereinafter, system (4.38) will be denoted by the "original system", while system (4.39) will be referred to as the "smoothed system".

In the following subsections, several theorems are presented to demonstrate that the behavior of the original system can be properly approximated by the behavior of the smoothed system.

4.3.2 The validity of the smoothed system

System (4.39) is a valid approximation of (4.38) if any solution of (4.38) is arbitrarily close to a solution of (4.39), and vice versa. In this subsection, two theorems are provided to demonstrate that the smoothed system is a valid approximation of the original system, and the accuracy of the smoothed system can be controlled by parameter γ in equation (4.39b).

The following theorem establishes that any solution of (4.38) is arbitrarily close to a solution of (4.39):

Theorem 11. *Assume that* $\mathbf{f}_a$ *is* C^1 *in a neighborhood of a solution* $(\widehat{y}, \widehat{u}, \widehat{\mathbf{z}}, \widehat{t})$ *of* (4.38).

Then, for a sufficiently small $\gamma > 0$*, the smoothed system* (4.39) *generically admits a solution* $(\widetilde{y}(\gamma), \widetilde{u}(\gamma), \widetilde{\mathbf{z}}(\gamma), \widetilde{t}(\gamma))$ *(implicitly parameterized by* γ*) arbitrarily close to the solution* $(\widehat{y}, \widehat{u}, \widehat{\mathbf{z}}, \widehat{t})$ *of the original system* (4.38).

Proof. The proof is given in Section A.12. □

The following theorem establishes that any solution of (4.39) is arbitrarily close to a solution of (4.38):

Theorem 12. *Assume that* $\mathbf{f}_a$ *is* C^1 *in a neighborhood of a solution* $(\widetilde{y}(\gamma), \widetilde{u}(\gamma), \widetilde{\mathbf{z}}(\gamma), \widetilde{t}(\gamma))$ *(implicitly parameterized by* γ*) of* (4.39).

Then, for a sufficiently small $\gamma > 0$, the original system (4.38) *generically admits a solution* $(\widehat{y}, \widehat{u}, \widehat{\mathbf{z}}, \widehat{t})$ *arbitrarily close to the solution* $(\widetilde{y}(\gamma), \widetilde{u}(\gamma), \widetilde{\mathbf{z}}(\gamma), \widetilde{t}(\gamma))$ *of the smoothed system* (4.39).

Proof. The proof is given in Section A.13. □

Theorem 11 demonstrates that all solutions of the original system are near solutions of the smoothed system. Similarly, Theorem 12 establishes that all solutions of the smoothed system are near solutions of the original system. Together, these theorems prove that the smoothed system (4.39) is indeed a valid approximation of system (4.38).

4.3.2.1 Example

Theorems 11 and 12 are illustrated by analyzing the three-bus system of Figure 32. In this example, however, the generator at bus 2 is replaced by a SVC with the same voltage setpoint, but with $b_{\min} = 0.8$ pu, $b_{\max} = 1.4$ pu and $K = 5$ (the SVC is modelled by equations (2.26) and (2.28)). Moreover, the SVC connected to bus 2 is used to control the voltage of bus 3 ($i = 3$ in (2.26) and $j = 2$ in (2.28)). The TP due to the lower saturation limit occurs at $t \approx 1.4886$ (this will later be verified in the solution curve of Figure 46). The solution for $t \approx 1.4886$ is given in the last row of Table 2, where $b_{\min} = 0.8 = K(V_{\text{spec}} - V_3) = 5(1 - 0.84)$.

Solution points for the smoothed system, where the saturation function in (2.26) is replaced by function (4.36), are shown in Table 2. Note that, with the decrease of γ, the smooth solution point approaches the original one.

Table 2 – Solution points for $t \approx 1.4886$.

Model	E_2	E_3	b
$\gamma = 1.2$	$1.032\angle{-0.3333}$	$0.8585\angle{-0.2825}$	0.8359
$\gamma = 0.12$	$1.004\angle{-0.3318}$	$0.8418\angle{-0.2832}$	0.8036
$\gamma = 0.012$	$1.002\angle{-0.3316}$	$0.8402\angle{-0.2833}$	0.8004
$\gamma = 0$	$1.001\angle{-0.3316}$	$0.84\angle{-0.2833}$	0.8

4.3.3 Transforming generic bifurcations into SNBs

The original system (4.38) can generically undergo two bifurcation types: SNB and LIB. Assuming that $\mathbf{f}_a$ is C^1, the BP may be a LIB point if this point is the TP of equation (4.38b). These TPs were graphically sketched in Figure 43. On the other hand, system (4.38) generically undergoes a SNB if the BP is not a TP of equation (4.38b).

Like Figures 33 and 34, the occurrence of both SNBs and LIBs due to saturation functions is sketched in Figure 45. This figure depicts the SNB as the birth of two solution

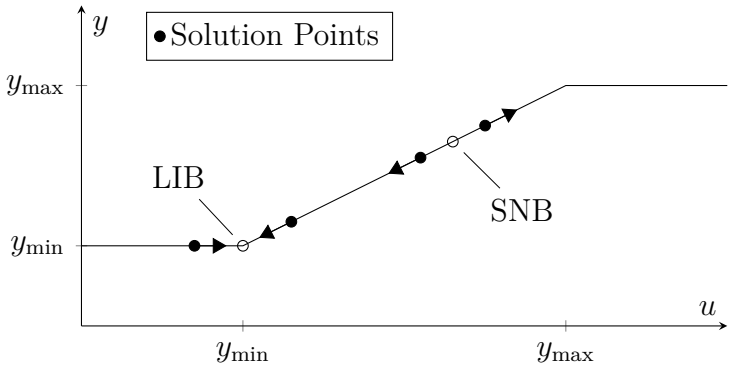

Figure 45 – Bifurcations due to the saturation function. The arrows indicate the direction of variation of the solution points with the increase of t.

points with the increase of t. The LIB point in this figure is the collision of two solution points with the increase of t.

In order to prove that generic bifurcation points of the original system and saddle-node bifurcation points of the smoothed system are arbitrarily close to each other, we demonstrate that solution points of the original system and of the smooth system vary in the same direction with the increase of t. This is somewhat analogous to Corollaries 1 and 2 provided in Section 4.2.

Theorem 13. *For any* smooth saturation function $g_\gamma(y)$*:*

$$\lim_{\gamma \to 0^+} g'_\gamma(y) = \begin{cases} 1, & \text{if } y_{min} < y < y_{max}\,, \\ 0, & \text{otherwise}\,, \end{cases} \tag{4.40}$$

for all $y \notin \{y_{min}, y_{max}, y_{crit}\}$.

Proof. The proof is given in Section A.14. □

Corollary 3 is a direct application of Theorem 13. This corollary is written in terms of a generic function $h(y, u)$. This function will become an implicit function $t(y, u)$ in Theorem 14, which prove the equivalency between bifurcation points of systems (4.38) and (4.39). Function $t(y, u)$ simply represents how t in the solution of systems (4.38) and (4.39) varies when a solution point moves in the yu-plane.

Corollary 3. *Let* $h(y, u) : \mathbb{R} \times \mathbb{R} \to \mathbb{R}$ *be any* C^1 *function defined in a neighborhood of* $(\widehat{y}, \mathrm{sat}(\widehat{y}))$*, where* $\widehat{y} \notin \{y_{min}, y_{max}, y_{crit}\}$ *(*y_{crit} *was defined in Property* [III] *of a* smooth saturation function*). Let* $\widetilde{y}$ *be sufficiently close to* $\widehat{y}$*.*

Then, in order to increase h*, both solutions* $(\widehat{y}, \mathrm{sat}(\widehat{y}))$ *and* $(\widetilde{y}, g_\gamma(\widetilde{y}))$ *should move in the same direction of* y*, i.e., they both should either increase* y *or decrease* y*.*

Proof. The proof is given in Section A.15. □

Theorem 14. *If* $\mathbf{f}_a$ *is* C^1 *in a neighborhood of either a SNB point or LIB point of the original system* (4.38)*, then this BP generically is arbitrarily close to a SNB point of the smoothed system* (4.39)*.*

Likewise, if $\mathbf{f}_a$ *is* C^1 *in a neighborhood of a SNB point of the smoothed system* (4.39)*, then this BP generically is arbitrarily close to either a SNB or a LIB point of the original system* (4.38)*.*

Moreover, assuming that a LIB occurs in the original system and that two solutions disappear with the increase of t*, then* t *at the BP of the smoothed system is lower than* t *at the BP of the original system.*

Proof. The proof is given in Section A.16. □

4.3.3.1 Example

Theorem 14 shows that saddle-node bifurcation points of the smoothed system (4.39) are arbitrarily close to generic bifurcation points of the original system (4.38) (namely saddle-node bifurcations and limit-induced bifurcations), and vice-versa. To illustrate the result of this theorem, the three-bus system of Figure 32 is again studied. The generator at bus 2 was replaced with a SVC, as explained in the example of Subsection 4.3.2.

Solution branches are shown in Figure 46 for this system. Corroborating the results of Theorems 11 and 12, Figure 46 shows that the solution branch of the smoothed system is near the solution branch of the original system. Corroborating the results of Theorem 14, the BPs of the original and smoothed systems approach each other when γ is decreased. A LIB occurs at the original system, while a SNB occurs at the smoothed system.

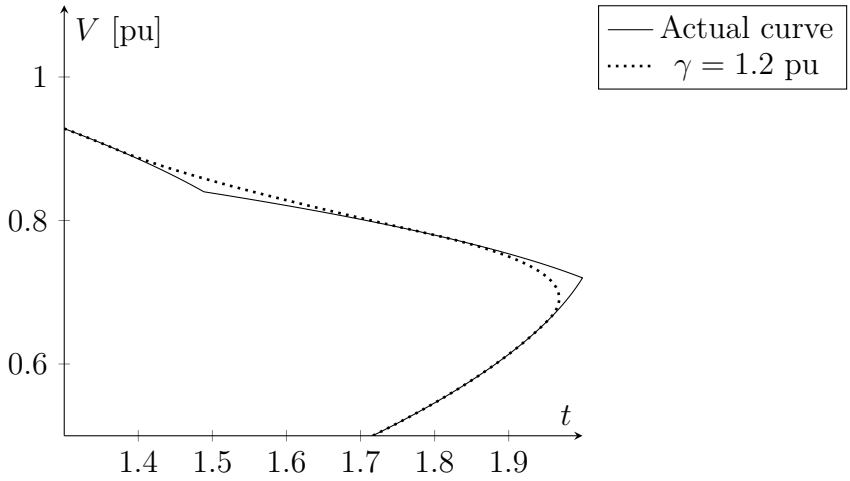

Figure 46 – Solution branches for bus 3.

4.4 Handling inequality constraints

In order to represent system (2.36) by system (4.1), the inequality constraints in (2.36b) should be included directly in function **h** of (4.1).

In this work, we propose to transform the following system:

$$\mathbf{f}(\mathbf{x}, t) = \mathbf{0}\,, \tag{4.41a}$$

$$g(\mathbf{x}, t) \geq 0\,, \tag{4.41b}$$

into the following system:

$$\mathbf{f}(\mathbf{x}, t) = \mathbf{0}\,, \tag{4.42a}$$

$$g(\mathbf{x}, t) = k^2\,, \tag{4.42b}$$

Hence, the inequality constraint is transformed into an equality constraint. When one equation is added to system (4.42), one new variable should also be added. This new variable is k, as shown in equation (4.42b).

Obviously, any solution $(\mathbf{x}, t) = (\widehat{\mathbf{x}}, \widehat{t})$ of (4.41) corresponds to two solutions of (4.42), namely $(\mathbf{x}, t, k) = (\widehat{\mathbf{x}}, \widehat{t}, -\sqrt{g(\widehat{\mathbf{x}}, \widehat{t})})$ and $(\mathbf{x}, t, k) = (\widehat{\mathbf{x}}, \widehat{t}, +\sqrt{g(\widehat{\mathbf{x}}, \widehat{t})})$.

On the other hand, any solution $(\mathbf{x}, t, k) = (\widehat{\mathbf{x}}, \widehat{t}, \widehat{k})$ of (4.42) is a solution of (4.41), because $g(\widehat{\mathbf{x}}, \widehat{t}) = \widehat{k}^2 \geq 0$ for all $k \in \mathbb{R}$.

Therefore, systems (4.41) and (4.42) are completely equivalent, in the sense that they share the same solution set. As a consequence, all bifurcation points of (4.41) are bifurcation points of (4.42). The main difference is that all CVIBs in (4.41) are invariably transformed into SNBs in (4.42), as established by the next theorem:

Theorem 15. *Each CVIB in system* (4.41) *invariably corresponds to a SNB in system* (4.42)

Proof. The proof is given in Section A.17. □

It is intuitive to note that CVIBs of (4.41) are transformed into SNBs of (4.42). Consider that (4.41) undergoes a CVIB at $t = t_{\text{crit}}$, where one solution exist for $t \leq t_{\text{crit}}$ and disappears for $t > t_{\text{crit}}$. This means that, in a neighborhood of $t = t_{\text{crit}}$:

- $g(\mathbf{x}(t), t) > 0$ for $t < t_{\text{crit}}$;
- $g(\mathbf{x}(t), t) = 0$ at $t = t_{\text{crit}}$;
- $g(\mathbf{x}(t), t) < 0$ for $t > t_{\text{crit}}$.

In relation to system (4.42), this means that:

- two solutions exist for $t < t_{\text{crit}}$, where $k(t) = -\sqrt{g(\mathbf{x}(t), t)}$ for one solution and $k(t) = \sqrt{g(\mathbf{x}(t), t)}$ for the other solution;

- these two solutions coalesce at $t = t_{\text{crit}}$, where $k(t) = -\sqrt{0} = \sqrt{0} = 0$;
- there is no solution for $t > t_{\text{crit}}$, because there is no $k \in \mathbb{R}$ satisfying (4.42b).

Moreover, the CVIB occurs in system (4.41), where both $\mathbf{f}$ and g are C^1 at the BP, thus system (4.42) is C^1 at the BP. The Jacobian matrix of this system is:

$$\begin{bmatrix} \partial_{\mathbf{x}}\mathbf{f} & \mathbf{0} \\ \partial_{\mathbf{x}} g & -2k \end{bmatrix}, \tag{4.43}$$

which clearly is singular when $k = 0$.

Two solutions of (4.42) coalesce at the BP and disappear. System (4.42) is differentiable and the Jacobian is singular at the BP, which proves that this BP is a SNB point.

Assume that the original system (2.36) has n state variables, n equality constraints and m inequality constraints. If the proposed approach were applied recursively to all inequality constraints, the final power system model would have $n+m$ variables and $n+m$ inequality constraints. If m is large, the final system of equations would be significantly larger than the original one. As a result, the final system of equations would be considerably harder to solve than the original system. To overcome this inconvenience, we may exploit the pattern of the inequalities in (2.36b). For example, every voltage limit of the form:

$$V_i \leq V_{i,\max}\,, \tag{4.44}$$

can be grouped into a single inequality constraint of the form:

$$\max_i \frac{V_i}{V_{i,\max}} \leq 1\,, \tag{4.45}$$

since $V_{i,\max} > 0 \;\forall\; i$.

However, g in this case would not be C^1. Note that the left-hand side of (4.45) is simply a $\|\cdot\|_\infty$ norm. Thus, (4.45) is equivalent to:

$$\lim_{p\to\infty} \sqrt[p]{\sum_i \left(\frac{V_i}{V_{i,\max}}\right)^p} \leq 1\,, \tag{4.46}$$

which can be approximated by:

$$\sqrt[p]{\sum_i \left(\frac{V_i}{V_{i,\max}}\right)^p} \leq 1\,, \tag{4.47}$$

for a sufficiently large $p < \infty$.

When inequation (4.45) is replaced by (4.47), we guarantee conservative results simply by noticing that every $\|\cdot\|_p$ unit ball is included in the $\|\cdot\|_\infty$ unit ball. In other words, every solution that satisfies (4.47) also satisfies (4.45).

Similar considerations made to develop (4.44) to (4.47) may be used in other situations. For example, the lower voltage limits in inequation (2.4) or for the apparent power of system branches in inequation (2.11) could be grouped in a similar way. The main advantage of (4.47) in relation to (4.44) is that only a few instances of equation (4.42b) are added to the final power system model, rather than one equation for each limit.

4.4.1 Example

Consider a simple two-bus system in which a load bus is connected to an infinite bus with voltage $V_\infty = 1$ through a transmission line with impedance $z = 0.01 + j0.1$. The complex power flow equation for this system is:

$$S_{\text{load}}(t) = P + jQ = V\angle\underline{\theta}\frac{\overline{V}_\infty - V\angle\underline{-\theta}}{\bar{z}} \tag{4.48}$$

where V is the voltage at the load bus and θ is the voltage angle at the same bus. Figure 47 shows the solution branch for the *scenario* given by $S_{\text{load}}(t) = t$.

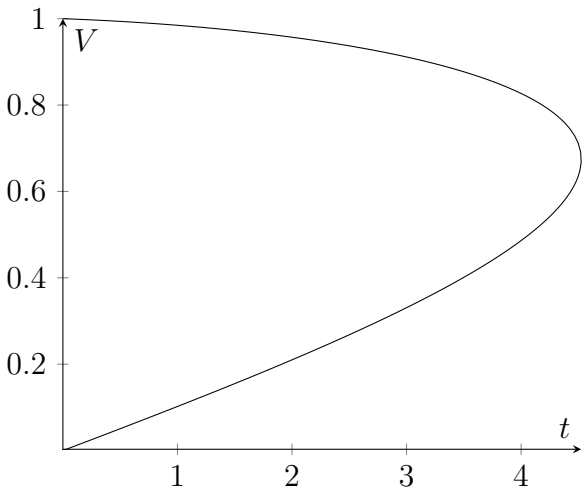

Figure 47 – Solution branch for the two-bus system.

Now assume that this two-bus system is also subjected to an undervoltage limit at the load bus given by $V \geq 0.9$. From Figure 47, the voltage limit is reached at $t_{\text{CVIB}} = 3.183$. To transform this CVIB into a SNB, the undervoltage limit is transformed into the following equation:

$$k^2 = V - 0.9\,, \tag{4.49}$$

which is equation (4.42b) for this example.

The auxiliary system has four real variables (V, θ, t, k) and three real equations (the complex equation (4.48) and the real equation (4.49)). The solution branch for the auxiliary system is shown in Figure 48. From this figure, it is clear that a SNB occurs in the auxiliary system and that $t_{\text{SNB}} = t_{\text{CVIB}}$.

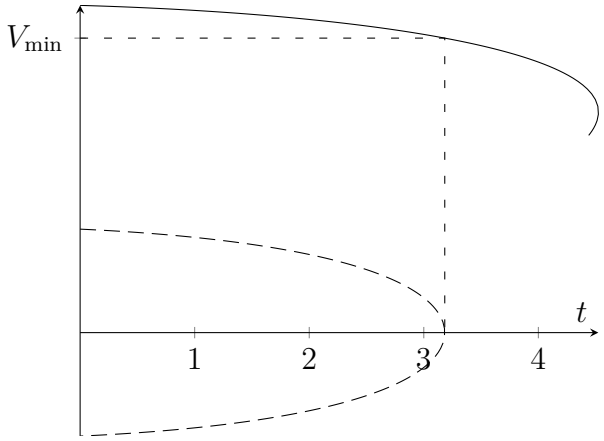

—— Value of V on the solution branch of system (4.41)
– – Value of k on the solution branch of system (4.42)

Figure 48 – Solution branch for the auxiliary system.

4.5 Global behavior of the proposed model

In Section 4.2, several theorems were introduced to corroborate that system (4.24) is a valid approximation of system (4.23). The only difference between these systems is that one instance of equation (4.12) was replaced by one instance of equation (4.22). The main theorems that prove the equivalence between (4.23) and (4.24) are Theorems 4, 5, 8, 9 and 10.

Likewise, Section 4.3 demonstrates the equivalence between systems (4.38) and (4.39) by means of Theorems 11, 12 and 14.

All aforementioned theorems are local, in the sense that all these theorems explore the local behavior of the power system near a solution or bifurcation point to demonstrate the equivalency between the original power flow model and the proposed power flow model. Moreover, these theorems assume that only one equation changes in the power system model.

This section aims for collecting the propositions of all previous sections into two theorems that establish a global equivalency between two distinct power system models, namely the traditional power system model (2.36):

$$\mathbf{f}(\mathbf{x}, t) = \mathbf{0}\,, \tag{4.50a}$$

$$\mathbf{g}(\mathbf{x}, t) \geq \mathbf{0}\,, \tag{4.50b}$$

and the proposed power system model (4.1):

$$\mathbf{h}(\mathbf{z}, t) = \mathbf{0}\,. \tag{4.51}$$

The dimensions of $\mathbf{f}$, $\mathbf{g}$ and $\mathbf{h}$ are n, m and $n + m$, respectively. Similarly, $\mathbf{x}$ is

a n-dimensional vector and $\mathbf{z}$ is a $(n+m)$-dimensional vector. The difference between systems (4.50) and (4.51) are:

- All instances of equation (4.12) in system (4.50a) are replaced by instances of equation (4.22) in order to build system (4.51);
- All instances of saturation functions (equation (4.34)) in system (4.50a) are replaced by instances of a *smooth saturation function* in order to build system (4.51);
- Every inequation of the form (4.41b) in system (4.50b) is replaced by one instance of equation (4.42b) to built system (4.51). For each equation (4.42b), variable k is appended to vector $\mathbf{x}$ in order to create vector $\mathbf{z}$.

The following theorem establishes that solutions of (4.50) and (4.51) are arbitrarily close to each other:

Theorem 16. *Suppose that, apart from all instances of equations* (4.12) *and* (4.34)*, function* $\mathbf{f}$ *of system* (4.50) *is* C^1 *(i.e., all non-smooth characteristics of* (4.50a) *can be categorized either in* (4.18) *or in* (4.34)*). Also suppose that* $\mathbf{g}$ *in* (4.50b) *is* C^1*.*

Then, any solution of (4.50) *generically is arbitrarily close to a solution of* (4.51)*. Likewise, any solution of* (4.51) *generically is arbitrarily close to a solution of* (4.50)*.*

Proof. The proof is given in Section A.18. □

The following theorem establishes that generic bifurcations of (4.50) and (4.51) are arbitrarily close to each other:

Theorem 17. *Suppose that, apart from all instances of equations* (4.12) *and* (4.34)*, function* $\mathbf{f}$ *of system* (4.50) *is* C^1 *(i.e., all non-smooth characteristics of* (4.50a) *can be categorized either in* (4.18) *or in* (4.34)*). Also suppose that* $\mathbf{g}$ *in* (4.50b) *is* C^1*.*

Then, any generic BP (a SNB point, LIB point or CVIB point) of (4.50) *generically is arbitrarily close to a SNB point of* (4.51)*. Likewise, any SNB point of* (4.51) *generically is arbitrarily close to a generic BP of* (4.50)*.*

Proof. The proof is given in Section A.19. □

Theorems 16 and 17 are the main results of all contributions of this chapter. Together, these theorems show how the (4.51) is a valid approximation of (4.50), both in terms of solution points and bifurcation points.

4.6 Complete formulation of the proposed model

In this chapter, a new power system model was proposed to transform system (2.36) into system (4.1). The main results of this chapter are given in Theorems 16 and 17, which prove the equivalence between systems (2.36) and (4.1).

Variables $\mathbf{p}$ and $\mathbf{u}$ are shared between systems (2.36) and (4.1). In its unreduced form, vector $\mathbf{z}$ of (4.1) is identical to $\mathbf{x}$ of (2.36). The reduction in (4.1) will be explained later in this section.

If the dimension of $\mathbf{f}$ is n and the dimension of $\mathbf{g}$ is m, then the dimension of $\mathbf{h}$ (in its unreduced form) is $n + m$. In comparison with (2.36), system (4.1) is composed of the following equations:

- $2n_{\text{bus}}$ real equations from nodal analysis (real and imaginary parts of (2.2));
- n_{area} equations of power interchange control;
- n_{slack} instances of equation (2.9) for slack generators, smoothed using *smooth step functions*;
- n_{gen} instances of equation (2.9) for non-slack generators, smoothed using *smooth step functions*;
- n_{LTC} instances of equation (2.13), smoothed using *smooth step functions*;
- n_{PST} instances of equation (2.14), smoothed using *smooth step functions*;
- n_{PST} instances of equation (2.15);
- n_{DC} instances of equation (2.19), smoothed using *smooth saturation functions*;
- n_{DC} instances of equation (2.22), smoothed using *smooth step functions*;
- n_{DC} instances of equation (2.23), smoothed using *smooth step functions*;
- n_{SVC} instances of either equation (2.26) or (2.27), smoothed using *smooth saturation functions* or *smooth step functions*, respectively;
- n_{STATCOM} instances of either equation (2.29) or (2.30), smoothed using *smooth saturation functions* or *smooth step functions*, respectively;
- n_{VLID} instances of equation (2.33), smoothed using *smooth step functions*.

Lastly, note that several equations of the form

$$f_1(y, u) = 0 \tag{4.52}$$

were replaced by several equations of the form

$$u = f_2(y)\,. \tag{4.53}$$

Variable u is directly defined by variable y in equation (4.53). Thus, both variable u and equation (4.53) can be removed from the set of equations, which leads to a reduced version of equation (4.1), as opposed to the (unreduced) one presented above. A discussion of this reduction in the number of equations and variables was presented in Subsection 4.2.4.

Equation (4.1) can be further reduced considering the grouping of inequality constraints described in Section 4.4. For example, inequality constraints such as (4.44) can be grouped as shown in (4.47).

4.7 Partial Conclusions

This chapter presented how the (nonsmooth) equation (2.36) can be approximated by the proposed (smooth) equation (4.1). Many theorems were developed to provide a solid foundation to the proposed power system model.

The following chapters show how useful the proposed model is in voltage stability analysis, justifying the theoretical foundations described in this chapter. In the next chapters, new VSA methods are proposed based solely in the saddle-node bifurcation, which is the only type of generic bifurcation that can occur in (4.1). If the original model (2.36) were used instead, the methods proposed in the next chapters would not provide a comprehensive analysis of the power system, because these methods would not capture any bifurcations besides SNBs.

The model proposed in this chapter is useful not only to the methods proposed in the next chapter, but also to many of the methods presented in Chapter 3: most methods presented in Chapter 3 also restrict the search for bifurcations to the search for SNBs, so these methods fail in case of LIBs and CVIBs.

5 PROPOSED METHOD FOR CONTINGENCY RANKING

Chapter 4 proposed a new power system model, in which the power system steady-state is represented uniquely by equation (4.1), where $\mathbf{h}$ is C^1. This chapter presents one application of this smooth model. Here, the smooth model is applied to contingency analysis in voltage stability analysis.

In this chapter, the power flow model proposed in Chapter 4 is used to assess voltage stability of a set of credible contingencies. Specifically, the VSM associated with all contingencies are computed in a efficient way.

When contingencies are analyzed using the original power flow model (2.36), neither the pre-contingency bifurcation type nor the post-contingency bifurcation type is known in advance. Furthermore, the bifurcation type can change due to the contingency. Without knowing beforehand the type of the occurring bifurcation and if this bifurcation type would change due to the contingency, the method must be able to compute different types of bifurcation, which makes the analysis more complex.

On the other hand, by transforming all bifurcations into SNBs, the smooth power flow model (4.1) unifies the computation of any bifurcation, which simplifies both analysis and implementation.

The proposed method is presented in Section 5.1. Results for this method are presented in Section 5.2. Lastly, Section 5.3 compares the proposed method to other methods in the VSA literature.

5.1 Proposed method

In Chapter 4, a new power system model was presented in which the power flow equations are represented by equation (4.1), where $\mathbf{h}$ is C^1. Hence, the Implicit Function Theorem guarantees that every bifurcation point is a point where $\partial_{\mathbf{z}}\mathbf{h}$ is singular. Then the bifurcation surface invariably satisfies by the following set of equations (equation (3.27)):

$$\mathbf{h}(\mathbf{z}, \mathbf{p}, \mathbf{u}) = \mathbf{0}\,, \tag{5.1a}$$

$$\partial_{\mathbf{z}}\mathbf{h}(\mathbf{z}, \mathbf{p}, \mathbf{u})\,\mathbf{v} = \mathbf{0}\,, \tag{5.1b}$$

$$\|\mathbf{v}\| = 1\,. \tag{5.1c}$$

Assume a particular *parameter variation scenario* given by $\mathbf{p} = \mathbf{p}(t)$. Also assume that $\mathbf{u}$ is constant. Thus, system (5.1) has $2n + 1$ equations (function $\mathbf{h}$ has dimension n) and $2n + 1$ variables (n-dimensional vector $\mathbf{x}$, n-dimensional vector $\mathbf{v}$ and scalar t). The solution set of this system of equations represent the set of bifurcation points that can be

reached for this particular *scenario*. A graphical visualization of the BP associated with a *scenario* was sketched in Figure 18.

Define function $\mathbf{H}$ as:

$$\mathbf{H}(\mathbf{z}, t, \mathbf{v}) = \begin{bmatrix} \mathbf{h}(\mathbf{z}, \mathbf{p}(t), \mathbf{u}) \\ \partial_{\mathbf{z}}\mathbf{h}(\mathbf{z}, \mathbf{p}, \mathbf{u})\,\mathbf{v} \\ \|\mathbf{v}\| - 1 \end{bmatrix}, \tag{5.2}$$

thus every bifurcation point $(\mathbf{z}, t, \mathbf{v})$ satisfies

$$\mathbf{H}(\mathbf{z}, t, \mathbf{v}) = \mathbf{0}\,. \tag{5.3}$$

As defined in equation (3.2), the VSM measures the distance between the current operating point (given by $\mathbf{p}(0)$)) and the bifurcation point (given by $\mathbf{p}(t_{\max})$). In order to compute VSM, it is necessary to compute the bifurcation point that satisfies equation (5.1). This equation can be solved directly or indirectly by using continuation methods (described in Section 3.3). In this section, assume for simplicity that VSM can be quantified by the value of t at the BP:

$$\text{VSM} = t_{\max}\,. \tag{5.4}$$

Suppose that this power system undergoes a large perturbation (for example, the tripping of a transmission line or a generation unit due to a short-circuit) and that the power system model changes from $\mathbf{h}$ to $\widetilde{\mathbf{h}}$. The bifurcation point of the post-contingency situation is given by:

$$\widetilde{\mathbf{H}}(\mathbf{z}, t, \mathbf{v}) = \mathbf{0} \tag{5.5}$$

where:

$$\widetilde{\mathbf{H}}(\mathbf{z}, t, \mathbf{v}) = \begin{bmatrix} \widetilde{\mathbf{h}}(\mathbf{z}, \mathbf{p}(t), \mathbf{u}) \\ \partial_{\mathbf{z}}\widetilde{\mathbf{h}}(\mathbf{z}, \mathbf{p}, \mathbf{u})\,\mathbf{v} \\ \|\mathbf{v}\| - 1 \end{bmatrix}. \tag{5.6}$$

The goal of contingency screening and ranking is to determine which contingencies are critical or unstable, where:

- critical contingencies are near the bifurcation point (and the system is near a voltage collapse);
- unstable contingencies have already crossed the bifurcation surface, and the system immediately becomes unstable.

Using the definition of VSM of equation (5.4), VSM is a small positive number for critical contingencies and VSM is negative for unstable contingencies. Figure 49 shows the bifurcation surface associated with the system under three situations:

- The bifurcation surface for the pre-contingency situation;
- The bifurcation surface after a critical contingency, where the system is near the BP;

- The bifurcation surface after an unstable contingency, where equation $\widetilde{\mathbf{h}}(\mathbf{z}, 0) = \mathbf{0}$ has no solution $\mathbf{z}$.

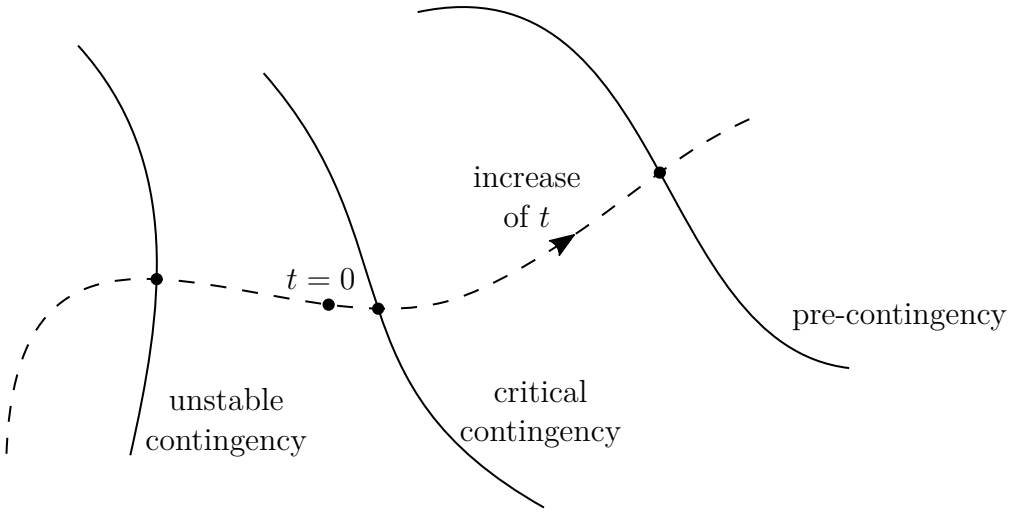

Figure 49 – Bifurcation surface after a contingency.

Each contingency is associated with a particular BP, as shown in Figure 49. In this section, a new method is proposed to accurately compute the BP for a set of credible contingencies in a efficient way.

Assume that the BP of the pre-contingency situation is known. In other words, the solution $(\mathbf{z}, t, \mathbf{v})$ of (5.3) is known. In order to compute the BP for a particular contingency, the solution of equation (5.5) should be computed (either directly or indirectly).

Given that a solution of (5.3) is already known, one possibility is to use this known solution as an initial estimate of the solution of (5.5) and apply an iterative solver, like Newton's method. This strategy is usually enough to compute the BP for most contingencies. However, in critical and unstable contingencies, the power system typically undergoes a large disturbance. As a consequence, the BPs of the pre-contingency and post-contingency situations are away from each other, and most numerical solvers are not able to reach the BP of the post-contingency case starting from the BP of the pre-contingency case.

In this chapter, we propose to apply a homotopy method to compute a solution of (5.5). A homotopy method basically defines a function $\mathbf{\Gamma}$ satisfying the following boundary conditions:

- $\mathbf{\Gamma}(\mathbf{z}_0, t_0, \mathbf{v}_0, 0) = \mathbf{0}$,
- $\mathbf{\Gamma}(\mathbf{z}, t, \mathbf{v}, 1) = \widetilde{\mathbf{H}}(\mathbf{z}, t, \mathbf{v}) \; \forall \; (\mathbf{z}, t, \mathbf{v})$,

where $(\mathbf{z}_0, t_0, \mathbf{v}_0)$ is an arbitrary initial point. Note that the dimension of $\mathbf{\Gamma}$ is the same dimension of $(\mathbf{z}, t, \mathbf{v})$.

Having defined function $\mathbf{\Gamma}$, one applies a continuation method (Section 3.3) to find

solutions of

$$\mathbf{\Gamma}(\mathbf{z}, t, \mathbf{v}, \mu) = \mathbf{0} \tag{5.7}$$

for increasing values of μ. The solution for $\mu = 0$ is known to be $(\mathbf{z}_0, t_0, \mathbf{v}_0)$, while the solution for $\mu = 1$ is the desired BP of the post-contingency situation (solution of (5.5)).

Figure 50 illustrates the solution branch of (5.7) for noncritical, critical and unstable contingencies. In this section, we assume that $(\mathbf{z}_0, t_0, \mathbf{v}_0)$ is the bifurcation point of the pre-contingency situation. Thus, the value of t at $\mu = 0$ shown in Figure 50 represents the pre-contingency VSM.

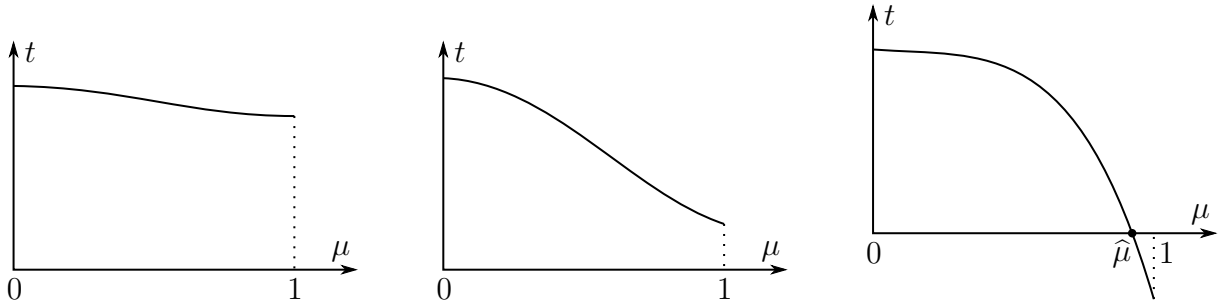

(a) Noncritical. (b) Critical. (c) Unstable.

Figure 50 – Solution branch of (5.7) for different contingencies.

In the unstable contingency shown in Figure 50, there is a $\widehat{\mu} \in (0, 1)$ in which $t = 0$ at the solution of (5.7). This is the value of μ at which the current operating point (given by $\mathbf{p} = \mathbf{p}(0)$) crosses the bifurcation surface, and the system loses the solution point.

Figure 50 shows the usual situation in which the solution branch of equation (5.7) does not undergo a bifurcation with the increase of μ for $\mu \in [0, 1]$. Even though this is generally the case (this statement will be corroborated in the results of Section 5.2), there might be atypical situations, e.g., the situation shown in Figure 51. This figure shows the case where a SNB (Subsection 4.1.1) occurs with the increase of μ, and μ starts to decrease after the turning point.

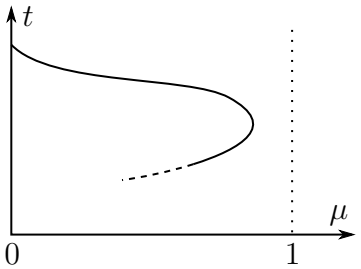

Figure 51 – Atypical solution branch of (5.7).

If one follows the solution branch shown in Figure 51, μ *might* restart to increase again and this solution branch *might* eventually reach the hyperplane $\mu = 1$. We cannot know beforehand if the solution branch of Figure 51 will reach $\mu = 1$. Even if it does, we

cannot predict how long it would take for a continuation procedure to track this entire solution branch. Thereat this work proposes to follow the solution branch only while μ is increasing. If μ starts decreasing for a particular contingency, then alternative methods should be applied to analyze this contingency specifically. Since very few contingencies behave like Figure 51, traditional methods like continuation power flow can be applied to these few contingencies without triggering a computational burden.

The Implicit Function Theorem guarantees that, if $\mathbf{\Gamma}$ is C^1, then every bifurcation of (5.7) with the increase of μ is a point of singularity of $\begin{bmatrix}\partial_{\mathbf{z}}\mathbf{\Gamma} & \partial_t\mathbf{\Gamma} & \partial_{\mathbf{v}}\mathbf{\Gamma}\end{bmatrix}$. Thus, if $\mathbf{\Gamma}$ is C^1, the situation sketched in Figure 51 will not occur as long as $\begin{bmatrix}\partial_{\mathbf{z}}\mathbf{\Gamma} & \partial_t\mathbf{\Gamma} & \partial_{\mathbf{v}}\mathbf{\Gamma}\end{bmatrix}$ is nonsingular on the solution branch. Note that the example of *smooth step function* in equation (4.19) is not C^2, and thus $\mathbf{\Gamma}$ is not C^1. This function will be C^1 if a C^2 *smooth step function* is used. For this chapter only, let all *smooth step functions* be instances of:

$$u = \frac{u_2 + u_1}{2} - \frac{u_1 - u_2}{\pi} \arctan \frac{(y - y_{\text{spec}})}{\gamma} \tag{5.8}$$

which can be shown to satisfy all properties of a *smooth step function*. In addition, (5.8) is an infinitely differentiable *smooth step function*. In all simulations of this chapter, $\gamma = 0.001$ will be used in all instances of (5.8). An example of a C^2 *smooth saturation function* is not necessary in this chapter, as no saturation function is employed in the studied power systems.

This chapter proposes to apply a continuation method to equation (5.7) to assess voltage stability of all power system branches (either transmission lines or transformers). For $\mu = 1$, both the series and shunt admittance of the branch must be zeroed, whereas the branch must be in-service for $\mu = 0$. In this work, let function $\mathbf{\Gamma}$ be an intermediary power system in which the branch admittances in equation (2.12) are given by (FLUECK; DONDETI, 2000):

$$y_{\text{se}}(\mu) = (1 - \mu)\, \widehat{y}_{\text{se}} \qquad\qquad y_{\text{sh}}(\mu) = (1 - \mu)\, \widehat{y}_{\text{sh}}\,, \tag{5.9}$$

where $\widehat{y}_{\text{se}}$ and $\widehat{y}_{\text{sh}}$ are, respectively, the original values of y_{se} and y_{sh} in the pre-contingency situation. From equation (2.12), it is possible to see that the branch is in-service for $\mu = 0$ and out-of-service for $\mu = 1$.

Note that functions $\mathbf{h}$ and $\widetilde{\mathbf{h}}$ are linear in relation to both y_{se} and y_{sh}, since y_{se} and y_{sh} only appear on the nodal equations of complex power. In other words, the complex powers $S_1 = E_1\overline{I_1}$ and $S_2 = E_2\overline{I_2}$ (where I_1 and I_2 are given in equation (2.12)) are linear in relation to the admittances. Therefore, function $\mathbf{H}$ can be separated into three distinct terms:

$$\mathbf{H}(\mathbf{z}, t, \mathbf{v}) \equiv \mathbf{H}_0(\mathbf{z}, t, \mathbf{v}) + \widehat{y}_{\text{se}}\, \mathbf{H}_{\text{se}}(\mathbf{z}, t, \mathbf{v}) + \widehat{y}_{\text{sh}}\, \mathbf{H}_{\text{sh}}(\mathbf{z}, t, \mathbf{v})\,, \tag{5.10}$$

where $\mathbf{H}_0$ is function $\mathbf{H}$ with the faulted branch removed, while $\mathbf{H}_{\text{se}}$ and $\mathbf{H}_{\text{sh}}$ are the linear coefficients of $\mathbf{H}$ in relation to y_{se} and y_{sh}, respectively. Note that $\widetilde{\mathbf{H}} \equiv \mathbf{H}_0$.

The homotopy described by equation (5.9) thus define the following function $\boldsymbol{\Gamma}$:

$$\begin{aligned}\boldsymbol{\Gamma}(\mathbf{z},t,\mathbf{v},\mu) &\equiv \widetilde{\mathbf{H}}(\mathbf{z},t,\mathbf{v}) + (1-\mu)\,\widehat{y}_{\text{se}}\,\mathbf{H}_{\text{se}}(\mathbf{z},t,\mathbf{v}) + (1-\mu)\,\widehat{y}_{\text{sh}}\,\mathbf{H}_{\text{sh}}(\mathbf{z},t,\mathbf{v}) \\ &\equiv (1-\mu)\,\widetilde{\mathbf{H}}(\mathbf{z},t,\mathbf{v}) + (1-\mu)\,\widehat{y}_{\text{se}}\,\mathbf{H}_{\text{se}}(\mathbf{z},t,\mathbf{v}) + (1-\mu)\,\widehat{y}_{\text{sh}}\,\mathbf{H}_{\text{sh}}(\mathbf{z},t,\mathbf{v}) + \mu\,\widetilde{\mathbf{H}}(\mathbf{z},t,\mathbf{v})\,,\end{aligned} \tag{5.11}$$

which reduces to:

$$\boldsymbol{\Gamma}(\mathbf{z},t,\mathbf{v},\mu) \equiv (1-\mu)\,\mathbf{H}(\mathbf{z},t,\mathbf{v}) + \mu\,\widetilde{\mathbf{H}}(\mathbf{z},t,\mathbf{v}) \tag{5.12}$$

showing that the homotopy described by equation (5.9) belongs to the class of the so-called convex homotopy methods (CHIANG; WANG, 2018):

$$\boldsymbol{\Gamma}(\mathbf{z},t,\mathbf{v},\mu) \equiv (1-\mu)\,\boldsymbol{\Gamma}_0(\mathbf{z},t,\mathbf{v}) + \mu\,\widetilde{\mathbf{H}}(\mathbf{z},t,\mathbf{v}) \tag{5.13}$$

where $\boldsymbol{\Gamma}_0$ is an arbitrary function satisfying $\boldsymbol{\Gamma}_0(\mathbf{z}_0,t_0,\mathbf{v}_0) = \mathbf{0}$. For the homotopy proposed in this work, $\boldsymbol{\Gamma}_0 \equiv \mathbf{H}$ and $(\mathbf{z}_0,t_0,\mathbf{v}_0)$ is the pre-contingency BP.

From the computational point of view, the only advantage of defining the admittances in equation (5.9) directly instead of using equation (5.12) is that the former only executes function $\mathbf{H}$ once per evaluation of $\boldsymbol{\Gamma}$, while the latter executes function $\mathbf{H}$ twice (one with the branch in-service and one with the branch out-of-service). However, equation (5.12) is more flexible as one does not need to modify branch parameters directly. Moreover, equation (5.12) can be used in contingencies other than branch contingencies.

The homotopy proposed in equation (5.12) will be compared to other convex homotopy methods, namely:

- The *Newton homotopy method*, defined by replacing the following function $\boldsymbol{\Gamma}_0$ into equation (5.13):

$$\boldsymbol{\Gamma}_0(\mathbf{z},t,\mathbf{v}) \equiv \widetilde{\mathbf{H}}(\mathbf{z},t,\mathbf{v}) - \widetilde{\mathbf{H}}(\mathbf{z}_0,t_0,\mathbf{v}_0)\,. \tag{5.14}$$

- The *fixed-point homotopy method*, defined by replacing the following function $\boldsymbol{\Gamma}_0$ into equation (5.13):

$$\boldsymbol{\Gamma}_0(\mathbf{z},t,\mathbf{v}) \equiv \mathbf{A}\begin{bmatrix}\mathbf{z}-\mathbf{z}_0\\ t-t_0\\ \mathbf{v}-\mathbf{v}_0\end{bmatrix}, \tag{5.15}$$

  where $\mathbf{A}$ is an arbitrary nonsingular matrix.

Both for *Newton homotopy methods* and *fixed-point homotopy methods*, the value of $\mathbf{z}_0$ is not restricted to be the pre-contingency bifurcation point, but rather it can be an arbitrary initial point.

As a remark, when many contingencies must be analyzed, it is useful to use the tangent vector as the predictor for the first continuation step. In this case, we estimate

$(\mathbf{z}(\mu), t(\mu), \mathbf{v}(\mu))$ in the following way:

$$\begin{bmatrix}\partial_{\mathbf{z}}\mathbf{\Gamma} & \partial_t\mathbf{\Gamma} & \partial_{\mathbf{v}}\mathbf{\Gamma}\end{bmatrix}\begin{bmatrix}d\mathbf{z}(\mu)\\ dt(\mu)\\ d\mathbf{v}(\mu)\end{bmatrix} + \partial_\mu\mathbf{\Gamma}\, d\mu = \mathbf{0}$$

$$\Rightarrow \begin{bmatrix}\partial_{\mathbf{z}}\mathbf{\Gamma} & \partial_t\mathbf{\Gamma} & \partial_{\mathbf{v}}\mathbf{\Gamma}\end{bmatrix}\begin{bmatrix}(\mathbf{z}(\mu)-\mathbf{z}_0)\\ (t(\mu)-t_0)\\ (\mathbf{v}(\mu)-\mathbf{v}_0)\end{bmatrix} = -\partial_\mu\mathbf{\Gamma}\,\mu\,, \quad (5.16)$$

where all Jacobian matrices are evaluated at point $(\mathbf{z}_0, t_0, \mathbf{v}_0)$.

In case of homotopy (5.12), the coefficient matrix $\begin{bmatrix}\partial_{\mathbf{z}}\mathbf{\Gamma} & \partial_t\mathbf{\Gamma} & \partial_{\mathbf{v}}\mathbf{\Gamma}\end{bmatrix}$ does not depend on the contingency being analyzed. Therefore, this matrix can be constructed and factorized only once, reducing the computational cost in the first prediction step.

5.1.1 The proposed algorithm

The method proposed in this chapter can be summarized by the following algorithm:

Step 1 Apply the continuation power flow on equation $\mathbf{h}(\mathbf{z}, t) = \mathbf{0}$ to compute the pre-contingency bifurcation point $(\mathbf{z}_0, t_0, \mathbf{v}_0)$ (solution of equation (5.3)).

Step 2 Build and factorize matrix $\begin{bmatrix}\partial_{\mathbf{z}}\mathbf{\Gamma} & \partial_t\mathbf{\Gamma} & \partial_{\mathbf{v}}\mathbf{\Gamma}\end{bmatrix}$, used to compute the tangent predictor as shown in equation (5.16).

Step 3 For each credible contingency:

- *3.1* Apply a continuation method on equation (5.12), with the goal to compute the solution of $\mathbf{\Gamma}(\mathbf{z}, t, \mathbf{v}, 1) = \mathbf{0}$ starting from the solution $(\mathbf{z}_0, t_0, \mathbf{v}_0)$ of $\mathbf{\Gamma}(\mathbf{z}, t, \mathbf{v}, 0) = \mathbf{0}$.
- *3.2* If the proposed continuation method stopped before $\mu = 1$ (i.e., this contingency behaves like Figure 51), then apply the continuation power flow on equation $\widetilde{\mathbf{h}}(\mathbf{z}, t) = \mathbf{0}$ to compute the post-contingency bifurcation point $(\mathbf{z}_1, t_1, \mathbf{v}_1)$.

The core of the proposed method is *Step 3.1*, which computes the bifurcation point for a given post-contingency scenario. Usually, the continuation power flow in *Step 3.2* has to be computed only for a few (if any) contingencies.

5.1.2 Example

A detailed analysis of the proposed method is provided for the IEEE 14-bus system (CHRISTIE, 1999). The contingency of the line between buses 1 and 5 is arbitrarily chosen in the analysis.

Assuming an increase in both generation and load proportionally to the base case, the continuation method (Section 3.3) is used to compute the VSM for the pre-contingency case, obtaining a VSM of 77.8%. This indicates that both generation and load can increase up to 77.8% before a voltage collapse. The continuation power flow provides $\mathbf{z}_0$ and t_0 at the BP, while $\mathbf{v}_0$ is an unit-vector tangent to the solution branch at the BP. This

vector might be a by-product of the continuation power flow computation, if the tangent predictor (equation (3.14)) is used.

The next step is to use another continuation method to find the solution of equation (5.7) at $\mu = 1$ (the post-contingency situation) from the solution of (5.7) at $\mu = 0$ (the pre-contingency situation). The result of this continuation procedure for the contingency of line 1—5 is shown in Figure 52. This figure also shows the estimate of VSM based on the linear sensitivity of VSM in relation to μ.

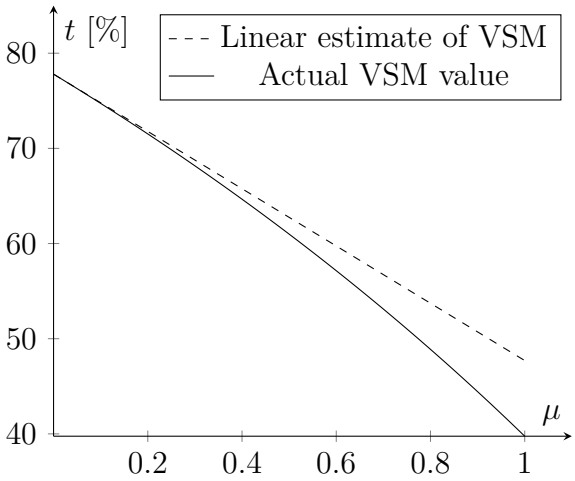

Figure 52 – Contingency of line 1—5.

The continuation process should compute the solution of (5.7) at $\mu = 1$ for as few values of μ as possible. Usually, it is possible to compute the solution of (5.7) at $\mu = 1$ with only one step from $\mu = 0$ to $\mu = 1$. However, only for critical contingencies, it may be necessary to decrease the step size. Therefore, the best approach is to start with a one-unit step-size and adaptatively decrease it if necessary.

In our implementation, the pre-contingency bifurcation for the 14-bus system is computed by means of the continuation power flow (see Section 3.3) in a time equivalent to 40 power flow executions, while the proposed method computes the bifurcation of the contingency case in a time equivalent to 2.3 power flow executions.

Consider now the contingency of line 1—2 instead of line 1—5. Using the proposed method, $t < 0$ at $\mu = 1$, indicating that the system loading should in fact be decreased to reach the bifurcation of the post-contingency situation (this case was sketched in Figure 50(c)). This emphasizes the ability of the proposed method to detect severe contingencies that would lead to an immediate voltage collapse, where there is no solution $\mathbf{z}$ for $t = 0$ and $\mu = 1$. The solution branch for contingency 1—2 is shown in Figure 53.

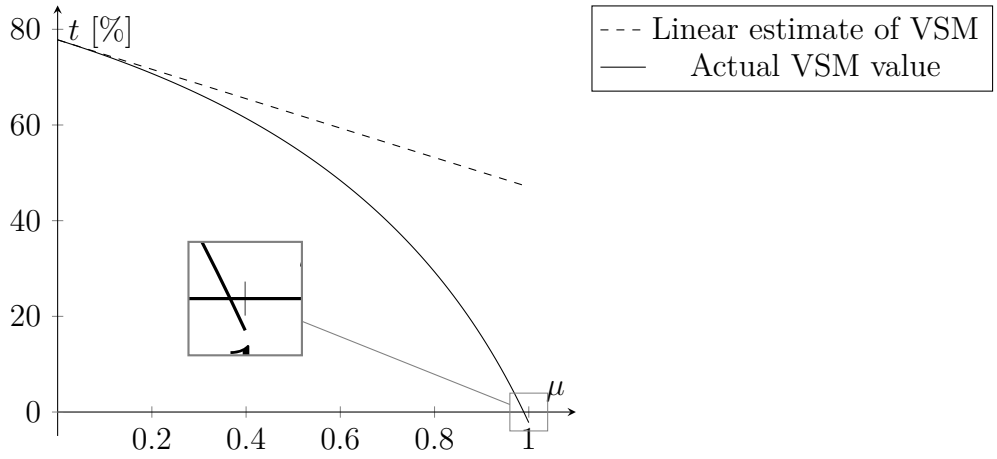

Figure 53 – Contingency of line 1—2.

5.2 Implementation results

In this section, the proposed method is applied to assess voltage stability for all branch contingencies (either a transmission line or a transformer) of different power systems. Each of these power systems is considered in one of the following subsections.

5.2.1 The IEEE 118-bus system

This is one of the IEEE standard test systems and its data can be obtained from (CHRISTIE, 1999). This power system has 186 branches. For 9 of these contingencies, the system becomes inoperable, since the contingency splits the system into two isolated islands. This situation can be detected (THEODORO et al., 2012) before the execution of our method and thus, these contingencies are excluded from the results presented here.

Table 3 highlights the accuracy of our method on estimating the contingency ranking for the most severe contingencies. Contingencies are ranked according to the VSM value (equation (5.4)). The table presents the ranking computed by three methods:

- the reference method, which uses the traditional power system model (Chapter 2) and continuation power flow to compute the VSM;
- the proposed method, using the smooth formulation (Chapter 4) and the homotopy described in Section 5.1;
- the linearization of the solution branch at the pre-contingency BP (shown as dashed lines in Figures 52 and 53).

Note that errors in VSM computation using the proposed method are only due to the smooth formulation and thus, these errors are usually negligible. Even though an (approximated) smooth power system model is used, the estimated ranking is almost identical to the exact ranking, not only for the critical contingencies shown in Table 3, but

Table 3 – Contingency ranking for the 118-bus system.

Contingency	Reference method	Proposed method	Linearization
8 — 5	1	1	1
75 — 118	2	2	122
38 — 37	3	3	5
100 — 103	4	4	103
38 — 65	5	5	3
76 — 77	6	6	77
103 — 110	7	7	104
68 — 69	8	8	176
4 — 5	9	9	17
26 — 30	10	10	2

for all contingencies in the power system model. Differences between the exact ranking and the estimated ranking only occur for contingencies whose VSMs are very close. Hence, these differences are unlikely to influence the contingency analysis.

Table 3 shows that the linearization ranking can be misleading. Contingency 75 — 118, for example, was ranked 122th according to the linearization, even though this is one of the most severe contingencies. The μt curve for this contingency is shown in Figure 54. From this figure, it is clear that the linearization at $\mu = 0$ cannot provide a good estimate of the BP at $\mu = 1$. In addition, this figure clarifies why the linearization cannot detect the severity of contingency 75 — 118. Figure 54 emphasizes that the relation between μ and VSM can be highly nonlinear.

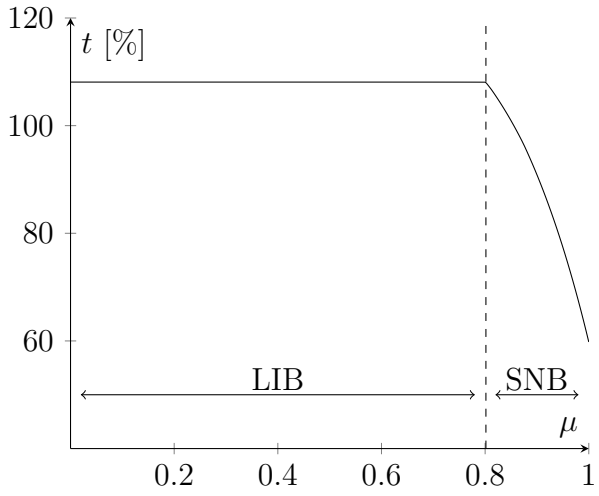

Figure 54 – Proposed homotopy for contingency 75 — 118.

From Figure 54 itself, we can see an abrupt change in the power system behavior at $\mu \approx 0.8$. This cusp point can be an evidence that the bifurcation type changes with the variation of μ. In fact, by classifying each BP in Figure 54 (NEVES; ALBERTO; CHIANG, 2020), we check that the bifurcation changes from LIB to SNB for $\mu \approx 0.8$.

Since every static bifurcation is transformed into a SNB when using the smooth model proposed in Chapter 4, the proposed method is able to seamlessly compute every point in the curve of Figure 54 without having to check the bifurcation type. This would also be the case in a transition from a SNB to CVIB, for example. Note that the traditional power system model cannot be used to detect LIBs or CVIBs using equation (5.1).

In Figures 55 and 56, all 177 contingencies are categorized according to the speed of the proposed method. In Figure 55, the proposed method is compared to the power flow computation. In Figure 56, the proposed method is compared to the reference method (shown in Table 3). These figures show that the proposed method is usually equivalent to a few power flow computations, and usually is more than 10 times faster than the reference method.

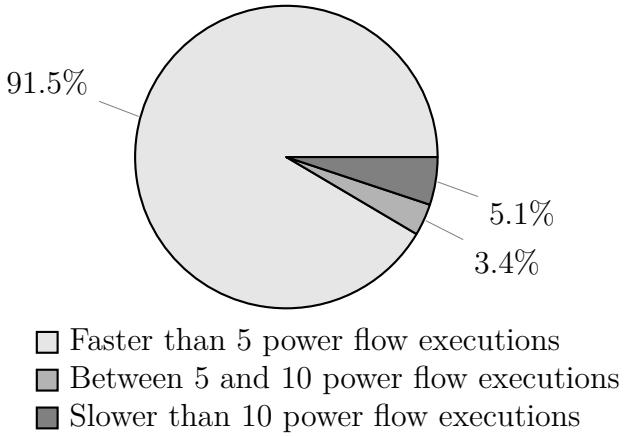

Figure 55 – Percentage of contingencies of the 118-bus system according to the speed of the proposed method to compute VSM of the post-contingency scenario in relation to the speed of the power flow computation.

All aforementioned results were obtained using the homotopy described by equation (5.9). Table 4 shows the same results using other homotopy methods, namely *Newton homotopy* (equation (5.14)) or *fixed-point homotopy* (equation (5.15)). The "quantile" field in this table gives the quantile of $\left\{\frac{\Delta t_{i,\text{reference method}}}{\Delta t_{i,\text{proposed}}}\right\}$, where $\Delta t_{i,\text{proposed}}$ represents the computational time expended by the proposed method on the ith contingency. For example, if the 30% quantile is 5, then the proposed method was (at least) 5 times faster than the reference method for 30% of all contingencies.

Table 4 indicates that the homotopy using equation (5.9) gave better results among the alternatives, since this homotopy was faster and did not encounter any atypical contingencies.

5.2.2 The PEGASE 1354-bus system

This system represents partially the size and complexity of the European transmission system (JOSZ et al., 2016; FLISCOUNAKIS et al., 2013), and its data can be

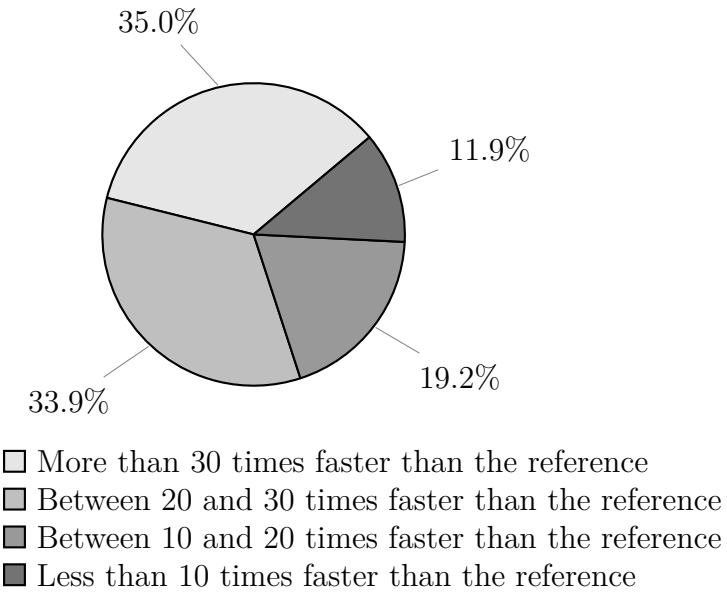

Figure 56 – Percentage of contingencies of the 118-bus system according to the speed of the proposed method to compute VSM of the post-contingency scenario in relation to the speed of the reference method.

Table 4 – IEEE 118-bus system: Comparison of homotopy methods (higher values of quantile are better).

Homotopy method	Equation (5.9)	Equation (5.14)	Equation (5.15) $\mathbf{A} = \mathbf{I}$	Equation (5.15) $\mathbf{A} = \partial_{(\mathbf{z},t,\mathbf{v})}\mathbf{H}$ evaluated at $(\mathbf{z}_0, t_0, \mathbf{v}_0)$
Number of *atypical* contingencies (Figure 51)	0	0	4	0
90% quantile	8.15	5.33	5.81	5.36
50% quantile	25.9	22.1	23.9	22.2
10% quantile	37.6	35.9	38.1	34.2

obtained from MATPOWER (ZIMMERMAN; MURILLO-SANCHEZ; THOMAS, 2011). This system has 1991 branches. 561 of these branches are necessary for the system to be connected. Thus, these contingencies are ignored in this analysis.

Table 5 highlights the accuracy of the proposed method in estimating the contingency ranking for the most severe contingencies. The same comments made for Table 3 are relevant for Table 5. This table reiterates that methods based on extrapolation can provide misleading results regarding the contingency ranking. The method proposed here, on the other hand, provides an accurate estimate of the exact contingency ranking

In Figures 57 and 58, all 1430 contingencies are categorized according to the speed of the proposed method. In Figure 57, the proposed method is compared to the power flow computation. In Figure 58, the proposed method is compared to the reference method. These figures show that the proposed method is usually equivalent to a few power flow

Table 5 – Contingency ranking for the 1354-bus system.

Contingency	Reference method	Proposed method	Linearization
3145 — 2918	1	1	253
3145 — 7770	2	2	606
4950 — 333	3	3	1421
9174 — 5658	4	4	213
6901 — 4874	5	5	9
6738 — 6901	6	6	7
5589 — 3608	7	7	1
1767 — 892	8	8	3
1001 — 892	9	9	53
455 — 333	10	10	5

computations, and usually is more than 10 times faster than the reference method.

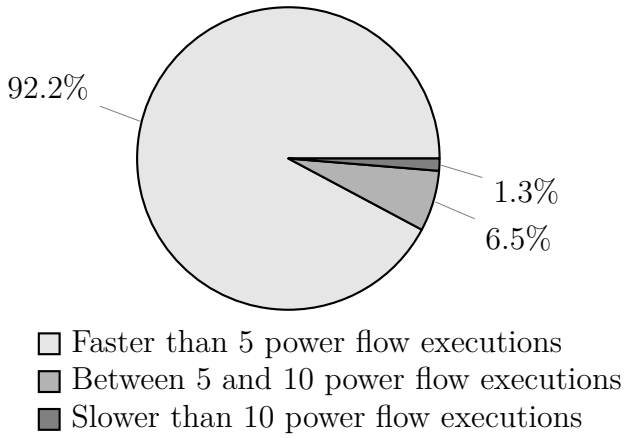

Figure 57 – Percentage of contingencies of the 1354-bus system according to the speed of the proposed method to compute VSM of the post-contingency scenario in relation to the speed of the power flow computation.

Table 6 shows the comparison of different homotopy methods in analyzing the 1354-bus system. For this system, all homotopy methods (except equation (5.15) with $\mathbf{A} = \mathbf{I}$) were equivalent in terms of robustness and performance.

This power system is also analyzed considering voltage limits. These limits are inequalities incorporated into inequation (2.36b), and they are transformed into equations as proposed in Section 4.4. Both undervoltage limits and overvoltage limits are gathered, as shown in inequation (4.47) using $p = 1000$. In this situation, the proposed method was faster than 10 power flow executions in 90.4% of the contingencies.

5.2.3 The PEGASE 2869-bus system

This system also represents the European transmission line, and it approaches the size of real power systems. This system has 4582 branches from which 778 are essential for

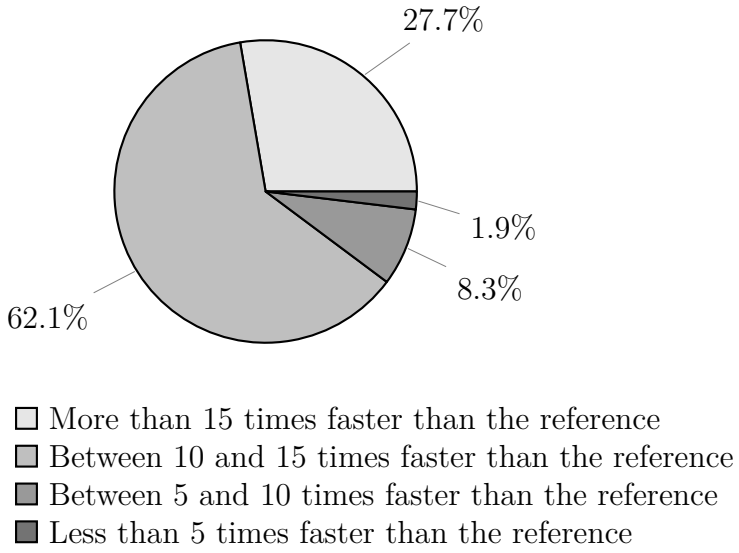

Figure 58 – Percentage of contingencies of the 1354-bus system according to the speed of the proposed method to compute VSM of the post-contingency scenario in relation to the speed of the reference method.

Table 6 – PEGASE 1354-bus system: Comparison of homotopy methods (higher values of quantile are better).

Homotopy method	Equation (5.9)	Equation (5.14)	Equation (5.15) $\mathbf{A} = \mathbf{I}$	Equation (5.15) $\mathbf{A} = \partial_{(\mathbf{z},t,\mathbf{v})}\mathbf{H}$ evaluated at $(\mathbf{z}_0, t_0, \mathbf{v}_0)$
Number of *atypical* contingencies (Figure 51)	0	0	5	0
90% quantile	9.91	9.70	2.39	9.75
50% quantile	13.6	13.8	12.2	13.8
10% quantile	17.3	18.1	17.2	18.1

the system to be connected. These contingencies are neglected in this analysis.

As for the 1354-bus system, none of the remaining 3804 contingencies behave like Figure 51, which shows that the proposed method is robust in analyzing all contingencies of large power systems. Table 7 highlights the accuracy of the proposed method in estimating the contingency ranking for the most severe contingencies. The same comments made for Table 3 are relevant for Table 7.

Note that the wrong classification of contingency 1767 — 892 is *not* a problem, since the difference in VSM between the 9th and 17th contingencies (according to the proposed method) is only 0.13%. This means that, in terms of severity, all contingencies ranked from 9th to 17th are basically equivalent.

In Figures 59 and 60, all 3804 contingencies are categorized according to the speed of the proposed method. In Figure 59, the proposed method is compared to the power flow computation. In Figure 60, the proposed method is compared to the reference method.

Table 7 – Contingency ranking for the 2869-bus system.

Contingency	Reference method	Proposed method	Linearization
8249 — 6139	1	1	2
4950 — 333	2	2	3591
6901 — 4874	3	3	1064
4858 — 8211	4	4	1
1956 — 8264	5	5	3
6738 — 6901	6	6	997
5589 — 3608	7	8	899
2154 — 5996	8	7	19
1767 — 892	9	17	960
838 — 6295	10	9	14

These figures show that the proposed method is usually equivalent to a few power flow computations, and usually is more than 10 times faster than the reference method.

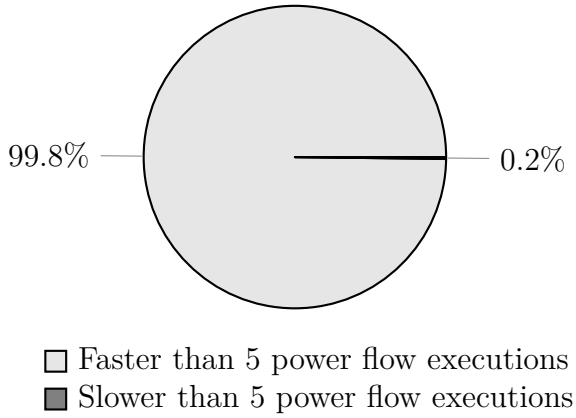

Figure 59 – Percentage of contingencies of the 2869-bus system according to the speed of the proposed method to compute VSM of the post-contingency scenario in relation to the speed of the power flow computation.

Table 8 shows the comparison of different homotopy methods in analyzing the 2869-bus system. The same way as for the 118-bus system, this table shows that the proposed homotopy performed slightly better than the alternatives.

This power system is also analyzed considering voltage limits. These limits are the inequalities in inequation (2.36b), and they are transformed into equations as proposed in Section 4.4. Both undervoltage limits and overvoltage limits are gathered as shown in inequation (4.47) using $p = 1000$. In this situation, the proposed method was faster than 10 power flow executions in 93.1% of the contingencies.

5.2.4 Conclusions

The results shown in this section demonstrate that the contingency ranking computed by the proposed method is very close to the exact one. The only source of error in

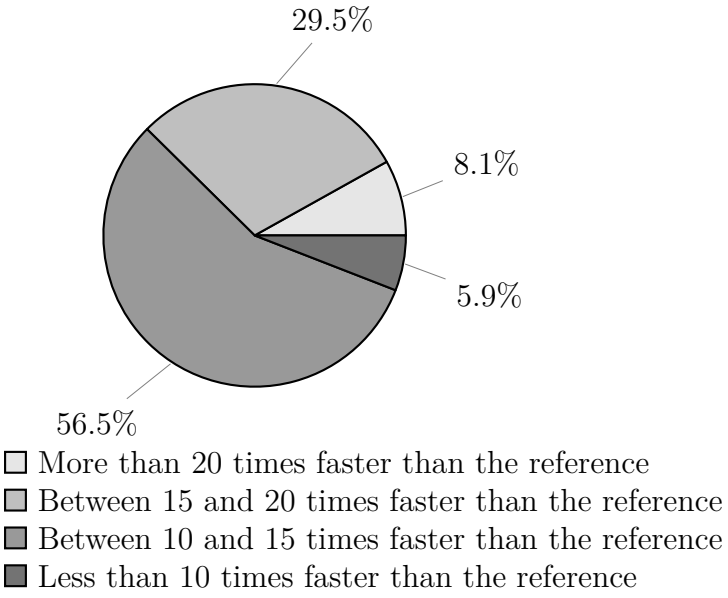

Figure 60 – Percentage of contingencies of the 2869-bus system according to the speed of the proposed method to compute VSM of the post-contingency scenario in relation to the speed of the reference method.

Table 8 – PEGASE 2869-bus system: Comparison of homotopy methods (higher values of quantile are better).

Homotopy method	Equation (5.9)	Equation (5.14)	Equation (5.15) $\mathbf{A} = \mathbf{I}$	Equation (5.15) $\mathbf{A} = \partial_{(\mathbf{z},t,\mathbf{v})}\mathbf{H}$ evaluated at $(\mathbf{z}_0, t_0, \mathbf{v}_0)$
Number of *atypical* contingencies (Figure 51)	0	0	7	0
90% quantile	11.0	10.7	1.43	10.6
50% quantile	14.2	13.8	2.33	13.6
10% quantile	19.1	18.7	16.7	18.3

the proposed method is the error due to the approximated model proposed in Chapter 4. Differences in the ranking using the proposed method and the reference method only occur for contingencies that produce almost the same value of VSM. These contingencies can be considered equivalent in terms of severity and hence the difference in the ranking is unlikely to influence the contingency analysis.

Even though the proposed method aims for accurately computing the VSM associated with each contingency, this method was consistently executed faster than the continuation power flow (often between 8-15 times faster, according to Tables 4, 6 and 8). This execution time is often between the cost of 5-10 power flow executions.

In relation to other homotopy methods, the homotopy described by equation (5.9) invariably produced good results in terms of speed, and performed best according to the number of atypical contingencies. Tables 4, 6 and 8 show that no contingencies were

problematic when using equation (5.9). In general, only a few contingencies are expected to behave like Figure 51. Hence the cost of analyzing these few atypical contingencies using the reference method would not be unacceptably high.

5.3 Comparison to other studies

This chapter proposed a new method to compute VSM of a set of credible contingencies by solving equation (5.5) using a homotopy method. Since equation (5.5) is in fact being solved, the proposed method does not rely on approximations to estimate the VSM for a given contingency.

In the literature on contingency ranking and screening, most methods (EJEBE et al., 1996; CHIANG; WANG; FLUECK, 1997; GREENE; DOBSON; ALVARADO, 1999; JIA; JEYASURYA, 2000; FLUECK; GONELLA; DONDETI, 2002; NEVES; ALBERTO; CHIANG, 2020) estimate VSM by means of extrapolations. Many critical contingencies represent a large disturbance and a very nonlinear change in the power flow behavior (this is clearly depicted in Figure 54), thus extrapolations can provide misleading results in relation to the severity of a contingency. Tables 3, 5 and 7 illustrate well these misleading results when using a linear extrapolation.

Most studies in the literature assume that a SNB occurs at the BP. In contrast, a key aspect of the proposed method is the application of the model proposed in Chapter 4. In this way, it is possible to compute generic bifurcations in the original power system (namely SNBs, LIBs and CVIBs) in a unified way, since all these bifurcations correspond to SNBs in the smooth power system model. The model proposed in Chapter 4 is seamlessly integrated in the method proposed in this chapter. As a result, the proposed method does not need to verify if the bifurcation type changes from the pre-contingency situation to the post-contingency situation. For example, the proposed method can compute the solution branch shown in Figure 54 without checking that the bifurcation changed from LIB to SNB.

Without the model proposed in Chapter 4, the homotopy method would fail to compute the post-contingency bifurcation point in the case of a change in the bifurcation type, because the characteristic equations of a bifurcation change from one bifurcation type to the other (according to the definitions in Section 4.1). In this case, the homotopy method would fail when it could not find a solution for the characteristic equations, which is the case simply because the characteristic equations changed during the continuation process.

6 PROPOSED METHOD FOR VSM COMPUTATION CONSIDERING PARAMETER UNCERTAINTIES

In the literature, parameter uncertainties in static voltage stability were addressed as described in Section 3.6. This chapter, on the other hand, describes how parameter uncertainties are addressed in this work, and how these uncertainties influence the computation of voltage stability margin. Moreover, a new method is proposed to compute voltage stability margin with special consideration for these uncertainties.

Parameter uncertainties should be taken into account in VSA because we cannot predict exactly how parameters will change with time. In other words, we cannot known in advance the *parameter variation scenario* $\mathbf{p}(t)$ shown in Figure 18. In general, the elements of $\mathbf{p}$ are loading parameters (recall that these elements usually parameterize the power of different load buses in the power system), which are intuitively uncontrollable (e.g., we cannot control how much load power a consumer is demanding at a specific bus). Loading uncertainties are intensified nowadays with the increase of intermittent and distributed generation, which are usually non-dispatchable as well.

The remaining of this chapter is divided as follows. Section 6.1 describes the new proposed model for dealing with parameter uncertainties in voltage stability assessment. Section 6.2 explains how this model is included in the voltage stability margin computation. Section 6.3 presents a robust and fast method to compute VSM considering parameter uncertainties. Several implementation results are reported in Section 6.4 for different power systems. Finally, Section 6.5 discusses the main features of the proposed method and the contributions of this chapter to the current VSA literature.

6.1 On the modelling of parameter uncertainties

In Section 3.2, the bifurcation surface was defined and a *parameter variation scenario* was described. Section 3.6 then presented a discussion on why it is important not only to use statistical information to predict the true *parameter variation scenario* but also to take uncertainties related to this *scenario* into account when computing VSM.

The true *parameter variation scenario* $\mathbf{p}$ cannot be predicted exactly. This is a consequence of the fact that any *parameter variation scenario* is one realization $\mathbf{p}(t)$ of a stochastic process $\{\mathbf{P}(t),\ t \geq 0\}$. Both the index set and the state space are continuous in this stochastic process. This work assumes that this stochastic process is a Brownian Motion (ROSS, 1995), which is a limit case of a Random Walk. In this case, process $\{\mathbf{P}(t),\ t \geq 0\}$ satisfies the following assumptions:

- $\{\mathbf{P}(t),\ t \geq 0\}$ has independent increments, which means that

$$\mathbf{P}(b) - \mathbf{P}(a) \tag{6.1}$$

and

$$\mathbf{P}(d) - \mathbf{P}(c) \tag{6.2}$$

are independent variables as long as intervals (a, b) and (c, d) do not overlap.
- $\{\mathbf{P}(t),\ t \geq 0\}$ has stationary increments, which means that the random variable given by

$$\mathbf{P}(t_0 + \Delta t) - \mathbf{P}(t_0) \tag{6.3}$$

is independent of t_0.
- $\{\mathbf{P}(t),\ t \geq 0\}$ is *memoryless*, in the sense that it satisfies the Markov property. In other words, the value of $\mathbf{p}(t)$ for $t > T$ depends only on the value of $\mathbf{p}(T)$, and not on the value of $\mathbf{p}(t)$ for $t < T$.

Assume the random variable $\mathbf{P}(t)$ can be decomposed into a purely deterministic term $\widehat{\mathbf{p}}(t)$ and a purely stochastic term $\widetilde{\mathbf{P}}(t)$ in the following form:

$$\mathbf{P}(t) = \widehat{\mathbf{p}}(t) + \widetilde{\mathbf{P}}(t)\,, \tag{6.4}$$

where the expectation of the stochastic term is zero ($E\{\widetilde{\mathbf{P}}(t)\} = 0\ \forall\ t \geq 0$). Thus, the expected path among all realizations of $\{\mathbf{P}(t),\ t \geq 0\}$ is equal to $\widehat{\mathbf{p}}(t)$. It is intuitive to note that the expected *parameter variation scenario*, given by $\widehat{\mathbf{p}}(t)$, is the trajectory to be considered when uncertainties are neglected. For example, *scenario* $\widehat{\mathbf{p}}(t)$ is the path assumed by continuation methods when computing a specific bifurcation point.

If $\{\widetilde{\mathbf{P}}(t),\ t \geq 0\}$ is a Brownian Motion, then the increment given by

$$\widetilde{\mathbf{P}}(t + t_0) - \widetilde{\mathbf{P}}(t_0) \tag{6.5}$$

follows a multivariate normal distribution with mean zero and covariance matrix proportional to t. Let this increment be given by:

$$\widetilde{\mathbf{P}}(t + t_0) - \widetilde{\mathbf{P}}(t_0) = \sqrt{t}\mathbf{A}\mathbf{Z} \tag{6.6}$$

where $\mathbf{Z}$ is a set of independent random variables following the standard normal distribution (i.e., $\mathbf{Z}$ is a standard normal random vector). Matrix $\mathbf{A}$ has full row rank[1] and is independent of t_0, since a Brownian Motion has stationary increments. It follows that the covariance matrix $\mathbf{\Sigma}(t)$ of $\widetilde{\mathbf{P}}(t + t_0) - \widetilde{\mathbf{P}}(t_0)$ is given by $t\mathbf{A}\mathbf{A}^T$, which is nonsingular for $t \neq 0$.

[1] In this work we assume the generic situation where there are no completely dependent random variables in $\mathbf{p}$. If, on the other hand, there are $m - m_0$ completely dependent random variables, one could split vector $\mathbf{p}$ as $\mathbf{p}^T = \left[\mathbf{p}_1^T, \mathbf{p}_2^T\right]$, where $\mathbf{p}_1 \in \mathbb{R}^{m_0}$ is a random vector with no completely dependent elements and $\mathbf{p}_2 = \mathbf{p}_2(\mathbf{p}_1)$ is a function of $\mathbf{p}_1$.

Equations (6.4) and (6.6) can be used to provide the probability density function of $\mathbf{P}(t)$ for any t, given that $\mathbf{P}(0) = \mathbf{p}(0) = \widehat{\mathbf{p}}(0)$ and $\widetilde{\mathbf{P}}(0) = \mathbf{0}$. Since (6.6) follows a multivariate normal distribution, the prediction region for $\widetilde{\mathbf{P}}(t)$ can be computed using the χ^2 distribution:

$$\widetilde{\mathbf{p}}^T \boldsymbol{\Sigma}(t)^{-1} \widetilde{\mathbf{p}} \leq F_m^{-1}(\sigma)\,, \tag{6.7}$$

where $F_m^{-1}(\sigma)$ is the inverse cumulative distribution function of the χ^2 distribution with m degrees of freedom (where m is the dimension of $\mathbf{p}$). Equation (6.7) basically says that, with probability σ, $\widetilde{\mathbf{P}}(t)$ is inside a hyper-ellipsoid centered at the origin.

Since the norm of $\boldsymbol{\Sigma}(t) = t\mathbf{A}\mathbf{A}^T$ increases with t, the volume of the hyper-ellipsoid (6.7) increases with t. This is intuitive: the uncertainty in vector $\mathbf{p}(t)$ should increase with time, since we are predicting a point further in the future.

With probability σ, equation (6.7) ensures that the realization of $\mathbf{P}(t)$ will be a function $\mathbf{p}(t)$ such that:

$$\left\| \frac{\mathbf{p}(t) - \widehat{\mathbf{p}}(t)}{\sqrt{t}} \right\|_\beta^2 \leq 1\,, \tag{6.8}$$

where the vector norm $\|\cdot\|_\beta = \sqrt{\langle \cdot, \cdot \rangle_\beta}$ is induced by the following inner product:

$$\langle \mathbf{x}, \mathbf{y} \rangle_\beta \equiv \mathbf{x}^T \frac{(\mathbf{A}\mathbf{A}^T)^{-1}}{F_m^{-1}(\sigma)} \mathbf{y} \equiv \mathbf{x}^T \mathbf{M}_\beta \mathbf{y}\,. \tag{6.9}$$

A graphical sketch of equations (6.7) and (6.8) is shown in Figure 61. Figure 61(c) is the superposition of the *scenario* shown in Figure 61(a) and the uncertainty regions shown in Figure 61(b). The dotted lines in Figure 61(c) show the boundary of the uncertainty region.

The uncertainty region in Figure 61(c) is a function of the probability σ: to increase the probability of function $\mathbf{p}(t)$ stay inside the uncertainty region, σ should be increased in (6.7), which in turn increases the volume of the ellipses in Figure 61(b) (note that F_m^{-1} is an increasing function of the probability σ).

In the remainder of this chapter, the structure of equation (6.8) is explored to provide specialized methods for voltage stability assessment.

6.2 Including parameter uncertainties in VSM computation

VSM is defined in equation (3.2) as a measure of the distance between the current operating point $\mathbf{p}(0)$ and the bifurcation point $\mathbf{p}(t_{\max})$, thus low values of VSM indicate that the system is currently near a bifurcation point, and preventive actions should be triggered to avoid a voltage collapse. When considering several *scenarios*, it is reasonable to define the overall VSM as the infimum of all VSM values associated with all credible *scenarios*. Mathematically, the overall VSM is the solution of the following optimization

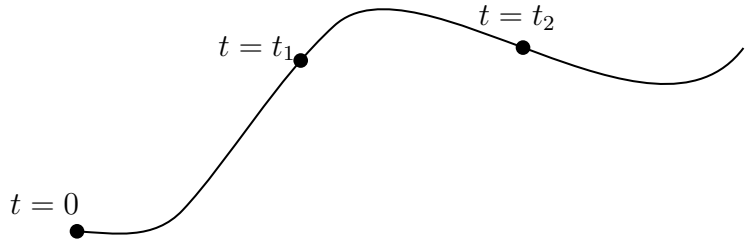

(a) Expected *scenario* $\widehat{\mathbf{p}}(t)$.

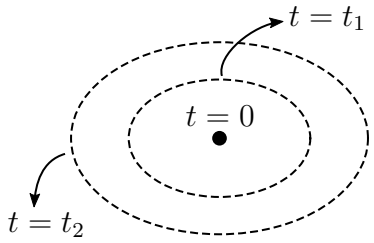

(b) Prediction region of vector $\widetilde{\mathbf{p}}(t)$ (equation (6.7)).

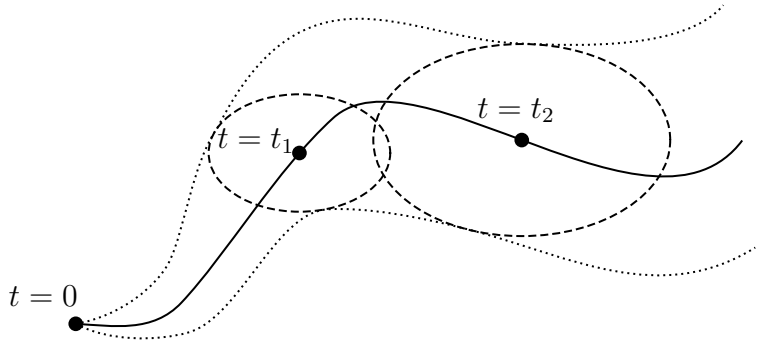

(c) Prediction region of vector $\mathbf{p}(t)$ (equation (6.8)).

Figure 61 – Graphical sketch of the uncertainty region for a given probability σ.

problem:

$$\begin{aligned} &\min_{i} && \text{VSM}(\mathbf{p}_i) \\ &\text{subject to} && \mathbf{p}_i \text{ is a credible parameter varation scenario} \end{aligned} \tag{6.10}$$

where $\mathbf{p}_i$ is a function that describes the ith credible *scenario* and VSM is a function that computes the voltage stability margin associated with a particular *scenario*. Note that the minimization of VSM proposed by this optimization problem agrees with the approach of minimizing VSM described in Sections 3.5 and 3.6.

From Section 6.1, within a probability σ, *scenario* $\mathbf{p}(t)$ (which is a realization of the stochastic process $\{\mathbf{P}(t),\ t \geq 0\}$) satisfies inequation (6.8). Thus, with probability σ, the VSM of the true *parameter variation scenario* is higher than the solution of the following optimization problem:

$$\begin{aligned} \text{VSM}_{\text{min}} = \quad &\min_{\mathbf{p}} && \text{VSM}(\mathbf{p}) \\ &\text{subject to} && \left\| \frac{\mathbf{p}(t) - \widehat{\mathbf{p}}(t)}{\sqrt{t}} \right\|_{\beta}^{2} \leq 1 \end{aligned} \tag{6.11}$$

where the optimal function $\mathbf{p}$ of this problem is the critical *scenario*, which produces the lowest VSM among all realizations of $\{\mathbf{P}(t),\ t \geq 0\}$ within a probability σ.

Intuitively, one should decrease the value of VSM_{min} to increase the confidence of the analysis (the less VSM_{min} is, the greater is the number of *scenarios* for which $\text{VSM} \geq \text{VSM}_{\text{min}}$). In fact, to increase the probability of the actual VSM be greater than VSM_{min}, σ should be increased from σ_0 to σ_1, which in turn increases the cumulative distribution function F_m^{-1}, concluding that the feasible set of problem (6.11) for a given σ_0 is a subset of the feasible set of problem (6.11) for $\sigma_1 > \sigma_0$. This proves that $\text{VSM}_{\text{min}}(\sigma_0) \geq \text{VSM}_{\text{min}}(\sigma_1)$.

For the computation of VSM, one usually needs only the final bifurcation point $\mathbf{p}(t_{\max})$, thus problem (6.11) can be reduced to the following:

$$\begin{aligned} \mathrm{VSM}_{\min} = \min_{t_{\max},\mathbf{p}_{\max}} \quad & \text{objective}(\mathbf{p}_{\max}) \\ \text{subject to} \quad & \mathbf{p}_{\max} \in \text{ bifurcation surface} \\ & \left\| \frac{\mathbf{p}_{\max} - \widehat{\mathbf{p}}(t_{\max})}{\sqrt{t_{\max}}} \right\|_\beta^2 \leq 1 \\ & \sqrt{t_{\max}} \geq 0 \end{aligned} \tag{6.12}$$

where the first constraint guarantees that $\mathbf{p}_{\max} = \mathbf{p}(t_{\max})$ is a bifurcation point. In comparison to (6.11), only the bifurcation point is required to solve this problem, as opposed to computing the whole *scenario* from $t = 0$ to $t = t_{\max}$. Moreover, problem (6.12) explicitly constraints $\sqrt{t_{\max}}$ to be non-negative, which was an implicit constraint on problem (6.11). Note that $t_{\max} \neq 0$ since $\mathbf{p}(0)$ (the current operating point) is not on the bifurcation surface.

From (3.2):

$$\text{objective}(\mathbf{p}_{\max}) \equiv d(\mathbf{p}_0, \mathbf{p}_{\max}) \equiv \|\mathbf{p}_{\max} - \mathbf{p}_0\|_\alpha \,, \tag{6.13}$$

where $\mathbf{p}_0 = \mathbf{p}(0)$ and it is assumed that the distance function d in (3.2) comes from a generic vector norm $\|\cdot\|_\alpha$.

The next section proposes a new method for solving problem (6.12).

6.3 The proposed method for computing VSM_{min}

In this section, problem (6.12) will be simplified to allow for fast computation of $\mathrm{VSM}_{\min}$. Moreover, a new method is proposed to solve the simplified problem.

6.3.1 Describing the bifurcation surface

This is the point where the power flow model proposed in Chapter 4 is useful. With this modelling, every bifurcation point, without exception, satisfies equation (5.1). In addition, every solution of (5.1) generically is a bifurcation point. This concludes that (5.1) describes the bifurcation surface, and problem (6.12) can be rewritten as:

$$\begin{aligned} \mathrm{VSM}_{\min} = \min_{t_{\max},\mathbf{p}_{\max},\mathbf{z},\mathbf{v}} \quad & \|\mathbf{p}_{\max} - \mathbf{p}_0\|_\alpha \\ \text{subject to} \quad & \mathbf{h}(\mathbf{z}, \mathbf{p}_{\max}) = \mathbf{0} \\ & \partial_{\mathbf{z}}\mathbf{h}(\mathbf{z}, \mathbf{p}_{\max})\ \mathbf{v} = \mathbf{0} \\ & \|\mathbf{v}\| = 1 \\ & \left\| \frac{\mathbf{p}_{\max} - \widehat{\mathbf{p}}(t_{\max})}{\sqrt{t_{\max}}} \right\|_\beta^2 \leq 1 \\ & \sqrt{t_{\max}} \geq 0 \end{aligned} \tag{6.14}$$

where the control vector $\mathbf{u}$ was omitted from function $\mathbf{h}$.

6.3.2 Describing the proposed hypercone

In order to implement inequation (6.8), it is necessary to estimate the expectation $\widehat{\mathbf{p}}(t)$ of the random process $\{\mathbf{P}(t), t \geq 0\}$. This expectation is usually difficult to obtain, so it is reasonable to use a linear approximation for $\widehat{\mathbf{p}}(t)$ given by a ray spanned by a constant vector $\widehat{\mathbf{p}}$:

$$\widehat{\mathbf{p}}(t) = \sqrt{t}\widehat{\mathbf{p}} \tag{6.15}$$

where $\widehat{\mathbf{p}}$ is a fixed vector, which provides the direction in which $\mathbf{p}$ is assumed to vary with the increase of t. In this definition it is assumed that $\mathbf{p}(0) = \mathbf{p}_0 = \mathbf{0}$, thus the origin of the parameter space is the current operating point (the coordinate system can be shifted to this end).

By replacing (6.15) in inequation (6.8):

$$\left\| \frac{\mathbf{p}_{\max}}{\sqrt{t_{\max}}} - \widehat{\mathbf{p}} \right\|_\beta^2 \leq 1\,, \tag{6.16}$$

which describes a cone whose vertex is at the origin in the m-dimensional parameter space[2]. This cone is sketched in Figure 62 for $m = 2$. The dotted ellipse in this figure is the boundary of the set $\{\mathbf{p} \mid \|\mathbf{p} - \widehat{\mathbf{p}}\|_\beta \leq 1\}$.

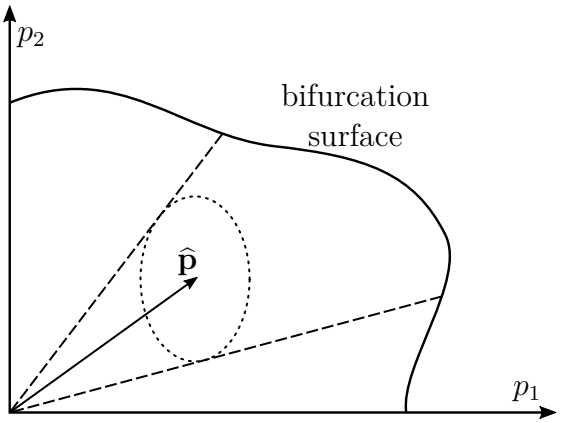

Figure 62 – Cone generated by inequation (6.16).

For each optimal bifurcation point $\mathbf{p}_{\max}$ of (6.12), there is an interval $[t_{\text{lower}}, t_{\text{upper}}]$ of optimal values of $t_{\max}$. When $t_{\text{lower}} < t_{\text{upper}}$ (this situation is sketched in Figure 63), there is a continuum of solutions of (6.12) distinguished by the value of $t_{\max}$. Hence, $t_{\max}$ does not directly influence the solution of problem (6.12). By exploring inequation (6.16), $t_{\max}$ can be removed from problem (6.12).

Since $\|\cdot\|_\beta$ is induced by the inner product $\langle\cdot,\cdot\rangle_\beta$, equation (6.16) can be expanded as follows:

$$\frac{\|\mathbf{p}_{\max}\|_\beta^2}{t_{\max}} - 2\frac{\langle \mathbf{p}_{\max}, \widehat{\mathbf{p}}\rangle_\beta}{\sqrt{t_{\max}}} + \|\widehat{\mathbf{p}}\|_\beta^2 - 1 \leq 0\,. \tag{6.17}$$

[2] For any $\mathbf{p}_{\max}$ satisfying (6.16) for a given $t_{\max}$, any $\mathbf{p} = k\mathbf{p}_{\max}$ $(k > 0)$ also satisfies (6.16) for $t = k^2 t_{\max}$

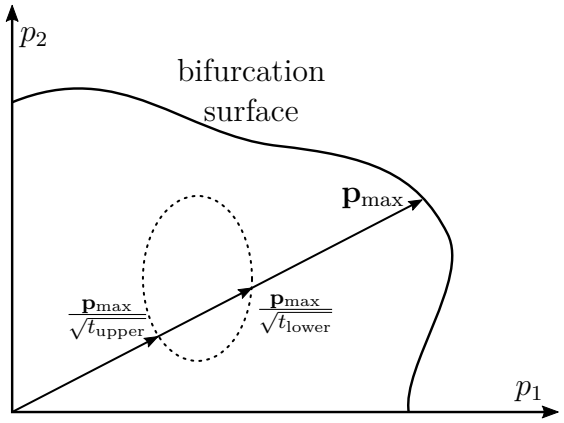

Figure 63 – Continuum $[t_{\text{lower}}, t_{\text{upper}}]$ of optimal values of $t_{\max}$.

In relation to $1/\sqrt{t_{\max}}$, the left-hand side of this inequation is a convex quadratic polynomial (note that $\|\mathbf{p}_{\max}\|_\beta^2 > 0$ since $\mathbf{p}_{\max} \neq \mathbf{0}$), so there is a $t_{\max}$ that satisfies this inequation if and only if there is at least one real solution $t_{\max}$ to the following equation:

$$\frac{\|\mathbf{p}_{\max}\|_\beta^2}{t_{\max}} - 2\frac{\langle \mathbf{p}_{\max}, \widehat{\mathbf{p}} \rangle_\beta}{\sqrt{t_{\max}}} + \|\widehat{\mathbf{p}}\|_\beta^2 - 1 = 0\,, \tag{6.18}$$

which only occurs when:

$$\langle \mathbf{p}_{\max}, \widehat{\mathbf{p}} \rangle_\beta^2 \geq \|\mathbf{p}_{\max}\|_\beta^2 (\|\widehat{\mathbf{p}}\|_\beta^2 - 1)\,. \tag{6.19}$$

Condition (6.19) is always satisfied when $\|\widehat{\mathbf{p}}\|_\beta^2 \leq 1$. This is clear from Figure 62 itself: if $\|\widehat{\mathbf{p}}\|_\beta^2 \leq 1$, then the ellipse would contain the origin, so problem (6.12) would be searching for the smallest VSM in the entire parameter space. This is not what we want, so hereinafter we assume $\|\widehat{\mathbf{p}}\|_\beta^2 > 1$.

There is a $\sqrt{t_{\max}} \geq 0$ that satisfies (6.17) if:

$$\frac{\|\mathbf{p}_{\max}\|_\beta^2}{\langle \mathbf{p}_{\max}, \widehat{\mathbf{p}} \rangle_\beta + \sqrt{\langle \mathbf{p}_{\max}, \widehat{\mathbf{p}} \rangle_\beta^2 - \|\mathbf{p}_{\max}\|_\beta^2 (\|\widehat{\mathbf{p}}\|_\beta^2 - 1)}} \tag{6.20}$$

is nonnegative, which only occurs when:

$$\langle \mathbf{p}_{\max}, \widehat{\mathbf{p}} \rangle_\beta \geq 0\,. \tag{6.21}$$

By joining inequations (6.19) and (6.21):

$$\langle \mathbf{p}_{\max}, \widehat{\mathbf{p}} \rangle_\beta \geq \|\mathbf{p}_{\max}\|_\beta \sqrt{\|\widehat{\mathbf{p}}\|_\beta^2 - 1}\,. \tag{6.22}$$

Therefore, problem (6.12) can be rewritten as:

$$\begin{aligned} \text{VSM}_{\min} = \quad & \min_{\mathbf{p}_{\max}} && \|\mathbf{p}_{\max}\|_\alpha \\ & \text{subject to} && \mathbf{p}_{\max} \in \text{ bifurcation surface} \\ & && \langle \mathbf{p}_{\max}, \widehat{\mathbf{p}} \rangle_\beta \geq \|\mathbf{p}_{\max}\|_\beta \sqrt{\|\widehat{\mathbf{p}}\|_\beta^2 - 1} \end{aligned}\,, \tag{6.23}$$

which shows that $t_{\max}$ was removed from the optimization variables of this problem.

The dot product $\langle \cdot, \cdot \rangle_\beta$ induces the following angle θ between two vectors $\mathbf{x}$ and $\mathbf{y}$:

$$\cos\theta = \frac{\langle \mathbf{x}, \mathbf{y} \rangle_\beta}{\|\mathbf{x}\|_\beta \|\mathbf{y}\|_\beta}\,, \tag{6.24}$$

so condition (6.22) can be rewritten as follows:

$$\cos\theta \geq \cos\theta_{\max} = \sqrt{1 - \frac{1}{\|\widehat{\mathbf{p}}\|_\beta^2}}\,. \tag{6.25}$$

This inequation defines how much the direction of $\mathbf{p}_{\max}$ can deviate from the direction of the expectation $\widehat{\mathbf{p}}$. This is sketched in Figure 64.

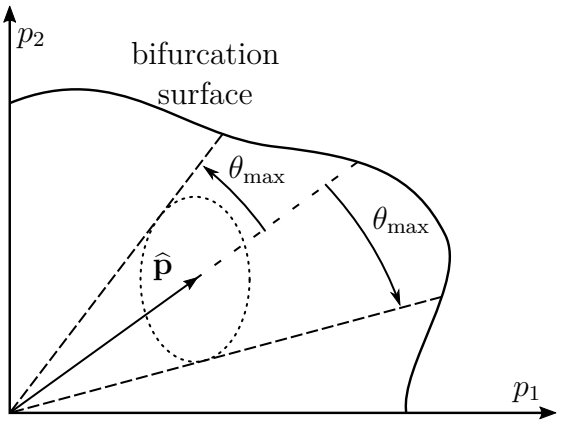

Figure 64 – Geometric interpretation of condition (6.22).

Inequation (6.25) can also be obtained by a geometric analysis of the cone: consider a vector $\mathbf{p}$ lying both on the boundary of the cone and on the boundary of the ellipse $\|\mathbf{p} - \widehat{\mathbf{p}}\|_\beta \leq 1$, as shown in Figure 65. It is easy to show that $\mathbf{p}$ and $\Delta\mathbf{p} = \mathbf{p} - \widetilde{\mathbf{p}}$ are β-orthogonal (i.e. they are orthogonal according to the inner product $\langle \cdot, \cdot \rangle_\beta$). Thus:

$$\sin\theta_{\max} = \frac{\|\Delta\mathbf{p}\|_\beta}{\|\widetilde{\mathbf{p}}\|_\beta} = \frac{1}{\|\widetilde{\mathbf{p}}\|_\beta}\,, \tag{6.26}$$

and consequently:

$$\cos\theta_{\max} = \sqrt{1 - \sin^2\theta_{\max}} = \sqrt{1 - \frac{1}{\|\widehat{\mathbf{p}}\|_\beta^2}}\,. \tag{6.27}$$

Remark

Note that (6.22) is precisely a second-order cone. For example, by defining the Cholesky decomposition $\mathbf{M}_\beta = \mathbf{U}^H\mathbf{U}$, condition (6.22) can be written as follows:

$$\left(\widehat{\mathbf{p}}^T\mathbf{M}_\beta\right)\mathbf{p}_{\max} \geq \|\mathbf{U}\mathbf{p}_{\max}\|_2 \sqrt{\|\widehat{\mathbf{p}}\|_\beta^2 - 1}\,. \tag{6.28}$$

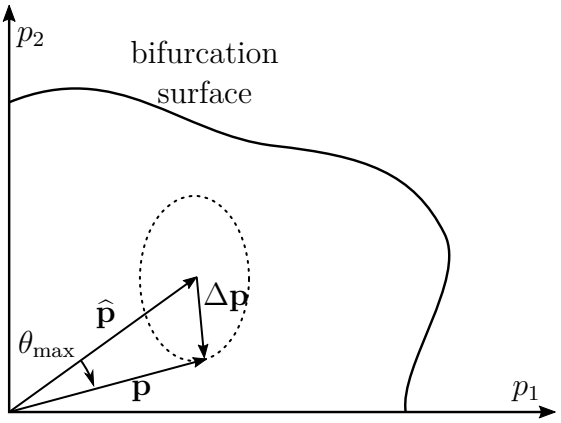

Figure 65 – Geometric interpretation of condition (6.22).

6.3.3 The proposed method

By using the modelling of the bifurcation surface described in Subsection 6.3.1 and the modelling of the hypercone described in Subsection 6.3.2, problem (6.12) is transformed into the following:

$$\begin{aligned} \text{VSM}_{\min} = \min_{\mathbf{p}_{\max},\mathbf{z},\mathbf{v}} \quad & \|\mathbf{p}_{\max}\|_\alpha \\ \text{subject to} \quad & \mathbf{h}(\mathbf{z},\mathbf{p}_{\max}) = \mathbf{0} \\ & \partial_{\mathbf{z}}\mathbf{h}(\mathbf{z},\mathbf{p}_{\max})\,\mathbf{v} = \mathbf{0} \\ & \|\mathbf{v}\| = 1 \\ & \langle \mathbf{p}_{\max}, \widehat{\mathbf{p}} \rangle_\beta \geq \|\mathbf{p}_{\max}\|_\beta \sqrt{\|\widehat{\mathbf{p}}\|_\beta^2 - 1} \end{aligned} \quad . \tag{6.29}$$

This subsection proposes a new method to solve problem (6.29). The kth iteration of the proposed method basically consists of the following steps:

Step 1 Compute the bifurcation point $\mathbf{p}_k = \sqrt{t_{\max}}\mathbf{u}_{k-1}$ for the *scenario* $\mathbf{p}(t) = \sqrt{t}\mathbf{u}_{k-1}$;

Step 2 Compute a linearization of the bifurcation surface at $\mathbf{p}_k$;

Step 3 Solve problem (6.29), with the saddle-node bifurcation equations replaced by the respective tangent hyperplane;

Step 4 Assign the solution $\mathbf{p}_{\max}$ of the previous step to $\mathbf{u}_k$.

Let $\mathbf{u}_0 = \widehat{\mathbf{p}}$, so the method first computes the bifurcation point associated with the expected *scenario*. Figures 66 and 67 provide a graphical description of the proposed algorithm.

In the following subsections, each of the proposed steps is described in detail.

6.3.3.1 Computing the bifurcation point

This step approaches the computation of the bifurcation point associated with a particular *scenario*. Several methods in the literature can be used for this computation. In this work, the first bifurcation point is computed by means of a continuation method (Section 3.3).

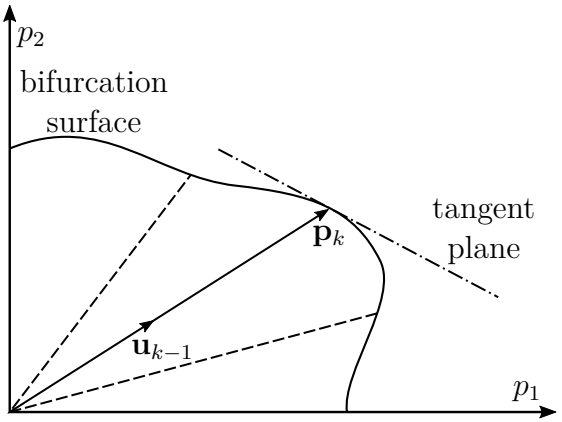

Figure 66 – The first and second steps compute $\mathbf{p}_k = t_{\max}\mathbf{u}_{k-1}$ and the tangent hyperplane.

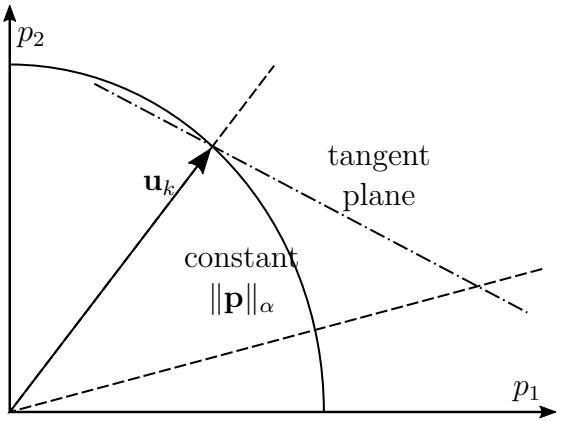

Figure 67 – The third and fourth steps solve problem (6.29) (with the bifurcation surface replaced by the tangent hyperplane) and assign its solution to $\mathbf{u}_k$.

Subsequent BPs are computed by solving equation (5.1) directly. In this case, the previous bifurcation point is used as an initial estimate of the solution of (5.1).

To avoid convergence problems, this work solves equation (5.1) using the damped version of the Newton's method described in (NEVES; ALBERTO, 2020), where the step size is adaptatively reduced to guarantee the global convergence to a minimum of $\|\mathbf{f}(\mathbf{x})\|_2$, where $\mathbf{f}(\mathbf{x}) = \mathbf{0}$ is the equation to be solved.

6.3.3.2 Linearizing the bifurcation surface

The normal vector to the bifurcation surface at the BP can be computed as described in Section 3.5. Specifically, equation (3.23) establishes that the tangent hyperplane at point $\mathbf{p}_k$ is given by:

$$\mathbf{n}^T(\mathbf{p} - \mathbf{p}_k) = 0 \Rightarrow \mathbf{n}^T\mathbf{p} = \eta\,, \tag{6.30}$$

where $\mathbf{n} = \partial_{\mathbf{p}}\mathbf{h}^T\mathbf{w}$ and $\eta = \mathbf{n}^T\mathbf{p}_k$. Vector $\mathbf{w}$ is the left eigenvector of the null eigenvalue of $\partial_{\mathbf{z}}\mathbf{h}$.

6.3.3.3 Solving the relaxed problem

By replacing the bifurcation surface equations (5.1) by its linearization (6.30), problem (6.29) is reduced to:

$$\begin{aligned} \mathrm{VSM}_{\min} = \quad & \min_{\mathbf{p}_{\max}} && \|\mathbf{p}_{\max}\|_\alpha \\ & \text{subject to} && \mathbf{n}^T\mathbf{p}_{\max} = \eta \\ & && \langle \mathbf{p}_{\max}, \widehat{\mathbf{p}} \rangle_\beta \geq \|\mathbf{p}_{\max}\|_\beta \sqrt{\|\widehat{\mathbf{p}}\|_\beta^2 - 1} \end{aligned} \tag{6.31}$$

From the computational point of view, problem (6.31) offers three main advantages over problem (6.29):

- variables $\mathbf{x}$ and $\mathbf{v}$ are removed from the optimization problem, so the dimension of problem (6.29) is greatly reduced (the dimension of vectors $\mathbf{x}$ and $\mathbf{v}$ usually is comparable to the dimension of $\mathbf{p}$);
- all nonlinearities associated with the power flow equations (equation (4.1)) and its respective bifurcation surface are isolated from the optimization problem, which makes (6.31) much easier to solve than (6.29);
- problem (6.31) is a convex optimization problem[3], which can be solved more efficiently than problem (6.29).

For convenience, variable $\mathbf{p}_{\max}$ of (6.31) is renamed to $\mathbf{p}$ in the remaining of this section.

Problem (6.31) is convex, so any solution to the Karush-Kuhn-Tucker (KKT) conditions (LUENBERGER; YE, 2008) define a global optimal point of problem (6.31). The KKT conditions for problem (6.31) are:

$$\nabla f_{\text{obj}}(\mathbf{p}) + \lambda\mathbf{n} + \mu\nabla g(\mathbf{p}) = \mathbf{0}\,, \tag{6.32a}$$

$$g(\mathbf{p})\mu = 0\,, \tag{6.32b}$$

$$\mathbf{n}^T\mathbf{p} = \eta\,, \tag{6.32c}$$

$$g(\mathbf{p}) \leq 0\,, \tag{6.32d}$$

$$\mu \geq 0\,, \tag{6.32e}$$

where

$$f_{\text{obj}}(\mathbf{p}) = \|\mathbf{p}\|_\alpha\,, \tag{6.33}$$

$$g(\mathbf{p}) \equiv \|\mathbf{p}\|_\beta \sqrt{\|\widehat{\mathbf{p}}\|_\beta^2 - 1} - \langle \mathbf{p}, \widehat{\mathbf{p}} \rangle_\beta \equiv \|\mathbf{p}\|_\beta \kappa - \langle \mathbf{p}, \widehat{\mathbf{p}} \rangle_\beta\,, \tag{6.34}$$

and ∇f_{obj} (resp. ∇g) is the gradient of f_{obj} (resp. g).

[3] Any vector norm $\|\cdot\|_\alpha$ is a convex function, and the intersection of the cone (6.22) and the plane (6.30) is a convex set.

From condition (6.32b), either $g(\mathbf{p})$ or μ must be zero. When $g(\mathbf{p}) = 0$, the optimal solution of (6.31) lies on the surface of the hypercone (as depicted in Figure 67), while $g(\mathbf{p}) < 0$ indicates that the optimal point is in the interior of the cone.

Consider initially that $\mu = 0$ (i.e., we assume the optimal point is in the interior of the cone). In this situation, (6.32) reduces to the following:

$$\nabla f_{\text{obj}}(\mathbf{p}) + \lambda \mathbf{n} = \mathbf{0}\,, \tag{6.35a}$$

$$\mathbf{n}^T \mathbf{p} = \eta\,, \tag{6.35b}$$

$$g(\mathbf{p}) \leq 0\,. \tag{6.35c}$$

This system of equations can be solved using Newton's method, starting from the value of $\mathbf{p}$ at the last iteration of the proposed procedure, given by $\mathbf{p}_{k-1}$. Linearizing the first equation with respect to $\mathbf{p}$ leads to:

$$\begin{aligned} &\nabla f_{\text{obj}}(\mathbf{p}) + \lambda \mathbf{n} + \mathbf{M}_\alpha(\mathbf{p}) \Delta \mathbf{p} = 0 \\ \Rightarrow\ &\Delta \mathbf{p} = -\mathbf{M}_\alpha(\mathbf{p})^{-1} (\nabla f_{\text{obj}}(\mathbf{p}) + \lambda \mathbf{n}) \end{aligned} \tag{6.36}$$

where $\mathbf{M}_\alpha(\mathbf{p})$ is the Hessian matrix of f_{obj} evaluated at $\mathbf{p}$. Usually $\|\cdot\|_\alpha$ is induced by an inner-product. In this case, if we define the objective function as $\|\mathbf{p} - \mathbf{p}_0\|_\alpha^2$, then $\mathbf{M}_\alpha$ is a constant matrix, $\nabla f_{\text{obj}}(\mathbf{p}) = \mathbf{M}_\alpha \mathbf{p}$ and Newton's method converge in one iteration:

$$\mathbf{p} + \Delta \mathbf{p} = \mathbf{p} - \mathbf{M}_\alpha^{-1} (\mathbf{M}_\alpha \mathbf{p} + \lambda \mathbf{n}) = -\lambda \mathbf{M}_\alpha^{-1} \mathbf{n}\,, \tag{6.37}$$

which defines the direction of the new vector $\mathbf{p}$, while the norm of $\mathbf{p}$ is determined by equation (6.35b). If $\mathbf{M}_\alpha = \mathbf{I}$, equation (6.37) basically establishes that $\mathbf{p}$ must be parallel to $\mathbf{n}$, which is a normal vector to the tangent hyperplane. This ensures that, when the solution of (6.31) is in the interior of the cone and the objective function is $\|\mathbf{p} - \mathbf{p}_0\|_2^2$, the proposed method is exactly the same as the *closest bifurcation method* of Section 3.5. Hence, the proposed method can be thought as a generalization of the method in Section 3.5.

Having computed the solution $\mathbf{p}^{(6.35)}$ of equations (6.35a) and (6.35b), the next step is to check if condition (6.35c) is satisfied. If this condition is satisfied, the solution of (6.31) has been found. Otherwise, our initial assumption that $\mu = 0$ was incorrect and the optimal solution of (6.31) lies on the boundary of the cone. In this case, $g(\mathbf{p}) = 0$ and (6.32) reduces to the following:

$$\nabla f_{\text{obj}}(\mathbf{p}) + \lambda \mathbf{n} + \mu \left(\frac{\mathbf{M}_\beta \mathbf{p}}{\|\mathbf{p}\|_\beta} \kappa - \mathbf{M}_\beta \widehat{\mathbf{p}} \right) = \mathbf{0}\,, \tag{6.38a}$$

$$\|\mathbf{p}\|_\beta \kappa - \langle \mathbf{p}, \widehat{\mathbf{p}} \rangle_\beta = 0\,, \tag{6.38b}$$

$$\mathbf{n}^T \mathbf{p} = \eta\,, \tag{6.38c}$$

$$\mu \geq 0\,. \tag{6.38d}$$

If $\mathbf{p}$ is a solution of equations (6.38a) and (6.38b), $k\mathbf{p}$ is also a solution of these equations[4] for all $k > 0$. Thus, equations (6.38a) and (6.38b) are invariant to the norm of $\mathbf{p}$, which is uniquely defined by equation (6.38c).

To simplify equation (6.38), (6.38c) is replaced by $\|\mathbf{p}\|_\beta^2 = 1$. This is convenient because occurrences of $\|\mathbf{p}\|_\beta$ can be simplified in equations (6.38a) and (6.38b):

$$\nabla f_{\text{obj}}(\mathbf{p}_2) + \lambda_2 \mathbf{n} + \mu_2 \left(\mathbf{M}_\beta \mathbf{p}_2 \kappa - \mathbf{M}_\beta \widehat{\mathbf{p}}\right) = \mathbf{0}\,, \tag{6.39a}$$

$$\kappa - \langle \mathbf{p}_2, \widehat{\mathbf{p}} \rangle_\beta = 0\,, \tag{6.39b}$$

$$\|\mathbf{p}_2\|_\beta^2 = 1\,. \tag{6.39c}$$

Equation (6.39) is slightly simpler than equation (6.38), and the solution of equation (6.38) can be obtained from the solution of (6.39) with the following:

$$(\mathbf{p}, \mu, \lambda) = (k\mathbf{p}_2, k\mu_2, k\lambda_2)\,, \tag{6.40}$$

where $k = \frac{\eta}{\mathbf{n}^T \mathbf{p}_2}$. However, it is not necessary to compute $(\mathbf{p}, \mu, \lambda)$, since the only information we need from the solution of (6.31) is the direction of $\mathbf{p}$ (this vector will invariably be scaled by *Step 1* of the proposed procedure).

Equation (6.39) can be solved with a damped Newton's method (NEVES; ALBERTO, 2020). To this end, the following Jacobian matrix must be evaluated and factorized:

$$\begin{bmatrix} \mathbf{M}_\alpha(\mathbf{p}_2) + \mu_2 \mathbf{M}_\beta \kappa & \mathbf{M}_\beta \mathbf{p}_2 \kappa - \mathbf{M}_\beta \widehat{\mathbf{p}} & \mathbf{n} \\ -\widehat{\mathbf{p}}^T \mathbf{M}_\beta & 0 & 0 \\ 2\mathbf{p}_2^T \mathbf{M}_\beta & 0 & 0 \end{bmatrix}. \tag{6.41}$$

If the dependency between the random variables in the stochastic process $\{\mathbf{P}(t),\ t \geq 0\}$ is negligible, $\mathbf{M}_\beta$ can be approximated by a diagonal matrix. If $\mathbf{M}_\alpha(\mathbf{p}_2)$ is also a diagonal matrix, then $\mathbf{M}_\alpha(\mathbf{p}_2) + \mu_2 \mathbf{M}_\beta \kappa$ is diagonal, and the linear system involving (6.41) can be solved very efficiently using the Schur complement of $\mathbf{M}_\alpha(\mathbf{p}_2) + \mu_2 \mathbf{M}_\beta \kappa$.

The last implementation aspect of the resolution of (6.31) is how to define the initial estimate of the solution of (6.39). Recall that equation (6.39) only needs to be solved when the solution $\mathbf{p}^{(6.35)}$ of (6.35a) and (6.35b) violates the hypercone condition (6.35c). This situation is sketched in Figure 68. Since we cannot go from $\mathbf{p}_{k-1}$ to $\mathbf{p}^{(6.35)}$ without leaving the cone, we use as starting point the vector $\mathbf{p}$ between $\mathbf{p}_{k-1}$ and $\mathbf{p}^{(6.35)}$ that lies on the cone surface. Specifically, the value of $\mathbf{p}$ is given by:

$$\mathbf{p} = \mathbf{p}_{k-1} + \gamma(\mathbf{p}^{(6.35)} - \mathbf{p}_{k-1}) \equiv \mathbf{p}_{k-1} + \gamma \mathbf{d}\,, \tag{6.42}$$

where γ is chosen so that $\mathbf{p}$ is in the cone surface:

$$\langle \mathbf{p}, \widehat{\mathbf{p}} \rangle_\beta = \kappa \|\mathbf{p}\|_\beta\,. \tag{6.43}$$

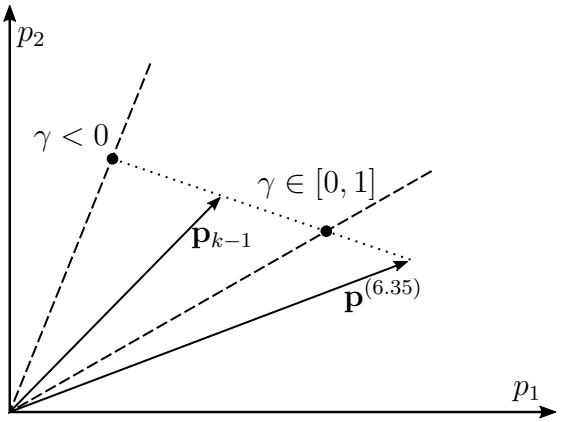

Figure 68 – Estimate of the solution of (6.39).

This equation is quadratic in relation to γ:

$$\begin{aligned}\langle \mathbf{p}_{k-1} + \gamma\mathbf{d}, \widehat{\mathbf{p}}\rangle_\beta^2 &= \kappa^2 \|\mathbf{p}_{k-1} + \gamma\mathbf{d}\|_\beta^2 \\ \Rightarrow \left(\langle \mathbf{p}_{k-1}, \widehat{\mathbf{p}}\rangle_\beta + \gamma\langle \mathbf{d}, \widehat{\mathbf{p}}\rangle_\beta\right)^2 &= \kappa^2 \left(\|\mathbf{p}_{k-1}\|_\beta^2 + 2\gamma\langle \mathbf{p}_{k-1}, \mathbf{d}\rangle_\beta + \gamma^2\|\mathbf{d}\|_\beta^2\right) \quad (6.44)\end{aligned}$$

One of the solutions of γ is guaranteed to belong to the interval $[0, 1]$, as depicted in Figure 68. This solution is used to compute $\mathbf{p}$. This vector $\mathbf{p}$ is then scaled so that $\|\mathbf{p}\|_\beta = 1$. In this way, equations (6.39b) and (6.39c) are both satisfied for the initial estimate of the solution of (6.39).

Lastly, the initial values for μ_2 and λ_2 are computed as follows:

$$\lambda_2 = -\frac{\mathbf{p}_2^T \nabla f_{\text{obj}}(\mathbf{p}_2)}{\mathbf{p}_2^T \mathbf{n}}\,, \quad (6.45a)$$

$$\mu_2 = \widehat{\mathbf{p}}^T \nabla f_{\text{obj}}(\mathbf{p}_2) + \lambda_2 \widehat{\mathbf{p}}^T \mathbf{n}\,. \quad (6.45b)$$

These equations can be obtained by pre-multiplying equation (6.39a) by $\mathbf{p}_2^T$ and $\widehat{\mathbf{p}}^T$, respectively.

6.3.4 Example

Consider a simple two-bus system, where an infinite bus with voltage $V_\infty = 1$ pu is connected to a load bus by means of a transmission line with impedance $z = 0.01 + j0.05$ pu. The (complex) power flow equation for this system is:

$$S = V\overline{I} = V\frac{\overline{V_\infty} - \overline{V}}{\overline{z}} = V\frac{1 - \overline{V}}{0.01 - j0.05} \quad (6.46)$$

where S is the complex power demanded by the load bus and V is the complex voltage at that bus. The state vector (vector $\mathbf{z}$ in (4.1)) is composed by the real and imaginary parts of V.

[4] Note that $k\,\partial_{\mathbf{p}}\|\mathbf{p}\| = \partial_{\mathbf{p}}\|k\mathbf{p}\| = \partial_{k\mathbf{p}}\|k\mathbf{p}\|\,k \;\Rightarrow\; \partial_{\mathbf{p}}\|\mathbf{p}\| = \partial_{k\mathbf{p}}\|k\mathbf{p}\|\;\forall\; k > 0$.

The random variables of this system are the active and reactive powers at the load bus. Therefore, vector $\mathbf{p}$ in (4.1) is composed by the real and imaginary parts of S.

Assume that, using a point estimator, the expected *scenario* for this two bus system is estimated:

$$\widehat{\mathbf{p}}(t) = \mathbf{p}_0 + \widehat{\mathbf{p}}\sqrt{t} = \begin{bmatrix} 1 \\ 0.5 \end{bmatrix} + \begin{bmatrix} 2.5 \\ 1.5 \end{bmatrix} \sqrt{t}\,, \tag{6.47}$$

where $\mathbf{p}_0$ is the current value of $\mathbf{p}$. Therefore, the initial power demand at the load bus is $S = 1 + j0.5$.

Also assume that the estimated covariance matrix $\mathbf{\Sigma}(t)$ at $t = 1$ for the random variables (real and imaginary parts of S) is the following positive definite matrix:

$$\mathbf{\Sigma}(1) = \mathbf{A}\mathbf{A}^T = \begin{bmatrix} 0.1 & 0.03 \\ 0.03 & 0.08 \end{bmatrix} \tag{6.48}$$

Assume that we want to compute a voltage stability margin with 95% probability. The inverse cumulative distribution function of a χ^2 distribution with 2 degrees of freedom at $p = 0.95\%$ is $F_2^{-1}(0.95) \approx 5.99$. Using equation (6.9), $\mathbf{M}_\beta$ is given by:

$$\mathbf{M}_\beta \approx \begin{bmatrix} 1.88 & -0.705 \\ -0.705 & 2.35 \end{bmatrix}. \tag{6.49}$$

Lastly, VSM should be defined by means of the vector norm $\|\cdot\|_\alpha$. Here, let $\|\cdot\|_\alpha$ be the Euclidean norm $\|\cdot\|_2$.

Optimization problem (6.29) is now completely defined:

$$\begin{aligned} \min_{\mathbf{p},\mathbf{z},\mathbf{v}} \quad & \|\mathbf{p} - \mathbf{p}_0\|_2 \\ \text{subject to} \quad & \mathbf{h}(\mathbf{z}, \mathbf{p}) = \mathbf{0} \\ & \partial_{\mathbf{z}}\mathbf{h}(\mathbf{z}, \mathbf{p})\,\mathbf{v} = \mathbf{0} \\ & \|\mathbf{v}\| = 1 \\ & \langle \mathbf{p} - \mathbf{p}_0, \widehat{\mathbf{p}} \rangle_\beta \geq \|\mathbf{p} - \mathbf{p}_0\|_\beta \sqrt{\|\widehat{\mathbf{p}}\|_\beta^2 - 1} \end{aligned} \tag{6.50}$$

where:

- $\mathbf{p}^T = \begin{bmatrix} P & Q \end{bmatrix}$, where $S = P + jQ$ is the demanded power in the load bus, as shown in equation (6.46);
- $\mathbf{z}^T = \begin{bmatrix} V_r & V_i \end{bmatrix}$, where $V = V_r + jV_i$ is the complex voltage at the load bus, as shown in equation (6.46);
- $\mathbf{p}_0^T = \begin{bmatrix} 1 & 0.5 \end{bmatrix}$ and $\widehat{\mathbf{p}}^T = \begin{bmatrix} 2.5 & 1.5 \end{bmatrix}$;
- equation $\mathbf{h}(\mathbf{z}, \mathbf{p}) = \mathbf{0}$ is a two-element equation given by the real and imaginary parts of equation (6.46);
- $\langle \mathbf{x}, \mathbf{y} \rangle_\beta \equiv \mathbf{x}^T\,\mathbf{M}_\beta\,\mathbf{y}$ and $\|\mathbf{x}\|_\beta^2 \equiv \langle \mathbf{x}, \mathbf{x} \rangle_\beta$.

In this small example, $\mathbf{p}$ is two dimensional, so the bifurcation surface is one-dimensional. Moreover, for this two-bus system it can be shown that the singularity condition (equation $\det \partial_{\mathbf{z}} \mathbf{h}(\mathbf{z}, \mathbf{p}) = 0$) reduces to:

$$\text{real}(V) = \frac{V_\infty}{2} \,. \tag{6.51}$$

Therefore, the values of $S = P + jQ$ on the bifurcation surface can be computed simply by varying the imaginary part of V in equation (6.46), while the real part is fixed at 0.5 pu. Figure 69 shows the bifurcation surface with imag(V) varying from -0.5 pu to 0.2 pu.

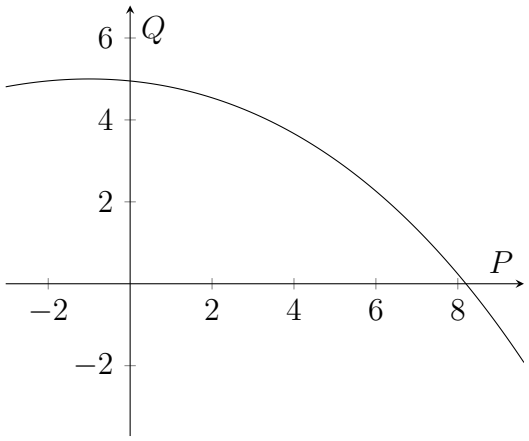

Figure 69 – Bifurcation surface for the two-bus system.

Using the eigendecomposition of $\mathbf{M}_\beta$, the hyperellipsoid and the hypercone shown in Figure 70 are computed.

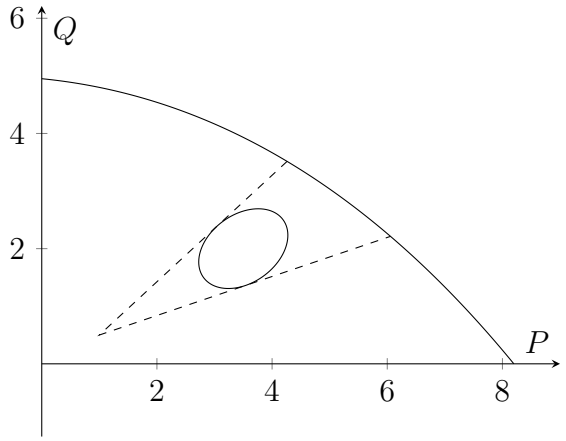

Figure 70 – Cone for the two-bus system.

The first bifurcation point is usually computed by means of a continuation method (Section 3.3). Basically, t is increased in (6.47) until the disappearance of the solution $\mathbf{z}$ of $\mathbf{h}(\mathbf{z}, \widehat{\mathbf{p}}(t)) = \mathbf{0}$. Specifically for this two-bus system, the maximum value of t satisfies the following complex equation:

$$(1 + j0.5) + (2.5 + j1.5)\sqrt{t} = (0.5 + jV_i)\frac{1 - (0.5 - jV_i)}{0.01 - j0.05} \,, \tag{6.52}$$

which is basically the combination of equations (6.46), (6.47) and (6.51). The variables of this equation are t and V_i. The solution is $(V_i, t) \approx (-0.226, 2.69)$, and the power at the BP is $\widehat{\mathbf{p}}(t)^T \approx \begin{bmatrix} 5.10 & 2.96 \end{bmatrix}$.

The next step is to compute the normal vector to the bifurcation surface at the BP. For practical power systems, this normal vector is computed using equation (6.30). However, for this two-bus system, V_r is constant at the bifurcation surface, and the normal vector satisfies the following equation:

$$\begin{bmatrix} \frac{dP}{dV_i} & \frac{dQ}{dV_i} \end{bmatrix} \mathbf{n} = 0\,, \tag{6.53}$$

where P and Q are functions of V_i computed as shown in (6.46), and $V = 0.5 + jV_i$. One vector $\mathbf{n}$ that satisfies (6.53) is $\mathbf{n} = \begin{bmatrix} 0.582 & 0.813 \end{bmatrix}^T$.

Next, the relaxed problem (6.31) is solved. Assuming that the solution to this problem is in the interior of the cone, equations (6.35a) and (6.35b) are solved. In this example, $\mathbf{M}_\alpha$ is the identity matrix, so equation (6.37) shows that the solution $\mathbf{p}^{(6.35)}$ is in the direction of $\mathbf{n}$ itself. To check if (6.35c) is satisfied, we compute $g(\mathbf{n}) \approx 0.494$. Since $g(\mathbf{n}) > 0$, our initial assumption about the solution of (6.31) being in the interior of the cone was wrong, and we need to constraint this problem to $g(\mathbf{p}) = 0$. In comparison to Figure 70, in Figure 71 we show both the tangent hyperplane (dotted line) and vector $\mathbf{p}^{(6.35)}$. Clearly $\mathbf{p}^{(6.35)}$ is out of the cone.

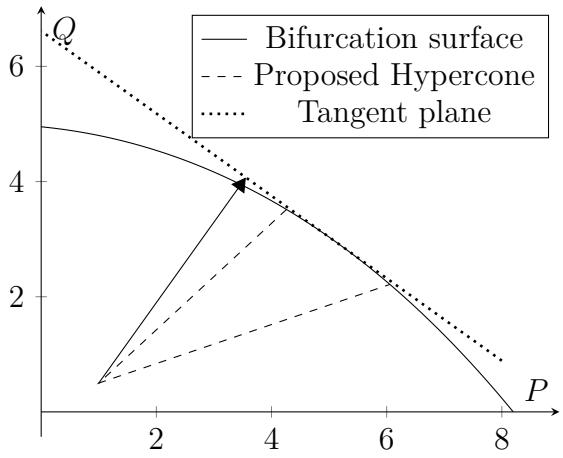

Figure 71 – Linearization of the bifurcation surface. The arrow represents vector $\mathbf{p}^{(6.35)}$.

In order to solve equation (6.39), the initial point is computed as described in Subsection 6.3.3. Basically, we compute a vector $\mathbf{p}$ in the boundary of the cone by moving from the current bifurcation point $\mathbf{p}_0 + \sqrt{2.69}\widehat{\mathbf{p}}$ in direction to vector $\mathbf{p}_0 + \mathbf{p}^{(6.35)}$. From Figure 71, the initial point is on the upper dashed line (upper boundary of the cone). Indeed, this initial point is the solution of (6.39), and problem (6.31) is solved. This concludes one iteration of the proposed method.

In the next iteration, we compute the bifurcation point associated with the upper boundary of the cone. By following the same steps as before, we can check that the solution

of (6.31) will still be the upper boundary of the cone, so the iterative procedure converged in two iterations.

6.4 Implementation results

In this section, the proposed method is applied to several practical power systems. Specifically, results are reported for the following systems:

- IEEE 118-bus system and IEEE 300-bus system (CHRISTIE, 1999);
- PEGASE 1354-bus system, PEGASE 2869-bus system, PEGASE 9241-bus system and PEGASE 13659-bus system (ZIMMERMAN; MURILLO-SANCHEZ; THOMAS, 2011; JOSZ et al., 2016; FLISCOUNAKIS et al., 2013).

In all simulations, the random variables in vector $\mathbf{p}$ are the demanded power (active and reactive) at all buses and the active power of all generators[5]. The threshold for entering vector $\mathbf{p}$ is 0.01 pu (e.g., a load power between -0.01 pu and 0.01 pu will not be considered a random variable, but rather a constant power).

We arbitrarily define the most likely *scenario* as the increase of the power of all buses proportionally to the base case:

$$\widehat{\mathbf{p}}(t) = (1 + \sqrt{t})\mathbf{p}_0\,, \tag{6.54}$$

where $\mathbf{p}_0$ is the initial value of the random variables. Similarly, we arbitrarily choose $\mathbf{M}_\beta$ in the following way:

$$\mathbf{M}_\beta = \operatorname{diag}\left(\frac{\mathbf{p}_0}{2}\right)^{-2}\,, \tag{6.55}$$

where $\operatorname{diag}(\mathbf{p}_0)$ is the diagonal matrix whose diagonal is $\mathbf{p}_0$. Note that, with this definition of $\mathbf{M}_\beta$, each element of $\mathbf{p}$ is allowed to deviate at most by 50% from the respective expected value. We reiterate that these choices for $\widehat{\mathbf{p}}$ and $\mathbf{M}_\beta$ were arbitrary. In practical situations, these values should be estimated using appropriate statistical methods.

Lastly, we define the VSM function:

$$\text{VSM} = \frac{1}{2}\|\mathbf{p} - \mathbf{p}_0\|_2^2 = \frac{1}{2}(\mathbf{p} - \mathbf{p}_0)^T(\mathbf{p} - \mathbf{p}_0)\,, \tag{6.56}$$

which is a quadratic function whose Hessian matrix is the identity matrix.

The initial VSM (computed for the expected scenario $\widehat{\mathbf{p}}$) and the minimum value of VSM (the optimal value of problem (6.29)) are reported in Table 9. This table also presents results from solving problem (6.29) directly using the method proposed in (NEVES;

[5] The active power output of synchronous generators is not really a random variable, but rather it is a function of the system loading (the active power is adjusted by speed governors and automatic generation control), which in turn is composed of random variables.

ALBERTO, 2020). This method is called "Reference method". Both methods are compared in terms of computed VSM and computational time, using the results of one continuation power flow (specifically, the continuation power flow associated with the expected *scenario* $\widehat{\mathbf{p}}$, which consists of the first execution of *Step 1*) as reference.

Table 9 – Results of the proposed method.

		Expected *Scenario*	Proposed method	Reference method
118-bus	VSM	f_{obj}	$0.598 f_{\text{obj}}$	$0.711 f_{\text{obj}}$
	Time	Δt	$8.27\Delta t$	$3.06\Delta t$
300-bus	VSM	f_{obj}	$0.533 f_{\text{obj}}$	$0.558 f_{\text{obj}}$
	Time	Δt	$3.54\Delta t$	$33.6\Delta t$
1354-bus	VSM	f_{obj}	$0.493 f_{\text{obj}}$	$0.493 f_{\text{obj}}$
	Time	Δt	$2.55\Delta t$	$6.26\Delta t$
2869-bus	VSM	f_{obj}	$0.592 f_{\text{obj}}$	$0.592 f_{\text{obj}}$
	Time	Δt	$2.06\Delta t$	$6.95\Delta t$
9241-bus	VSM	f_{obj}	$0.698 f_{\text{obj}}$	$0.698 f_{\text{obj}}$
	Time	Δt	$4.72\Delta t$	$7.94\Delta t$
13659-bus	VSM	f_{obj}	$0.351 f_{\text{obj}}$	$0.942 f_{\text{obj}}$
	Time	Δt	$5.73\Delta t$	$48.6\Delta t$

All results shown in Table 9 represent feasible points (i.e., all results represent points on the bifurcation surface and in the interior of the cone). Hence, the results of both methods can be compared by its final VSM (better solutions have smaller values of VSM). It can be seen from Table 9 that the proposed method returned a better (or equal) solution than the reference method in all simulations. Furthermore, the proposed method is usually faster than the reference method.

The reason for the robustness of the proposed method in comparison to the reference method is mainly due to the fact that all nonlinearities in the bifurcation surface (5.1) are isolated from the optimization problem (6.31). In the proposed method, there is one specific step to compute the bifurcation point for a specific *scenario* (*Step 1*) and one specific step to compute a new *scenario* (*Step 3*). On the other hand, the reference method tries to solve problem (6.29) directly by means of a quasi-Newton SQP algorithm. The reference method tries to move on the bifurcation surface (represented by the highly nonlinear bifurcation equations shown in (5.1)) and decrease the VSM while confined to the cone. In this procedure, the update steps in the reference method can become small enough to stop the algorithm prematurely, which is the case of the 118-bus system. In other situations, the small update steps are not sufficient for the optimization algorithm to converge within a maximum number of iterations. The maximum number of iterations of the reference method was reached for the 300-bus and the 13659-bus systems shown in Table 9, which explains why the computational time of the reference method for these

systems was considerably larger than the respective results of the proposed method. These comments also apply to other general-purpose optimization algorithms (e.g., interior-point algorithms), which hardly solve problem (6.29) for the systems considered in this section.

To illustrate the results provided by the proposed method, Figure 72 shows the solution branch for the 13659-bus system both for the most credible *parameter variation scenario* (given by (6.54)) and for the most critical *scenario*, given by:

$$\widehat{\mathbf{p}}(t) = \mathbf{p}_0 + \sqrt{t}\mathbf{p}_{\max}\,, \tag{6.57}$$

where $\mathbf{p}_{\max}$ is the solution of problem (6.29), computed using the proposed method.

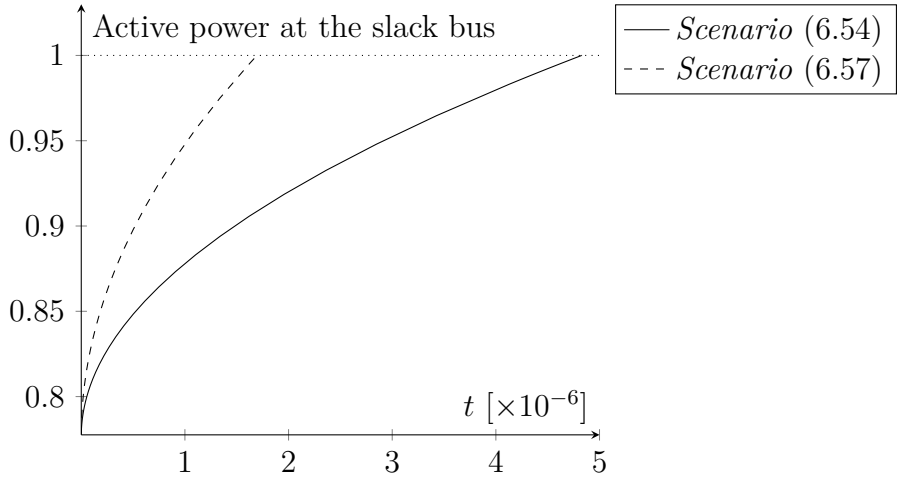

Figure 72 – 13659-bus system: solution curves before and after the proposed method

The curves depicted in Figure 72 refer to the active power generation at the slack bus with the increase of t. This slack generator has an active power upper bound of 1 pu. The power system cannot withstand an increase of load after this limit is reached, which is represented as the loss of the solution of equation (4.1) at a bifurcation point. Indeed, Figure 72 shows that the bifurcation occurs when the active power reaches 1 pu. Note that the maximum value of t for *scenario* (6.57) is 35.1% of the maximum value of t for *scenario* (6.54), in agreement with the results reported in Table 9.

6.5 Partial Conclusions

This chapter presents several relevant contributions to the current literature of uncertainty analysis on voltage stability. These contributions can be concisely described in the following items:

- A solid foundation to the treatment of uncertainties in voltage stability was proposed in Section 6.1. By using statistical information about vector $\mathbf{p}$ (specifically, its expected value and covariance matrix), the prediction region for the future behavior of the random variables is completely defined. Subsection 6.3.2 demonstrates that this prediction region is a second-order cone in the parameter space.

- A new method is proposed to solve problem (6.29). The new method alternates between solving the bifurcation equations (5.1) and the convex second-order cone optimization problem (6.31). A simple and efficient way of solving problem (6.31) is also proposed.

The results shown in Section 6.4 corroborate that the proposed method is more robust than general-purpose optimization methods for solving problem (6.29). The proposed method has distinct steps for computing bifurcation points of a particular *scenario* and for computing a new *scenario*. In this way, all nonlinearities of the power flow model are isolated from the search for the critical *scenario*. The proposed method has converged successfully in every simulation on which it was tested.

It should be emphasized that the modelling of Chapter 4 is essential in the proposed method. This model is necessary to represent the bifurcation surface by equation (5.1), as described in Subsection 6.3.1.

The proposed method is fast and can be applied on model-based voltage stability analysis of real power systems. As shown in Table 9, the proposed method is usually executed in a time equivalent to a few continuation power flow computations[6]. Therefore, the proposed method has potential for practical applications to real, large-scale power systems.

[6] As a reference, the proposed method was applied to the 13659-bus system (as shown in Table 9) in about 22 seconds on a Intel Core i7-8565U laptop.

7 PROPOSED METHOD FOR VSM CORRECTION

Chapter 6 proposed a method for computation of the voltage stability margin considering parameter uncertainties. By applying the proposed method, we are able to compute the locally closest bifurcation point associated with an arbitrary probability. The distance to this closest bifurcation point quantifies VSM, which provides a robust measure to the voltage collapse.

As discussed in Chapter 6, the control vector $\mathbf{u}$ of equation (4.1) is held constant during the computation of VSM. Thus, the distance to a voltage collapse is computed assuming that control variables remain unchanged. The computed VSM is then used to judge if the power system is prone to a voltage collapse:

- If the value of VSM is unacceptably small, then control actions are needed to increase the distance to the collapse. These control actions are represented by changes in vector $\mathbf{u}$ of equation (4.1).
- Otherwise, no control actions are necessary to improve voltage stability of the current operating point.

In this way, we avoid modifying vector $\mathbf{u}$ unless necessary. This is desirable, since these control variables are manually operated. In addition, some control variables are mechanically switched (e.g., switched capacitors), which are prone to mechanical wear. On the other hand, some variables directly influence economic factors (e.g., generation re-dispatch). There are costs associated with all these control variables, thus changes in these variables should be minimized.

In this chapter, a new method is proposed to increase the value of VSM defined in Chapter 6 to a minimum admissible value. The proposed method usually provides a small number of control actions that are sufficient to increase the VSM. Moreover, the proposed method is fast, with potential for online voltage stability assessment.

It should be noted that the method for control selection described in this chapter aims exclusively for increasing the VSM. This method can be combined with other methods, such as optimal power flow. In this case, the optimal power flow provides an optimal control vector $\mathbf{u}$, and this vector is then modified by the method proposed in this chapter to improve voltage stability. Changes in vector $\mathbf{u}$ provided by the optimal power flow usually imply an increase in power system operation costs. This reiterates that control actions should be minimized in the proposed method.

7.1 Handling Control Selection on VSA

In order to take parameter uncertainties into voltage stability analysis, Chapter 6 defines VSM by means of the following optimization problem (problem (6.29)):

$$\begin{aligned} \mathrm{VSM}_{\min} = \min_{\mathbf{p}_{\max},\mathbf{z},\mathbf{v}} \quad & \|\mathbf{p}_{\max}\|_{\alpha} \\ \text{subject to} \quad & \mathbf{h}(\mathbf{z},\mathbf{p}_{\max}) = \mathbf{0} \\ & \partial_{\mathbf{z}}\mathbf{h}(\mathbf{z},\mathbf{p}_{\max})\,\mathbf{v} = \mathbf{0} \\ & \|\mathbf{v}\| = 1 \\ & \langle \mathbf{p}_{\max}, \widehat{\mathbf{p}} \rangle_{\beta} \geq \|\mathbf{p}_{\max}\|_{\beta} \sqrt{\|\widehat{\mathbf{p}}\|_{\beta}^{2} - 1} \end{aligned} \quad . \tag{7.1}$$

Note that this problem is solved for a specific value of the control vector $\mathbf{u}$. In particular, this optimization problem has one solution $(\mathbf{p}_{\max}, \mathbf{z}, \mathbf{v})$ for each value of vector $\mathbf{u}$. As a result, there is an implicit function $\mathrm{VSM}_{\min}(\mathbf{u})$ that maps each control vector $\mathbf{u}$ into the corresponding solution of problem (7.1).

Let $\mathbf{u}_0$ be the initial value of $\mathbf{u}$, according to the current operating point. In addition, let $\underline{\mathrm{VSM}}$ be the minimum admissible value of VSM. Our goal is to increase VSM up to $\underline{\mathrm{VSM}}$ changing as few elements of $\mathbf{u}$ as possible[1]. Mathematically, this is equivalent to the following optimization problem:

$$\begin{aligned} \min_{\Delta\mathbf{u}} \quad & \text{number of nonzero elements of } \Delta\mathbf{u} \\ \text{subject to} \quad & \mathrm{VSM}_{\min}(\mathbf{u}_0 + \Delta\mathbf{u}) \geq \underline{\mathrm{VSM}} \\ & \mathbf{u}_{\min} \leq \mathbf{u} + \Delta\mathbf{u} \leq \mathbf{u}_{\max} \end{aligned} \quad , \tag{7.2}$$

where $\mathbf{u}_{\min}$ and $\mathbf{u}_{\max}$ are bound constraints imposed to the control variables.

This problem is intrinsically combinatorial, due to its objective function. Furthermore, this is a nested optimization problem, since the evaluation of function $\mathrm{VSM}_{\min}(\mathbf{u})$ itself is the resolution of an optimization problem. These points emphasize that problem (7.2) cannot be solved in real time for online voltage stability assessment. In the next section, a new method is proposed to estimate the solution of problem (7.2).

7.2 The Proposed Method

In the proposition of methods to solve problem (7.2), there is a trade-off between execution speed and quality of the results. The combinatorial nature of problem (7.2) prevents methods from finding the global optimal solution of this problem in the case of large power systems (which may have thousands of control possibilities).

The method proposed in this work should be fast enough to provide control actions necessary to avoid an incoming collapse. Thus, the focus here is speed rather than accuracy.

[1] As described at the beginning of this chapter, there is a cost in modifying each element of $\mathbf{u}$, thus changes in this vector should be minimized.

In this way, an approximation of the true global solution or problem (7.2) is often acceptable for real time operation.

The following method is proposed to estimate the solution of (7.2):

Step I For the current estimate of vector $\mathbf{u}$, compute the solution $\mathrm{VSM}_{\min}(\mathbf{u})$ of problem (7.1) using the method described in Chapter 6;

Step II Compute the gradient $\nabla\mathrm{VSM}_{\min}(\mathbf{u})$ in order to linearize function $\mathrm{VSM}_{\min}(\mathbf{u})$ at point $\mathbf{u}$;

Step III Compute a vector $\Delta\mathbf{u}$ such that:

$$\mathrm{VSM}_{\min}(\mathbf{u}) + \nabla\mathrm{VSM}_{\min}(\mathbf{u}) \cdot \Delta\mathbf{u} \geq \underline{\mathrm{VSM}}\,, \tag{7.3a}$$

$$\mathbf{u}_{\min} \leq \mathbf{u} + \Delta\mathbf{u} \leq \mathbf{u}_{\max}\,. \tag{7.3b}$$

From all vectors $\Delta\mathbf{u}$ that satisfy those conditions, choose one with the minimum number of nonzero elements.

Step IV Update $\mathbf{u} \leftarrow \mathbf{u} + \Delta\mathbf{u}$ and go to *Step I*.

This iterative procedure is repeated until one of the following stop criteria is met:

Condition I The value $\mathrm{VSM}_{\min}(\mathbf{u})$ computed at *Step I* satisfies the following:

$$\mathrm{VSM}_{\min}(\mathbf{u}) \geq \underline{\mathrm{VSM}}\,. \tag{7.4}$$

Condition II There is no update $\Delta\mathbf{u}$ that satisfies the following:

$$\nabla\mathrm{VSM}_{\min}(\mathbf{u}) \cdot \Delta\mathbf{u} > 0\,, \tag{7.5a}$$

$$\mathbf{u}_{\min} \leq \mathbf{u} + \Delta\mathbf{u} \leq \mathbf{u}_{\max}\,. \tag{7.5b}$$

Condition I is the desired situation, in which we were able to reach the threshold $\underline{\mathrm{VSM}}$ for a given vector $\mathbf{u}$ such that $\mathbf{u}_{\min} \leq \mathbf{u} \leq \mathbf{u}_{\max}$. In this case, vector $\mathbf{u} - \mathbf{u}_0$ gives a set of control actions that are sufficient to improve voltage stability of the current operating point.

On the other hand, *Condition II* shows the situation where the method is not able to increase VSM. *Condition II* is satisfied when the linearization of $\mathrm{VSM}_{\min}(\mathbf{u})$ around the current vector $\mathbf{u}$ does not admit an increase in VSM subject to the bound constraints $\mathbf{u}_{\min} \leq \mathbf{u} \leq \mathbf{u}_{\max}$. In other words, the method stopped at a local maximum of function $\mathrm{VSM}_{\min}(\mathbf{u})$ subject to $\mathbf{u}_{\min} \leq \mathbf{u} \leq \mathbf{u}_{\max}$. This local maximum may be a global maximum, which basically establishes that the set of controls in vector $\mathbf{u}$ is not sufficient to increase VSM up to $\underline{\mathrm{VSM}}$. Hence, one should either lower the value of $\underline{\mathrm{VSM}}$ or add new elements to vector $\mathbf{u}$ (which will increase the global maximum of $\mathrm{VSM}_{\min}(\mathbf{u})$).

Figure 73 provides a sketch of one iteration of the proposed method when only one control variable is available. The dashed straight line represents the linearized VSM function at the current control value u. From this linearization, one concludes that u must be increased in order to raise VSM up to $\underline{\text{VSM}}$.

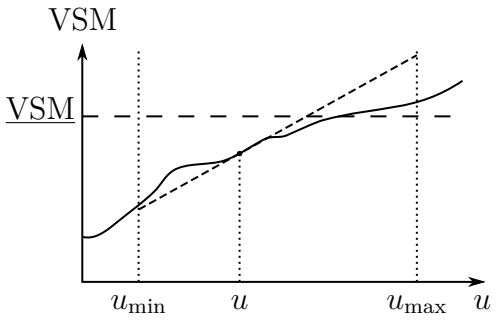

Figure 73 – Sketch of the proposed control-selection method.

Note that this iterative procedure can only provide an estimate of the solution of problem (7.2). When this method is able to increase VSM satisfactorily (i.e., the method stopped due to *Condition I*), there is no guarantee that the number of nonzero elements in $\mathbf{u} - \mathbf{u}_0$ is minimal. On the other hand, when the method stops due to *Condition II*, there is no guarantee that the local maximum $\mathbf{u}$ is in fact the global maximum of $\text{VSM}_{\min}(\mathbf{u})$ subject to $\mathbf{u}_{\min} \leq \mathbf{u} \leq \mathbf{u}_{\max}$.

Nevertheless, we expect that the proposed procedure will usually provide satisfactory results for real time analysis. In normal situations, the *Steps I* to *IV* will be iterated only a few times. As a consequence, problem (7.1) will be solved only a few times, and the execution time will be appropriate for online VSA. Moreover, we expect that only a few elements of $\Delta\mathbf{u}$ are nonzero after each execution of *Step III*. Thus, only a small number of control variables will be modified during the execution of the proposed method.

7.3 Implementation Details

This section provides a detailed description of the proposed procedure. Specifically, in the two following subsections, implementation details are provided for the second and third steps of the proposed algorithm. These are the core steps of the proposed method for control selection.

7.3.1 *Step II*

$\text{VSM}_{\min}(\mathbf{u})$ is computed from the solution of problem (7.1). Thus, in order to compute the gradient $\nabla\text{VSM}_{\min}(\mathbf{u})$, it is necessary to compute the Jacobian of the solution of (7.1) in relation to $\mathbf{u}$.

To simplify the computation, we again replace the bifurcation equations (5.1) by

its linearization:

$$\begin{bmatrix} \partial_{\mathbf{z}}\mathbf{h} & \partial_{\mathbf{p}}\mathbf{h} & \partial_{\mathbf{u}}\mathbf{h} & \mathbf{0} \\ \partial_{\mathbf{z}}(\partial_{\mathbf{z}}\mathbf{h}\,\mathbf{v}) & \partial_{\mathbf{p}}(\partial_{\mathbf{z}}\mathbf{h}\,\mathbf{v}) & \partial_{\mathbf{u}}(\partial_{\mathbf{z}}\mathbf{h}\,\mathbf{v}) & \partial_{\mathbf{z}}\mathbf{h} \\ \mathbf{0} & \mathbf{0} & \mathbf{0} & \partial_{\mathbf{v}}\|\mathbf{v}\| \end{bmatrix} \begin{bmatrix} \mathbf{z}-\mathbf{z}^* \\ \mathbf{p}-\mathbf{p}^* \\ \mathbf{u}-\mathbf{u}^* \\ \mathbf{v}-\mathbf{v}^* \end{bmatrix} = \begin{bmatrix} \mathbf{0} \\ \mathbf{0} \\ 0 \end{bmatrix}, \tag{7.6}$$

where $(\mathbf{z}^*, \mathbf{p}^*, \mathbf{v}^*)$ is the current bifurcation point, computed at *Step I* for the current value of $\mathbf{u} = \mathbf{u}^*$. The Jacobian matrix is evaluated at this current bifurcation point.

Note that variables $\mathbf{z}$ and $\mathbf{v}$ only appear in the bifurcation equations of problem (7.1). Hence, when these equations are replaced by (7.6), variables $\mathbf{z}$ and $\mathbf{v}$ can be removed from the optimization problem by means of a Kron reduction. By removing $2n$ equations of this linear system, the $2n$ variables $\mathbf{z}$ and $\mathbf{v}$ are removed, leading to the following one-dimensional linear equation:

$$\mathbf{n}_{\mathbf{p}}^T(\mathbf{p}-\mathbf{p}^*) + \mathbf{n}_{\mathbf{u}}^T(\mathbf{u}-\mathbf{u}^*) = 0\,, \tag{7.7}$$

where $\mathbf{n}_{\mathbf{p}}$ and $\mathbf{n}_{\mathbf{u}}$ are normal vectors that result from the Kron reduction.

If $\mathbf{w}$ is the left eigenvector of the null eigenvalue of matrix $\partial_{\mathbf{z}}\mathbf{h}$, we can left-multiply the first row of equation (7.6) by $\mathbf{w}^T$ to obtain:

$$\begin{aligned} \mathbf{w}^T \begin{bmatrix} \partial_{\mathbf{z}}\mathbf{h} & \partial_{\mathbf{p}}\mathbf{h} & \partial_{\mathbf{u}}\mathbf{h} & \mathbf{0} \end{bmatrix} \begin{bmatrix} \mathbf{z}-\mathbf{z}^* \\ \mathbf{p}-\mathbf{p}^* \\ \mathbf{u}-\mathbf{u}^* \\ \mathbf{v}-\mathbf{v}^* \end{bmatrix} = \mathbf{w}^T\mathbf{0} = \begin{bmatrix} \mathbf{0} & \mathbf{w}^T\partial_{\mathbf{p}}\mathbf{h} & \mathbf{w}^T\partial_{\mathbf{u}}\mathbf{h} & \mathbf{0} \end{bmatrix} \begin{bmatrix} \mathbf{z}-\mathbf{z}^* \\ \mathbf{p}-\mathbf{p}^* \\ \mathbf{u}-\mathbf{u}^* \\ \mathbf{v}-\mathbf{v}^* \end{bmatrix} \\ \Rightarrow \left(\mathbf{w}^T\partial_{\mathbf{p}}\mathbf{h}\right)(\mathbf{p}-\mathbf{p}^*) + \left(\mathbf{w}^T\partial_{\mathbf{u}}\mathbf{h}\right)(\mathbf{u}-\mathbf{u}^*) = \mathbf{0}\,, \end{aligned} \tag{7.8}$$

which has the same form as equation (7.7). Thus, $\mathbf{n}_{\mathbf{p}} = \partial_{\mathbf{p}}\mathbf{h}^T\mathbf{w}$ and $\mathbf{n}_{\mathbf{u}} = \partial_{\mathbf{u}}\mathbf{h}^T\mathbf{w}$. Hence, there is no need to actually perform a Kron reduction in equation (7.6).

When the bifurcation equations are replaced by its linearization, problem (7.1) becomes:

$$\begin{aligned} \text{VSM}_{\min} = \quad & \min_{\mathbf{p}} && \|\mathbf{p}\|_\alpha \\ & \text{subject to} && \mathbf{n}_{\mathbf{p}}^T(\mathbf{p}-\mathbf{p}^*) + \mathbf{n}_{\mathbf{u}}^T(\mathbf{u}-\mathbf{u}^*) = 0\,, \\ & && \langle \mathbf{p}, \widehat{\mathbf{p}} \rangle_\beta \geq \|\mathbf{p}\|_\beta \sqrt{\|\widehat{\mathbf{p}}\|_\beta^2 - 1} \end{aligned} \tag{7.9}$$

where $\mathbf{p}$ is the only optimization variable, and the solution $\mathbf{p}$ of this optimization problem is a function of the control vector $\mathbf{u}$.

The first-order optimality conditions (LUENBERGER; YE, 2008) of problem (7.9)

are:

$$\nabla_{\mathbf{p}}\|\mathbf{p}\|_{\alpha} + \lambda\mathbf{n}_{\mathbf{p}} + \mu\nabla_{\mathbf{p}}g(\mathbf{p}) = \mathbf{0}\,, \tag{7.10a}$$

$$\mu\, g(\mathbf{p}) = 0\,, \tag{7.10b}$$

$$\mathbf{n}_{\mathbf{p}}^{T}(\mathbf{p}-\mathbf{p}^{*}) + \mathbf{n}_{\mathbf{u}}^{T}(\mathbf{u}-\mathbf{u}^{*}) = 0\,, \tag{7.10c}$$

$$g(\mathbf{p}) \leq 0\,, \tag{7.10d}$$

$$\mu \geq 0\,, \tag{7.10e}$$

where λ and μ are dual variables, while $g(\mathbf{p}) \equiv \|\mathbf{p}\|_{\beta}\sqrt{\|\widehat{\mathbf{p}}\|_{\beta}^{2}-1} - \langle\mathbf{p},\widehat{\mathbf{p}}\rangle_{\beta}$.

From equation (7.10), the solution of the problem solved in *Step I* either satisfies $\mu = 0$ (i.e., the solution of this optimization problem is in the interior of the uncertainty cone) or satisfies $g(\mathbf{p}) = 0$ (i.e., the solution lies on the boundary of the cone). Each of these cases are analyzed separately in order to compute the gradient vector $\nabla\mathrm{VSM}_{\min}(\mathbf{u})$.

The solution is in the interior of the cone

In this case, $\mu = 0$ and equation (7.10) becomes:

$$\nabla_{\mathbf{p}}\|\mathbf{p}\|_{\alpha} + \lambda\mathbf{n}_{\mathbf{p}} = \mathbf{0}\,, \tag{7.11a}$$

$$\mathbf{n}_{\mathbf{p}}^{T}(\mathbf{p}-\mathbf{p}^{*}) + \mathbf{n}_{\mathbf{u}}^{T}(\mathbf{u}-\mathbf{u}^{*}) = 0\,, \tag{7.11b}$$

whose derivative with respect to $\mathbf{u}$ is given by:

$$\begin{bmatrix}\mathbf{M}_{\alpha} & \mathbf{n}_{\mathbf{p}}\\ \mathbf{n}_{\mathbf{p}}^{T} & 0\end{bmatrix}\begin{bmatrix}\partial_{\mathbf{u}}\mathbf{p}\\ \partial_{\mathbf{u}}\lambda\end{bmatrix} = \begin{bmatrix}\mathbf{0}\\ -\mathbf{n}_{\mathbf{u}}^{T}\end{bmatrix}\,, \tag{7.12}$$

where $\mathbf{M}_{\alpha}$ is the Hessian matrix of the objective function at point $\mathbf{p}^{*}$. Usually, the objective function is defined in such a way that $\mathbf{M}_{\alpha}$ is a diagonal matrix. In this case, linear system (7.12) can be solved very efficiently using the Schur complement of matrix $\mathbf{M}_{\alpha}$.

After the computation of $\partial_{\mathbf{u}}\mathbf{p}$, the gradient $\nabla\mathrm{VSM}_{\min}(\mathbf{u})$ can be computed with the following matrix product:

$$\nabla\mathrm{VSM}_{\min}(\mathbf{u})^{T} = \partial_{\mathbf{u}}\mathrm{VSM}_{\min}(\mathbf{p}) = \partial_{\mathbf{p}}\mathrm{VSM}_{\min}(\mathbf{p})\,\partial_{\mathbf{u}}\mathbf{p} = \partial_{\mathbf{p}}\|\mathbf{p}\|_{\alpha}\,\partial_{\mathbf{u}}\mathbf{p} \tag{7.13}$$

The solution is on the boundary of the cone

In this case, $g(\mathbf{p}) = 0$ and equation (7.10) becomes:

$$\nabla_{\mathbf{p}}\|\mathbf{p}\|_{\alpha} + \lambda\mathbf{n}_{\mathbf{p}} + \mu\nabla_{\mathbf{p}}g(\mathbf{p}) = \mathbf{0}\,, \tag{7.14a}$$

$$g(\mathbf{p}) = 0\,, \tag{7.14b}$$

$$\mathbf{n}_{\mathbf{p}}^{T}(\mathbf{p}-\mathbf{p}^{*}) + \mathbf{n}_{\mathbf{u}}^{T}(\mathbf{u}-\mathbf{u}^{*}) = 0\,, \tag{7.14c}$$

whose derivative with respect to $\mathbf{u}$ is given by:

$$\begin{bmatrix} \mathbf{M}_\alpha + \mu\mathbf{G}(\mathbf{p}) & \nabla_{\mathbf{p}} g(\mathbf{p}) & \mathbf{n}_{\mathbf{p}} \\ \nabla_{\mathbf{p}} g(\mathbf{p})^T & 0 & 0 \\ \mathbf{n}_{\mathbf{p}}^T & 0 & 0 \end{bmatrix} \begin{bmatrix} \partial_{\mathbf{u}}\mathbf{p} \\ \partial_{\mathbf{u}}\mu \\ \partial_{\mathbf{u}}\lambda \end{bmatrix} = \begin{bmatrix} \mathbf{0} \\ \mathbf{0} \\ -\mathbf{n}_{\mathbf{u}}^T \end{bmatrix}, \tag{7.15}$$

where $\mathbf{G}$ is the Hessian matrix of function $\mathbf{g}$:

$$\mathbf{G}(\mathbf{p}) = \sqrt{\|\widehat{\mathbf{p}}\|_\beta^2 - 1}\left(\frac{\mathbf{M}_\beta}{\|\mathbf{p}\|_\beta} - \frac{(\mathbf{M}_\beta\mathbf{p})(\mathbf{M}_\beta\mathbf{p})^T}{\|\mathbf{p}\|_\beta^3}\right) = \kappa\left(\frac{\mathbf{M}_\beta}{\|\mathbf{p}\|_\beta} - \frac{(\mathbf{M}_\beta\mathbf{p})(\mathbf{M}_\beta\mathbf{p})^T}{\|\mathbf{p}\|_\beta^3}\right), \tag{7.16}$$

where $\langle \mathbf{x}, \mathbf{y} \rangle_\beta \equiv \mathbf{x}^T\mathbf{M}_\beta\mathbf{y}$ and $\|\mathbf{x}\|_\beta \equiv \sqrt{\langle \mathbf{x}, \mathbf{x} \rangle_\beta}$.

If both $\mathbf{M}_\alpha$ and $\mathbf{M}_\beta$ are diagonal matrices, then $\mathbf{M}_\alpha + \frac{\mu\kappa}{\|\mathbf{p}\|_\beta}\mathbf{M}_\beta$ is also a diagonal matrix. Hence, $\mathbf{M}_\alpha + \mu\mathbf{G}(\mathbf{p})$ is a rank-one update of a diagonal matrix. In this situation, the linear system (7.15) can be solved efficiently using the Schur complement of $\mathbf{M}_\alpha + \mu\mathbf{G}(\mathbf{p})$, which in turn is computed using the Sherman–Morrison formula (since this matrix is a rank-one update of a diagonal matrix).

After the computation of $\partial_{\mathbf{u}}\mathbf{p}$, the gradient $\nabla\mathrm{VSM}_{\min}(\mathbf{u})$ can be calculated with equation (7.13).

7.3.2 *Step III*

At the end of *Step II*, the linearization of function $\mathrm{VSM}_{\min}(\mathbf{u})$ is known. The objective of *Step III* is to find a vector $\Delta\mathbf{u}$ such that:

$$\mathrm{VSM}_{\min}(\mathbf{u}) + \nabla\mathrm{VSM}_{\min}(\mathbf{u}) \cdot \Delta\mathbf{u} \geq \underline{\mathrm{VSM}}\,, \tag{7.17a}$$

$$\mathbf{u}_{\min} \leq \mathbf{u} + \Delta\mathbf{u} \leq \mathbf{u}_{\max}\,. \tag{7.17b}$$

In order to minimize the number of nonzero elements in $\Delta\mathbf{u}$, only one control variable will be modified at a time. If we only change the control variable i, the change Δu_i needed to increase the margin to $\underline{\mathrm{VSM}}$ is given by:

$$\partial_{u_i}\mathrm{VSM}_{\min}(\mathbf{u})\Delta u_i \geq \underline{\mathrm{VSM}} - \mathrm{VSM}_{\min}(\mathbf{u}) > 0\,, \tag{7.18}$$

and the minimum value of $|\Delta u_i|$ needed to increase the VSM up to the desired value is given by:

$$|\Delta u_i|_{\min} = \left|\frac{\Delta\mathrm{VSM}}{\partial_{u_i}\mathrm{VSM}_{\min}(\mathbf{u})}\right|, \tag{7.19}$$

where $\Delta\mathrm{VSM} = \underline{\mathrm{VSM}} - \mathrm{VSM}_{\min}(\mathbf{u})$.

However, Δu_i is bounded to:

$$u_{\min,i} - u_i \leq \Delta u_i \leq u_{\max,i} - u_i\,, \tag{7.20}$$

thus the maximum admissible value for $|\Delta u_i|$ is given by:

$$|\Delta u_i|_{\max} = \begin{cases} u_{\max,i} - u_i, & \text{if } \partial_{u_i} \mathrm{VSM}_{\min}(\mathbf{u}) \geq 0\,, \\ u_i - u_{\min,i}, & \text{if } \partial_{u_i} \mathrm{VSM}_{\min}(\mathbf{u}) < 0\,, \end{cases} \tag{7.21}$$

If $|\Delta u_i|_{\min} \leq |\Delta u_i|_{\max}$, then $\Delta u_i = |\Delta u_i|_{\min} \operatorname{sign}\left(\partial_{u_i} \mathrm{VSM}_{\min}(\mathbf{u})\right)$ satisfies both (7.18) and (7.20), and a possible solution to *Step III* has been computed. This solution might not be unique, since there might be several values of i for which $|\Delta u_i|_{\min} \leq |\Delta u_i|_{\max}$. Despite that, all these solutions share the same information: it is possible to increase the linearization of $\mathrm{VSM}_{\min}$ up to $\underline{\mathrm{VSM}}$ by changing only one control variable.

On the other hand, if $|\Delta u_i|_{\min} > |\Delta u_i|_{\max}\ \forall\ i$, then it is not possible to increase VSM satisfactorily by changing only one control variable. In this case the control variable i that is most promising in increasing VSM is the variable i that maximizes:

$$\Delta\mathrm{VSM}_i = |\partial_{u_i} \mathrm{VSM}_{\min}(\mathbf{u})| \cdot |\Delta u_i|_{\max}\,, \tag{7.22}$$

which is the variable i that maximizes:

$$\frac{|\partial_{u_i} \mathrm{VSM}_{\min}(\mathbf{u})|}{\Delta\mathrm{VSM}} \cdot |\Delta u_i|_{\max} = \frac{|\Delta u_i|_{\max}}{|\Delta u_i|_{\min}} \tag{7.23}$$

This variable i is modified accordingly and the value of ΔVSM is updated by:

$$\Delta\mathrm{VSM} \leftarrow \Delta\mathrm{VSM} - \Delta\mathrm{VSM}_i\,, \tag{7.24}$$

to reflect the increase in VSM due to the change in variable i. The search for a new control variable to increase VSM is then restarted.

This algorithm can be summarized in the following pseudo-code:

Step 1 Define variable $\Delta\mathrm{VSM} \leftarrow \underline{\mathrm{VSM}} - \mathrm{VSM}_{\min}(\mathbf{u})$.

Step 2 Find the index i that minimizes $k_i = \frac{|\Delta u_i|_{\max}}{|\Delta u_i|_{\min}}$, where $|\Delta u_i|_{\min}$ and $|\Delta u_i|_{\max}$ are computed as shown in equations (7.19) and (7.21), respectively.

Step 3 If $k_i = 0$ (i.e., either $|\Delta u_i|_{\max} = 0$ or $\partial_{u_i} \mathrm{VSM}_{\min}(\mathbf{u}) = 0$), then no control variables are available to increase VSM, so stop the algorithm. Otherwise, go to the next step.

Step 4 If $k_i \geq 1$ (i.e., $|\Delta u_i|_{\min} \leq |\Delta u_i|_{\max}$), then control variable i is sufficient to increase VSM. Assign $\Delta u_i \leftarrow |\Delta u_i|_{\min} \operatorname{sign}\left(\partial_{u_i} \mathrm{VSM}_{\min}(\mathbf{u})\right)$ and stop the algorithm. Otherwise, go to the next step.

Step 5 Variable i is not sufficient to increase VSM satisfactorily. However, variable i is the most promising control variable to increase VSM.
Assign $\Delta u_i \leftarrow |\Delta u_i|_{\max} \operatorname{sign}\left(\partial_{u_i} \mathrm{VSM}_{\min}(\mathbf{u})\right)$, update ΔVSM according to equation (7.24) and return to *Step 2*.

This pseudo-code provides guidelines to execute *Step III* of the proposed procedure. However, two implementation details should be addressed:

- The pseudo-code described above generates a set of control actions that aim for increasing VSM to exactly $\underline{\text{VSM}}$. Thus, it is expected that $\text{VSM}_{\min}(\mathbf{u})$ will converge to $\underline{\text{VSM}}$, which does *not* mean that the condition (7.4) will be satisfied. This is depicted in Figure 74.

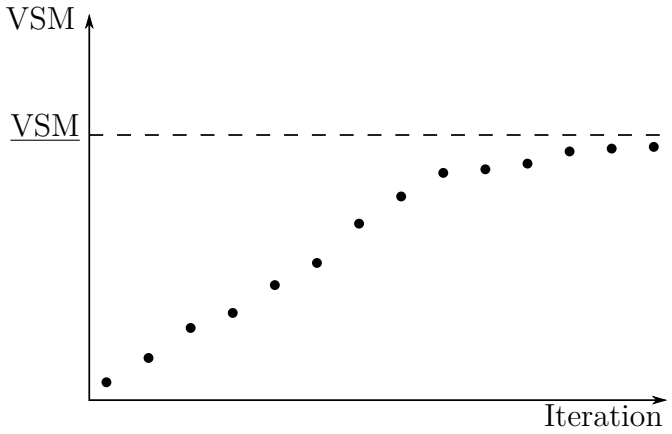

Figure 74 – Convergence of VSM to $\underline{\text{VSM}}$

To overcome this problem, *Step III* should simply aim at a value of margin greater than $\underline{\text{VSM}}$. In this case, the initial value of ΔVSM in the pseudo-code described above is higher than $\underline{\text{VSM}} - \text{VSM}_{\min}(\mathbf{u})$. The target value can be constant, as shown in Figure 75, where condition (7.4) becomes true at the iteration highlighted in the figure.

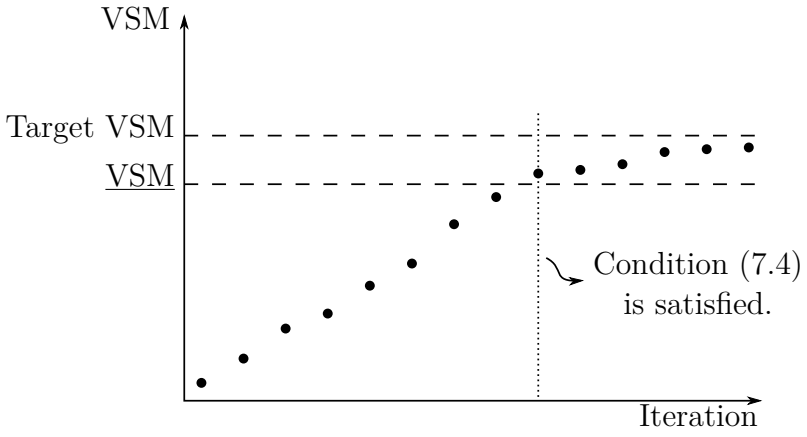

Figure 75 – Convergence of VSM to target $\text{VSM}_{\text{target}}$.

Another possibility is to adapt the target value according to the difference between $\underline{\text{VSM}}$ and $\text{VSM}_{\min}(\mathbf{u})$. For example, we may define the target value as

$$\text{VSM}_{\text{target}} = \underline{\text{VSM}} + \rho \cdot (\underline{\text{VSM}} - \text{VSM}_{\min}(\mathbf{u}))\,, \tag{7.25}$$

where $\rho > 0$ is a constant factor. In this way, the difference of the target and desired values of VSM decreases as we approach $\underline{\text{VSM}}$. In the implementation used in this work, we use $\rho = 0.1$.

- If ΔVSM is large, then the number of control actions computed by *Step III* may be large. Since function $\text{VSM}_{\text{min}}(\mathbf{u})$ is nonlinear, this large amount of control variations does not necessarily reflect in a large increase in VSM. In order to avoid modifying unnecessary control variables, we may limit the number of control actions in each execution of *Step III* to a fixed value. In the implementation of this work, at most 10 elements of $\Delta\mathbf{u}$ are nonzero after each execution of *Step III*.

7.3.3 Line-search technique

The last implementation aspect of the proposed procedure is related to the nonlinear behavior of function $\text{VSM}_{\text{min}}(\mathbf{u})$. The control selection in *Steps II* and *III* compute a vector $\Delta\mathbf{u}$ based on the linearization of $\text{VSM}_{\text{min}}(\mathbf{u})$ at the current value of $\mathbf{u}$. According to this linearization, $\text{VSM}_{\text{min}}(\mathbf{u}+\Delta\mathbf{u})$ is greater than $\text{VSM}_{\text{min}}(\mathbf{u})$. However, since function $\text{VSM}_{\text{min}}(\mathbf{u})$ is nonlinear, the value of $\text{VSM}_{\text{min}}(\mathbf{u})$ might actually decrease between two consecutive iterations of the proposed procedure. As a result, the proposed method may encounter divergence problems.

To avoid this situation, we may explicitly disallow a decrease in $\text{VSM}_{\text{min}}(\mathbf{u})$. This is possible by means of a line-search technique, which simply reduces the value of $\tau > 0$ to satisfy the following condition:

$$\text{VSM}_{\text{min}}(\mathbf{u}+\tau\Delta\mathbf{u}) > \text{VSM}_{\text{min}}(\mathbf{u})\,. \tag{7.26}$$

This condition is true for a sufficiently small τ, because $\Delta\mathbf{u}$ was chosen to satisfy $\nabla\text{VSM}_{\text{min}}(\mathbf{u})\cdot\Delta\mathbf{u} > 0$. In the implementation of this work, we start with $\tau = 1$ and multiply τ by 0.5 until condition (7.26) is satisfied.

7.4 Regarding discrete control variables

In addition to being manually operated, many control variables in vector $\mathbf{u}$ are associated with a discrete behavior, such as the tap position of a transformer. In some situations, these discrete control variables lead to large variations in the power system performance. This is the case of large switchable capacitor banks and load shedding, for example. Usually, these large discrete changes cannot be accurately approximated by a continuous modelling. As a result, some of the elements of vector $\mathbf{u}$ are discrete, and the original problem (7.2) becomes a mixed-integer optimization problem.

In this situation, the proposed method should be adapted to handle discrete control variables. *Step III* is the only step of the proposed procedure that needs to be modified to deal with discrete variables in vector $\mathbf{u}$. In this case, some elements of vector $\Delta\mathbf{u}$ computed by *Step III* can only assume discrete values.

Assume that the control variable u_i can only assume discrete values. Then, the control change Δu_i can only assume discrete values. In this case, the value of $|\Delta u_i|_{\text{min}}$

(equation (7.19)) in the pseudo-code of Subsection 7.3.2 should be rounded up to the next discrete value. On the other hand, the value $|\Delta u_i|_{\max}$ computed by (7.21) already is a valid discrete value, since u_i, $u_{\min,i}$ and $u_{\max,i}$ are valid discrete values. The computation of *Step III* then proceeds in the same way described in the pseudo-code of Subsection 7.3.2.

With this modification, the update vector $\Delta\mathbf{u}$ is valid both for continuous and discrete variables in vector $\mathbf{u}$. However, we must ensure that the update vector $\tau\Delta\mathbf{u}$ used in the line search technique (equation (7.26)) is also valid.

Subsection 7.3.3 proposed to successively update vector $\Delta\mathbf{u}$ with

$$\Delta\mathbf{u} \leftarrow k\Delta\mathbf{u} \tag{7.27}$$

until condition

$$\mathrm{VSM}_{\min}(\mathbf{u}+\Delta\mathbf{u}) > \mathrm{VSM}_{\min}(\mathbf{u}) \tag{7.28}$$

is satisfied. The implementation used in this work uses $k = 1/2$. In order to guarantee that every vector $\Delta\mathbf{u}$ is valid, we replace the update (7.27) by the following:

$$\Delta\mathbf{u} \leftarrow \mathrm{round}\,(k\Delta\mathbf{u}) \tag{7.29}$$

where the round function simply rounds the discrete elements of the input vector towards zero.

7.5 Example

In this section, the proposed method will be illustrated using the IEEE 14-bus power system (CHRISTIE, 1999). In this example, all parameters in vector $\mathbf{p}$ are load parameters. With the load modelled as constant power, those parameters are the active and reactive power demanded at each bus.

Consider that, in the most likely *parameter variation scenario*, all system loads increase proportionally to the base case. By using a continuation power flow, we are able to increase the system load up to 76.0%.

Now, consider that there is uncertainty associated with this load growth direction, as described in Chapter 6. In this example, we arbitrarily choose matrix $\mathbf{M}_\beta$ in the same way as in the results of Chapter 6:

$$\mathbf{M}_\beta = \mathrm{diag}\left(\frac{\mathbf{p}_0}{2}\right)^{-2}, \tag{7.30}$$

where diag is a function that transforms a vector into a diagonal matrix, while vector $\mathbf{p}_0$ is the initial value of vector $\mathbf{p}$ in the base case situation.

Lastly, the objective function of problem (7.1) is redefined to $\frac{1}{2}\|\mathbf{p}_{\max}-\mathbf{p}_0\|_2^2$, whose Hessian matrix is the identity matrix.

Having defined the objective function and the uncertainty region, problem (7.1) can now be solved. By using the method proposed in Chapter 6, the final value of the objective function is given by $0.258 \approx \frac{1}{2}(0.604\|\mathbf{p}_0\|_2)^2$, which is equivalent to a variation of 60.4% in $\mathbf{p}_0$. In other words, the distance to a bifurcation point decreased from 76.0% to 60.4% when uncertainties were taken into account.

For illustration purposes, assume that a distance of 60.4% to a voltage collapse is too small, and that this value should be increased to 76.0%. In this way, control actions must be selected to increase the VSM considering parameter uncertainties to the value of VSM that was obtained before considering uncertainties.

In this example, assume that the following control variables are available to increase the VSM:

- Variable shunt susceptances are available at buses 3, 5 and 10. Each variable susceptance can vary between -0.4 pu and 0.4 pu, and its initial value is 0 pu.
- All three transformers are manually operated on-load tap changers. The tap position of each transformer ($|t|$ in equation (2.12)) is bounded between 0.8 pu and 1.2 pu, and their initial positions are given by the system data (CHRISTIE, 1999).
- The active power provided by the generator connected at bus 2, initially fixed at 0.4 pu, can vary between 0 pu and 1 pu.
- The voltage setpoint of all three synchronous condensers (connected to buses 3, 6 and 8) can be adjusted between 0.9 pu and 1.1pu. Their initial values are given by the system data (CHRISTIE, 1999).

7.5.1 First iteration

7.5.1.1 *Step I*

After the first execution of *Step I*, problem (7.1) is solved and a VSM value of $\frac{1}{2}(60.4\%\|\mathbf{p}_0\|_2)^2$ was computed. Since this value is less than the desired VSM of $\frac{1}{2}(76.0\%\|\mathbf{p}_0\|_2)^2$, the algorithm proceeds to *Step II*.

7.5.1.2 *Step II*

The solution computed in *Step I* lies on the boundary of the cone. In this situation, the linear system given by (7.15) should be solved. Then, the gradient is calculated using equation (7.13).

The final value of the gradient is shown in Table 10. The values of these derivatives are expected:

- The sensitivity of VSM in relation to shunt susceptances are positive, which agrees with the fact that there is a lack of reactive power in the system at the bifurcation

point. If this reactive power were provided by capacitor banks, the system load could be further increased, which in turn increases the VSM.

Note that the order of those derivatives are also expected: a capacitor bank of 1 pu connected to bus 10 is more promising to improve voltage stability than the same capacitor connected at bus 3, because bus 10 belongs to the load side of the system, while bus 3 belongs to its generation side.

- According to the notation of equation (2.12), an increase in the value of $|t|$ of each of the transformers is expected to increase the voltage at buses 7, 9 and 6. From the IEEE 14-bus system data, we can see that an increase in $|t|$ thus increases the voltage at the load side of the system, when compared to the voltage at the generation side. This increase in the load-side voltage allows larger power transfers through the transmission system, increasing the VSM.
- When the active power of the generator at bus 2 is held constant, the increase in system load is compensated exclusively by the increase in generation at the slack bus. An increase in the generation at bus 2 is then expected to alleviate the active power transfer on the lines connected to the slack bus, hence increasing the VSM.
- At the bifurcation point, all synchronous condensers are operating at their reactive power limits. As a result, none of these condensers is operating on voltage control (as described by equation (2.9)), and the value of the setpoint voltage will have no (local) effect on the value of VSM.

Table 10 – IEEE 14-bus system — Gradient of VSM in relation to control variables

Control variable	i	Derivative $\partial_{u_i}\mathrm{VSM}_{\min}(\mathbf{u})$
Susceptance at bus 3	1	0.0805
Susceptance at bus 5	2	0.0949
Susceptance at bus 10	3	0.1503
Tap of transformer 4—7	4	0.2262
Tap of transformer 4—9	5	0.1287
Tap of transformer 5—6	6	0.2651
Active power of generator at bus 2	7	0.0368
Voltage setpoint of generator at bus 3	8	0
Voltage setpoint of generator at bus 6	9	0
Voltage setpoint of generator at bus 8	10	0

7.5.1.3 *Step III*

This step selects control actions to take based on the gradient vector computed in *Step II*. These control actions should increase VSM from its current value to the target value, as defined by (7.25), where $\rho = 0.1$. This defines the following value of ΔVSM:

$$\Delta\mathrm{VSM} = \mathrm{VSM}_{\mathrm{target}} - \mathrm{VSM}_{\min}(\mathbf{u}) = (1+\rho)(\underline{\mathrm{VSM}} - \mathrm{VSM}_{\min}(\mathbf{u}))\,, \tag{7.31}$$

which, for this iteration, is given by $(1+0.1)\left(\frac{1}{2}(76.0\%\|\mathbf{p}_0\|_2)^2 - \frac{1}{2}(60.4\%\|\mathbf{p}_0\|_2)^2\right) = 0.167$.

With this initial value, the pseudo-code of Subsection 7.3.2 is executed. Table 11 shows the values of variables $|\Delta u_i|_{\min}$, $|\Delta u_i|_{\max}$ and k_i at the first iteration of this pseudo-code. The rows in this table are sorted in descending order with respect to k_i. Hence, these rows are sorted according to the effectiveness in improving voltage stability.

Table 11 – IEEE 14-bus system — Control Selection

Control variable	i	$\|\Delta u_i\|_{\min}$	$\|\Delta u_i\|_{\max}$	k_i
Susceptance at bus 10	3	1.11	0.4	0.3605
Tap of transformer 4—7	4	0.7374	0.1775	0.2407
Susceptance at bus 5	2	1.757	0.4	0.2276
Tap of transformer 5—6	6	0.6292	0.127	0.2019
Susceptance at bus 3	1	2.073	0.4	0.1929
Active power of generator at bus 2	7	4.533	0.6	0.1324
Tap of transformer 4—9	5	1.296	0.168	0.1296
Voltage setpoint of generator at bus 3	8	∞	0.09	0
Voltage setpoint of generator at bus 6	9	∞	0.03	0
Voltage setpoint of generator at bus 8	10	∞	0.01	0

Table 11 shows that $k_3 < 1$, which means that the most promising control action is not sufficient to increase VSM satisfactorily, and more than one control variable must be modified to increase VSM up to the target level. By executing the algorithm described in Subsection 7.3.2, the control variables will be successively modified in the order presented in Table 11. In fact, it can be shown that the algorithm of Subsection 7.3.2 simply selects the smallest set $\mathcal{S}$ such that

$$\sum_{i\in\mathcal{S}} k_i \geq 1\,. \tag{7.32}$$

In this first execution of *Step III*, $\mathcal{S} = \{3, 4, 2, 6\}$, for which $\sum_{i\in\mathcal{S}} k_i = 1.031$. The first three variables are fixed at their limits, while the last one is adjusted to increase VSM to the target value:

- Variables u_3, u_4 and u_2 are fixed at 0.4 pu, 1.2 pu and 0.4 pu, respectivelly.
- The change Δu_6 in the tap position of transformer 5—6 is given by:

$$\begin{aligned} |\Delta u_6| &= \frac{1 - k_3 - k_4 - k_2}{k_6} |\Delta u_6|_{\max} \\ &\approx \frac{1 - 0.3605 - 0.2407 - 0.2276}{0.2019} 0.127 \approx 0.1077\,, \end{aligned} \tag{7.33}$$

  and $u_6 = 1.181$ pu.

7.5.2 Second iteration

7.5.2.1 *Step I*

With the control variables modified as computed by *Step III*, problem (7.1) is solved again, obtaining a VSM value of $\frac{1}{2}(80.6\%\|\mathbf{p}_0\|_2)^2$. Hence, the selected control actions

indeed increased VSM up to the desired value of $\frac{1}{2}(76.0\%\|\mathbf{p}_0\|_2)^2$. The execution of the proposed method then stops due to *Condition I*.

7.6 Simulation Results

In this section, the proposed method is applied to select control actions with the aim of improving voltage stability of several power systems. All power systems studied in Chapter 6 will be analyzed here.

Each power system is operating in a different condition. As a result, the initial value of VSM is different for each power system. Hence, it is difficult to define a desired value of VSM that is common to all these systems. In this section, the desired value of VSM (VSM in problem (7.2)) is twice the initial value of VSM, for all analyzed systems.

For all simulations, the elements of vector $\mathbf{p}$ are load parameters in the power system (active and reactive power demanded by loads in all buses). In contrast to Chapter 6, the active power output of generators are not included in vector $\mathbf{p}$. On the other hand, these parameters will be included in the control vector $\mathbf{u}$.

The same way as in Chapter 6, matrix $\mathbf{M}_\beta$ (such that $\langle \mathbf{p}_{\max}, \widehat{\mathbf{p}} \rangle_\beta = \mathbf{p}_{\max}^T \mathbf{M}_\beta \mathbf{p}$ in problem (6.29)) is arbitrarily defined in the following way:

$$\mathbf{M}_\beta = \operatorname{diag}\left(\frac{\widehat{\mathbf{p}}}{2}\right)^{-2}, \tag{7.34}$$

where $\widehat{\mathbf{p}}$ is the most likely direction of loading variation. In this section, $\widehat{\mathbf{p}}$ is proportional to the initial value of power system loading. In addition, VSM is also defined as in Chapter 6:

$$\text{VSM} = \frac{1}{2}\|\mathbf{p} - \mathbf{p}_0\|_2^2 = \frac{1}{2}(\mathbf{p} - \mathbf{p}_0)^T(\mathbf{p} - \mathbf{p}_0)\,, \tag{7.35}$$

For all power systems, the control variables in vector $\mathbf{u}$ are composed of:

- The active power output of generators. Bounds to these variables are defined by the original power system data, if available. Otherwise, active power variables can deviate in 20% from its initial value.
- The voltage setpoint of generators. These variables are limited between 90% and 110% of its initial value.
- Variable susceptance devices connected to 10% of the system buses. These buses were arbitrarily picked among all buses. Each variable susceptance is initially set to 0 pu and is bounded between -0.5 pu and 0.5 pu.

The results for all power systems are summarized in Table 12. All results are given using the continuation power flow associated with the most credible *scenario* as reference. When uncertainties are considered, the final value of voltage stability margin is reduced and the computational time increases. On top of that, the computational time

also increases when control actions are selected to improve voltage stability. Note that the final value of VSM after control selection is at least two times greater than the VSM before control selection.

Table 12 – Control Selection — Implementation results

System	IEEE 118-bus system
Initial VSM (Continuation Power Flow Method)	f_{obj}
Execution time	Δt
VSM considering parameter uncertainties (Chapter 6)	$0.831 f_{\text{obj}}$
Execution time	$1.61\Delta t$
VSM after control changes	$1.66 f_{\text{obj}}$
Execution time	$7.66\Delta t$
Number of available control variables	100
Number of selected control actions	12
System	IEEE 300-bus system
Initial VSM (Continuation Power Flow Method)	f_{obj}
Execution time	Δt
VSM considering parameter uncertainties (Chapter 6)	$0.809 f_{\text{obj}}$
Execution time	$1.89\Delta t$
VSM after control changes	$1.62 f_{\text{obj}}$
Execution time	$6.99\Delta t$
Number of available control variables	162
Number of selected control actions	2
System	PEGASE 1354-bus system
Initial VSM (Continuation Power Flow Method)	f_{obj}
Execution time	Δt
VSM considering parameter uncertainties (Chapter 6)	$0.891 f_{\text{obj}}$
Execution time	$1.16\Delta t$
VSM after control changes	$2.13 f_{\text{obj}}$
Execution time	$2.61\Delta t$
Number of available control variables	654
Number of selected control actions	1
System	PEGASE 2869-bus system
Initial VSM (Continuation Power Flow Method)	f_{obj}
Execution time	Δt
VSM considering parameter uncertainties (Chapter 6)	$0.942 f_{\text{obj}}$

Execution time	$3.34\Delta t$
VSM after control changes	$2.24 f_{\text{obj}}$
Execution time	$6.22\Delta t$
Number of available control variables	1306
Number of selected control actions	1
System	PEGASE 9241-bus system
Initial VSM (Continuation Power Flow Method)	f_{obj}
Execution time	Δt
VSM considering parameter uncertainties (Chapter 6)	$0.904 f_{\text{obj}}$
Execution time	$1.86\Delta t$
VSM after control changes	$2.13 f_{\text{obj}}$
Execution time	$3.53\Delta t$
Number of available control variables	3813
Number of selected control actions	1
System	PEGASE 13659-bus system
Initial VSM (Continuation Power Flow Method)	f_{obj}
Execution time	Δt
VSM considering parameter uncertainties (Chapter 6)	$0.921 f_{\text{obj}}$
Execution time	$2.32\Delta t$
VSM after control changes	$2.21 f_{\text{obj}}$
Execution time	$8.47\Delta t$
Number of available control variables	9549
Number of selected control actions	1

The first point to be highlighted in this table is the execution time. In agreement with the results reported in Chapter 6, the computational cost of considering uncertainties in VSM computation is only a few times higher than the computation neglecting these uncertainties (i.e., the continuation power flow execution). On top of that, the control selection method proposed in Section 7.2 executes the method of Chapter 6 only a few times. As a result, the overall method (computing the VSM considering uncertainties and selecting controls to increase this value to the desired VSM) is less than 10 times slower than the computation of a single continuation power flow. These results reveal that the proposed method has good potential to be applied in real-time voltage stability assessment of large power systems, since it can be executed in a time-scale of a few minutes for large, real-sized systems.

The second point to be highlighted refers to the number of control actions needed to

restore the voltage stability margin. Note that the control actions selected by the proposed method are only a small subset of the complete set of available control variables. This agrees with the objective function of the original optimization problem (7.2). Moreover, note that more control actions were needed to improve voltage stability of smaller systems (118-bus system and 300-bus system). This is due to the following reasons:

- The initial distance to collapse is greater for the IEEE test-systems. In other words, the PEGASE systems are more prone to a voltage collapse. Hence, the initial value of VSM for the IEEE systems is greater than the VSM of the PEGASE systems, and doubling the VSM of the IEEE systems is then more difficult than doubling the VSM of the PEGASE systems.
- The simulations in this section consider that only load parameters are included in vector $\mathbf{p}$. This means that only load parameters are varied to compute the VSM, while the active power of all generators (but the slack generator) are fixed. The slack generator is responsible for meeting the loading deviations in the whole system. As a consequence, the system is less robust to load variations occurring far from the slack bus, which explains why larger systems are more prone to a voltage collapse in these simulations. In these larger systems, the value of VSM can be easily doubled by modifying the active power output of an appropriate generator, usually located far from the slack bus.
- The data for the IEEE test-systems were obtained from (CHRISTIE, 1999), which provides no information related to active power limits of generators. In this section, we arbitrarily admit 20% variation from the current value to set up limits the active power of these generators. In contrast, the data for the PEGASE systems were obtained from (ZIMMERMAN; MURILLO-SANCHEZ; THOMAS, 2011), which provides bounds to the active power of generators. Some of these generators admit large variations of active power, thus these generators can provide large variations in VSM as compared to the generators in the IEEE systems.

The voltage collapse occurs when the increase of active power generated at the slack bus is not able to compensate the load increase in remote buses. Thus, it is expected that the most promising control actions to restore stability refer to the increase in active power of remote generators. In fact, with the exception of 4 control variables for the 118-bus system and 1 control variable for the 300-bus system, all control actions selected by the proposed method refer to the increase of generation in the system.

The greater distance to collapse of the IEEE systems means that these systems can withstand a larger load increase before the collapse. With load increases, there are large voltage drops in these systems before the collapse. As a result, control variables that aim for increasing the voltage of system buses are effective in increasing the VSM. Besides the controls that increase the active power generation, all remaining controls selected for

the IEEE systems refer to increase of voltage setpoint of generators.

7.7 Partial Conclusions

This chapter proposed a new method for control selection that aims for increasing the value of VSM computed by the method of Chapter 6. The method of this chapter is build on top of the method of Chapter 6. This method usually provides a small number of control actions that increase the VSM to the desired value.

Similarly to the method of Chapter 6, the method proposed in this chapter isolates the control selection from the bifurcation surface nonlinearities by means of a linearization. Even though the control variables are selected based on a linearization, the nonlinearities of the power system model are taken into account in each execution of the method of Chapter 6.

The proposed method was tested in several different power systems with promising results. The results of Section 7.6 show that the propose method is able to double the initial value of VSM with a small number of control actions. Moreover, the proposed method is usually executed in a time equivalent to less than 10 continuation power flow executions. This highlights that the proposed method has good potential for voltage stability assessment by not only computing VSM with uncertainties taken into account, but also defining control variables that increase the VSM to a predefined minimum value.

8 CONCLUSIONS

The contributions of this thesis range from further developing the theoretical foundations of voltage stability to the proposition of new, enhanced models, methods and computational tools for voltage stability margin calculation and control. These contributions can be summarized in the following topics:

- A new model was proposed to represent power systems. This new model transforms every generic static bifurcation of the original model into saddle-node bifurcations. The main purpose of this new model is to unify the search for bifurcations: any method developed to deal with SNB can be seamlessly applied to compute any generic static bifurcation of the proposed model. Not only new methods can be proposed based on this power system model, but also many existing traditional methods in the literature can be enhanced by this new model. A solid theoretical foundation is given to prove that the proposed model is indeed a valid approximation of the original model.
- A new method was developed for dealing with contingency analysis in voltage stability. The proposed method can fast and accurately rank the voltage stability margin of contingencies in a power system. The new method applies the proposed power flow model to compute VSM due to any type of bifurcation, avoiding potential issues due to the change of the bifurcation type due to a contingency.
- A new method to deal with uncertainties in voltage stability was proposed. By further developing the foundations of the treatment of parameter uncertainties in VSA, an optimization problem is proposed to compute a robust measure of voltage stability margin. Moreover, an efficient method is proposed to solve this optimization problem. The proposed method is generic and can be applied not only to loading parameter uncertainties, but also to arbitrary parameter uncertainties. Furthermore, the method can compute arbitrary bifurcation points due to the proposed power flow model.
- A novel method was proposed for selecting control variables to increase the voltage stability margin up to a predefined value by means of a small number of control actions. These control actions can be composed of arbitrary parameters in the power flow model. The method is robust, by taking uncertainties into account. In addition, the method is fast, usually executed in a time equivalent to a few evaluations of continuation power flow. By exploring the proposed smooth power flow model, the method takes into account arbitrary bifurcations in the power system.

The models and methods proposed in this thesis present new, innovative contributions to the current literature in relation to:

- Modelling:
  - The proposed power flow model makes only a few assumptions about the power system model, and this new model can be applied to several devices besides the ones described in this thesis. In this way, the proposed model can be easily extended to include generic devices in the power system. Besides the methods discussed in this document, any method that computes SNBs can take advantage of the proposed model to be able to detect generic bifurcations.
  - The treatment of uncertainties in voltage stability assessment is further clarified (from the statistical point of view) by the new model presented in this PhD. This uncertainty model is generic, which can incorporate arbitrary parameters in the power flow model.
- Voltage stability margin computation:
  - While the literature on contingency analysis usually prioritize speed rather than accuracy, the proposed method for contingency ranking presents a good trade-off between speed and accuracy. The proposed method is able to give a precise ranking of contingencies without sacrificing performance, while still being able to detect generic static bifurcations.
  - The method proposed for voltage stability margin computation considering uncertainties is more robust than the alternatives in the literature. This robustness is achieved by a practical decoupling between bifurcation point computation and uncertainty evaluation. At the same time, the proposed method is still fast on computing a robust measure of voltage stability margin.
- Voltage stability margin control: the proposed method is able to select a small amount of control actions to increase the voltage stability margin to a predefined value. To our knowledge, this is the first method that deals with control selection taking uncertainties into account. Moreover, the method scales well with large systems, and its execution time remains on a range of a few continuation power flow executions.

By gathering all these contributions, this PhD thesis presents a comprehensive computational framework to statically assess voltage stability of generic power systems, providing methods for contingency analysis, uncertainty evaluation and control selection. All methods were tested on large-scale power systems with promising results, showing potential to be applied in real-time voltage stability analysis of real power systems.

8.1 Published Papers

During this PhD, three journal papers were published or accepted:

NEVES, L. S.; ALBERTO, L. F. C.; CHIANG, H.-D. A fast method for detecting limit-induced bifurcation in electric power systems. **Electric Power Systems Research**, v. 180, p. 106101, 2020. ISSN 0378-7796.

NEVES, L. S.; ALBERTO, L. F. C. On the computation of the locally closest bifurcation point considering loading uncertainties and reactive power limits. **IEEE Transactions on Power Systems**, v. 35, n. 5, p. 3885–3894, 2020.

NEVES, L. S.; ALBERTO, L. F. C.; CHIANG, H.-D. Smooth power flow model for unified voltage stability assessment: Theory and computation. **IEEE Transactions on Power Systems**, 2021. In press.

In addition, three conference papers were also published or accepted:

NEVES, L. S.; ALBERTO, L. F. C. Voltage stability monitoring using artificial neural networks. In: **13th Latin-American Congress on Electricity Generation and Transmission**. [S.l.: s.n.], 2019.

NEVES, L. S.; ALBERTO, L. F. C. Equivalence between geometric and optimization approaches on computing the power system closest bifurcation. In: **Conferência Brasileira de Dinâmica, Controle e Aplicações**. [s.n.], 2019. Disponível em: <http://soac.eesc.usp.br/index.php/dincon/xivdincon/paper/view/1962/1212>.

NEVES, L. S.; ALBERTO, L. F. C.; CHIANG, H.-D. Fast contingency screening for voltage stability analysis considering both SNBs and SIBs. In: **Power Systems Computation Conference**. [S.l.: s.n.], 2021. In press.

Furthermore, several other papers are currently being developed regarding the contributions of this research.

BIBLIOGRAPHY

ABE, S. et al. Load flow convergence in the vicinity of a voltage stability limit. **IEEE Transactions on Power Apparatus and Systems**, PAS-97, n. 6, p. 1983–1993, 1978.

AFFONSO, C. M. et al. Mw and mvar management on supply and demand side for meeting voltage stability margin criteria. **IEEE Transactions on Power Systems**, v. 19, n. 3, p. 1538–1545, 2004.

AJJARAPU, V.; CHRISTY, C. The continuation power flow: a tool for steady state voltage stability analysis. **IEEE Transactions on Power Systems**, IEEE, v. 7, n. 1, p. 416–423, fev. 1992. ISSN 0885-8950.

ALVARADO, F.; DOBSON, I.; HU, Y. Computation of closest bifurcations in power systems. **IEEE Transactions on Power Systems**, v. 9, n. 2, p. 918–928, maio 1994. ISSN 1558-0679.

AVALOS, R. J. et al. Equivalency of Continuation and Optimization Methods to Determine Saddle-Node and Limit-Induced Bifurcations in Power Systems. **IEEE Transactions on Circuits and Systems I: Regular Papers**, v. 56, n. 1, p. 210–223, jan. 2009. ISSN 1549-8328.

CANIZARES, C. A. On bifurcations, voltage collapse and load modeling. **IEEE Transactions on Power Systems**, v. 10, n. 1, p. 512–522, fev. 1995.

CANIZARES, C. A. Calculating optimal system parameters to maximize the distance to saddle-node bifurcations. **IEEE Transactions on Circuits and Systems I: Fundamental Theory and Applications**, v. 45, n. 3, p. 225–237, 1998.

CANIZARES, C. A.; ALVARADO, F. L. Point of collapse and continuation methods for large AC/DC systems. **IEEE Transactions on Power Systems**, IEEE, v. 8, n. 1, p. 1–8, fev. 1993. ISSN 0885-8950.

CANIZARES, C. A. et al. Point of collapse methods applied to AC/DC power systems. **IEEE Transactions on Power Systems**, IEEE, v. 7, n. 2, p. 673–683, maio 1992. ISSN 0885-8950.

CAPITANESCU, F.; CUTSEM, T. V. Preventive control of voltage security margins: a multicontingency sensitivity-based approach. **IEEE Transactions on Power Systems**, v. 17, n. 2, p. 358–364, 2002.

CAPITANESCU, F.; CUTSEM, T. V. Unified sensitivity analysis of unstable or low voltages caused by load increases or contingencies. **IEEE Transactions on Power Systems**, IEEE, v. 20, n. 1, p. 321–329, fev. 2005. ISSN 0885-8950.

CAPITANESCU, F. et al. Contingency filtering techniques for preventive security-constrained optimal power flow. **IEEE Transactions on Power Systems**, v. 22, n. 4, p. 1690–1697, nov. 2007.

CHIANG, H.-D. et al. On voltage collapse in electric power systems. **IEEE Transactions on Power Systems**, v. 5, n. 2, p. 601–611, 1990.

CHIANG, H.-D. et al. CPFLOW: a practical tool for tracing power system steady-state stationary behavior due to load and generation variations. **IEEE Transactions on Power Systems**, v. 10, n. 2, p. 623–634, maio 1995. ISSN 0885-8950.

CHIANG, H.-D.; WANG, C.-S.; FLUECK, A. J. Look-ahead voltage and load margin contingency selection functions for large-scale power systems. **IEEE Transactions on Power Systems**, IEEE, v. 12, n. 1, p. 173–180, fev. 1997. ISSN 0885-8950.

CHIANG, H.-D.; WANG, T. Novel homotopy theory for nonlinear networks and systems and its applications to electrical grids. **IEEE Transactions on Control of Network Systems**, v. 5, n. 3, p. 1051–1060, 2018.

CHRISTIE, R. **Power Systems Test Case Archive**. 1999. <https://labs.ece.uw.edu/pstca/>.

CUTSEM, T. V. A method to compute reactive power margins with respect to voltage collapse. **IEEE Transactions on Power Systems**, v. 6, n. 1, p. 145–156, 1991.

CUTSEM, T. V. An approach to corrective control of voltage instability using simulation and sensitivity. **IEEE Transactions on Power Systems**, v. 10, n. 2, p. 616–622, 1995.

CUTSEM, T. V.; VOURNAS, C. **Voltage Stability of Electric Power Systems**. 1. ed. Boston, MA: Springer, 1998. (Power Electronics and Power Systems). ISBN 978-0-387-75536-6.

DOBSON, I. Observations on the geometry of saddle node bifurcation and voltage collapse in electrical power systems. **IEEE Transactions on Circuits and Systems I: Fundamental Theory and Applications**, v. 39, n. 3, p. 240–243, mar. 1992. ISSN 1057-7122.

DOBSON, I. Distance to Bifurcation in Multidimensional Parameter Space: Margin Sensitivity and Closest Bifurcations. In: **Bifurcation Control**. [S.l.]: Springer Berlin Heidelberg, 2004. p. 49–66.

DOBSON, I.; CHIANG, H.-D. Towards a theory of voltage collapse in electric power systems. **Systems & Control Letters**, Elsevier BV, v. 13, n. 3, p. 253–262, set. 1989. ISSN 0167-6911.

DOBSON, I.; LU, L. Computing an optimum direction in control space to avoid stable node bifurcation and voltage collapse in electric power systems. **IEEE Transactions on Automatic Control**, IEEE, v. 37, n. 10, p. 1616–1620, out. 1992. ISSN 0018-9286.

DOBSON, I.; LU, L. Voltage collapse precipitated by the immediate change in stability when generator reactive power limits are encountered. **IEEE Transactions on Circuits and Systems I: Fundamental Theory and Applications**, IEEE, v. 39, n. 9, p. 762–766, set. 1992. ISSN 1057-7122.

DOBSON, I.; LU, L. New methods for computing a closest saddle node bifurcation and worst case load power margin for voltage collapse. **IEEE Transactions on Power Systems**, IEEE, v. 8, n. 3, p. 905–913, ago. 1993. ISSN 0885-8950.

EJEBE, G. C. et al. Methods for contingency screening and ranking for voltage stability analysis of power systems. **IEEE Transactions on Power Systems**, v. 11, n. 1, p. 350–356, 1996.

FENG, Z.; AJJARAPU, V.; LONG, B. Identification of voltage collapse through direct equilibrium tracing. **IEEE Transactions on Power Systems**, v. 15, n. 1, p. 342–349, fev. 2000. ISSN 0885-8950.

FENG, Z.; AJJARAPU, V.; MARATUKULAM, D. J. A practical minimum load shedding strategy to mitigate voltage collapse. **IEEE Transactions on Power Systems**, v. 13, n. 4, p. 1285–1290, nov. 1998. ISSN 0885-8950.

FENG, Z.; AJJARAPU, V.; MARATUKULAM, D. J. A comprehensive approach for preventive and corrective control to mitigate voltage collapse. **IEEE Transactions on Power Systems**, v. 15, n. 2, p. 791–797, maio 2000. ISSN 0885-8950.

FLATABO, N. et al. A method for calculation of margins to voltage instability applied on the norwegian system for maintaining required security level. **IEEE Transactions on Power Systems**, v. 8, n. 3, p. 920–928, 1993.

FLATABO, N.; OGNEDAL, R.; CARLSEN, T. Voltage stability condition in a power transmission system calculated by sensitivity methods. **IEEE Transactions on Power Systems**, v. 5, n. 4, p. 1286–1293, 1990.

FLISCOUNAKIS, S. et al. Contingency Ranking With Respect to Overloads in Very Large Power Systems Taking Into Account Uncertainty, Preventive, and Corrective Actions. **IEEE Transactions on Power Systems**, v. 28, n. 4, p. 4909–4917, nov. 2013. ISSN 0885-8950.

FLUECK, A. J.; DONDETI, J. R. A new continuation power flow tool for investigating the nonlinear effects of transmission branch parameter variations. **IEEE Transactions on Power Systems**, v. 15, n. 1, p. 223–227, 2000.

FLUECK, A. J.; GONELLA, R.; DONDETI, J. R. A new power sensitivity method of ranking branch outage contingencies for voltage collapse. **IEEE Transactions on Power Systems**, v. 17, n. 2, p. 265–270, 2002.

GAO, B.; MORISON, G. K.; KUNDUR, P. Voltage stability evaluation using modal analysis. **IEEE Transactions on Power Systems**, v. 7, n. 4, p. 1529–1542, 1992.

GAO, B.; MORISON, G. K.; KUNDUR, P. Towards the development of a systematic approach for voltage stability assessment of large-scale power systems. **IEEE Transactions on Power Systems**, v. 11, n. 3, p. 1314–1324, 1996.

GREENE, S.; DOBSON, I.; ALVARADO, F. L. Sensitivity of the loading margin to voltage collapse with respect to arbitrary parameters. **IEEE Transactions on Power Systems**, v. 12, n. 1, p. 262–272, fev. 1997. ISSN 0885-8950.

GREENE, S.; DOBSON, I.; ALVARADO, F. L. Contingency ranking for voltage collapse via sensitivities from a single nose curve. **IEEE Transactions on Power Systems**, v. 14, n. 1, p. 232–240, 1999.

HAESEN, E. et al. A Probabilistic Formulation of Load Margins in Power Systems With Stochastic Generation. **IEEE Transactions on Power Systems**, v. 24, n. 2, p. 951–958, maio 2009. ISSN 0885-8950.

HALE, J. K.; KOCAK, H. **Dynamics and Bifurcations**. 1. ed. New York, NY: Springer-Verlag, 1991. (Texts in Applied Mathematics). ISBN 978-0-387-97141-4.

HATZIARGYRIOU, N. et al. Definition and classification of power system stability – revisited & extended. **IEEE Transactions on Power Systems**, v. 36, n. 4, p. 3271–3281, 2021.

HISKENS, I.; CHAKRABARTI, B. Direct calculation of reactive power limit points. **International Journal of Electrical Power & Energy Systems**, v. 18, n. 2, p. 121–129, fev. 1996. ISSN 0142-0615.

IBA, K. et al. Calculation of critical loading condition with nose curve using homotopy continuation method. **IEEE Transactions on Power Systems**, v. 6, n. 2, p. 584–593, 1991.

IEEE Task Force on Load Representation for Dynamic Performance. Load representation for dynamic performance analysis (of power systems). **IEEE Transactions on Power Systems**, IEEE, v. 8, n. 2, p. 472–482, maio 1993. ISSN 0885-8950.

JIA, Z.; JEYASURYA, B. Contingency ranking for on-line voltage stability assessment. **IEEE Transactions on Power Systems**, v. 15, n. 3, p. 1093–1097, 2000.

JIANFEN, Z. et al. Probabilistic Voltage Stability Analysis Based on Unscented Transformation and Maximum Entropy Principle. **American Journal of Electrical Power and Energy Systems**, v. 5, n. 6, p. 81–90, 2016. ISSN 2326-9200.

JOSZ, C. et al. AC Power Flow Data in MATPOWER and QCQP Format: iTesla, RTE Snapshots, and PEGASE. **ArXiv e-prints**, mar. 2016.

KATAOKA, Y. A probabilistic nodal loading model and worst case solutions for electric power system voltage stability assessment. **IEEE Transactions on Power Systems**, v. 18, n. 4, p. 1507–1514, nov. 2003. ISSN 0885-8950.

KUNDUR, P. **Power System Stability and Control**. 1. ed. [S.l.]: McGraw-Hill, Inc, 1994. ISBN 0-07-035958-X.

KWATNY, H.; PASRIJA, A.; BAHAR, L. Static bifurcations in electric power networks: Loss of steady-state stability and voltage collapse. **IEEE Transactions on Circuits and Systems**, v. 33, n. 10, p. 981–991, 1986.

LEE, B. H.; LEE, K. Y. A study on voltage collapse mechanism in electric power systems. **IEEE Transactions on Power Systems**, v. 6, n. 3, p. 966–974, 1991.

LOF, P.-A. et al. Fast calculation of a voltage stability index. **IEEE Transactions on Power Systems**, v. 7, n. 1, p. 54–64, 1992.

LUENBERGER, D. G.; YE, Y. **Linear and Nonlinear Programming**. [S.l.]: Springer US, 2008.

MANSOUR, M. R.; ALBERTO, L. F. C.; RAMOS, R. A. Preventive Control Design for Voltage Stability Considering Multiple Critical Contingencies. **IEEE Transactions on Power Systems**, v. 31, n. 2, p. 1517–1525, mar. 2016. ISSN 0885-8950.

MANSOUR, M. R. et al. A New and Fast Method for Preventive Control Selection in Voltage Stability Analysis. **IEEE Transactions on Power Systems**, v. 28, n. 4, p. 4448–4455, nov. 2013. ISSN 0885-8950.

MORISON, G. K.; GAO, B.; KUNDUR, P. Voltage stability analysis using static and dynamic approaches. **IEEE Transactions on Power Systems**, v. 8, n. 3, p. 1159–1171, 1993.

NEVES, L. S.; ALBERTO, L. F. C. Equivalence between geometric and optimization approaches on computing the power system closest bifurcation. In: **Conferência Brasileira de Dinâmica, Controle e Aplicações**. [s.n.], 2019. Disponível em: <http://soac.eesc.usp.br/index.php/dincon/xivdincon/paper/view/1962/1212>.

NEVES, L. S.; ALBERTO, L. F. C. Voltage stability monitoring using artificial neural networks. In: **13th Latin-American Congress on Electricity Generation and Transmission**. [S.l.: s.n.], 2019.

NEVES, L. S.; ALBERTO, L. F. C. On the computation of the locally closest bifurcation point considering loading uncertainties and reactive power limits. **IEEE Transactions on Power Systems**, v. 35, n. 5, p. 3885–3894, 2020.

NEVES, L. S.; ALBERTO, L. F. C.; CHIANG, H.-D. A fast method for detecting limit-induced bifurcation in electric power systems. **Electric Power Systems Research**, v. 180, p. 106101, 2020. ISSN 0378-7796.

NEVES, L. S.; ALBERTO, L. F. C.; CHIANG, H.-D. Fast contingency screening for voltage stability analysis considering both SNBs and SIBs. In: **Power Systems Computation Conference**. [S.l.: s.n.], 2021. In press.

NEVES, L. S.; ALBERTO, L. F. C.; CHIANG, H.-D. Smooth power flow model for unified voltage stability assessment: Theory and computation. **IEEE Transactions on Power Systems**, 2021. In press.

NOCEDAL, J.; WRIGHT, S. **Numerical Optimization**. 1. ed. [S.l.]: Springer-Verlag New York, 1999. (Springer Series in Operations Research and Financial Engineering). ISBN 0-387-98793-2.

OBADINA, O. O.; BERG, G. J. Identifying electrically weak and strong segments of a power system from a voltage stability viewpoint. **IEE Proceedings C - Generation, Transmission and Distribution**, v. 137, n. 3, p. 205–212, 1990.

OVERBYE, T. J. A power flow measure for unsolvable cases. **IEEE Transactions on Power Systems**, v. 9, n. 3, p. 1359–1365, 1994.

PIERCE JR, H. E. et al. Common Format For Exchange of Solved Load Flow Data. **IEEE Transactions on Power Apparatus and Systems**, PAS-92, n. 6, p. 1916–1925, nov. 1973. ISSN 0018-9510.

ROSS, S. M. **Stochastic Processes**. 2. ed. [S.l.]: John Wiley & Sons, Inc, 1995. ISBN 978-0-471-12062-9.

SAUER, P. W.; PAI, M. A. Power system steady-state stability and the load-flow jacobian. **IEEE Transactions on Power Systems**, v. 5, n. 4, p. 1374–1383, 1990.

SCHLUETER, R. A. et al. Methods for determining proximity to voltage collapse. **IEEE Transactions on Power Systems**, v. 6, n. 1, p. 285–292, 1991.

SEYDEL, R. **Practical Bifurcation and Stability Analysis**. 3. ed. [S.l.]: Springer-Verlag New York, 2010. (Interdisciplinary Applied Mathematics). ISBN 978-1-4419-1740-9.

SONG, H. et al. Reactive reserve-based contingency constrained optimal power flow (rccopf) for enhancement of voltage stability margins. **IEEE Transactions on Power Systems**, v. 18, n. 4, p. 1538–1546, 2003.

SOUZA, A. Z. de. Tangent vector applied to voltage collapse and loss sensitivity studies. **Electric Power Systems Research**, Elsevier BV, v. 47, n. 1, p. 65–70, out. 1998. ISSN 0378-7796.

TAMURA, Y.; MORI, H.; IWAMOTO, S. Relationship between voltage instability and multiple load flow solutions in electric power systems. **IEEE Transactions on Power Apparatus and Systems**, PAS-102, n. 5, p. 1115–1125, 1983.

TAYLOR, C. **Power System Voltage Stability**. 1. ed. Singapore: McGraw-Hill, 1994. ISBN 0-07-113708-4.

THEODORO, E. et al. Algebraic-graph method for identification of islanding in power system grids. **International Journal of Electrical Power & Energy Systems**, v. 35, n. 1, p. 171–179, 2012. ISSN 0142-0615.

TIRANUCHIT, A. et al. Towards a computationally feasible on-line voltage instability index. **IEEE Transactions on Power Systems**, v. 3, n. 2, p. 669–675, 1988.

TIRANUCHIT, A.; THOMAS, R. J. A posturing strategy against voltage instabilities in electric power systems. **IEEE Transactions on Power Systems**, v. 3, n. 1, p. 87–93, 1988.

VAAHEDI, E. et al. Voltage stability contingency screening and ranking. **IEEE Transactions on Power Systems**, v. 14, n. 1, p. 256–265, 1999.

VENIKOV, V. A. et al. Estimation of electrical power system steady-state stability in load flow calculations. **IEEE Transactions on Power Apparatus and Systems**, v. 94, n. 3, p. 1034–1041, 1975.

WANG, L.; CHIANG, H.-D. Group-based line switching for enhancing contingency-constrained static voltage stability. **IEEE Transactions on Power Systems**, v. 35, n. 2, p. 1489–1498, 2020.

WANG, R.; LASSETER, R. H. Re-dispatching generation to increase power system security margin and support low voltage bus. **IEEE Transactions on Power Systems**, v. 15, n. 2, p. 496–501, 2000.

WANG, X. et al. Preventive/corrective control for voltage stability using direct interior point method. In: **Proceedings of the 20th International Conference on Power Industry Computer Applications**. [S.l.: s.n.], 1997. p. 312–317.

WANG, Y.; CHIANG, H.-D.; WANG, T. A two-stage method for assessment of voltage stability in power system with renewable energy. In: **2013 IEEE Electrical Power Energy Conference**. [S.l.: s.n.], 2013. p. 1–6.

WU, Q. et al. Voltage security enhancement via coordinated control. **IEEE Transactions on Power Systems**, v. 16, n. 1, p. 127–135, 2001.

ZENG, Z. C. et al. A simplified approach to estimate maximum loading conditions in the load flow problem. **IEEE Transactions on Power Systems**, v. 8, n. 2, p. 646–654, 1993.

ZHANG, J.; DOBSON, I.; ALVARADO, F. L. Quantifying transmission reliability margin. **International Journal of Electrical Power & Energy Systems**, v. 26, n. 9, p. 697–702, nov. 2004. ISSN 0142-0615.

ZHANG, J. F. et al. Voltage stability analysis based on probabilistic power flow and maximum entropy. **IET Generation, Transmission Distribution**, v. 4, n. 4, p. 530–537, abr. 2010. ISSN 1751-8687.

ZHAO, J.; CHIANG, H.-D.; LI, H. A new contingency parameterization cpf model and sensivity method for voltage stability control. In: **IEEE Power Engineering Society General Meeting, 2005**. [S.l.: s.n.], 2005. p. 1681–1687.

ZHAO, J. et al. A novel preventive control approach for mitigating voltage collapse. In: **2006 IEEE Power Engineering Society General Meeting**. [S.l.: s.n.], 2006.

ZHU, P.; TAYLOR, G.; IRVING, M. A novel Q-Limit guided Continuation Power Flow method. In: **2008 IEEE Power and Energy Society General Meeting - Conversion and Delivery of Electrical Energy in the 21st Century**. [S.l.]: IEEE, 2008. p. 1–7. ISSN 1932-5517.

ZIMMERMAN, R. D.; MURILLO-SANCHEZ, C. E.; THOMAS, R. J. MATPOWER: Steady-State Operations, Planning, and Analysis Tools for Power Systems Research and Education. **IEEE Transactions on Power Systems**, v. 26, n. 1, p. 12–19, fev. 2011. ISSN 0885-8950.

Appendix

APPENDIX A – PROOFS

A.1 Proof of Theorem 2

If $(\widehat{y}, \widehat{u})$ is of the form (y, u_1) where $y < y_{\text{spec}}$, the proof is given by property [I] of a *smooth step function*.

If $(\widehat{y}, \widehat{u})$ is of the form (y, u_2) where $y > y_{\text{spec}}$, the proof is given by property [II] of a *smooth step function*.

Lastly, assume that $u_1 < u_2$ and that $(\widehat{y}, \widehat{u})$ is of the form (y_{spec}, u) where $u_1 \leq u \leq u_2$. Then, for any $\varepsilon > 0$, properties [I] and [II] ensure the existence of $\delta > 0$ such that, for any $\gamma \in (0, \eta)$, the following equations are satisfied:

$$g_\gamma(y_{\text{spec}} - \varepsilon) < u_1 + \varepsilon\,, \tag{A.1a}$$

$$g_\gamma(y_{\text{spec}} + \varepsilon) > u_2 - \varepsilon\,. \tag{A.1b}$$

g_γ is continuous, so the Intermediate Value Theorem establishes that there is a $y \in [y_{\text{spec}} - \varepsilon, y_{\text{spec}} + \varepsilon]$ such that $g_\gamma(y) = u$ for any value $u \in [g_\gamma(y_{\text{spec}} - \varepsilon), g_\gamma(y_{\text{spec}} + \varepsilon)]$.

Inequation (A.1) guarantees that $[u_1 + \varepsilon, u_2 - \varepsilon] \subset [g_\gamma(y_{\text{spec}} - \varepsilon, g_\gamma(y_{\text{spec}} + \varepsilon)]$. Therefore, for any $u \in [u_1 + \varepsilon, u_2 - \varepsilon]$, there is a $y \in [y_{\text{spec}} - \varepsilon, y_{\text{spec}} + \varepsilon]$ such that $g_\gamma(y) = u$. Since $\varepsilon > 0$ can be arbitrarily small, the theorem is demonstrated for any $(\widehat{y}, \widehat{u}) = (y_{\text{spec}}, u)$ where $u \in [u_1, u_2]$.

The proof is analogous for the case where $u_2 < u_1$.

The last part of the proof can be graphically visualized in Figure 76. For any $\varepsilon > 0$ there is a $\delta > 0$ such that the smooth function intersects both squares shown in Figure 76 for any $\gamma \in (0, \delta)$. This figure corroborates the statement of Theorem 2.

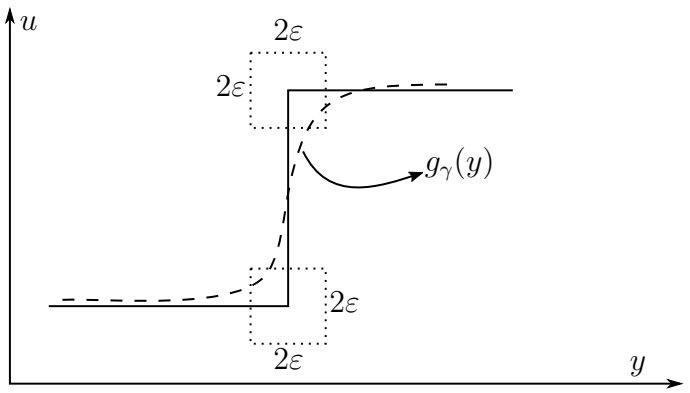

Figure 76 – Graphical visualization of Theorem 2.

A.2 Proof of Theorem 3

If $\widehat{y} \neq y_{\text{spec}}$, the proof is given by properties [I] and [II].

If $\widehat{y} = y_{\text{spec}}$, then property [III] guarantees that $\min\{u_1, u_2\} \leq g_\gamma(y_{\text{spec}}) \leq \max\{u_1, u_2\}$, concluding the proof.

A.3 Proof of Theorem 4

Since function $\mathbf{f}_a$ is C^1 in a neighborhood of $(\widehat{y}, \widehat{u}, \widehat{\mathbf{z}}, \widehat{t})$ and $\begin{bmatrix} \partial_{\mathbf{z}} \mathbf{f}_a & \partial_t \mathbf{f}_a \end{bmatrix}$ is generically nonsingular, the Implicit Function Theorem (Theorem 1) guarantees the existence and uniqueness of continuously differentiable functions $\mathbf{z}(y, u)$ and $t(y, u)$ such that $\mathbf{f}_a(y, u, \mathbf{z}(y, u), t(y, u)) \equiv \mathbf{0}$ in a neighborhood of $(\widehat{y}, \widehat{u}, \widehat{\mathbf{z}}, \widehat{t})$.

Theorem 2 establishes that, for a sufficiently small $\gamma > 0$, there is a solution $(\widetilde{y}, \widetilde{u}) = (\widetilde{y}(\gamma), \widetilde{u}(\gamma))$ of (4.22) arbitrarily close to a solution $(\widehat{y}, \widehat{u})$ of (4.18). Since functions $\mathbf{z}(y, u)$ and $t(y, u)$ are continuous, the smoothed system admits a solution $(\widetilde{y}, \widetilde{u}, \mathbf{z}(\widetilde{y}, \widetilde{u}), t(\widetilde{y}, \widetilde{u}))$ arbitrarily close to the solution $(\widehat{y}, \widehat{u}, \mathbf{z}(\widehat{y}, \widehat{u}), t(\widehat{y}, \widehat{u}))$ of the original system.

A.4 Proof of Theorem 5

Similarly to Theorem 4, there generically are unique C^1 functions $\mathbf{z}(y, u)$ and $t(y, u)$ such that $\mathbf{f}_a(y, u, \mathbf{z}(y, u), t(y, u)) \equiv \mathbf{0}$ in a neighborhood of $(\widehat{y}, \widehat{u}, \widehat{\mathbf{z}}, \widehat{t})$.

Theorem 3 establishes that, for a sufficiently small $\gamma > 0$, there is a solution $(\widehat{y}, \widehat{u})$ of (4.18) arbitrarily close to a solution $(\widetilde{y}, \widetilde{u}) = (\widetilde{y}(\gamma), \widetilde{u}(\gamma))$ of (4.22). Since functions $\mathbf{z}(y, u)$ and $t(y, u)$ are continuous, the original system admits a solution $(\widehat{y}, \widehat{u}, \mathbf{z}(\widehat{y}, \widehat{u}), t(\widehat{y}, \widehat{u}))$ arbitrarily close to the solution $(\widetilde{y}, \widetilde{u}, \mathbf{z}(\widetilde{y}, \widetilde{u}), t(\widetilde{y}, \widetilde{u}))$ of the smoothed system.

A.5 Proof of Theorem 6

Assume, for simplicity, that $\widehat{y} < y_{\text{spec}}$.

For any $\varepsilon > 0$ and $\delta > 0$ arbitrarily small, property [I] of a *smooth step function* guarantees the existence of a arbitrarily small γ such that:

$$u_1 - \varepsilon < g_\gamma(y) < u_1 + \varepsilon \,, \tag{A.2}$$

for any y in the compact $[\widehat{y} - \delta, \widehat{y} + \delta]$.

By the Mean Value Theorem:

$$g'_\gamma(y) = \frac{g_\gamma(\widehat{y} + \delta) - g_\gamma(\widehat{y} - \delta)}{2\delta} \,, \tag{A.3}$$

for some $y \in [\widehat{y} - \delta, \widehat{y} + \delta]$.

By joining equations (A.2) and (A.3):

$$-\frac{\varepsilon}{\delta} < g'_\gamma(y) < \frac{\varepsilon}{\delta}\,, \tag{A.4}$$

for some $y \in [\widehat{y}-\delta, \widehat{y}+\delta]$. For this value of y:

$$\begin{aligned}\mu'(y) &= \partial_y h(y, g_\gamma(y)) + \partial_u h(y, g_\gamma(y)) \times g'_\gamma(y) \\ &\Rightarrow \partial_y h(y, g_\gamma(y)) - |\partial_u h(y, g_\gamma(y))| \times \frac{\varepsilon}{\delta} < \mu'(y) < \partial_y h(y, g_\gamma(y)) + |\partial_u h(y, g_\gamma(y))| \times \frac{\varepsilon}{\delta}\,.\end{aligned} \tag{A.5}$$

Since h is C^1, $\partial_u h(y, g_\gamma(y))$ is bounded. Moreover, if $\varepsilon > 0$ and $\delta > 0$ are sufficiently small, then $\partial_y h(y, g_\gamma(y))$ (where $y \in [\widehat{y}-\delta, \widehat{y}+\delta]$ and $g_\gamma(y) \in [u_1-\varepsilon, u_1+\varepsilon]$) and $\partial_y h(\widehat{y}, \widehat{u})$ have the same sign. Hence, if ε is sufficiently small, then the sign of $\mu'(y)$ is equal to the sign of $\partial_y h(y, g_\gamma(y))$, which in turn is equal to the sign of $\partial_y h(\widehat{y}, \widehat{u})$, concluding the proof.

The proof is completely analogous for the case where $\widehat{y} > y_{\text{spec}}$.

A.6 Proof of Corollary 1

Given solution $(\widehat{y}, \widehat{u})$ of (4.18), Theorem 6 establishes the existence of a solution $(\widetilde{y}, \widetilde{u})$ of (4.22). These solutions are arbitrarily close to each other.

An infinitesimal variation of h in relation to infinitesimal variations in y and u is given by:

$$dh = \partial_y h\, dy + \partial_u h\, du\,. \tag{A.6}$$

If these infinitesimal variations in y and u are restricted to equation $c(y, u) = 0$, then:

$$\partial_y c\, dy + \partial_u c\, du = 0 \Rightarrow \frac{du}{dy} = -\frac{\partial_y c}{\partial_u c}\,, \tag{A.7}$$

thus the total derivative $\frac{dh}{dy}$ is given by:

$$\frac{dh}{dy} = \partial_y h + \partial_u h \frac{du}{dy} = \partial_y h - \partial_u h \frac{\partial_y c}{\partial_u c}\,. \tag{A.8}$$

For equation (4.18), $c(y, u)$ is either $u - u_1$ or $u - u_2$. Thus $\partial_y c = 0$ and $\partial_u c = 1$, and:

$$\frac{dh}{dy}(\widehat{y}, \widehat{u}) = \partial_y h(\widehat{y}, \widehat{u})\,. \tag{A.9}$$

For equation (4.22), $c(y, u) \equiv u - g_\gamma(y)$. Thus $\partial_y c = -g'_\gamma(y)$ and $\partial_u c = 1$, and:

$$\frac{dh}{dy}(\widetilde{y}, \widetilde{u}) = \partial_y h(\widetilde{y}, \widetilde{u}) + \partial_u h(\widetilde{y}, \widetilde{u})\, g'_\gamma(\widetilde{y})\,. \tag{A.10}$$

Theorem 6 guarantees that $\partial_y h(\widehat{y}, \widehat{u}) \times (\partial_y h(\widetilde{y}, \widetilde{u}) + \partial_u h(\widetilde{y}, \widetilde{u})\, g'_\gamma(\widetilde{y})) > 0$. This concludes that the sign of $\frac{dh}{dy}$ for solution $(\widehat{y}, \widehat{u})$ is equal to the sign of $\frac{dh}{dy}$ for solution $(\widetilde{y}, \widetilde{u})$.

A.7 Proof of Theorem 7

Assume, for simplicity, that $u_1 < u_2$. In this situation, property [V] of a *smooth step function* guarantees that g_γ is convex for $y < y_{\text{spec}}$ and concave for $y > y_{\text{spec}}$.

Property [III] guarantees that there is $\alpha > 0$ such that $u_1 + \alpha \leq g_\gamma(y_{\text{spec}}) \leq u_2 - \alpha$ for all γ. Let $r < \min\{\alpha, u_2 - \widehat{u}, \widehat{u} - u_1\}$. Thus, the following inequations are satisfied:

$$u_1 + r < g_\gamma(y_{\text{spec}}) < u_2 - r\,, \tag{A.11a}$$

$$u_1 + r < \widehat{u} < u_2 - r\,. \tag{A.11b}$$

Let Δ_1 and Δ_2 be defined in such a way that:

$$g_\gamma(y_{\text{spec}} - \Delta_1) = u_1 + r\,, \tag{A.12a}$$

$$g_\gamma(y_{\text{spec}} + \Delta_2) = u_2 - r\,. \tag{A.12b}$$

The first inequation in (A.11) guarantees that $\Delta_1 > 0$ and $\Delta_2 > 0$.

For any $\varepsilon \in (0, r)$ and $\delta \in (0, r)$ arbitrarily small, properties [I] and [II] of a *smooth step function* guarantee the existence of a sufficiently small γ such that:

$$u_1 - \varepsilon < g_\gamma(y_{\text{spec}} - \delta) < u_1 + \varepsilon\,, \tag{A.13a}$$

$$u_2 - \varepsilon < g_\gamma(y_{\text{spec}} + \delta) < u_2 + \varepsilon\,, \tag{A.13b}$$

and since g_γ is continuous and $\varepsilon < r$, the Intermediate Value Theorem establishes that $\Delta_1 < \delta$ and $\Delta_2 < \delta$.

Since g_γ is convex for $y < y_{\text{spec}}$ and concave for $y > y_{\text{spec}}$, then:

$$g'_\gamma(y_{\text{spec}} - \Delta_1) \geq \frac{g_\gamma(y_{\text{spec}} - \Delta_1) - g_\gamma(y_{\text{spec}} - \delta)}{\delta - \Delta_1}\,, \tag{A.14a}$$

$$g'_\gamma(y_{\text{spec}} + \Delta_2) \geq \frac{g_\gamma(y_{\text{spec}} + \delta) - g_\gamma(y_{\text{spec}} + \Delta_2)}{\delta - \Delta_2}\,. \tag{A.14b}$$

By replacing (A.12) and (A.13) into (A.14):

$$g'_\gamma(y_{\text{spec}} - \Delta_1) > \frac{r - \varepsilon}{\delta - \Delta_1}\,, \tag{A.15a}$$

$$g'_\gamma(y_{\text{spec}} + \Delta_2) > \frac{r - \varepsilon}{\delta - \Delta_2}\,. \tag{A.15b}$$

g_γ is convex for $y \leq y_{\text{spec}}$, thus $g'_\gamma(y) > g'_\gamma(y_{\text{spec}} - \Delta_1)\ \forall\ y \in [y_{\text{spec}} - \Delta_1, y_{\text{spec}}]$. Similarly, g_γ is concave for $y \geq y_{\text{spec}}$ and $g'_\gamma(y) > g'_\gamma(y_{\text{spec}} + \Delta_2)\ \forall\ y \in [y_{\text{spec}}, y_{\text{spec}} + \Delta_2]$. Therefore:

$$\begin{aligned} g'_\gamma(y) > \min\{g'_\gamma(y_{\text{spec}} - \Delta_1), g'_\gamma(y_{\text{spec}} + \Delta_2)\}\ \forall\ y \in [y_{\text{spec}} - \Delta_1, y_{\text{spec}} + \Delta_2] \\ \Rightarrow g'_\gamma(y) > \min\left\{\frac{r - \varepsilon}{\delta - \Delta_1}, \frac{r - \varepsilon}{\delta - \Delta_2}\right\}\ \forall\ y \in [y_{\text{spec}} - \Delta_1, y_{\text{spec}} + \Delta_2]\,. \end{aligned} \tag{A.16}$$

The Intermediate Value Theorem establishes the existence of $y \in [y_{\text{spec}} - \Delta_1, y_{\text{spec}} + \Delta_2]$ such that $g_\gamma(y) = u$ for all u in $[u_1 + r, u_2 - r]$. Since $\widehat{u}$ is in this interval, there is a $y \in [y_{\text{spec}} - \Delta_1, y_{\text{spec}} + \Delta_2]$ such that $g_\gamma(y) = \widehat{u}$.

For this pair $(y, \widehat{u})$:

$$\begin{aligned}
\mu'(y) &= \partial_y h(y, g_\gamma(y)) + \partial_u h(y, g_\gamma(y)) \times g'_\gamma(y) \\
&\Rightarrow \mu'(y) \times \partial_u h(y, g_\gamma(y)) = \partial_y h(y, g_\gamma(y)) \times \partial_u h(y, g_\gamma(y)) + \partial_u h(y, g_\gamma(y))^2 \times g'_\gamma(y) \\
&\Rightarrow \mu'(y) \times \partial_u h(y, g_\gamma(y)) > \partial_y h(y, g_\gamma(y)) \times \partial_u h(y, g_\gamma(y)) \\
&\qquad + \partial_u h(y, g_\gamma(y))^2 \times \min\left\{ \frac{r - \varepsilon}{\delta - \Delta_1}, \frac{r - \varepsilon}{\delta - \Delta_2} \right\}, \quad \text{(A.17)}
\end{aligned}$$

where the last inequation results from (A.16).

Point $(y, \widehat{u})$ is arbitrarily close to point $(y_{\text{spec}}, \widehat{u})$, because δ can be arbitrarily small (which leads to even smaller values of Δ_1 and Δ_2). Moreover, since h is C^1, both $\partial_y h$ and $\partial_u h$ are bounded on a neighborhood of $(y_{\text{spec}}, \widehat{u})$. If this neighborhood is sufficiently small, then $\partial_u h > 0$ and $\mu'(y) \times \partial_u h(y, g_\gamma(y))$ in inequation (A.17) is positive (note that $\delta - \Delta_1 > 0$ and $\delta - \Delta_2 > 0$ can be made arbitrarily small by reducing δ). This proves the theorem for the case where $u_1 < u_2$.

By following the same steps for $u_1 > u_2$, the final inequation is $\mu'(y) \times \partial_u h(y, g_\gamma(y)) < 0$, which completes the proof of the theorem.

A.8 Proof of Corollary 2

Given solution $(\widehat{y}, \widehat{u})$ of (4.18), Theorem 7 establishes the existence of a solution $(\widetilde{y}, \widetilde{u})$ of (4.22). These solutions are arbitrarily close to each other.

An infinitesimal variation of h in relation to infinitesimal variations in y and u is given by:

$$dh = \partial_y h \, dy + \partial_u h \, du \,. \quad \text{(A.18)}$$

If these infinitesimal variations in y and u are restricted to equation $c(y, u) = 0$, then:

$$\partial_y c \, dy + \partial_u c \, du = 0 \Rightarrow \frac{dy}{du} = -\frac{\partial_u c}{\partial_y c} \,, \quad \text{(A.19)}$$

thus the total derivative $\frac{dh}{dy}$ is given by:

$$\frac{dh}{du} = \partial_u h + \partial_y h \, \frac{dy}{du} = \partial_u h - \partial_y h \, \frac{\partial_u c}{\partial_y c} \,. \quad \text{(A.20)}$$

For equation (4.18), $c(y, u) \equiv y - y_{\text{spec}}$. Thus $\partial_u c = 0$ and $\partial_y c = 1$, and:

$$\frac{dh}{du}(\widehat{y}, \widehat{u}) = \partial_u h(\widehat{y}, \widehat{u}) \,. \quad \text{(A.21)}$$

For equation (4.22), $c(y,u) \equiv u - g_\gamma(y)$. Thus $\partial_y c = -g'_\gamma(y)$ and $\partial_u c = 1$, and:

$$\frac{dh}{du}(\widetilde{y},\widetilde{u}) = \partial_u h(\widetilde{y},\widetilde{u}) + \frac{\partial_y h(\widetilde{y},\widetilde{u})}{g'_\gamma(\widetilde{y})}\,. \tag{A.22}$$

Theorem 6 guarantees that:

$$\Big(g'_\gamma(\widetilde{y})\,(u_2-u_1)\Big) \times \left(\partial_u h(\widetilde{y},\widetilde{u}) + \frac{\partial_y h(\widetilde{y},\widetilde{u})}{g'_\gamma(\widetilde{y})}\right) \times \partial_u h(\widehat{y},\widehat{u}) > 0\,. \tag{A.23}$$

Therefore, the sign of $\frac{dh}{dy}$ for solution $(\widehat{y},\widehat{u})$ is equal to the sign of $\frac{dh}{dy}$ for solution $(\widetilde{y},\widetilde{u})$ if $g'_\gamma(\widetilde{y})\,(u_2-u_1) > 0$. Indeed this is true, because g_γ is increasing near y_{spec} if $u_1 < u_2$ and decreasing near y_{spec} if $u_1 > u_2$ (see Figure 31, for example).

A.9 Proof of Theorem 8

$\mathbf{f}_a$ is C^1 at the SNB point of the original system and $\begin{bmatrix}\partial_{\mathbf{z}}\mathbf{f}_a & \partial_t\mathbf{f}_a\end{bmatrix}$ is generically nonsingular. Thus, there are C^1 functions $\mathbf{z}(y,u)$ and $t(y,u)$ such that $\mathbf{f}_a(y,u,\mathbf{z}(y,u),t(y,u)) \equiv \mathbf{0}$ in a neighborhood of the BP.

Assume, for simplicity, that two solution points coalesce and disappear with the increase of t. The proof for the opposite situation is analogous.

If $\widehat{y} \neq y_{\text{spec}}$, then $\widehat{u}$ is either u_1 or u_2, and the SNB is similar to the one shown in Figure 33(a). Two distinct solutions approach each other at the BP with the increase of t. Let these two solutions of (4.23b) be $(\widehat{y}-\delta_1,\widehat{u})$ and $(\widehat{y}+\delta_2,\widehat{u})$ for sufficiently small values of $\delta_1 > 0$ and $\delta_2 > 0$. For these two solutions, Corollary 1 guarantees that, for a sufficiently small $\gamma > 0$, there are two distinct solutions of (4.24b) that approach each other with the increase of t. Hence, there is at least one local maximum of function t subject to equation (4.24b). This maximum is invariably the collision of two solution points. g_γ in equation (4.24b) is C^1, thus this maximum is a SNB of the smoothed system.

On the other hand, if $\widehat{y} = y_{\text{spec}}$, then $\min\{u_1,u_2\} < \widehat{u} < \max\{u_1,u_2\}$, and the SNB is similar to the one shown in Figure 33(b). Two solution points (of (4.23b)) $(y_{\text{spec}},\widehat{u}-\delta_1)$ and $(y_{\text{spec}},\widehat{u}+\delta_2)$ approach each other and coalesce at the BP, and Corollary 2 ensure the existence of two nearby solutions of (4.24b) that approach each other with the increase of t. Thus, there is at least one SNB point in the smoothed system arbitrarily close to the SNB point of the original system.

A.10 Proof of Theorem 9

From the LIB conditions, $\mathbf{f}_a$ is C^1 at the LIB point of the original system and $\begin{bmatrix}\partial_{\mathbf{z}}\mathbf{f}_a & \partial_t\mathbf{f}_a\end{bmatrix}$ is nonsingular. Thus, there are C^1 functions $\mathbf{z}(y,u)$ and $t(y,u)$ such that $\mathbf{f}_a(y,u,\mathbf{z}(y,u),t(y,u)) \equiv \mathbf{0}$ in a neighborhood of the BP.

For simplicity, assume that two solution points coalesce and disappear with the increase of t. Also assume that $u_1 < u_2$ and that the LIB point occurs at $(\widehat{y}, \widehat{u}) = (u_1, y_{\text{spec}})$. In this situation, the LIB is the one shown in Figure 34(a). This figure shows that two solution branches coalesce at (u_1, y_{spec}) with the increase of t. One solution point is of the form $(y_{\text{spec}}, u_1+\Delta_1)$, where $\Delta_1 > 0$ is sufficiently small. The other solution is $(y_{\text{spec}}-\Delta_2, u_1)$, with $\Delta_2 > 0$ sufficiently small. When u is decreased in the first solution, $t(y_{\text{spec}}, u)$ increases. Similarly, when y is increased in the second solution, $t(y, u_1)$ increases.

Corollary 2 guarantees the existence of a solution $(\widetilde{y}_1, \widetilde{u}_1)$ of (4.24b), arbitrarily close to $(y_{\text{spec}}, u_1 + \Delta_1)$, such that $t(y, u)$ increases when u decreases. Note that g_γ is an increasing function in a vicinity of y_{spec} when $u_1 < u_2$, thus $t(y, u)$ increases in the solution $(\widetilde{y}_1, \widetilde{u}_1)$ of (4.24b) when y decreases. Similarly, Corollary 1 guarantees the existence of a solution $(\widetilde{y}_2, \widetilde{u}_2)$ of (4.24b), arbitrarily close $(y_{\text{spec}} - \Delta_2, u_1)$, such that $t(y, u)$ increases when y increases.

This proves that there is at least one local maximum of $t(y, u)$ subject to equation (4.24b), which proves the existence of a SNB point of the smoothed system for $y \in [\widetilde{y}_2, \widetilde{y}_1]$.

Points $(y_{\text{spec}}, u_1 + \Delta_1)$ and $(y_{\text{spec}} - \Delta_2, u_1)$ are arbitrarily close to the LIB point. Thus, points $(\widetilde{y}_1, \widetilde{u}_1)$ and $(\widetilde{y}_2, \widetilde{u}_2)$ are arbitrarily close to the LIB point. Hence, the SNB point of the smoothed system is arbitrarily close to the LIB point of the original system. It remains to show that $\widetilde{t} < \widehat{t}$.

Let $\widetilde{u}_1 < u_1 + \alpha$ and $\widetilde{y}_2 > y_{\text{spec}} - \zeta$, where α and ζ were defined in properties [III] and [IV] of a *smooth step function*. Property [III] guarantees that $\widetilde{y}_1 < y_{\text{spec}}$, and the SNB point occurs for:

$$\widetilde{y} \in (y_{\text{spec}} - \zeta, y_{\text{spec}})\,, \tag{A.24}$$

and property [IV] guarantees that:

$$g_\gamma(\widetilde{y}) > u_1 \;\forall\; \gamma > 0\,. \tag{A.25}$$

From Figure 34(a) itself, it can be seen that

$$\partial_y t(y, u) > 0\,, \tag{A.26a}$$

$$\partial_u t(y, u) < 0\,, \tag{A.26b}$$

for all (y, u) in a neighborhood of (y_{spec}, u_1).

The proof that $\widetilde{t} < \widehat{t}$ comes from the Fundamental Theorem of Calculus:

$$\widehat{t} - \widetilde{t} = \int_{\mathcal{C}} t(y, u)\, d\mathbf{r}(y, u) \tag{A.27}$$

where $\mathcal{C}$ is any path from $(\widetilde{y}, \widetilde{u})$ to $(\widehat{y}, \widehat{u})$. For convenience, choose the straight line between these two endpoints:

$$\mathbf{r}(t) = (y(t), u(t)) = (\widetilde{y} + (\widehat{y} - \widetilde{y})\, t, \widetilde{u} + (\widehat{u} - \widetilde{u})\, t),\,, \tag{A.28}$$

and equation (A.27) lowers to:

$$\widehat{t} - \widetilde{t} = \int_0^1 \left(\partial_y t(y,u)\, y'(t) + \partial_u t(y,u)\, u'(t)\right)\, dt$$
$$= \int_0^1 \left(\partial_y t(y,u)\, (\widehat{y} - \widetilde{y}) + \partial_u t(y,u)\, (\widehat{u} - \widetilde{u})\right)\, dt\,. \quad \text{(A.29)}$$

When $(\widehat{y}, \widehat{u}) = (y_{\text{spec}}, u_1)$, equations (A.24), (A.25) and (A.26) ensure that the integrand in (A.29) is positive, and thus $\widehat{t} - \widetilde{t} > 0$, concluding the proof.

With the proper adaptations, this proof is also valid for the generic case in which $u_1 > u_2$ and/or $\widehat{u} = u_2$ and/or the solution point disappears with the decrease of t.

A.11 Proof of Theorem 10

$\mathbf{f}_a$ is C^1 at the SNB point of the smoothed system and $\begin{bmatrix}\partial_{\mathbf{z}}\mathbf{f}_a & \partial_t \mathbf{f}_a\end{bmatrix}$ is generically nonsingular. Thus, there are C^1 functions $\mathbf{z}(y,u)$ and $t(y,u)$ such that $\mathbf{f}_a(y,u,\mathbf{z}(y,u),t(y,u)) \equiv \mathbf{0}$ in a neighborhood of the BP.

Any SNB point of the smoothed system is invariably either a local minimum of $t(y,u)$ or a local maximum of this function, constrained to equation (4.24b). There are two solution points of (4.24b) that approach each other either with the increase of t or with the decrease of t. Since γ is sufficiently small, corollaries 1 and 2 guarantees the existence of two solutions of (4.23b) that approach each other either with the increase of t or with the decrease of t.

Hence, the original system (4.23) admits two distinct solutions for a given t and these solutions coalesce and disappear either with the increase of t or the decrease of t. This behavior represents invariably either the behavior of a saddle-node bifurcation or a limit-induced bifurcation, concluding the proof.

A.12 Proof of Theorem 11

Since function $\mathbf{f}_a$ is C^1 in a neighborhood of $(\widehat{y}, \widehat{u}, \widehat{\mathbf{z}}, \widehat{t})$ and $\begin{bmatrix}\partial_{\mathbf{z}}\mathbf{f}_a & \partial_t \mathbf{f}_a\end{bmatrix}$ is generically nonsingular, the Implicit Function Theorem (Theorem 1) guarantees the existence and uniqueness of continuously differentiable functions $\mathbf{z}(y,u)$ and $t(y,u)$ such that $\mathbf{f}_a(y,u,\mathbf{z}(y,u),t(y,u)) \equiv \mathbf{0}$ in a neighborhood of $(\widehat{y}, \widehat{u}, \widehat{\mathbf{z}}, \widehat{t})$.

Property [I] of a *smooth saturation function* establishes that, for a sufficiently small $\gamma > 0$, there is a solution $(\widetilde{y}, \widetilde{u}) = (\widetilde{y}(\gamma), \widetilde{u}(\gamma))$ of (4.39b) arbitrarily close to a solution $(\widehat{y}, \widehat{u})$ of (4.38b). Since functions $\mathbf{z}(y,u)$ and $t(y,u)$ are continuous, the smoothed system admits a solution $(\widetilde{y}, \widetilde{u}, \mathbf{z}(\widetilde{y}, \widetilde{u}), t(\widetilde{y}, \widetilde{u}))$ arbitrarily close to the solution $(\widehat{y}, \widehat{u}, \mathbf{z}(\widehat{y}, \widehat{u}), t(\widehat{y}, \widehat{u}))$ of the original system.

A.13 Proof of Theorem 12

Similarly to Theorem 11, there generically are unique C^1 functions $\mathbf{z}(y,u)$ and $t(y,u)$ such that $\mathbf{f}_a(y,u,\mathbf{z}(y,u),t(y,u)) \equiv \mathbf{0}$ in a neighborhood of $(\widetilde{y},\widetilde{u}) = (\widetilde{y}(\gamma),\widetilde{u}(\gamma))$.

Property [I] of a *smooth saturation function* establishes that, for a sufficiently small $\gamma > 0$, there is a solution $(\widehat{y},\widehat{u})$ of (4.38b) arbitrarily close to a solution $(\widetilde{y},\widetilde{u})$ of (4.39b). Since functions $\mathbf{z}(y,u)$ and $t(y,u)$ are continuous, the original system admits a solution $(\widehat{y},\widehat{u},\mathbf{z}(\widehat{y},\widehat{u}),t(\widehat{y},\widehat{u}))$ arbitrarily close to the solution $(\widetilde{y},\widetilde{u},\mathbf{z}(\widetilde{y},\widetilde{u}),t(\widetilde{y},\widetilde{u}))$ of the smoothed system.

A.14 Proof of Theorem 13

Property [I] of a *smooth saturation function* ensures that, for all $\delta > 0$ and $\varepsilon > 0$, there is a $\gamma > 0$ such that:

$$\mathrm{sat}(y-\delta) - \varepsilon < g_\gamma(y-\delta) < \mathrm{sat}(y-\delta) + \varepsilon\,, \tag{A.30a}$$

$$\mathrm{sat}(y) - \varepsilon < g_\gamma(y) < \mathrm{sat}(y) + \varepsilon\,, \tag{A.30b}$$

$$\mathrm{sat}(y+\delta) - \varepsilon < g_\gamma(y+\delta) < \mathrm{sat}(y+\delta) + \varepsilon\,, \tag{A.30c}$$

where sat is the original saturation function, given by (4.34).

If $y < y_{\mathrm{crit}}$, where y_{crit} is defined in property [III] of a *smooth saturation function*). Then g_γ is convex in a neighborhood of y:

$$\frac{g_\gamma(y) - g_\gamma(y-\delta)}{\delta} \leq g'_\gamma(y) \leq \frac{g_\gamma(y+\delta) - g_\gamma(y)}{\delta}\,. \tag{A.31}$$

By joining inequations (A.30) and (A.31):

$$\frac{\mathrm{sat}(y) - \mathrm{sat}(y-\delta)}{\delta} - 2\frac{\varepsilon}{\delta} \leq g'_\gamma(y) \leq \frac{\mathrm{sat}(y+\delta) - \mathrm{sat}(y)}{\delta} + 2\frac{\varepsilon}{\delta}\,. \tag{A.32}$$

When $\varepsilon > 0$ goes to zero, $\gamma > 0$ also goes to zero, thus:

$$\frac{\mathrm{sat}(y) - \mathrm{sat}(y-\delta)}{\delta} \leq \lim_{\gamma\to 0^+} g'_\gamma(y) \leq \frac{\mathrm{sat}(y+\delta) - \mathrm{sat}(y)}{\delta}\,. \tag{A.33}$$

The Squeeze Theorem guarantees that, when δ goes to zero:

$$\lim_{\gamma\to 0^+} g'_\gamma(y) = \mathrm{sat}'(y) = \begin{cases} 1, & \text{if } y_{\min} < y < y_{\max}\,, \\ \text{undefined}, & \text{if } y \in \{y_{\min}, y_{\max}\}\,, \\ 0, & \text{otherwise}\,, \end{cases} \tag{A.34}$$

for all $y < y_{\mathrm{crit}}$ such that $y \neq y_{\min}$. By using the same procedure, the same result is shown for $y > y_{\mathrm{crit}}$.

A.15 Proof of Corollary 3

The derivative of $h(y, \text{sat}(y))$ with respect to y is:

$$\partial_y h(y, \text{sat}(y)) + \partial_u h(y, \text{sat}(y)) \times \text{sat}'(y)\,. \tag{A.35}$$

Likewise, the derivative of $h(y, g_\gamma(y))$ with respect to y is

$$\partial_y h(y, g_\gamma(y)) + \partial_u h(y, g_\gamma(y)) \times g'_\gamma(y)\,. \tag{A.36}$$

Property [I] ensures that $g_\gamma(\widehat{y})$ is arbitrarily close to $\text{sat}(\widehat{y})$ with the decrease of γ. Moreover, Theorem 13 guarantees that $g'_\gamma(\widehat{y})$ also approaches $\text{sat}'(\widehat{y})$ with the decrease of γ. Therefore:

$$\lim_{\gamma \to 0^+} \frac{d}{dt}\left(h(y, g_\gamma(y))\right) = \frac{d}{dt}\left(h(y, \text{sat}(y))\right) \;\forall\; y \notin \{y_{\min}, y_{\max}, y_{\text{crit}}\}\,. \tag{A.37}$$

Both total derivatives are continuous at $\widehat{y}$. Then, the sign of these total derivatives will be the same for a sufficiently small $\gamma > 0$ and for $\widetilde{y}$ sufficiently close to $\widehat{y}$.

A.16 Proof of Theorem 14

$\mathbf{f}_a$ is C^1 at the BP and $\begin{bmatrix}\partial_{\mathbf{z}}\mathbf{f}_a & \partial_t \mathbf{f}_a\end{bmatrix}$ is generically nonsingular. Thus, there are C^1 functions $\mathbf{z}(y,u)$ and $t(y,u)$ such that $\mathbf{f}_a(y,u,\mathbf{z}(y,u),t(y,u)) \equiv \mathbf{0}$ in a neighborhood of the BP.

Assume that two solution points approach each other and collide at the BP with the increase of t. Also assume that this bifurcation point is a bifurcation of the original system (4.38). Then, in a neighborhood of this BP, Corollary 3 ensures that two solutions of the smoothed system (4.39), arbitrarily close to the BP of the original system, approach each other with the increase of t. Since g_γ is C^1, this bifurcation point is a SNB of the smoothed system.

The proof for the generic case follows similar procedures. A detailed demonstration is analogous to the proofs of Theorems 8, 9 and 10 provided in Section 4.2.

A.17 Proof of Theorem 15

Assume that the bifurcation occurs at $t = t_{\text{crit}}$, where one solution exists for $t \leq t_{\text{crit}}$ and disappears for $t > t_{\text{crit}}$.

Since a CVIB occurs at the BP, $\mathbf{f}$ is C^1 and $\partial_{\mathbf{x}}\mathbf{f}$ is nonsingular at the BP (conditions [II] and [III] of a CVIB). Therefore, the Implicit Function Theorem establishes the existence and uniqueness of a C^1 function $\mathbf{x}(t)$ such that $\mathbf{f}(\mathbf{x}(t), t) \equiv \mathbf{0}$ in a neighborhood of $t = t_{\text{crit}}$.

From this function $\mathbf{x}(t)$, define $\mu : \mathbb{R} \to \mathbb{R}$ as $\mu(t) \equiv g(\mathbf{x}(t), t)$. Therefore, equation (4.42b) can be rewritten as:

$$\mu(t) = k^2 \,. \tag{A.38}$$

Since both g and $\mathbf{x}$ are C^1, μ is C^1. Moreover, a CVIB occurs at $t = t_{\text{crit}}$, and thus $\mu'(t_{\text{crit}}) \neq 0$. Since the solution point disappears with the increase of t, $\mu'(t_{\text{crit}}) < 0$.

Hence, there is a $\delta > 0$ for which μ is strictly decreasing in the compact interval $\mathcal{I} = [t_{\text{crit}} - \delta, t_{\text{crit}} + \delta]$, i.e., $\mu'(t) < 0 \; \forall \; t \in \mathcal{I}$. μ is bijective and continuous in $\mathcal{I}$, concluding that μ is a homeomorphism in $\mathcal{I}$. Thus, there is a continuous variable transformation $\nu = \mu(t)$ with continuous inverse $t = \mu^{-1}(\nu)$, which transforms (A.38) into the normal form (SEYDEL, 2010) of a saddle-node bifurcation given by:

$$\nu = k^2 \,. \tag{A.39}$$

The SNB occurs at $\nu = k = 0$. Therefore, the bifurcation occurs for $t = \mu^{-1}(\nu) = \mu^{-1}(0) = t_{\text{crit}}$. The SNB occurs for $t = t_{\text{crit}}$ and $\mathbf{x} = \mathbf{x}(t_{\text{crit}})$, concluding the proof.

A.18 Proof of Theorem 16

Let $(\mathbf{x}_0, t_0)$ be a solution of (4.50). This solution satisfies (4.50b), thus:

$$\mathbf{g}(\mathbf{x}_0, t_0) \geq \mathbf{0} \,, \tag{A.40}$$

thus there is a vector $\mathbf{k}_0$ such that:

$$k_{0,i} = \sqrt{g_i(\mathbf{x}_0, t_0)} \; \forall \; i \,, \tag{A.41}$$

where $k_{0,i}$ is the ith element of $\mathbf{k}_0$. Vector $\mathbf{z}_0 = \begin{bmatrix} \mathbf{x}_0^T & \mathbf{k}_0^T \end{bmatrix}$ satisfies:

$$\mathbf{f}_0(\mathbf{z}, t) \equiv \begin{bmatrix} \mathbf{f}(\mathbf{x}, t) \\ g_1(\mathbf{x}, t) - k_1^2 \\ \vdots \\ g_m(\mathbf{x}, t) - k_m^2 \end{bmatrix} = \mathbf{0} \,. \tag{A.42}$$

All inequality constraints were transformed into equality constraints when (4.50) was transformed into $\mathbf{f}_0(\mathbf{z}, t) = \mathbf{0}$. In order to transform $\mathbf{f}_0$ into function $\mathbf{h}$ of equation (4.51), all instances of (4.12) must be replaced by (4.22) and all instances of the saturation function must be replaced by *smooth saturation functions*.

Define:

- n_{step} as the number of instances of equation (4.12);
- n_{sat} as the number of instances of the saturation function (4.34);
- $N = n_{\text{step}} + n_{\text{sat}}$.

Generically, each TP is due to one device limit at a time. Therefore, it is possible to rewrite equation $\mathbf{f}_0(\mathbf{z}, t) = \mathbf{0}$ into the following

$$\mathbf{f}_{a,0}(\mathbf{z}, t) = \mathbf{0}\,, \tag{A.43a}$$

$$f_{b,0}(\mathbf{z}, t) = 0\,, \tag{A.43b}$$

where function $\mathbf{f}_{a,0}$ is locally C^1. Hence, one can apply either Theorem 4 or Theorem 11 to prove the existence of a solution $(\mathbf{z}_1, t_1)$ of

$$\mathbf{f}_1(\mathbf{z}, t) = \mathbf{0} \tag{A.44}$$

arbitrarily close to $(\mathbf{z}_0, t_0)$, where $\mathbf{f}_1$ is defined as:

$$\mathbf{f}_1(\mathbf{z}, t) \equiv \begin{bmatrix} \mathbf{f}_{a,1}(\mathbf{z}, t) \\ f_{b,1}(\mathbf{z}, t) \end{bmatrix}\,. \tag{A.45}$$

$\mathbf{f}_{a,1} \equiv \mathbf{f}_{a,0}$ and $f_{b,1}(\mathbf{z}, t) = 0$ is either equation (4.24b) (related to a *smooth step function*) or (4.39b) (related to *smooth saturation function*).

Function $\mathbf{f}_1$ is clearly C^1 in a neighborhood of $(\mathbf{z}_1, t_1)$. Therefore, we can apply either Theorem 4 or Theorem 11 again to prove the existence of a solution $(\mathbf{z}_2, t_2)$ of

$$\mathbf{f}_2(\mathbf{x}, t) = \mathbf{0} \tag{A.46}$$

arbitrarily close to $(\mathbf{x}_1, t_1)$. Equation (A.46) is equation (A.44) with one instance of either (4.23b) or (4.38b) replaced by one instance of either (4.24b) or (4.39b), respectively.

If we recursively replace all N occurrences of either (4.18) or (4.34) in the original equation (A.42), then we obtain a function $\mathbf{h} \equiv \mathbf{f}_N$ that is C^1 everywhere and that admits a solution $(\mathbf{z}_N, t_N)$ arbitrarily close to $(\mathbf{z}_{N-1}, t_{N-1})$, which in turn is arbitrarily close to $(\mathbf{z}_{N-2}, t_{N-2})$ and so on. Hence, the solution $(\mathbf{z}_N, t_N)$ of equation (4.51) is arbitrarily close to the solution $(\mathbf{z}_0, t_0)$ of equation (A.42).

The final function $\mathbf{f}_N$ is independent of the order in which the nonsmooth functions are replaced by their smooth equivalents. Thus, $\mathbf{f}_N$ is independent of the original solution $(\mathbf{x}_0, t_0)$.

The proof when $(\mathbf{z}_0, t_0)$ is a solution of (4.51) is analogous. In this which case, Theorems 5 and 12 are applied recursively to prove the existence of a solution $(\mathbf{z}_N, t_N)$, arbitrarily close to $(\mathbf{z}_0, t_0)$, such that:

$$\mathbf{f}_N(\mathbf{z}_N, t_N) \equiv \begin{bmatrix} \mathbf{f}(\mathbf{x}_N, t_N) \\ g_1(\mathbf{x}_N, t_N) - k_1^2 \\ \vdots \\ g_m(\mathbf{x}_N, t_N) - k_m^2 \end{bmatrix} = \mathbf{0}\,, \tag{A.47}$$

where $\mathbf{z}_N = \begin{bmatrix} \mathbf{x}_N^T & \mathbf{k}_N^T \end{bmatrix}$ and $(\mathbf{x}_N, t_N)$ is a solution of (4.50).

A.19 Proof of Theorem 17

The proof is analogous to the proof of Theorem 16, where instead of applying Theorems 4, 5, 11 and 12 recursively, one applies Theorems 8, 9, 10, 14 and 15 recursively.